

**One-step gold nanoparticle size-shift assay using
synthetic binding proteins and dynamic light scattering**

By

Thanisorn Mahatnirunkul

Submitted in accordance with the requirements for the degree of
Doctor of Philosophy

The University of Leeds

School of Biomedical Sciences, Faculty of Biological Sciences

September 2017

I confirm that the work submitted is my own and that appropriate credit has been given
where reference has been made to the work of others.

This copy has been supplied on the understanding that it is copyright material and that no
quotation from the thesis may be published without proper acknowledgement.

Acknowledgement

I would like to express my deepest gratitude to my supervisor, Prof. Paul Millner, for his invaluable guidance, support, advice, jokes and for being a great supervisor throughout my PhD time. I also would like to thank all members in the Millner group in the past and present for academic discussion in a very friendly manner especially Asif, Kaniz, Por and Shazana for all the food, cakes and coffee to comfort me after a long day of experiment. Special thanks go to Dr. Carolyn Jackson for being the best lab manager. Also, Dr. Jack Goode and Dr. Lewis McKenzie for your kind editorial assistance, I am really appreciated.

I would like to thank the BSTG for Affimer production support especially my co-supervisors, Prof. Michael McPherson and Dr. Darren Tomlinson. As well as Anna, Cristian and Tom, thank you for being very patient with my limited molecular biology knowledge. I would also like to thank Prof. John Colyer for his guidance throughout this project. Additionally, I would like to thank all people who have facilitated my project in terms of equipment: Particle CIC in Faculty of Engineering for DLS, Martin Fuller for TEM, Dr. James Robinson for SPR, Rachel Gasior for ICP-MS and Dr. James Ault and his FBS mass spectrometry unit for all the mass spectra. Thank you for your trainings and special tips when using all the equipment.

I would not have this PhD opportunity without my sponsor. Thank you the Royal Thai Government and National Nanotechnology Center of Thailand (NANOTEC) for financial support. Another group of person that I would like to thank is all my friends in Leeds for poker lessons, drinks, parties, late night talks and all the cherished memories we have been sharing during my stay in the UK. Especially the original Leeds 2012, poker gangster, Sukhothai crews and all MSc Bionanotechnology friends (especially Jo, Stella and Iril) without you guys my life here would not be completed. My endless thanks go to Aleena who always makes me laugh and keeps me sane along the journey. As well as all my Thai friends back home, thank you for always there for me whenever I need you guys.

To my family, Daddy, Mommy and my sister Pearl aka Purzy, a very big thanks to you for the unmeasurable love and support you have given me all my life. I would not have come this far in life without you guys. I am really sorry for being far away for so long. I specially dedicate this work to all of you and I cannot wait to go home.

Abstract

Gold nanoparticles (AuNPs) have attracted significant interest for biosensing applications because of their distinctive optical properties including light scattering. Dynamic light scattering (DLS) is an analytical tool used routinely for measuring the hydrodynamic size of colloids and nanoparticles in liquid environment. By combining the light scattering properties of AuNPs with DLS, a label-free, facile and sensitive assay has been developed. There have been several reports showing that NP-coupled DLS size shift assays are capable of quantitative analysis for target analytes ranging from metal ions to proteins as well as being a tool for biomolecular interaction studies.

The principle of the assay developed is to immobilise bioreceptors (antibodies, oligonucleotides or synthetic binding proteins) specific to the target analyte onto AuNPs to produce nanobiosensors. When the analyte is added to the system, binding of the target protein to the immobilised bioreceptors leads to a size increase of the functionalised AuNPs. The hydrodynamic diameter (D_H) can then be measured by DLS for complete quantitation. However, the ability to use synthetic binding proteins (Affimers) in optical sensing has not been investigated. Here, anti-myoglobin (Mb) Affimers were selected by biopanning of a phage display library and subcloned into a bacterial plasmid for expression in a prokaryotic system. These Affimers were then expressed and characterised before being used as bioreceptors in the NP-coupled DLS size shift assay. The Affimer functionalised AuNPs were compared to those using polyclonal antibodies (IgG) as bioreceptors.

The Affimer nanobiosensors could selectively detect Mb with a limit of detection of 554 fM when multiple Affimer clones were immobilized onto the AuNPs, which was comparable to IgG based nanobiosensors (LOD = 148 fM). These findings suggest that in general a polyclonal reagent is optimum for the assay. In addition, other factors, such as AuNP size and concentration, related to the assay were investigated. The detection range of the size shift assay could be tailored to each analyte by selecting the appropriate AuNP size and concentration. This fundamental data will serve as a base for future studies of using Affimers in DLS based sensing applications.

Abbreviations

10Fn3	10 th domain of fibronectin type 3
AAS	Atomic absorption spectroscopy
Ab	Antibody
AF	Aflatoxin
Affimer-AuNP	Affimer conjugated gold nanoparticle
AFM	Atomic force microscopy
AFP	Alpha-fetoprotein
Ag@Au CSNP	Silver-core gold-shell nanoparticle
AgNP	Silver nanoparticle
AuNP	Gold nanoparticle
AuNR	Gold nanorod
Biotin HPDP	N-[6-(biotinamido)hexyl]-3'-(2'-pyridyldithio)propionamide
Biotin NHS	Biotin N-hydroxysuccinimide
BLI	Bio-layer interferometry
BPH	Benign prostate hyperplasia
BSTG	The Leeds BioScreening Technology Group
cal	Calprotectin
CDK	Cyclin-dependent kinases
cDNA	Complementary DNA
CDR	Complementarity determining region
CEA	Carcinoembryonic antigen
CFCA	Calibration-free concentration analysis
CM	Carboxymethylated dextran
Con A	Concanavalin A
CTAB	Cetrimonium bromide
Cys	Cysteine
Cyt c	Horse heart cytochrome c
<i>D</i>	Translational diffusion coefficient
DCS	Differential centrifugal sedimentation
D _H	Hydrodynamic diameter
DHLA	Dihydrolipoic acid

DLS	Dynamic light scattering
DMSO	Dimethyl sulfoxide
DNA	Deoxyribonucleic acid
dNTP	Deoxynucleotide
DSC	Differential scanning calorimeter
dsDNA	Double stranded DNA
DTSSP	3,3'-dithiobis(sulfosuccinimidyl propionate)
DTT	Dithiothreitol
ECL	Enhanced chemiluminescence
<i>E.coli</i>	<i>Escherichia Coli</i>
EDA	1,2-ethylenediamine
EDC	1-ethyl-3-[3-dimethylaminopropyl] carbodiimide
EDTA	Ethylenediaminetetracetic acid
ELISA	Enzyme-linked immunosorbent assay
FRET	Fluorescence resonance energy transfer
GADPH	Glyceraldehyde 3-phosphate dehydrogenase
GC-MS	Gas chromatography-mass spectrometry
GO _x	Glucose oxidase
GSH	Glutathione
HBsAg	Hepatitis B antigen
hCG	Human chorionic gonadotropin
HER2	Human epidermal growth factor receptor type 2
HIV	Human immunodeficiency virus
HPLC	High-performance liquid chromatography
HPV	Human papilloma virus
HRP	Horseradish peroxidase
ICP-MS	Inductively coupled plasma mass spectrometry
IgG	Immunoglobulin G
IgG-AuNPs	IgG conjugated gold nanoparticle
IO	Iron oxide
IPTG	Isopropyl β -D-1-thiogalactopyranoside
K _a	Association rate constant

K_b	Dissociation rate constant
K_D	Dissociation constant
kcps	Kilo counts per second
LB	Luria-Bertani
LOD	Limit of detection
LRR	Leucine-rich repeat modules
LSPR	Localised surface plasmon resonance
mAb	Monoclonal antibody
Mb	Myoglobin
Mb-AuNP	Myoglobin conjugated gold nanoparticle
MC-LR	Microcystin-LR
Met	Methionine
MFP	Mean free path
MI	Myocardial infarction
miRNA	Micro RNA
MMP	Micro magnetic nanoparticle
MMM _Q	Melamine monomer's migratory quantity
Mr	Molecular weight
MRSA	Methicillin-resistant <i>Staphylococcus aureus</i>
MUA	11-mercaptoundecanoic acid
MWCO	Molecular weight cut-off
Ni ²⁺ -NTA	Nickel-nitrilotriacetic acid
NNLS	Non-negative least squares
NOS	Nopaline synthase
NP	Nanoparticle
NTA	Nanoparticle tracking analysis
OD	Optical density
pAb	Polyclonal antibody
pagA	Protective antigen precursor
PAP	Prostatic acid phosphatase
<i>p</i> -ATP	Para-aminothiophenol
PBS	Phosphate buffered saline

PCR	Polymerase chain reaction
PCS	Photon correlation spectroscopy
PDB	Protein data bank
PDI	Protein disulphide isomerase
PEG	Polyethylene glycol
pI	Isoelectric point
PNA	Peptide nucleic acid
PP	Pancreatic polypeptide
ppb	Parts per billion
ppm	Parts per million
ppt	Parts per trillion
PSA	Prostate specific antigen
QCM	Quartz crystal microbalance
QCM-D	Quartz crystal microbalance with dissipation monitoring
QD	Quantum dot
RB	Rhodamine B
RIA	Radioimmunoassay
RNA	Ribonucleic acid
RTags	Raman tags
SDS-PAGE	Sodium dodecyl sulphate-polyacrylamide gel electrophoresis
SELEX	Systematic evolution of ligands by exponential enrichment
SERS	Surface-enhanced Raman spectroscopy
SLS	Static light scattering
SOB	Super optimum broth
SOC	SOB with catabolite repression
SPR	Surface plasmon resonance
ssDNA	Single stranded DNA
ssRNA	Single stranded RNA
strep-AuNP	Streptavidin coated gold nanoparticle
sulfo-NHS	N-hydroxysulfosuccinimide
TCEP	Tris(2-carboxyethyl)phosphine hydrochloride
TEM	Transmission electron microscopy

TMB	3,3',5,5'-tetramethylbenzidine
TNF- α	Tumour necrosis factor alpha
TNT	2,4,6-trinitrotoluene
TrxA	Thioredoxin
TxB	<i>Clostridium difficile</i> toxin B
VOC	Volatile organic compound
WHO	World Health Organization

Table of Contents

Acknowledgement	i
Abstract	ii
Abbreviation	iii
List of Figures	xii
List of Tables	xvii
Chapter 1 Introduction	1
1.1 Overview.....	2
1.2 Biosensing system	4
1.2.1 Classification of biosensing platform	5
1.2.2 Labelled vs label-free sensing platform	9
1.3 Metal nanoparticles	12
1.3.1 Synthesis of gold nanoparticles	12
1.3.2 Functionalisation of AuNPs	13
1.3.3 Gold nanoparticles as a biosensing system	20
1.4 AuNP size-shift based method	30
1.4.1 Dynamic light scattering.....	30
1.4.2 Principle of nanoparticle-coupled dynamic light scattering assay	37
1.4.3 Applications of nanoparticle-coupled DLS assay	42
1.4.4 Challenges in the development of nanoparticle-coupled dynamic light scattering detection	63
1.5 Bioreceptors	65
1.5.1 Oligonucleotides and aptamers	65
1.5.2 Antibodies and their alternatives	67
1.6 Project aims and impact statement: potential applications	79
Chapter 2 Materials and Methods.....	83

2.1	Materials.....	83
2.1.1	Inorganic materials.....	83
2.1.2	Organic materials	83
2.1.3	Antibodies	83
2.1.4	Buffers and solutions	84
2.1.5	Kits and consumables.....	85
2.1.6	Growth media for bacteria and antibiotics.....	85
2.1.7	Phage display and phage ELISA related materials	86
2.1.8	Subcloning Affimer DNA related materials.....	86
2.1.9	Expression and purification of Affimer related materials.....	87
2.1.10	Gold nanoparticles (AuNPs)	87
2.2	Methods	88
2.2.1	Affimer production.....	88
2.2.2	Characterisation of Affimers	96
2.2.3	Preparation of nanobiosensors.....	99
2.2.4	Characterisation of nanobiosensors	101
2.2.5	Nanoparticle (NP)-coupled dynamic light scattering (DLS) size shift assay	104
Chapter 3	Affimer production and characterisation	107
3.1	Introduction.....	107
3.2	Affimer production	108
3.2.1	Phage display screening	108
3.2.2	Phage ELISA	109
3.2.3	DNA sequencing	111
3.2.4	Subcloning.....	113

3.2.5	Expression and purification.....	117
3.3	Affimer characterisations	121
3.3.1	Immunoprecipitation (pull-down assay).....	121
3.3.2	ELISA analysis with purified Affimers	123
3.3.3	Binding kinetics	124
3.3.4	Affimer pair selection.....	135
3.4	Discussion	138
Chapter 4	Functionalisation of gold nanoparticles (AuNPs).....	141
4.1	Introduction.....	141
4.2	Biotinylation of bioreceptors.....	142
4.2.1	Antibodies (IgGs)	142
4.2.2	Affimers	144
4.3	Preparation of AuNP nanobiosensors	149
4.3.1	Streptavidin coated AuNPs	149
4.3.2	Conjugation of bioreceptors onto the AuNP surface.....	152
4.3.3	Optimising functionalisation	155
4.4	Quantification of bioreceptors on the AuNP surface.....	161
4.5	Discussion	167
Chapter 5	NP-coupled DLS size shift assay	171
5.1	Introduction.....	171
5.2	Kinetics study.....	171
5.3	Detection of myoglobin using NP-coupled DLS size shift assay	177
5.3.1	Antibody (IgG) based assay	177
5.3.2	Paired Affimer based assay	181
5.3.3	Multiple Affimer based assay.....	184

5.3.4	TEM images	187
5.4	Non-specific control	190
5.5	Effect of NP size	192
5.6	Effect of NP concentration	195
5.7	Stability of nanobiosensors	199
5.8	Versatility of NP-coupled DLS size shift assay using Affimers	202
5.9	Discussion	205
Chapter 6	General discussion	209
6.1	General discussion.....	209
6.2	Affimer production and characterisation.....	210
6.3	Nanoparticle (NP) coupled dynamic light scattering (DLS) size shift assay using synthetic binding proteins	211
6.4	Future work and opportunities	216
References.....		219
Appendices.....		235

List of Figures

Figure 1-1 The overview of biosensing platform.	4
Figure 1-2 Schematic of SPR principle.....	8
Figure 1-3 The number of publications derived via the Sciencedirect search engine, using the term “gold nanoparticle* and sensing”.	11
Figure 1-4 Schematic of functionalisation of AuNP probes.	14
Figure 1-5 3,3'-dithobis(sulfosuccinimidyl propionate) (DTSSP) molecule.	17
Figure 1-6 EDC crosslinking pathway.	18
Figure 1-7 The bio-bar-code assay method.	25
Figure 1-8 Schematic of main components of a lateral flow pregnancy strip.....	27
Figure 1-9 Schematic of a DLS instrument.....	31
Figure 1-10 Showing correlograms obtained from different sizes of particles.	33
Figure 1-11 The stabilization mechanisms of colloidal AuNP dispersion.	38
Figure 1-12 Schematic of non-crosslinking aggregation mechanisms.....	39
Figure 1-13 Schematic of interparticle crosslinking aggregation mechanism.....	41
Figure 1-14 Structures of theophylline and caffeine.	66
Figure 1-15 Antibody (IgG) molecular structure.....	68
Figure 1-16 Molecular structure of an Affimer.....	77
Figure 1-17 Schematic of NP-coupled DLS size shift assay.	80
Figure 3-1 Molecular structure of myoglobin.....	107
Figure 3-2 ELISA to validate biotinylation of myoglobin.....	108
Figure 3-3 Phage ELISA to show binding of myoglobin Affimer binders.	109
Figure 3-4 Phage ELISA histogram for anti-myoglobin Affimers.....	110
Figure 3-5 DNA sequencing results for anti-myoglobin Affimers.	111
Figure 3-6 Gel electrophoresis for anti-myoglobin Affimer inserts.....	113

Figure 3-7 Schematic of incorporating Affimers into pET11a vector.	114
Figure 3-8 pETT11a vector map	114
Figure 3-9 Gel electrophoresis for linearised pETT11a vector.....	115
Figure 3-10 Subcloned DNA sequences of anti-myoglobin Affimer subclones.	116
Figure 3-11 SDS-PAGE gel of purified anti-Mb Affimers.	118
Figure 3-12 SDS-PAGE gel of purified anti-Mb Affimers without heating step to the cell lysates.	120
Figure 3-13 SDS-PAGE gel for pull-down Mb using Affimers.	122
Figure 3-14 Direct ELISA results for six anti-Mb Affimers together with negative controls.	123
Figure 3-15 Real time binding data of SPR experiment on anti-Mb Affimers and its negative control.	125
Figure 3-16 Real time binding data of anti-Mb Affimer E3 and anti-yeast-SUMO Affimer on an expanded scale.....	126
Figure 3-17 Comparison graph of five anti-Mb Affimers SPR binding data.....	127
Figure 3-18 Typical SPR binding curve.	128
Figure 3-19 One-site binding model data fitting.....	130
Figure 3-20 Two-site binding model data fitting.	131
Figure 3-21 Summary of overall K_D values for anti-myoglobin Affimers.	134
Figure 3-22 Schematic of Affimer pair ELISA.	135
Figure 3-23 Affimer pair ELISA data for anti-Mb Affimers.....	137
Figure 4-1 Antibody (IgG) structure.	142
Figure 4-2 Biotin hydrazide reaction.....	143
Figure 4-3 ELISA to show biotinylation of anti-myoglobin IgG (anti-Mb IgG) for AuNP functionalisation.	144
Figure 4-4 Schematic of biotin maleimide interaction to Affimer.....	145

Figure 4-5 ELISA to show biotinylation of C2 Affimer.....	145
Figure 4-6 Mass spectra of C2 Affimer.....	146
Figure 4-7 Graphics illustrate the possible orientations of streptavidin on AuNP surface.....	151
Figure 4-8 Size distribution plots of all streptavidin coated AuNPs (strep-AuNPs) with different core diameters.	151
Figure 4-9 ECL dot blot immunoassay.....	152
Figure 4-10 The absorbance spectra of strep-AuNPs before and after conjugation with IgG or C2 Affimer.....	153
Figure 4-11 Size distribution plots of streptavidin coated AuNPs before and after functionalisation with IgGs and C2 Affimers.....	154
Figure 4-12 Effect of incubation time on AuNP functionalisation via the streptavidin-biotin interaction for AuNPs with 40 nm core diameter.	156
Figure 4-13 Effect of incubation time on AuNP functionalisation via the streptavidin-biotin interaction for different sizes of AuNPs.	157
Figure 4-14 Effect of bioreceptor concentration used in AuNP functionalisation via the streptavidin-biotin interaction for AuNPs with 40 nm core diameter.	158
Figure 4-15 Effect of bioreceptor concentration used in AuNP functionalisation via the streptavidin-biotin interaction for different sizes of AuNPs.	160
Figure 4-16 Concentration of gold from 1 ml AuNP nanobiosensors.....	162
Figure 4-17 The number of bioreceptor molecules conjugated onto AuNP surface compared between the direct and indirect quantification methods.....	164
Figure 4-18 Number of streptavidin on AuNP (molecule/NP).....	165
Figure 4-19 Number of bioreceptors on AuNP (molecule/NP).....	166
Figure 5-1 Size distribution plots of all functionalised AuNPs used in the kinetics study.....	173

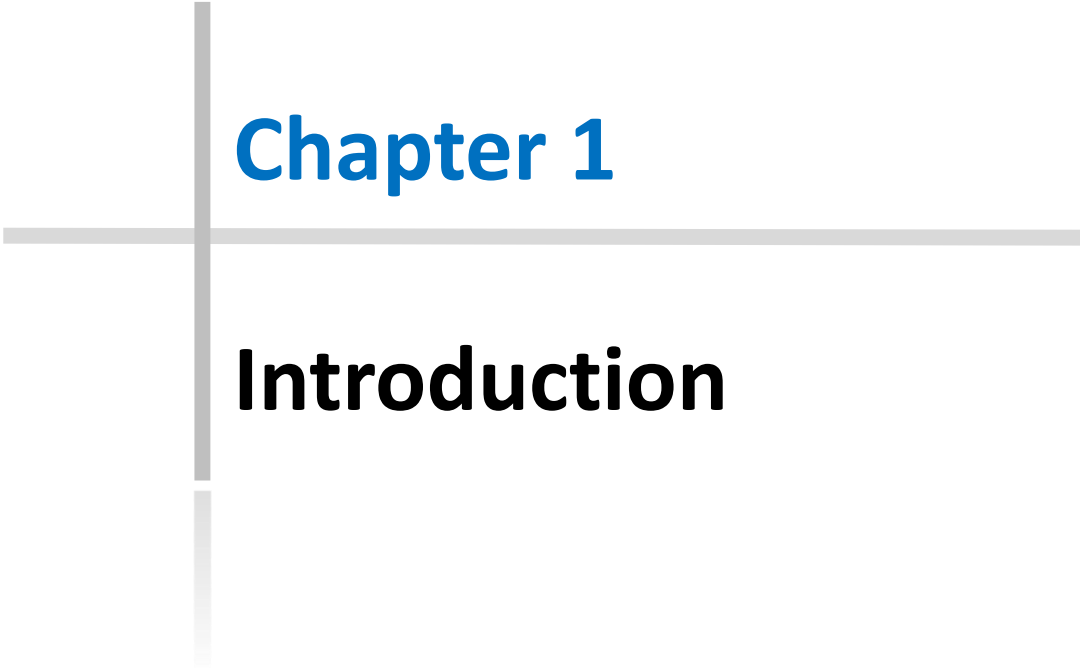
Figure 5-2 The average hydrodynamic diameter (D_H) of a 1:1 volume ratio mixture of myoglobin conjugated AuNPs (Mb-AuNPs) and three different nanobiosensors over 24 h.....	174
Figure 5-3 The average hydrodynamic diameter (D_H) of a 1:1 volume ratio mixture of myoglobin conjugated AuNPs (Mb-AuNPs) and three different nanobiosensors in an expanded scale.....	175
Figure 5-4 The size distributions of all three mixed solutions.....	176
Figure 5-5 Size shift of Mb mixed with IgG nanobiosensors after incubating at RT for 30 min.....	177
Figure 5-6 One-site, (A); and two-site, (B) model fittings of an assay for Mb using IgG conjugated AuNPs in the concentration range of 10 fM – 10 nM.....	180
Figure 5-7 Size shift of Mb mixed with paired Affimer nanobiosensors after incubating at RT for 30 min in comparison with negative control.	181
Figure 5-8 One-site, (A); and two-site, (B) model fittings of an assay for Mb using paired Affimers conjugated AuNPs.....	183
Figure 5-9 Size shift of Mb mixed with multiple Affimer nanobiosensors after incubating at RT for 30 min in comparison with negative control.	184
Figure 5-10 One-site, (A); and two-site, (B) model fittings of an assay for Mb using multiple Affimer conjugated AuNPs.	186
Figure 5-11 Size distribution plots of multiple Affimer nanobiosensors with and without Mb and their corresponded TEM images.....	188
Figure 5-12 Size shift of BSA mixed with multiple anti-myoglobin Affimer nanobiosensors after incubating at RT for 30 min.	190
Figure 5-13 Size shift of Mb mixed with anti-calprotectin Affimer nanobiosensors after incubating at RT for 30 min.	191
Figure 5-14 Effect of AuNP size on the DLS assay for Mb detection.	193
Figure 5-15 Limit of detections (LODs) of DLS assay for Mb detection using different AuNP core diameters.	194

Figure 5-16 Effect of AuNP nanobiosensor concentration on the DLS assay for Mb detection..	196
Figure 5-17 Dynamic ranges of DLS assay for Mb detection using four different nanobiosensor concentrations.	198
Figure 5-18 Mean D_H of AuNP probes used in stability study.	199
Figure 5-19 DLS assay for Mb detection performed on day 1, 3, 7 and 35 to study the stability of nanobiosensors.	200
Figure 5-20 Size shift of toxin B mixed with anti-toxin B paired Affimer nanobiosensors after incubating at RT for 30 min.	203
Figure 5-21 Two-site model fitting of an assay for toxin B using anti-toxin B paired Affimer conjugated AuNPs.	204

List of Tables

Table 1-1: Chemical sensing application	48
Table 1-2: Biological sensing applications.....	57
Table 1-3: Other applications.....	62
Table 1-4: Examples of secondary structure based binding mechanism non-antibody (Ab) binding proteins.	72
Table 1-5: Examples of loop based binding mechanism non-Ab binding proteins. .	73
Table 2-1: Summary of all antibodies used in this project	83
Table 2-2: Summary of buffers used in this project.....	84
Table 2-3: Summary of all growth media for bacteria used in this project	85
Table 2-4: Summary of PCR 25 µl reaction set up for Affimer DNA amplification ...	93
Table 2-5: Thermocycling conditions of PCR.....	93
Table 2-6: Showing the volume of supplement reagents in lysis buffer used for Affimer extraction	95
Table 2-7: Appropriate g forces used for AuNPs with different core diameter	100
Table 3-1: Affimer insert sequences for six selected anti-myoglobin Affimers.....	112
Table 3-2: Data from one-site binding model.....	132
Table 3-3: Data from two-site binding model.....	132
Table 4-1: Summary of all selected anti-myoglobin Affimers masses obtained by mass spectrometry.....	147
Table 4-2: Summary of all selected biotinylated anti-myoglobin Affimers masses obtained by mass spectrometry.	148
Table 4-3: Mean D_H of streptavidin coated AuNPs (strep-AuNPs).	150
Table 4-4: Mean D_H of strep-AuNPs before and after conjugation with IgGs and C2 Affimers via the streptavidin-biotin interaction.	154
Table 4-5: Comparison of theoretical and ICP-MS measured NP concentrations..	163

Table 5-1: Original sizes of all functionalised AuNPs used in the kinetics study measured by DLS.....	172
Table 5-2: Binding parameters derived from one- and two-site fitting models of myoglobin assay using IgG-AuNP nanobiosensors.	179
Table 5-3: Binding parameters derived from one- and two-site fitting models of myoglobin assay using paired-AuNP nanobiosensors.	182
Table 5-4: Binding parameters derived from one- and two-site fitting models of myoglobin assay using multiple Affimer-AuNP nanobiosensors.	185
Table 5-5: Apparent K_D s of five selected anti-myoglobin Affimers from SPR data.	187
Table 5-6: Binding parameters derived from a two-site fitting model of toxin B assay using anti-toxin B paired Affimer nanobiosensors.....	204



Chapter 1

Introduction

Chapter 1 Introduction

1.1 Overview

Nanoparticles (NPs) are particles with sizes ranging from 10 to a few 100s of nm. They possess unique characteristics in between those of bulk materials and molecular scale materials. NPs have attracted massive interests for biomedical applications e.g. for cellular imaging or biosensing, especially with their distinctive optical properties. Metal nanoparticles, particularly gold, have been extensively studied because of their facile synthesis and modifiable surface chemistry. In biosensing applications, gold nanoparticles (AuNPs) were first introduced as optical labels, electrochemical markers or signal amplifiers (Pissuwan et al., 2010; Kaittanis et al., 2010). However, in the past decade, the trend has shifted to a designed biosensing assay using AuNPs as a platform not just as a signal amplifier. With their unique optical properties, they allow various detection systems to be established.

Dynamic light scattering (DLS) is an analytical tool used routinely for measuring the hydrodynamic size of colloids and nanoparticles in a liquid environment. By combining the light scattering properties of AuNPs with DLS, a label-free, facile and sensitive assay can be developed. One of the most interesting assays is the NP-coupled DLS size-shift assay. The principle is to conjugate bioreceptors on AuNPs. When the target analyte is added to the system, the binding of the target and immobilised binding protein will lead to size increase or aggregation of AuNPs. The size increase then can be measured by DLS for complete quantitation. The concept of this assay was previously investigated and proved that it is possible with various type of bioreceptors, mostly antibodies (Abs).

There are some disadvantages regarding antibodies, e.g. they are large multimeric molecules, expensive to produce and with reproducibility issues and so there has been attention to find an alternative to antibodies. Amongst antibody mimetics, synthetic binding proteins are undergoing intense development. The Affimer is one of synthetic binding proteins that exhibits the promising property of

being an effective bioreceptor with similar or better specificity to antibodies, but is more easily produced and more thermodynamically and chemically stable.

The challenge in developing assays is to produce a stable detection probe with reliable binding property as the key principle relies on the specific binding event between the bioreceptors on NP surfaces and the target analyte. Work in this thesis has been carried out to investigate whether the Affimer can be used as bioreceptors in a nanoparticle size-shift assay. The work involved screening of the Affimers library for Affimer that bound equine heart myoglobin and characterizing them for size-shift assay applications. Myoglobin from equine heart was selected as a model analyte because it is an inexpensive and common protein, but is also an important biomarker for skeletal and cardiac muscle damage. With more stable bioreceptors, it is expected that this will open up more opportunities to develop cheaper and more robust assay systems.

1.2 Biosensing system

A biosensor is an analytical platform involving three main components (Figure 1-1), which are the recognition element, transduction and output systems. The recognition process utilizes the specific binding of an analyte – both biological and chemical – to a biomolecule often called a bioreceptor. This process is known as the biorecognition event. After the specific binding phenomenon occurs, a transducer system plays an important role in converting this event into a measurable signal that is proportional to the amount of analyte. Finally, those signals are amplified and displayed by the proper signal processing instrument.

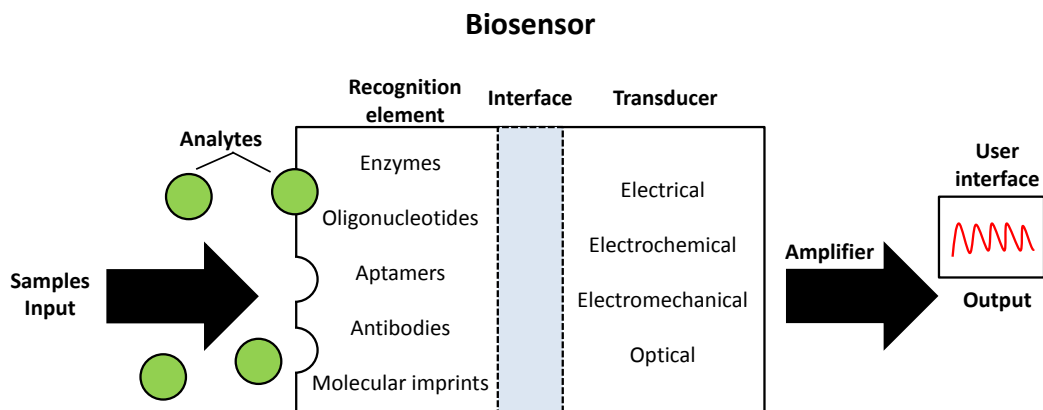


Figure 1-1 The overview of biosensing platform.

The biosensing field has grown rapidly since its concept was first introduced worldwide by Clark and Lyons (1962). They developed a biosensing device for glucose detection, which was based on electrochemical detection of oxygen using suitable immobilised enzymes. Since then, these biosensor has become a promising platform for detection of innumerable analytes. The main application that draws researchers' attention is the diagnostics via determination of various disease biomarkers as well as in drug discovery. However, the applications of biosensing platforms are not restricted to the biomedical field but includes wide range of applications in other fields such as food industries, environmental monitoring and even national security (Luong et al., 2008).

1.2.1 Classification of biosensing platform

Biosensing platforms can be classified using several principles. However, the biological recognition process and the signal transduction method are the two main criteria used for categorization.

1.2.1.1 *Electrochemical sensing*

Electrochemical techniques for transduction processes in biosensors have been used for a long time and this approach was the first ever transducer element introduced alongside the biosensor concept (Rushworth et al., 2013). Also, electrochemical techniques are sensitive but with reasonable cost. This kind of system can be miniaturized into a hand-held device or even implantable biosensors, which are suitable for lab-on-a-chip development. However, some electrochemical biosensor systems, such as impedimetric biosensors, still face problems with consistency when it comes to repetitive analysis (Luong et al., 2008; Pavesi and Fauchet, 2008). There are several types of electrochemical techniques; amperometric, potentiometric, impedimetric or conductometric systems. Amperometric techniques directly convert the reaction rate of biomolecular event into a quantifiable current. Potentiometric biosensors, by comparison measures a voltage change across the electrode surface. Impedimetric sensors measure the change of impedance across the electrode surfaces, whereas, the method that utilizes sensing materials and measures their capabilities to transport charge is known as conductometric biosensor (Yoo and Lee, 2010).

1.2.1.2 *Electromechanical sensing*

Another type of transduction is found in electromechanical biosensors. These sensors measure the change of mass on the sensor surface due to biomolecular recognition. They can be categorized into several subgroups, such as quartz crystal microbalances (QCM), acoustic wave sensors, microcantilever sensors and others. QCM – the most common technique – measures decrease in frequency that corresponds to change in mass of an oscillating crystal when bound to an analyte

(Tamayo et al., 2013; Rushworth et al., 2013), while acoustic wave sensors measure the overall change of sensor resonant frequency by using piezoelectric materials as a sensor surface. The frequency of oscillation depends on the material's mass. Thus, as analytes bind to the material, the mass will be increased and frequency reduces. The concentration of extra mass can be calculated using the change in frequency from the Sauerbrey equation (Chambers et al., 2008) . To fulfil the assumptions required for the equation, however, mass adsorbed must be small compared to the mass of the quartz crystal used, also the Sauerbrey equation only applies to rigid bodies. Therefore, QCM with dissipation monitoring or QCM-D was developed to solve this problem for soft materials (such as films, polymers and some biological macromolecules) or in a liquid environment as these samples or conditions always violate the rules of the Sauerbrey equation. With QCM-D, dissipation is monitored alongside the frequency by measuring the amplitude of oscillatory decay, which enables the viscoelasticity to be revealed (Dixon, 2008). The last subgroup utilizes cantilever flexibility as a key component. There are two modes of operation; (i) bending (or static) mode, which measures the deflection of the cantilever when the analyte binds and (ii) resonant (or dynamic) mode, in which measuring the resonant frequency change when analyte binds. This type of biosensor is highly sensitive, label-free and can be miniaturized (Tamayo et al., 2013).

1.2.1.3 Optical sensing

Optical biosensors can be roughly classified into label-based and label-free systems. Label-based platforms are systems that utilize optical labels, i.e. chromophores or fluorophores, as a transducer element. Sometimes the systems are based on the fact that many biomolecules have intrinsic fluorescence or synthetic fluorophores can be attached to be used as probes. Tagging a ligand with a fluorophore or development of a fluorescent analogue can require a multifaceted and time-consuming approach, which makes sensor fabrication more complicated (Pavesi and Fauchet, 2008; Shinde et al., 2012). Frequently, colored matrices or

interferents can compromise assay results and therefore label-free platforms are preferable.

Surface plasmon resonance (SPR) is a well-known label-free technique for measuring biomolecular interactions, providing kinetic parameters as well as concentration analysis. In a recent times, SPR is able to perform calibration-free concentration analysis (CFCA). This method allows the active concentration of analyte to be determined without a calibration curve. It is based on mass transport limitations. This condition is when the binding rate is proportional to the transport rate of the analyte to the sensor surface. The active concentration can be calculated directly from the slopes of the curve by injecting the analyte at two different flow rates (e.g. 5 and 100 $\mu\text{l}/\text{min}$), (Visentin et al., 2016). Moreover, SPR imaging is also developing. This is used in a microarray format and combines the sensitivity of SPR and spatial imaging (Damborsky et al., 2016). SPR techniques dominate the market for optical sensing because they can provide the real-time quantitative analysis with very high sensitivity. Also, SPR has a high-throughput potential as it is an automatic system. Nevertheless, there are some drawbacks of using SPR, as it requires an expert operator for measurement and data analysis. Additionally, the cost of SPR equipment and consumables (“chips”) is considerable, similar to most optical sensing systems. Furthermore, the technique itself cannot differentiate the effect of non-specific binding and the detection of low molecular weight samples is still limited (Ahmed et al., 2010; Damborsky et al., 2016).

SPR occurs when polarized light is applied to a glass prism-metal surface under total internal reflection (TIR) conditions. TIR is the point when all the incoming light reflects within the prism. This phenomenon will occur only at above a certain incidence angle. At the TIR condition, the reflected light produces an electrical field called an evanescent field on the surface. The wavelength of the evanescent wave is the same as that of the incident light but the amplitude decreases exponentially with increasing distance from the surface. When the prism is coated with a conducting material like gold, photons from the incident light interact with the outer shell or conduction band electrons of the gold and surface plasmons are generated, which are confined to the surface of the gold. These plasmons also produce an extended

evanescent wave across the gold surface and buffer solution. The conversion of photons to plasmons can occur when both momentum and energy of the process are maintained. The momentum can be referred to as a vector function with magnitude and direction of wave properties of both photons and plasmons. Resonance occurs when the momentum of incoming light is equal to the momentum of the plasmons. With this interaction, the photons convert to plasmons causing a dip in the reflected light intensity. At a specific angle where the maximum loss of the reflected light intensity occurs is called resonance angle, or SPR angle. To sustain this SPR phenomenon, the correct angle of incident light is required, but it is very sensitive to changes in refractive index at the surface. Therefore, any changes at the interface between the gold and the buffer, such as binding of molecule on the surface will alter the momentum of the surface plasmons and their associated evanescent wave. Regarding this, the SPR phenomenon no longer occurs at the same angle and leads to an SPR shift. The SPR configuration can be set up by detecting the SPR angle shifts at the sensor surface against time. The change corresponds to the biomolecule concentration. A schematic of the SPR principle is shown in Figure 1-2.

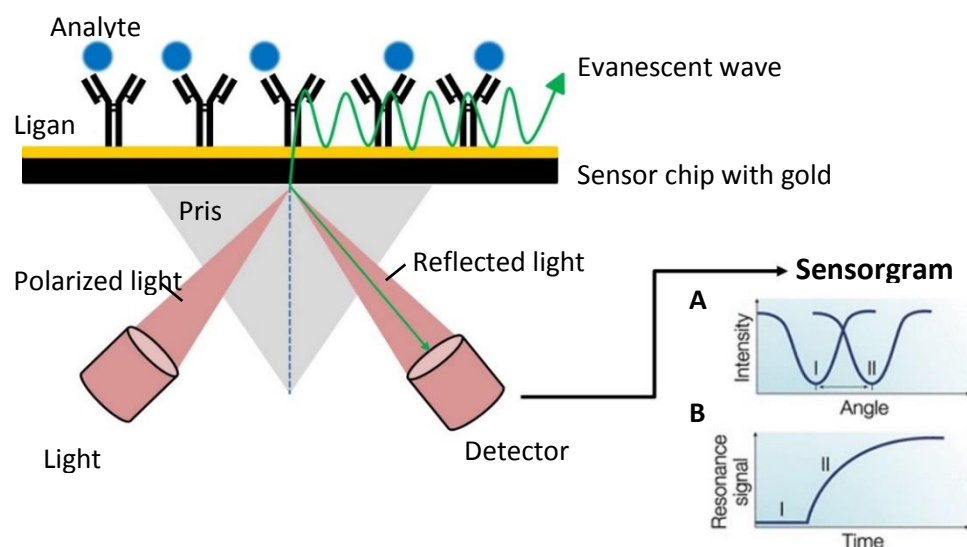


Figure 1-2 Schematic of SPR principle. Ligands are immobilised on the sensor surface, while the analyte is flowed through the flow cell over the chip. The light source is fixed with incident angle and optical detection placed for SPR angle change. (A), when the analyte-ligand binding occurs, the plasmon generated absorbs light at a different angle (II) from when ligands present on the chip surface only (I), causing the point of minimum intensity shifts; (B), this change in shift is a resonance signal used for monitoring binding in real time.

Apart from SPR, there are other optical sensing platforms that have been commercialized. For examples, bio-layer interferometry (BLI) is another widely used technique commercialized under the Octet system by ForteBio (Cooper, 2006). The principle of BLI is shining the white light to the optical sensor surface and collect the reflected light. The thickness of the surface layers disturbs the reflected light. The waves of light travelling back to the detector can interact either constructively or destructively to each other causing a phase-shift of light wave pattern. This particular pattern correlates to the optical thickness and is directly measured in real time. Another interesting optical sensing platform is ellipsometry. It measures the polarization change of incident light when it is reflected from the sensor surface in the form of an amplitude ratio and a phase difference. This change is based on the surface properties e.g. refractive index, surface thickness. The technique is mostly used in non-destructive measurement of thickness and optical constants of optical layers at the interface. Data obtained from ellipsometry, however, requires an appropriate optical model fitting and calculations especially for biological molecules (Garipcan et al., 2011; Damborsky et al., 2016). In terms of biosensing applications, there have been several reports reporting the success of ellipsometry in detection of various analytes such as proteins (Bombarová et al., 2015), carbohydrate tumor markers (Zhang et al., 2011), toxins (Nabok et al., 2011) and viruses (Qi et al., 2010). In addition, it was used for a binding profile study of influenza virus and its glycan receptor in a microarray format (Fei et al., 2015).

1.2.2 Labelled vs label-free sensing platform

The trends in biosensing platforms have moved towards label-free sensing systems. The established platforms, i.e. enzyme-linked immunosorbent assay (ELISA) or radioimmuno assay (RIA), were introduced to the analytical field over 40 years ago and are currently using as gold standards for many applications, especially biomarkers detection or protein analysis (Johnson and Krauss, 2017).

The definitions of labelled and label-free techniques are diverse. Generally, label-free techniques exploit unique molecular properties of capture molecules (ligands), target molecules or sensor constructs. For examples, QCM based methods or mass spectrometry utilize molecular weight of target molecules, whilst SPR uses the refractive index changes of reflected light through a prism sensor chip coated with metal thin film. On the contrary, labelled techniques directly tag any foreign molecules to either a ligand or a target molecule in the system in which can disturb its intrinsic properties. For instance, almost all fluorescent-based sensing platforms are labelled-techniques as fluorophores are tagged onto a detection molecules e.g. IgG. Another example is ELISA because it involves tagging a secondary antibody (Ab) with reporter system such as the enzyme horseradish peroxidase (HRP). Nonetheless, the immobilization of ligand or target molecule onto an optical substrate, especially in nanoparticle sensors, is not considered as labelling as the measurement is made from the optical change of the AuNP probe as a result of a binding event.

Though the use of labelled techniques have been established for a long time, there are many drawbacks. First, the tagging process is often complex and time-consuming, which makes sensor fabrication more complicated and expensive. Also, having foreign molecules attached to either one of the component can compromise the assay results by interfering with the true binding interaction. In addition, some larger proteins might be tagged with more than one fluor molecules leading to overestimate in quantification and so fluor to detection molecule ratio must often be determined. Conversely, not every protein can be labeled well, especially smaller proteins (Ferrigno, 2016). Consequently, label-free systems have become increasingly preferred. With the emergence of nanotechnology, more opportunities to develop label-free assay systems have arisen, especially the use of nanoparticles (NPs). NPs are good candidate materials onto which to attach bioreceptors because of their exceptional physical, chemical properties and high surface to volume ratio. The number of publications via the literature search using key words 'gold nanoparticle*' and 'sensing' via ScienceDirect has increased from around 2000 entries in 2009 to over 6000 entries in 2017 (Figure 1-3).

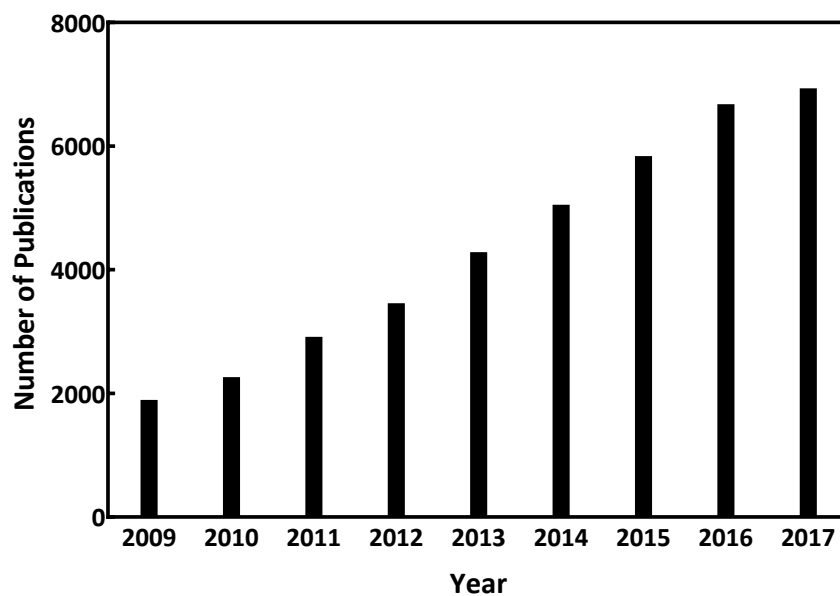


Figure 1-3 The number of publications derived via the Sciencedirect search engine, using the term “gold nanoparticle* and sensing” between the years 2009 to 2017. (Note “*” allows nanoparticle and nanoparticles to be found)

1.3 Metal nanoparticles

Metal nanoparticles, particularly gold, have been extensively studied because of their facile synthesis and modifiable surface chemistry. AuNP's unique optical property is owing to the collective oscillation of electrons in the conduction band at the surface in resonance with a specific wavelength of incident electromagnetic radiation. This phenomenon is known as surface plasmon resonance (SPR) or localised SPR (LSPR). AuNPs have their oscillation resonance frequency in the near UV region so AuNPs are seen in the form of pink colloid solution. This LSPR phenomenon is very sensitive to AuNP size, shape, ligand, interparticle distance and surrounding environment, including the dielectric constant/refractive index of the medium, and temperature. Because AuNPs have a high surface area to volume ratio, changing these parameters directly affects the LSPR and leads to colour change in the solution (Wang and Ma, 2009; Ma et al., 2010; Dreaden et al., 2012). These tuneable optical properties of AuNPs enables many possibilities in creating new optical sensing platforms. AuNPs comprise of two main parts, which are the metal core and the surface layer. Biosensing applications can be designed to modify their surface coating or alter the core properties. Besides the optical properties mentioned, AuNPs also have high surface area, conductivity and catalytic properties. Again, these properties open up many opportunities in using AuNP to improve or generate new electrical and electrochemical sensing systems (Jans and Huo, 2012; Saha et al., 2012).

1.3.1 Synthesis of gold nanoparticles

The history of AuNP synthesis can be tracked back to 1857 when Michael Faraday gave a lecture about synthesis of gold solution. He described the reduction of gold chloride compounds (e.g. sodium chloroaurate, NaAuCl_4) using phosphorus in carbon disulphide as a reducing agent (Faraday, 1857). The product solution had a beautiful ruby colour despite the yellow colour of the starting NaAuCl_4 solution. He concluded that the ruby solution obtained was the dispersion of very fine gold

particles in the solution. Unfortunately, at that time the technology was not available to prove the idea.

To date, there have been several methods of AuNP synthesis reported. The most common protocol and routinely used widespread is the citrate reduction method that uses citrate as a reducing and stabilizing agent at the same time. The process, developed by Turkevich et al., (1951), involves treating hydrogen tetrachloroaurate (HAuCl_4) with boiling citric acid. The particle size can be controlled by adjusting the proportion of gold and citrate used in the protocol (Frens, 1973). Another well-known method was established by Brust et al. (1994) and is known as the Brust and Schiffrin method. It was developed based on the fact that citrate-stabilized AuNPs still tend to form irreversible aggregates when a functionalization process is required. Brust et al. (1994) introduced a two phase system that can produce AuNP with a capping ligand, such as alkane thiols, to further stabilise the AuNP dispersion.

1.3.2 Functionalisation of AuNPs

The modifiable surface chemistry of AuNPs is another reason why they attract a lot of attention as materials of choice in sensing applications. Various types of bioreceptor such as polymers, oligonucleotides or proteins can be conjugated onto AuNP surface by a wide range of chemistries. This section describes the method of functionalisation of AuNPs and how to confirm the functionalisation process.

1.3.2.1 Functionalisation methods

The functionalisation of AuNPs can be roughly divided into two main methods; physical adsorption and covalent interactions. Figure 1-4 shows a schematic representation of functionalisation on an AuNP surface. Regarding physical interactions, these rely on non-covalent processes. Proteins can directly

adsorb onto AuNPs surface via ionic interaction between the negatively charged surface of the AuNP and positively charged side chains of proteins at the optimum pH condition (Figure 1-4A). Also, AuNP surfaces are hydrophobic and can be used for conjugation via hydrophobic-hydrophobic interaction (Figure 1-4B). Despite the physical interaction method being simple to perform, the binding interactions may not be strong enough to maintain the functionalised molecules throughout the preparation process that contains multiple washing steps or high salt concentrations in the buffer. In addition, if the AuNP surface is not saturated with the bioreceptor or not blocked properly, there is a high chance of non-specific binding to occur, and the sensitivity of the assay might be decreased. Moreover, high concentrations of bioreceptor are required in the preparation and orientation of bioreceptors on the surface is not guaranteed, which might affect their binding response as well (Wang and Ma, 2009; Jazayeri et al., 2016).

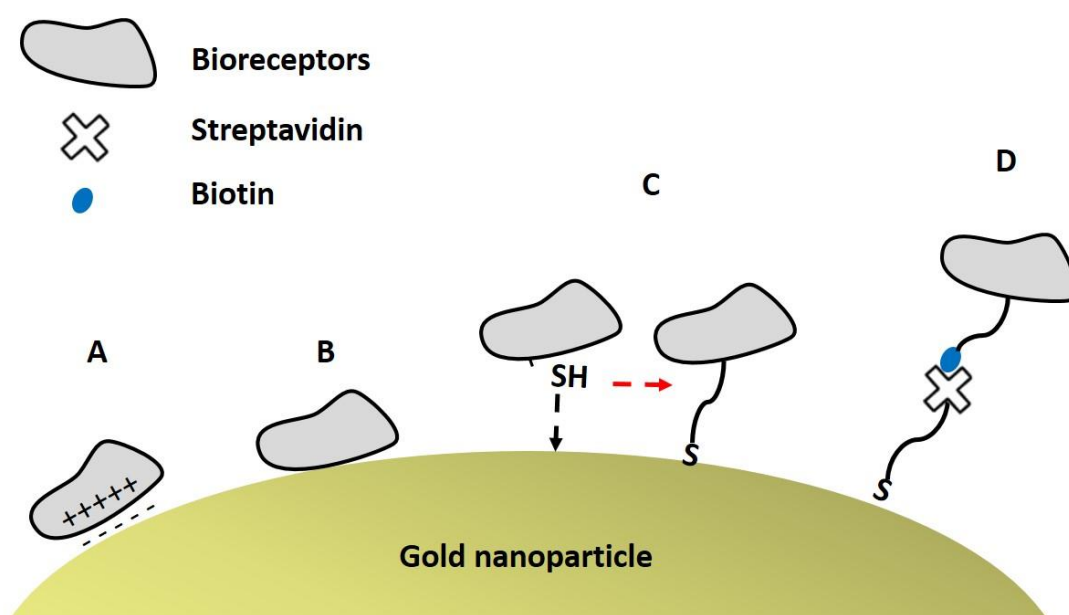


Figure 1-4 Schematic of functionalisation of AuNP probes. Representing physical (A-B) and chemical (C-D) interaction; (A), ionic interaction between negatively charged AuNP surface and positively charged side chains of protein; (B), hydrophobic interaction; (C), dative binding between free conducting electrons of sulphur and gold surface; (D), specific recognition by an adapter (streptavidin-biotin interaction).

However, there have been a number of researchers using this method for conjugation. For examples, Wang and coworkers used physical adsorption method to prepare anti-hepatitis B antigen-antibody conjugated AuNPs (Wang et al., 2012) and Huang et al., (2015) prepared anti-*Listeria monocytogenes* mAb conjugated AuNP probes by the same method (Huang et al., 2015). It was suggested in both papers that the conditions used for physical adsorption must be optimal for the conjugated molecules.

Chemical interaction, on the contrary, are more complicated and multiple steps are required, but the covalent bond formed possesses high stability to a range of conditions. In addition, using this functionalisation pathway the orientation of functionalised molecules can be controlled and this method requires less amount of the bioreceptor to be conjugated. A key aspect of chemical coupling methods lies in the use of self-assembled monolayers (SAMs) on gold via thiol interaction. SAMs show spontaneous assembly of an organic molecules onto a surface to form a well-defined arrays of molecules (Bain et al., 1989). For example, the Nuzzo group (Bain et al., 1989; Love et al., 2005) showed formation of SAMs by alkanethiol molecules on planar gold. This well-ordered molecular array can serve as tethering layer for conjugation to the AuNP surface.

Chemical coupling can be performed in several ways. For example, chemical adsorption of thiol containing proteins can occur via dative binding between free conducting electrons of sulphur atoms and the gold surface (Figure 1-4C). Normally, gold is an inert material but it can be oxidised in the presence of thiol group to form a thiolate-gold (RS-Au) bond, which is a covalent bond. The forming bond is very stable (~ 425 kJ/mol) and as strong as a gold-gold bond (Evans and Ulman, 1990; Häkkinen, 2012). Another approach to chemical coupling is using specific recognition between molecules as adapters on the surface such as protein A-antibody, streptavidin-biotin interactions (Figure 1-4D). By using these molecules as adapters not only provides strong interaction, but the molecule itself can act as a blocking agent to prevent non-specific binding to the AuNP surface too (Wang and Ma, 2009).

The high affinity interaction between biotin-avidin interaction are established and exploited for a long time (Wilchek and Bayer, 1990b). Biotin – also known as vitamin B₇ or vitamin H – is a small molecule used extensively in biomedical applications as it is versatile for linking biomolecules via avidins as crosslinkers. There are various biotinylation reagents for different types of biomolecules i.e. biotin-N-hydroxysuccinimide ester (biotin-NHS) for coupling to primary amine, biotin-hydrazide for coupling to carbohydrate or biotin-maleimide for thiol coupling. This allows many approaches for conjugating AuNPs to biomolecules. Avidin is a hetero-tetrameric glycoprotein derived from egg white. However, it has a high isoelectric point (pI), which can cause non-specific absorption of the molecule to negatively charge surfaces. As an alternative, streptavidin (derived from *Streptomyces avidinii*) and Neutravidin (deglycosylated avidin) can be used instead. The binding affinity still remains the same but their lower pIs mean they are negative at neutral pH. One molecule of avidin can theoretically bind to four molecules of biotin so it is possible to use a biotin tagged alkanethiol and use streptavidin to couple to biotin tagged bioreceptors. For example, Ahmed et al. (2013) constructed an impedance-based electrochemical immunosensors using neutravidin and biotin tagged whole antibodies for bacterial (*Streptococcus pyogenes*) detection.

The biotin-avidin interaction is non-covalent and with a very high affinity ($K_D = 10^{-15}$ M); this is comparable to covalent bonding (Hermanson, 2008). The advantage of the biotin-avidin system is its resistance to fairly harsh chemical and physical conditions (Wilchek and Bayer, 1990a). Regarding AuNP functionalisation, in work done by Gestwicki et al., (2000), streptavidin-coated 10 nm AuNPs were conjugated to the biotinylated target receptor, concanavalin A, to enhance contrast in transmission electron microscopy (TEM). Correspondingly, biotin-labeled mouse IgG antibody was added to streptavidin stabilised AuNPs for 1 h, followed by centrifugation to remove the excess biotinylated molecules. This method successfully conjugated the mouse IgG antibody to AuNPs as a sensing probe for detection of the mouse IgG (Liu and Huo, 2009).

In addition, a crosslinker can also be used to link the proteins to AuNPs. For instance, Driskell et al., (2011) prepared anti-human influenza A virus antibody conjugated AuNPs by using 3,3'-dithiobis(sulfosuccinimidyl propionate) (DTSSP) as a bifunctional linker to link the antibodies to the gold surface. DTSSP contains an amine-reactive N-hydroxysulfosuccinimide (sulfo-NHS) groups at each end with a cleavable disulphide bridge in the middle (Figure 1-5). Therefore, a thiolate monolayer on gold surface could be formed via a thiol-gold bond, whilst the sulfo-NHS end can react with a primary amine (-NH₂) on antibody molecules and form a peptide bond. The conjugation was performed in two steps, which reflected the complexity of preparation.

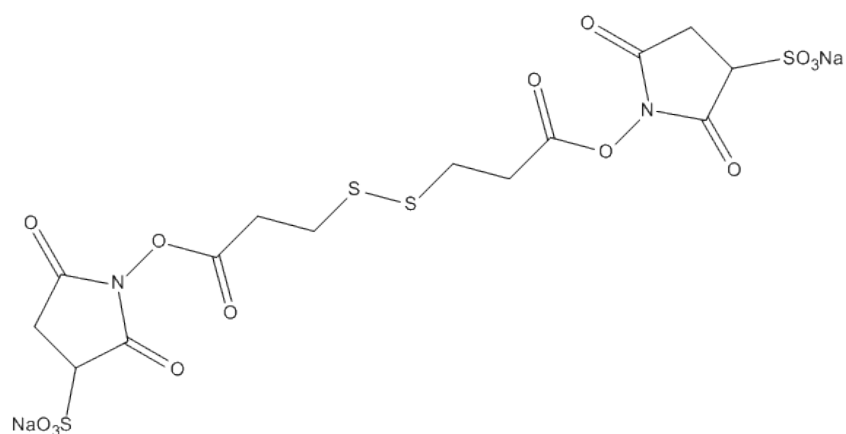


Figure 1-5 3,3'-dithiobis(sulfosuccinimidyl propionate) (DTSSP) molecule. This crosslinking reagent contains cleavable disulphide bridge and primary amine reactive.

1-ethyl-3-[3-dimethylaminopropyl] carbodiimide (EDC) is another linker used to conjugate proteins to AuNPs (Jazayeri et al., 2016). Carboxylic-AuNPs can be coupled to proteins using EDC via its carbodiimide reactive group, forming an unstable intermediate (o-acylisourea) as shown in Figure 1-6. The primary amine group of protein can then react with this intermediate and form a stable peptide bond (Hermanson, 2008). This was used by several groups. For instance, Di Pasqua et al., (2009) successfully demonstrated conjugation of anti-*Escherichia coli* O157:H7 antibody to AuNPs pendant carboxylic acid groups. Also, Aslan (2004) conjugated (+)-

biotinyl-3,6,9,-trioxaundecanediamine onto carboxyl-terminated alkanthiol adsorped AuNPs via EDC chemistry. The prepared AuNPs were used in an aggregation study in the presence of streptavidin. Other work involved dihydrolipoic acid (DHLA) capped AuNPs and $G\alpha_{i1}$ subunit (of heterotrimeric G-proteins), (Singh et al., 2013).

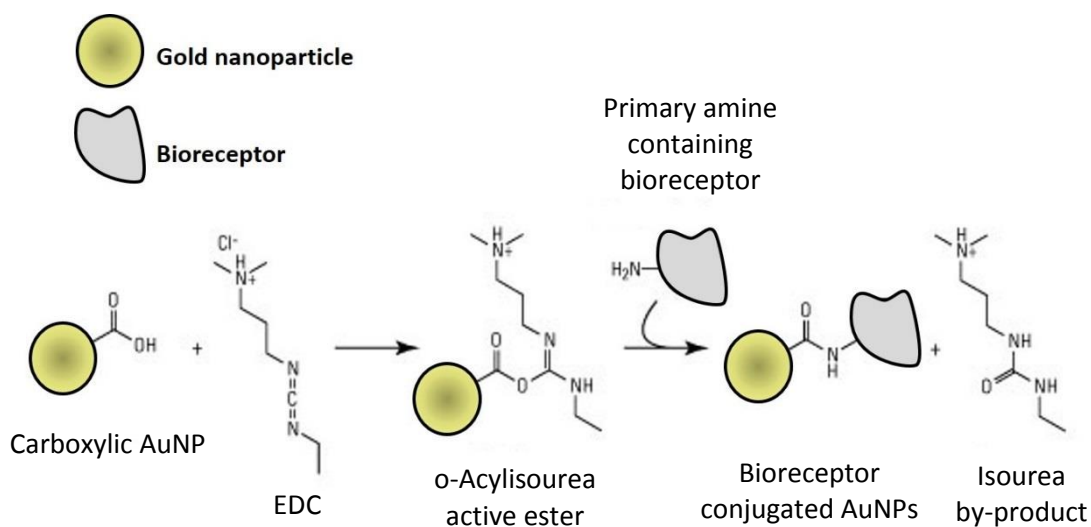


Figure 1-6 EDC crosslinking pathway. EDC can react with carboxylic group yielding an unstable intermediate. The presence of primary amine results in a stable amide bond formation.

1.3.2.2 Confirmation of the functionalisation process

There are various methods reported for confirmation of AuNP functionalisation. There includes UV-visible spectrophotometry, dynamic light scattering (DLS), differential centrifugal sedimentation (DCS), longitudinal SPR, atomic force microscopy (AFM) and TEM. Among those methods, UV-spectrophotometry is one of the most common techniques as it is a fast, simple and instruments are found in most laboratories (Kumar et al., 2008; Zhang et al., 2015; D'Agata et al., 2017). Upon conjugation, the absorbance spectrum of the conjugated

AuNP will shift slightly to a longer wavelength because of the local refractive index shift resulting in changing LSPR properties of the particles (Pollitt et al., 2015; Filbrun and Driskell, 2016).

In addition to UV-spectrophotometry, there were several studies using DLS as a tool confirming the conjugation of antibodies onto AuNPs. Jans et al., (2009) demonstrated the use of DLS in detection of bioconjugation by using protein A adsorption onto AuNPs as an example. The hydrodynamic diameter (D_H) was measured and plotted against the concentration of protein A added to the AuNPs. A linear relationship was observed until the full coverage of AuNPs was reached and their size became stable. Although proteins have an intrinsic weak light scattering intensity, they cannot be detected by DLS unless a high concentration is used. However, when they fully adsorb onto the AuNP surface, the diameter of the AuNPs is expected to increase at least by twice the diameter of the protein molecule. Accordingly, Bell et al., (2013) demonstrated that DLS, nanoparticle tracking analysis (NTA) and DCS could be used to monitor IgG protein adsorption to AuNPs and gave comparable results to UV-visible spectrophotometry.

The use of DLS and NTA for conjugation confirmation is exemplified in the work undertaken by James and Driskell (2013). They conducted a systemic experiment to investigate the use of NTA and DLS for monitoring AuNP conjugation. They found out that both DLS and NTA could provide information about the optimal amount of protein required for full coverage of AuNPs along with the optimal conditions suitable for the conjugation process. Moreover, Huang et al., (2015) investigated the amount of anti-*Listeria monocytogenes* monoclonal antibodies onto AuNPs by using DLS. They found out that when different concentrations of the antibodies were added, the mean D_H linearly increased from 102 ± 2.5 nm to 112.7 ± 2.0 nm and levelled off when 10 $\mu\text{g/ml}$ of the antibodies were reached. Additionally, DLS was also reported as a tool for surface interaction studies between DNA and AuNPs (Wang et al., 2014).

All of the methods indicated above, nevertheless, cannot directly quantify the number of proteins attach per AuNP and only give a relative surface coverage

estimation. Previously, the quantitation of proteins bound on a AuNP surface was done by quantifying the excess proteins (i.e. not conjugated) recovered. This indirect method usually overestimates the amount of proteins bound to AuNPs, since some proteins might stick to the container used and is counted as conjugated material. Until recently, Filbrun and Driskell (2016) proposed a fluorescence-based method for quantification of immobilised antibodies on AuNPs. The method is based on the dissolution of AuNPs by potassium iodide (KI)/iodine (I_2) solution. Here, gold can be dissolved by the oxidant generated with the iodine-iodide system. The oxidant triiodide ion (I_3^-) could be produced via the reaction of I_2 and I^- (Green, 2014). Once the AuNPs were fully dissolved, atomic absorption spectroscopy (AAS) was used to quantify the gold. At the same time, a fluorescent dye, called NanoOrange, was used to quantify antibodies released after the dissolution of the AuNPs. It should be noted that the protein solution was desalted to get rid of interferents. In comparison with indirect quantitation using excess antibodies in the supernatant during preparation process, this direct method gave significantly difference results but corresponded to the NTA size analysis of surface coverage of AuNPs.

1.3.3 Gold nanoparticles as a biosensing system

Initially, AuNPs were mostly used in the transduction process by acting as optical labels, electrochemical markers or signal amplifiers (Pissuwan et al., 2010; Kaittanis et al., 2010). However, in the past decades the trend has shifted to a biosensing assays using AuNPs as a platform not just a signal amplifier (Huang, 2007). Here are some examples of using AuNPs for biosensing.

1.3.3.1 AuNPs in electrical and electrochemical sensing

AuNPs have found applications in electrical and electrochemical sensing because of their exceptional conductivity and catalytic properties. Also, AuNPs have a high surface area to volume ratio, which makes them even more reactive and applicable for sensing applications (Saha et al., 2012). The development of an

electronic nose sensor is an example worth mentioning. Peng et al., (2010) successfully produced a nanosensor array for detection of volatile organic compounds (VOCs), which differentiates between healthy and cancer patients. The background of this valuable tool lies in various organic molecules used as capping monolayers on the AuNPs. The functionalised AuNPs were then dispersed on top of gold electrodes by drop casting methods. The data acquired from this new tool were comparable with the gold standard, gas chromatography-mass spectrometry (GC-MS) for VOCs.

Another applications of AuNPs in electrochemical sensing is their use as 'electron wires'. AuNPs enable electron transfer between redox proteins and the electrode surface, since most oxidoreductases used in electrochemical sensors are surrounded by protein in which becomes an insulating shells. As a result, the electrons cannot transfer to the electrode effectively, leading to reduced sensor performances (Li et al., 2010). Brown et al., (1996) was the first to demonstrate the use of AuNPs as electron wires. The untreated colloidal AuNPs were used with SnO₂ electrodes to detect horse heart cytochrome c (Cyt c). Direct electron transfer was proved to occur at uncoated submonolayers of colloidal AuNPs on SnO₂ electrode when Cyt c electrostatically-bound to the AuNPs. They suggested that AuNPs could be used as mediators to protect direct contact between the protein and metal surface, which can lead to structural and functional changes. However, it was found out that aggregated AuNPs were not effective in electron transfer.

1.3.3.2 AuNPs in QCM-based sensing

QCM is a technique that measures binding events through a change of frequency that corresponds to a change in the mass of an oscillating crystal. The role of AuNPs in QCM-based sensing is mostly as a "mass enhancer" to intensify the frequency changes. In a study conducted by Kim et al., (2007), it was shown that AuNPs were effective as signal enhancers in a QCM biosensor. They used N-[6-(biotinamido)hexyl]-3'-(2'-pyridyldithio)propionamide or biotin-HPDP modified

AuNPs on a gold coated QCM electrode instead of using biotinylated bovine serum albumin (BSA) as a control to detect streptavidin. The detection limit was 50 ng/ml.

There have been several reports of AuNP enhanced QCM-based sensing platforms. For example, Chen et al., (2011) described using oligonucleotide functionalised-AuNP to amplify a QCM-D signal in the detection of mercury(II) ions (Hg^{2+}). The sensor was able to detect the presence of Hg^{2+} in a drinking water source with detection limit of around 4 nM. Similarly, DNA-conjugated AuNPs were used to detect *Bacillus anthracis*, the anthrax causative agent (Hao et al., 2011). DNA complementary to the target DNA was immobilised on AuNPs and used as a signal amplifier for the QCM biosensor. Chu et al., (2012) successfully developed a sensor for gliadin, the protein responsible for causing food allergies, e.g. in coeliac disease, in food products by covering a QCM electrode with 25 nm AuNPs before immobilising anti-gliadin antibodies. With the high surface area of AuNPs, more antibodies could be conjugated and the sensitivity of the technique was improved. They reported that a 48% frequency shift could be observed with only 2 ppm of gliadin presented in commercial food products.

1.3.3.3 AuNPs in optical sensing

1.3.3.3.1 Fluorescence-based sensing

AuNPs have a broad energy bandwidth and high molar extinction coefficient so they are an excellent materials for fluorescence-resonance energy transfer (FRET)-based assays. AuNPs can act as fluorescence quenchers; for example, a mercury(II) (Hg^{2+}) sensing platform was successfully developed using rhodamine B (RB) fluorophore conjugated to AuNPs. RB exhibited a very weak fluorescent signal when adsorbed on AuNPs. With Hg^{2+} present, RB was freed from the surface and could re-establish its fluorescence. The assay took only 10 min to perform and the limit of detection (LOD) was 2 ppb from a pond water sample (Huang and Chang, 2006). Another interesting example of AuNPs in a fluorescence based assay is the chemical sensors developed by You et al., (2007). The main principle was to create a

fluorophore displacement protein sensor array. Six different non-covalent fluorescent polymer conjugates AuNPs were used. Before proteins were present, fluorescent property of the polymers was quenched by the AuNPs. By adding the proteins into the system, displacement of proteins triggered the fluorescent signal. They tested 52 unknown protein samples with seven different proteins using the sensor and the method showed an accuracy of 94.2%.

1.3.3.3.2 Surface Enhanced Raman Scattering (SERS)-based sensing

Raman spectroscopy uses an inelastic scattering process, known as Raman scattering or the Raman effect. It is a process where an incident photon interacts with a molecule and forces it into a higher vibrational state. Then, the photon is emitted upon relaxation to a lower vibrational state producing Raman scattered light. A spectrophotometer can separate the scattered light by wavelength and the results are presented as a graph between the Raman intensity vs wave-number giving a Raman shift, which is unique for each individual molecule. Therefore, these patterns can be used as a fingerprint to detect a target of interest (Saha et al., 2012). However, the use of Raman spectroscopy is limited because of its low scattered light intensity. By using plasmonic NPs or metal nanoparticles like AuNPs, the signal can be improved by up to 10^{11} order of magnitudes owing to their localised surface plasmons (LSRs). This method is called surface-enhanced Raman spectroscopy (SERS). When the frequencies of NPs' LSP and Raman scattered light are in resonance, the increase in Raman intensity is obtained. This is via the extra energy put into the transition via coupling the LSPs to the change in vibrational states. Sun et al., (2007) tagged both ssDNA and nonfluorescent Raman tags (RTags) onto AuNPs forming detection probes, which successfully detected the target DNA. Also, it proved to be effective after the probes were kept for three months.

1.3.3.3.3 Detection based on the surface chemistry of AuNPs

The DNA bio-bar-code is a well-known method that exemplifies the exploitation of the AuNP high surface area. Nam et al., (2003) discovered an ultrasensitive method for protein detection using AuNPs. Prostate-specific antigen (PSA) was used as model analyte to demonstrate the method. Two types of particles were used; anti-PSA monoclonal antibody conjugated magnetic microparticles (MMPs) and DNA encoded PSA-conjugated AuNPs together with anti-PSA polyclonal antibody (Figure 1-7A). Figure 1-7B shows the bio-barcode assay method.

First, MMPs was used to capture free PSA from solution and the unbound PSA was removed by using a magnetic separator. Then, the modified AuNPs were added to form a sandwich format. The AuNPs reacted with the bound PSA on MMPs and provided DNA strands for signal amplification. Following this, dehybridization was performed to release oligonucleotides off the AuNP surface, quantitation was effected based on the amplified oligonucleotides. Because of the high surface area of AuNPs, the detection limit for PSA was in the aM range. Later, this method was also modified and used for DNA detection. The performance of the assay was comparable with conventional PCR-based techniques (Nam et al., 2004).

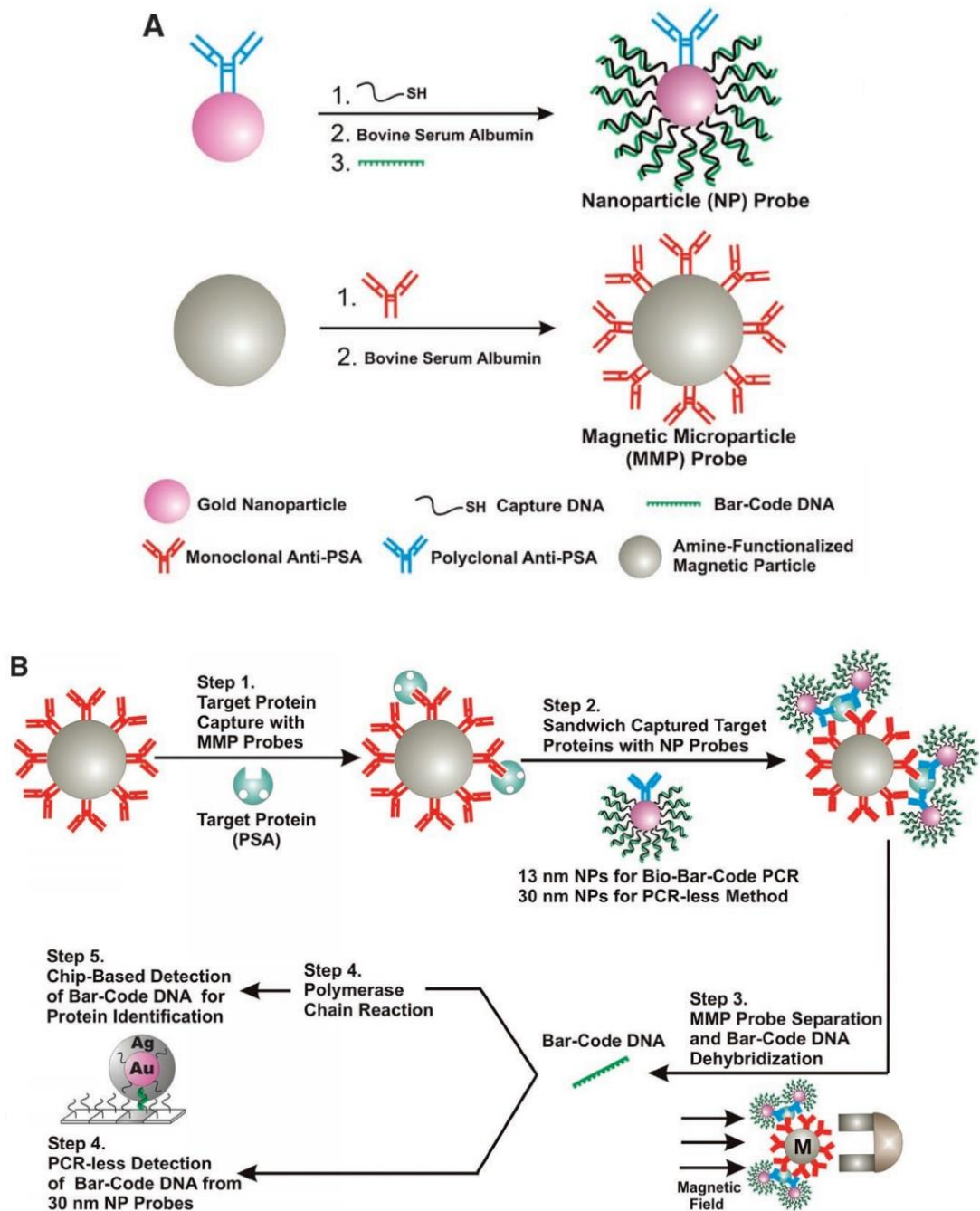


Figure 1-7 The bio-bar-code assay method. (A), two types of probes used in the assay: (i), anti-PSA monoclonal antibody conjugated magnetic microparticles (MMPs); and (ii), DNA encoded PSA- and anti-PSA polyclonal antibody-conjugated AuNPs. (B), PSA detection via bio-bar-code assay. First, free PSA was captured by MMPs then the complexes were sandwiched by DNA/pAb modified AuNPs. Magnetic separation was applied, following with dehybridization to release the bar-code DNA, which later used for quantitation. This figure was taken from Nam et al. (2003).

1.3.3.3.4 Detection based on LSPR

With respect to LSPR, as stated earlier, AuNPs can strongly absorb and scatter light at their own SPR wavelength region and this property is dependent on NP size and shape. As a wide range of sizes and different shapes of AuNPs can be easily prepared, this makes the SPR wavelength tailorable from the visible region to near IR region. Not only the size and shape, but also modification of their surface chemistry or changing the inter-particle interactions can affect the SPR band of AuNPs. Mainly, this SPR shift of AuNPs can be detected either by measuring light absorption or light scattering (Jans and Huo, 2012).

1.3.3.3.4.1 Detection based on light absorption

For light absorption measurement, LSPR of AuNPs is used. When the analyte of interest binds or comes close to the surface of AuNPs, the LSPR spectrum will shift to a longer wavelength (red-shift), which can be detected by UV-visible spectrophotometry. Also, this property enables a colorimetric assay platform to be established. The disadvantages of this type of detection are its relatively low sensitivity and limitation to colorless samples only. Here are some examples of the AuNPs colorimetric sensing platform.

A well-known application of AuNPs in optical sensing is the home-use pregnancy strip. Monoclonal anti- α -subunit of human chorionic gonadotropin (hCG) antibodies were conjugated onto AuNPs and used as probes of detection – hCG is a glycoprotein hormone found in pregnant woman. The strip is made mainly with nitrocellulose membrane to facilitate the transport of the urine sample to different components by capillary action. Figure 1-8 shows a schematic of main components of a pregnancy strip. At one end of the strip, there is a layer of sample addition pad and the probes embedded pad on top of the membrane. Another end contains an absorbent pad. Right before the absorbent pad, there are two lines; test and control line. The test line has immobilised antibodies against β -subunit of hCG, whereas the control line has immobilised antibodies against monoclonal anti- α -subunit of hCG

antibodies. Therefore, when urine sample is applied and transported pass the two lines, if there is hCG presented both lines will turn pink. But if there is no hCG, only the control line will produce colour (Marks, 2007; Lee, 2008).

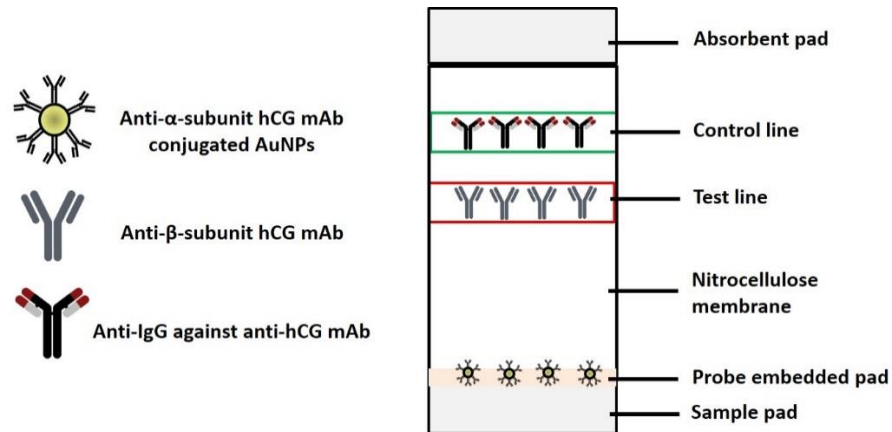


Figure 1-8 Schematic of main components of a lateral flow pregnancy strip. The strip is made of nitrocellulose membrane. At one end, it contains a sample pad with anti- α -subunit hCG mAb conjugated AuNPs embedded pad on top. There are test and control lines near the other end of the strip comprising of anti- β -subunit hCG mAb and anti-IgG against anti-hCG mAb, respectively. When urine sample is applied to the sample pad and transported to the absorbent pad by capillary action, if hCG is present, test and control lines will appear red but without hCG only the control line will turn red.

Mirkin et al., (1996) reported the use of this sensing technique for DNA detection. Two non-complementary DNAs were immobilised on AuNPs and acted as the probes of detection. The target DNA could bind to both DNAs and when added to the system, caused crosslinking between the particles. Quantitation could be performed by measuring the change in absorbance. Detection limits in the fM range could be obtained. In addition, with slight adaptation based on this technique, Aslan et al., (2004) published a paper describing glucose detection using competitive assay format. High molecular weight dextran-coated AuNPs were used as probes of detection. Aggregation of AuNPs was caused by adding concanavalin A (con A). By adding glucose to the system, it competed with the dextran-AuNPs for binding to con A, leading to deaggregation of AuNPs. The SPR shifted back to its near-red wavelength.

In addition to proteins, DNAs or small biomolecules, this technique has been applied to detection of metal ions as well. Kim et al., (2001) developed a simple colorimetric technique for lead (Pb^{2+}), cadmium (Cd^{2+}) and mercury (Hg^{2+}) trace detection in aqueous solution. 11-mercaptoundecanoic acid (MUA) were functionalised onto AuNPs, and in the presence of these ions, ion-templated chelation occurred and led to aggregation of AuNPs, which could be observed by the naked eye. Similarly, Si et al., (2007) reported the detection of Hg^{2+} using carboxylated peptide-functionalized AuNPs as probes. In the presence of Hg^{2+} , the probes aggregated and SPR of AuNPs shifted to around 670 nm, which again could be observed by the naked eye.

1.3.3.3.4.2 Detection based on light scattering

In terms of detection based on light scattering properties of AuNPs, it can provide better sensitivity than light absorption based. According to the light scattering theory, the intensity of scattered light increases with increased particle size and the light scattering intensity is proportional to the 6th power of the radius of the particle for Rayleigh scattering (Yguerabide and Yguerabide, 1998). AuNPs are known to scatter light stronger than fluorescent molecules and even stronger as compared to polymer beads. Principally, this detection can be divided into two different categories;

(i) Scattered light intensity/wavelength change-based methods

For this category, similarly to the absorption based techniques, the chemical/biological binding event can be detected directly by measuring the intensity of scattered light or wavelength change. Mainly, the instrument involved is a spectrophotometer or sometimes the change can be observed by the naked eye. Complete quantification can be done by using the relationship of observed scattered light and concentration of analyte (Jans and Huo, 2012). Storhoff et al., (2004)

successfully developed a 'spot-and-read' technique for identifying nucleic acid sequences. Around 33 zmol of methicillin-resistant *Staphylococcus aureus* (MRSA) DNA in the 1- μ l volume analysed on a glass slide could be detected without any signal amplification. Two oligonucleotide-conjugated AuNPs were used as probes and after the hybridization of the DNAs, the NP probes crosslinked and led to a SPR shift. The mixed samples were spotted onto a glass slide and illuminated with white light. The scattered yellow to orange light was observed if the complexes were formed due to a plasmon band red-shift.

Another experiment by Xiang et al., (2009) developed a method investigating the interaction between glycogen and biomacromolecules. With the presence of glycogen and citrate-capped AuNPs, the NPs formed clusters. When a biomacromolecule that could interact with glycogen was added, the aggregation of the NPs was reduced. As a result, the light scattering intensity was also reduced. Spectrofluorimeter was used in this measurement. Correspondingly, Zhang et al., (2010) reported the detection of adenosine in human urine using modified AuNP with adenosine structure-switching aptamers. The LOD was 1.8 nM, which was comparable to high-performance liquid chromatography (HPLC).

(ii) Size-shift based method

With this type of optical sensing, the chemical/biological binding event is detected by the change in size of AuNP probes. Dynamic light scattering (DLS) is the main instrument used for this method (Jans and Huo, 2012). The principle of DLS and the assay will be discussed further in the following section.

1.4 AuNP size-shift based method

DLS has become a common technique used routinely for determination of particle size and size distribution since it was first marketed in the 1970s. The measurement takes a short duration to perform and convenient to use. Also, it is a non-destructive measurement and samples in the submicron range can be measured; the amount of sample required is minimal (Hassan et al., 2015; Zheng, Bott, et al., 2016). In order to understand the assay better, the principles of DLS and the assay are described in the following sections, together with applications of the technique in various fields.

1.4.1 Dynamic light scattering

Scattering techniques for particle sizing rely on two characteristics of colloidal suspensions, which is the scattering effect of colloids known as the Tyndall effect and Brownian motion (Hassan et al., 2015). There are two types of scattering technique for sizing particle. The first one is static light scattering (SLS), which measures time averaged scattering intensity at different scattering angles. This type of measurement can only be done with particles of size at least greater than $\lambda/20$ so the range of detection is around 50 nm – 2000 μm (Hassan et al., 2015; Brar and Verma, 2011). Another type called dynamic light scattering (DLS) can be used with much smaller particles. DLS, which is sometimes known as photon correlation spectroscopy (PCS), measures the size of the particles related to Brownian motion (Brar and Verma, 2011; Hassan et al., 2015; Zheng, Bott, et al., 2016). Depending on the diffusion coefficient of these particles undergoing Brownian motion, as larger particles move slower than small particles, then scattering intensities fluctuate. So what exactly DLS measures is the fluctuation of scattering light intensity based upon time, triggered by particle movement. A schematic of a DLS instrument is shown in Figure 1-9.

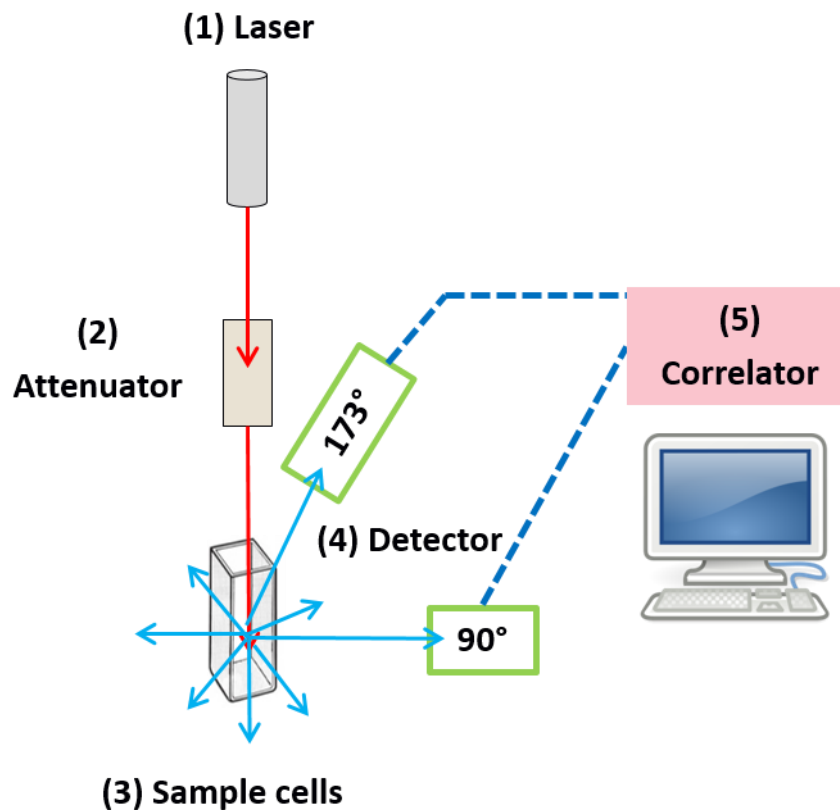


Figure 1-9 Schematic of a DLS instrument. The DLS main components are (1), laser light source; (2), attenuator to adjust the power of laser beam passed to the sample; (3), sample holder for a cuvette; (4), detector used to detect the scattered light from the sample (both 90° and 173° angle of detection can be used) and (5), a correlator.

There are five main components of DLS: (1) laser light source; (2) attenuator to adjust the power of laser beam passed to the sample; (3) sample holder for a cuvette; (4) detector used to detect the scattered light from the sample. It can be placed in two different positions, 90° and 173° angle of detection, depending on the model; and (5) correlator, which is a signal comparator. It calculates the fluctuation rate of the scattering intensity detected by the detector. It compares the intensity at sequential time intervals. More details will be discussed in the following paragraph. This information is passed onto the software to analyse and report as a particle size later. There are several companies selling DLS instruments, Malvern Instruments is the company dominating the DLS machine market in the UK. While, Beckman Coulter Inc., Microtrac, Micromeritics Instrument Corporation and Agilent Technologies are

major companies in the US market as well as Horiba, Ltd. – a global worldwide company from Japan – who dominates the Asian market.

The most important component that allows the principle of DLS is called the correlator. It is a signal comparator that compares the degree of similarity between two different signals, or one signal with itself at varying time intervals. If the same signal is compared at a small difference in time interval, there will be a strong relationship between the two signals recorded. However, if the signal is compared at a much later time, we can predict that the two signals have little or no correlation at all. Based on this relationship in DLS measurements, a correlation compares scattering intensity signals detected from colloidal suspensions. The correlation is reported as a correlation coefficient. Perfect correlation is indicated as 1 whereas no correlation is represented with zero. A correlation graph (correlogram) is plotted between the correlation coefficient and time (Figure 1-10). With small particles in the sample, the decay of correlation function occurs more rapidly (Figure 1-10A) compared with large particles (Figure 1-10B). The information received from DLS is mainly derived from the correlogram plot, for example, the average size of sample is from the time at which the correlation starts to decay. The shape of the curve also gives the detail about sample polydispersity. The broader the line, the more polydispersity the sample is and *vice versa*.

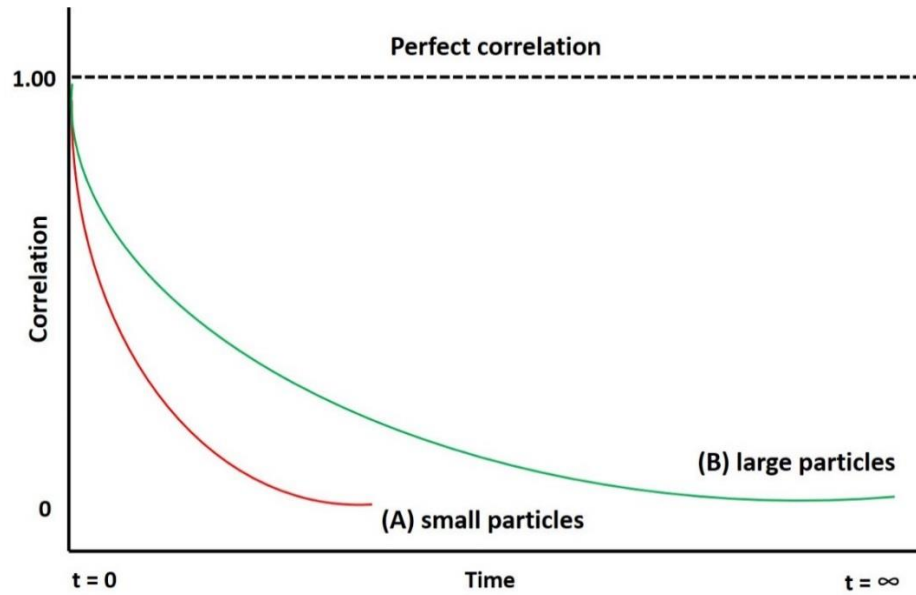


Figure 1-10 Showing correlograms obtained from different sizes of particles. Decay of correlation function of small particles, (A); and large particles, (B).

In terms of analysis, a correlation function ($G(\tau)$) is analysed to gain particle size information. For a monodisperse particle sample, $G(\tau)$ decays exponentially with the delay time τ and is given as

$$G(\tau) = A(1 + B \cdot e^{-2Dq^2\tau}) \quad (1-1)$$

where A and B are baseline and intercept of the correlation function, respectively, D is the translational diffusion coefficient of the particles, and q is the magnitude of the scattering vector, which can be calculated from the equation 1-2. Here, n is a refractive index of the dispersant, while λ is a wavelength of the laser used and θ is the light scattering angle.

$$q = \left(\frac{4\pi n}{\lambda}\right) \sin\left(\frac{\theta}{2}\right) \quad (1-2)$$

Whereas, for a polydisperse particle sample, sum of all exponential decays in the correlation function will be used instead. By using the translational diffusion coefficient (D) derived from these equations, the average particle size can be calculated via the Stokes-Einstein equation shown below.

$$D_H = \frac{kT}{6\pi\eta D} \quad (1-3)$$

where k is the Boltzmann's constant, T is an absolute temperature and η is solvent viscosity. The diameter obtained from DLS is called the hydrodynamic diameter (D_H) because it is based on how the particles movement in fluid form. It is reported based on the diameter of a sphere that has the same D (Hassan et al., 2015).

Regarding practical data analysis, there are several methods to extract information from the raw data obtained from DLS. The most common technique used is called the method of cumulants. It is the method recommended in the international standard ISO 224112:2017. This method obtains the average size of the particles by fitting a single exponential to the correlation function (Hassan et al., 2015). Other methods reported for DLS analysis are non-negative least squares (NNLS) (Morrison et al., 1985), CONTIN (Ju et al., 1992) and exponential sampling (Bertero and Pike, 1991).

Normally, DLS reports both the average hydrodynamic diameter and the size distribution of the sample. The size distribution graph can be presented in three ways; intensity-, volume- or number-weighted distributions. The first one is obtained by plotting the size on the X-axis and relative intensity of the scattered light on the Y-axis. This is the best representative of sample population data as it is generated from the measured data directly. The volume-weighted distribution is converted from intensity distribution via Mie theory, which is later used in calculating number-weighted distributions.

One of the shortcomings of DLS is that the average hydrodynamic diameter or mean D_H of NP is reported based on the scattered light intensity of the particle.

Therefore, particles with a larger size scatter to a larger extent. Accordingly, with polydispersed sample, the average size will be susceptible to the large sized particles within the population. However, DLS is still preferable for designing an NP aggregation assay because it means that only a small change in size can be detected by DLS by observing the average size. In other words, if only a small portion of aggregates form in the system, DLS is still able to report that. This was verified by Zheng et al. (2016). In the experiment, citrate-stabilised AuNPs with diameter of 20 and 100 nm were used to represent dispersed and aggregated populations respectively. It was reported that even with only 0.001% of 100 nm AuNPs presence in the system, the average size of well-dispersed 20 nm AuNPs increased from 23 to 27 nm.

In addition, there are several factors affecting the efficacy of DLS in terms of particle sizing. Temperature is a very important factor as it directly affects the viscosity of the samples, which can cause a non-random movement and eventually lead to misinterpretation of the NP size (Brar and Verma, 2011). Another factor needed to be considered is the saturation of detector, which is a systemic error issue. Too strongly scattered light can saturate the detector and leads to miscounting of photons by the detector. It is strongly recommended by the Malvern's user manual that the photon count rate should be in a few hundred kilo counts per second (kcps). This can be easily prevented by attenuating the laser power in the system. Besides systemic errors that can be prevented, multiple scattering processes give another error that might occur and lead to a dramatic error in particle sizing by DLS. Multiple scattering occurs when photon of scattered light is re-scattered again by another particles before reaching the detector. This re-scattered photon will affect the intensity fluctuation compared by the correlator and lead to miscalculation of particle size, which normally undervalues the actual size of the particles.

The photon mean free path (MFP) is one of the factors regulating the extent of multiple scattering. The MFP basically represents the average distance travelled by scattered photons from the scattering volume before re-scattering occurs. The term scattering volume refers to the actual volume within the sample from which

photons are directly detected by the photomultiplier. To avoid multiple scattering, back scattering angle detection can be introduced. As shown in Figure 1-9, the detector can be arranged at two different angles. At 173° , the backscattering angle, the scattered light path length is shorter, or in other words, scattered photons have to travel further to reach the detector when it is placed at 90° and the further the photon travels the more chances are that it will be re-scattered. Nevertheless, it was reported that back scattering angle detection did not greatly reduce multiple scattering effects better than 90° detection (Zheng et al., 2016). To this end, it was explained that there were other factors affecting this process such as concentration of NPs and laser power.

In the same paper by Zheng et al., (2016), the NP concentration was found to be another factor associated with multiple scattering. The concentration analysis was performed using 100 nm citrate-capped AuNPs. The results indicated that a linear relationship between scattering light intensity and concentration was observed until a certain concentration (the peak point). Above this peak point, the intensity dropped with further increase in NP concentration. It was explained by Zheng et al., (2016) that this might be due to the reduction in laser power by absorption/scattering effects of AuNPs before and after the scattering volume. Subsequently, the intensity of scattered light at the detector was reduced. In order to observe multiple scattering, the graph between mean D_H and NP concentrations was plotted. The concentration where the average size started to drop indicated the possible beginning of multiple scattering. It was strongly suggested that the best concentration of NP used should be the one that give strongest scattering light intensity but shows no multiple scattering.

1.4.2 Principle of nanoparticle-coupled dynamic light scattering assay

In terms of chemical and biological sensing, DLS was first proposed as a tool in an aggregation assay in 1975. Cohen and Benedek (1975) used polymer beads coated with BSA to detect anti-BSA Ab in the serum. When the antibodies bound to BSA, agglutination occurred and could be detected by DLS. The DLS could report the change in the average size of the polymer beads and this could be used to quantify the amount of antibody presented in the solution. However, this technique was abandoned because it could not be used as a practical application. One of the main obstacles at that time was the low scattering intensity of polymer beads. Therefore, background scattering, e.g. from proteins in blood, interfered with the actual scattering from the sample and quantification was not possible. Nevertheless, the arrival of AuNPs led to a renewed interest in using DLS for agglutination or aggregation assays, as AuNPs have a thousand time stronger scattering as compared with similar size polymer beads. This distinctive property is due to the SPR signal mentioned earlier.

For any particle aggregation assay, it is very important to understand control of the NP aggregation process, because aggregation should only occur in the presence of analytes and random cluster formation should be avoided. AuNPs are in a colloidal dispersion; thus stabilization relies on the balance between interparticle attractive (e.g. van der Waal force) and repulsive forces, known as colloidal stabilization effects. There are three stabilization mechanisms (Figure 1-11), which are electrostatic, steric and electrosteric stabilization. Electrostatic stabilization utilizes the charge of molecules on the NP surface to maintain the repulsive forces, whilst, steric stabilization uses grafted macromolecules (i.e. proteins, polymers) on the surfaces to act as barriers in order to prevent the particles moving closer together when van der Waals attractive forces become a dominant factor. For electrosteric stabilization, the first two mechanisms are combined by using macromolecules with charges, like DNA (negatively charged polymers) (Dunn, 1986; Zhao et al., 2008).

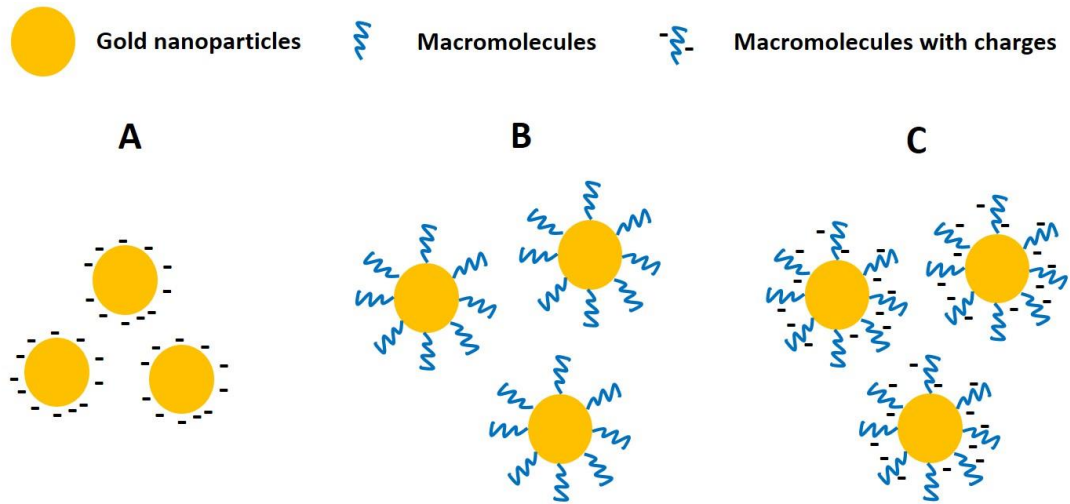


Figure 1-11 The stabilization mechanisms of colloidal AuNP dispersion. There are three different mechanisms: (A), electrostatic stabilization; (B), steric stabilization using macromolecules; (C), electrosteric stabilization.

In general, to control the aggregation of NPs, there are two main approaches, which are non-crosslinking aggregation or interparticle crosslinking aggregation mechanisms. The first can be caused without the formation of interparticle bond but by removal of colloidal stabilization effects. For examples, the loss of charge surfaces (Figure 1-12A) or removal of polymer molecules on the surfaces (Figure 1-12B).

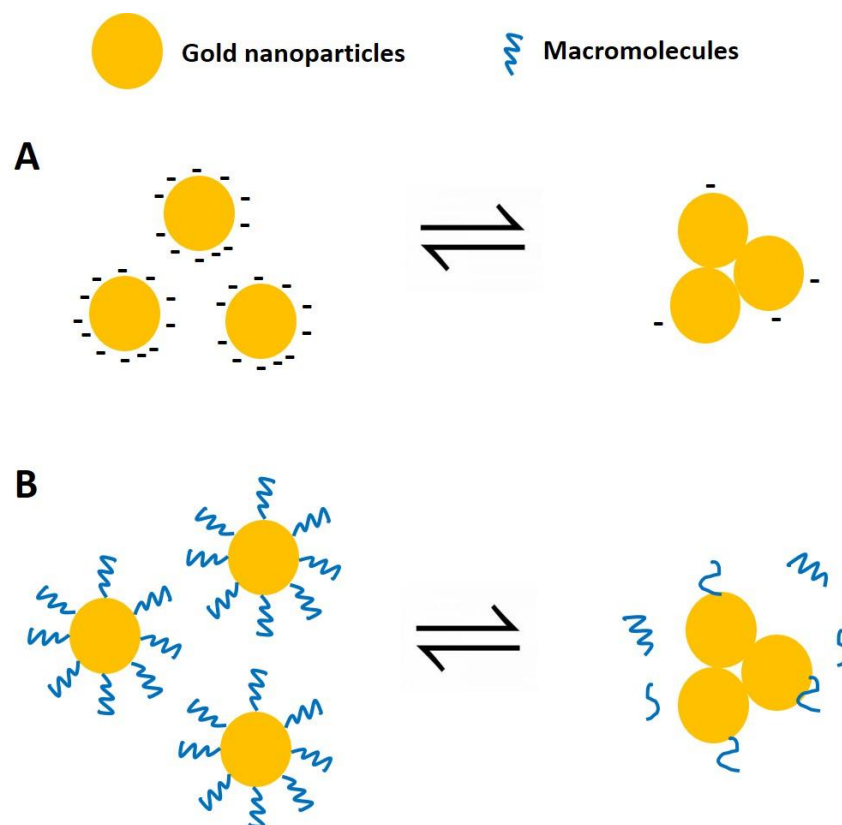


Figure 1-12 Schematic of non-crosslinking aggregation mechanisms; A), via loss of charge surfaces; B), via removal of polymers on nanoparticle surfaces.

In contrast, the latter mechanism focuses on the formation of interparticle bonding to crosslink the particles, which leads to complex formation and aggregation (Zhao et al., 2008). There are several ways to bring about interparticle crosslinking (Figure 1-13). For example, via direct interaction between different modified receptors on NP surfaces such as DNA complementary base pairs, or via using other molecules to crosslink the nanoparticles together, known as crosslinker molecules. Regarding this mechanism, multiple binding sites for crosslinker molecules are required and the binding and the aggregation rate depends on crosslinking reaction, which is often slower than with a non-crosslinking mechanism. Still, it is a common method selected by researchers in designing aggregation assays (Sato et al., 2003). Various aggregation assay platforms can be designed based on controlling NP aggregation, either with or without crosslinking molecules. Principally, the platforms can be divided into two categories; direct and indirect assays. Regarding the direct

assay, it is more straightforward than the latter as it measures the shift to a larger size NP. In contrast, the indirect assay's biorecognition process is based on the removal of the aggregation and measures the shift to a smaller size of NP.

In the case of interparticle crosslinking aggregation mechanism, there are several platforms designed. Two different modified NPs can be used for cluster forming (Figure 1-13A, Pathway A). One of the NP probes are modified with bioreceptors, whereas another NPs are modified with complementary molecules, for examples, two complementary DNAs that can hybrid the target analyte at the same time. Another platform is using multiple binding sites crosslinking molecules like polyclonal antibody (pAb) (Liu and Huo, 2009) or multiple NP modified with different binding molecules to the same target (Figure 1-13B, Pathway C) (Dai et al., 2008; Liu et al., 2008). This is the most common methods used in numerous studies. In addition, the target analyte with multi-binding sites such as multimeric molecules or large molecule with high number of antigen epitopes can be detected with one type of bioreceptor-conjugated NPs as shown in Figure 1-13C, Pathway E (Driskell et al., 2011; Nietzold and Lisdat, 2012; Huang et al., 2015). It should be noted that the aggregation process of NPs is reversible in every platform. This mean that indirect assay can be designed. By removing the crosslinking molecules or breaking the binding interaction, it is possible to quantify the analyte as well (Figure 1-13A-C, Pathway B, D and F). This type of assay favours the quantitation of small molecules that have restrict area for crosslinking molecule to bind. By tagging the small analytes on NP surface and couples with its specific bioreceptors-modified NPs, the aggregate can be formed. With the presence of the free analytes, there will be a competitive binding to the receptor NPs in which leads to deaggregation and smaller size observed. That is why sometimes indirect assay is called competitive assay.

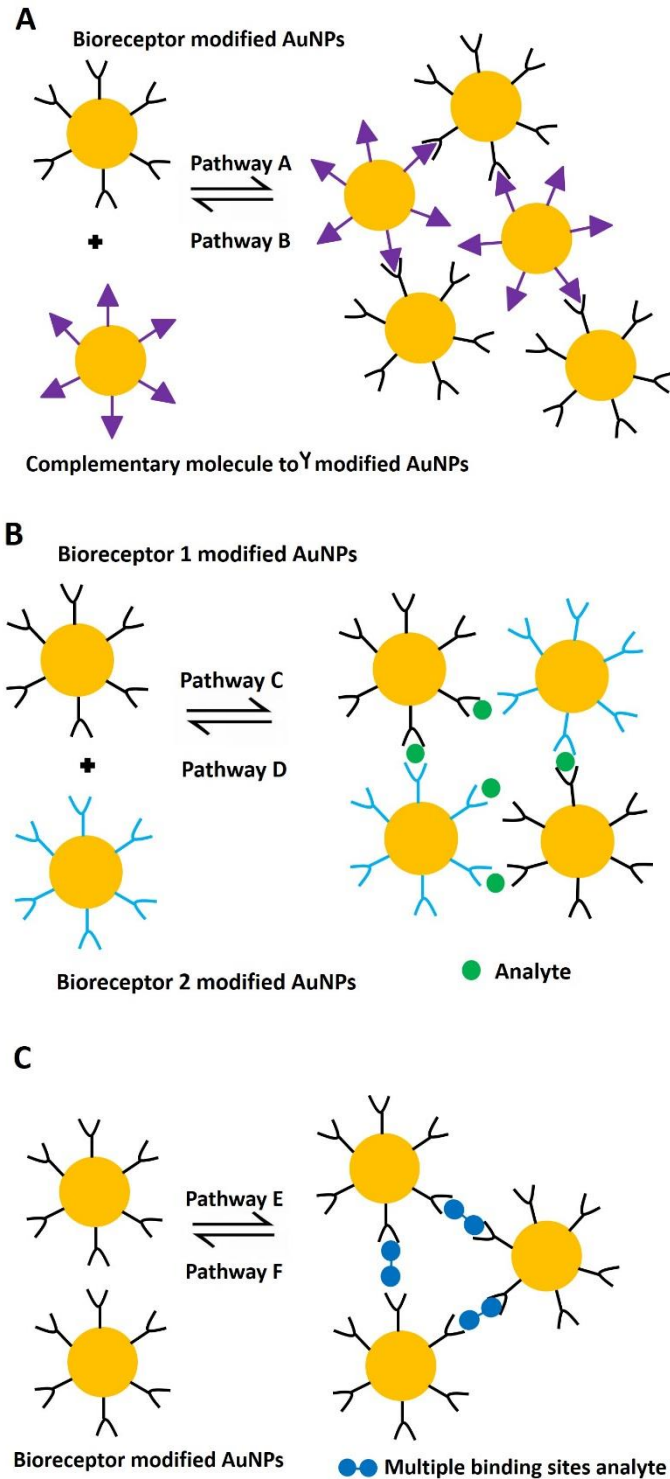


Figure 1-13 Schematic of interparticle crosslinking aggregation mechanism. (A), two different complementary molecules modified AuNPs are used as detection probes; (B), two different binding molecules to the same target are modified on AuNPs and used as detection probes; (C), target analyte with multiple binding sites can be detected with one type of modified AuNPs; pathway A, C and D represents the direct assay format, whereas pathway B, D and F represents the indirect assay format.

Similarly, for non-crosslinking aggregation mechanism, the direct assay can be performed by destabilization process of the colloidal AuNP dispersion. Basically, by adding the analytes, the stabilization of probes is destroyed, leading to an aggregate formation and can be detected using DLS (Figure 1-12A) like most of metal ions detection (Kalluri et al., 2009; Beqa et al., 2011; Durgadas et al., 2011). Whereas, in the indirect/competitive assay format, NP probes are aggregated prior the presence of the analyte. By adding the analytes, the analyte itself might act as a stabilizer for the NPs as seen in experiment done by (Wang et al., 2010).

In summary, NP-enable DLS assay principle is fundamentally all about the controlling aggregation of NPs. The specific aggregation/deaggregation of the NP probes can be detected with DLS. For complete quantitation, calibration curve can be obtained using standard solutions. The combination of NP distinctive light scattering property and DLS potential to detect a small change in size provides a great opportunity to establish new assay.

1.4.3 Applications of nanoparticle-coupled DLS assay

There are several papers reported the use of DLS in chemical and biological sensing, including other applications. Table 1-1, 1-2 and 1-3 summarize some of DLS sensor examples in recent years categorized by target analytes. The next section describes NP coupled DLS sensing platform applications in the literature.

1.4.3.1 Chemical sensing

Relevant chemical sensing papers are summarized in Table 1-1.

1.4.3.1.1 Metal ions

Heavy metal ions are a major public health problem, especially in drinking or ground water. Detection of these metal ions is extremely important for the prevention of a metal ion poisonings. There were reports of using DLS based sensing platform in detection of arsenic (As^{3+}) (Kalluri et al., 2009), lead (II)(Pb^{2+}) (Beqa et al., 2011; Miao et al., 2011), copper (II)(Cu^{2+}) (Miao et al., 2012), and mercury(II)(Hg^{2+}) (Xiong and Ling, 2012; Ma et al., 2014).

In 2009, Kalluri and a group of scientists in Bangladesh successfully developed an AuNP-DLS based assay for As^{3+} detection (Kalluri et al., 2009). They modified AuNPs with three different thiol containing compounds via the Au-S interaction, which were glutathione (GSH), dithiothreitol (DTT) and cysteine (Cys). The crosslinking between modified AuNPs was based on the binding of As^{3+} to DTT via the As-S bond, whilst for GSH and Cys, there is no free thiol group left after conjugation with the AuNPs so the binding of As^{3+} occurred via the As-O bond instead. The DLS intensity was increased after the presence of As^{3+} . They also suggested that bigger AuNPs have more surface area per individual NP compared with smaller ones so that is reason why the sensitivity could be improved with increasing AuNP size. The detection limit of the assay was reported at 3 ppt when 110 nm of AuNPs were used. The reported data were comparable with the data obtained from inductively coupled plasma mass spectrometry (ICP-MS). They concluded that their DLS technique had a three orders of magnitude better detection than the WHO limit guidelines for detection of As^{3+} .

Pb^{2+} is another metal ions heavily investigated by researchers as it is a compound found in common objects, i.e. paints or plastic toys, or army related materials like ammunition. Beqa et al., (2011) successfully demonstrated that GSH coated AuNPs could be used to detect Pb^{2+} via DLS as low as 100 ppt from plastic toys, paints and water samples within 20 min. The DLS could be used with gold nanorods (AuNRs) and silver nanoparticles (AgNPs) in quantitative assays for Pb^{2+} (Durgadas et al., 2011). The detection limits for both techniques were as low as 25 nM and 0.25 pM, respectively. Another DLS based method developed for Pb^{2+}

detection was developed by Miao et al., (2011). They utilized Pb^{2+} -specific DNAzymes to disaggregate of two different oligonucleotide-conjugated AuNPs. Using a similar principle, the Miao group later developed an assay for Cu^{2+} ions, but this time unmodified AuNPs were used instead (Miao et al., 2012). The principle of the assay was based on the ability of Cu^{2+} to cleave the DNAzyme from double-stranded (ds) to single-stranded DNA (ssDNA). The ssDNA fragment's was able to coat bare AuNPs, which protecting them from aggregate with the presence of sodium chloride (NaCl) salt, and the extent of aggregation proportionally to the concentration of Cu^{2+} was reported via DLS measurement mean hydrodynamic diameter (D_H) of the AuNPs.

Recently after, Hg^{2+} is another metal ions that has been detected using a DLS-based assay. Oligonucleotide- and Hg^{2+} aptamer conjugated AuNPs were used as probes for detection of Hg^{2+} (Xiong and Ling, 2012; Ma et al., 2014). Both reports used the same principle, where DLS was used to recover the average D_H of modified-AuNPs in the presence of Hg^{2+} . The mean D_H increased after NaCl salt was added to the system, as Hg^{2+} disrupted the structure of the oligonucleotide and aptamer resulting in lack of protection of the AuNP surface and aggregation. These methods gave detection limits in the nanomolar range.

1.4.3.1.2 Small chemicals and biomolecules

When it comes to small biomolecules, glucose is one of the most common targets for developing a sensing platform. There have been various types of glucose sensors established including DLS based sensors. Recently, Miao et al., (2013) proved that by conjugating two different pre-designed oligonucleotides onto AuNPs, the glucose level could be measured with DLS. By crosslinking the two modified AuNPs with another specific oligonucleotides (named Oligo-3), the AuNPs formed an aggregate. In the presence of glucose, glucose oxidase (GOx) and Fe^{2+} , Oligo-3 was cleaved and could not hybridized the two AuNPs. This eventually led to a proportional decrease in the mean size of AuNPs detected by DLS with detection limit of 38 μ M. The selectivity of the assay was tested against five other sugars and

it showed good selectivity for glucose. In another work by Miao et al. (2014), 8.3 pM of glucose was determined by DLS and AuNPs in human serum. This time ssDNA coated AuNPs were used as probes. By adding glucose to the system, the ssDNAs were cleaved and could not be adsorbed onto AuNPs. Therefore, when NaCl was added, AuNPs aggregated and DLS was again used as signal transducer. The aggregation assay format coupled with DLS measurement has proved to be useful for detection of other molecules. Yang et al., (2011) demonstrated a one-step sandwich-format for adenosine detection. An adenosine binding aptamer was split into two fragments and conjugated onto AuNPs (mean $D_H = 31$ nm). Upon binding adenosine, crosslinking of AuNPs could occur because an adenosine aptamer complex had been formed and D_H increased substantially. This method improved the limit of detection (LOD) to around 7 nM. Also, the change in mean D_H was selective to adenosine as there was no response observed in the presence of its analogues such as uridine, cytidine and guanosine.

Applications of the AuNP-DLS sensing platform have extended to security uses as well, and an interesting target analyte worth mentioning is 2,4,6-trinitrotoluene (TNT), a well-known explosive. Dasary et al., (2010) successfully established AuNP probes coupled with DLS for TNT detection with a detection limit of 100 pM. Para-aminothiophenol (*p*-ATP) was conjugated onto AuNPs because of its ability to form strong π -donor-acceptor interactions with TNT, which led to aggregation. In this work, they compared the DLS assay with a colorimetric assay and found that the LOD could be lowered using DLS. They also pointed out that with low levels of TNT in the solution, only dimers were formed, not larger aggregates. The colorimetric assay could not differentiate between monomers and dimers but DLS could do so, because it is sensitive in small changes in particle size. Similar to this experiment, the same principle was applied by Lin et al., (2012) but 1,2-ethylenediamine (EDA) was coated onto AuNPs instead and 0.4 pM of TNT could be determined.

1.4.3.1.3 Toxins

The AuNP-coupled DLS sensing assay has found applications in measuring environmental, agricultural and food contaminants. Here are some examples:

In 2010, Wang et.al. demonstrated the use of antibody-modified gold nanorods (AuNRs) in detection of microcystin-LR (MC-LR), a water contaminant from cyanobacteria that can cause liver cancer if exposed for a long time (Wang et al., 2010). A competitive assay format was used in this experiment. First, either side-by-side or end-to-end nanorod (NR) assemblies were formed via crosslinking of anti-MC-LR antibody modified AuNRs and MC-LR-OVA antigen modified AuNRs. The addition of toxin analyte competed with the antigen AuNRs and disrupted the assemblies resulting in reduction of mean D_H . The acquisition time of the assay was faster than ELISA, which was the established method to which the DLS assay compared.

Regarding food toxins, aflatoxins (AFs) are common mycotoxins produced from *Aspergillus*, and are well-known as carcinogens mainly affecting the liver. The established methods for AFs detection are time-consuming and labour intensive. In 2013, Xu et al. demonstrated that a gold nanorod (AuNR) coupled DLS based system could quantify the amount of AFB1, which is the most toxic type of AF, in peanut samples. Again, a competitive format was applied, but this time the AFB1-BSA antigen were immobilised onto AuNR surfaces protecting the rods from aggregation. Next, anti-AFB1 antibodies were added to the system and crosslinked the AuNRs causing aggregation. Competition occurred when AFB1 in the sample was added to the system. Free AFB1 competed with AFB1-conjugated AuNRs and prevented the rods from aggregating and consequently D_H changed from 776 nm to 80 nm with the 20 ng/ml of AFB1. This technique proved to quantify as low as 0.16 ng/ml of AFB1 and took only 45 min to perform. With the same principle, a competitive assay was applied by Zhang et al., (2013) for aflatoxin M1 (AFM) determination. Yet, this time there were two different probes, which were anti-AFM modified magnetic beads and AFM-BSA conjugated AuNPs. The AFM analyte competed with AFM-BSA AuNPs for binding to antibody-magnetic beads. The unbound AuNPs were separated and

measured by DLS. A linear relationship between the average size of the AuNPs and AFM concentrations was found with a LOD of 27.5 ng/L in milk samples.

In addition, melamine is a contaminant substance used in food containers that can migrate into food and cause health issues. It is also an illegal additive used to increase protein level in milk products. Ma et al. was the first group utilizing DLS in melamine sensing. Using citrate-stabilised AuNPs as probes Ma et al., (2014), crosslinking between AuNPs were based on the binding of melamine directly to the AuNPs. It was reported that the change in mean D_H could be observed with only 0.05 ppm of melamine from milk sample. The effect of pH was also tested and showed no effect on the DLS measurement. Whereas, another group from China used thymine containing DNA coated AuNPs to detect melamine monomer's migratory quantity (MMM_Q) (Wu et al., 2014). They exploited the hydrogen bonding between melamine and the thymine base and showed a detection limit of 2 µg/L. In addition, there was a reported AuNP-based DLS assay for the food contaminant cholera toxin, a protein enterotoxin from *Vibrio cholera*, which is a major cause of epidemic outbreak in developing countries (Khan et al., 2015). Anti-cholera antibodies were immobilised on AuNPs and acted as detection agents. The presence of cholera toxin caused aggregation of the particles and led to a shift in size, which was later detected by DLS.

Table 1-1 Chemical sensing application

Analyte	Probe	Detection limit	Source of sample	References
Metal ions				
Arsenic (As ³⁺)	Glutathione (GSH)-dithiothreitol (DTT)-cysteine (CYS) modified AuNPs	3 ppt	Ground water	(Kalluri et al., 2009)
Lead(II) (Pb ²⁺)	GSH-conjugated AuNPs	100 ppt	Paints Plastics Water samples	(Beqa et al., 2011)
	Aza-crown-ether-modified silver nanoparticles (AgNPs)	0.20 pM 0.22 pM 0.25 pM	Yangtze water East Lake water Drinking water	(Zhang et al., 2011)
	Oligonucleotide-conjugated AuNPs coupled with Pb ²⁺ -dependent DNAzyme	35 pM	Drinking water	(Miao et al., 2011)
	GSH modified gold nanorods (AuNRs)	0.025 mM	Deionized water	(Durgadas et al., 2011)
Copper(II) (Cu ²⁺)	Unmodified AuNPs	60 pM	River water	(Miao et al., 2012)
Mercury(II) (Hg ²⁺)	Oligonucleotide-conjugated AuNPs	0.43 nM	River/Pond water	(Xiong and Ling, 2012)
Mercury(II) (Hg ²⁺)	Hg ²⁺ aptamer-DNA AuNPs	0.1 nM	Lake water	(Ma et al., 2014)

Table 1-1: Chemical sensing application (continue)

Analyte	Probe	Detection limit	Source of sample	References
Small chemicals				
2,4,6-Trinitrotoluene (TNT)	Para-aminothiophenol conjugated AuNPs	100 pM	4:1 Ethanol/Acetonitrile	(Dasary et al., 2010)
Adenosine	ssDNA-conjugated AuNPs	7 nM	10 mM PBS buffer (pH 7.3)	(Yang et al., 2011)
2,4,6-Trinitrotoluene (TNT)	1,2-ethylenediamine (EDA) capped AuNPs	0.4 pM	Tap water	(Lin et al., 2012)
Glucose	Oligonucleotide conjugated AuNPs	38 pM	Human serums	(Miao et al., 2013)
Glucose	ssDNA adsorbed AuNPs	8.3 pM	Human serums	(Miao et al., 2014)
Toxins				
Microcystin-LR (MC-LR)	AuNRs assemblies side-by-side/ene-to-end by anti-MC-LR antibody modified and MC-LR-OVA antigen modified AuNRs	Side-by-side: 0.45 ng/ml End-to-end: 5 pg/ml	Water spike with MC-LR standards	(Wang et al., 2010)
Aflatoxin B1 (AFB)	AFB1-BSA conjugated AuNRs	0.16 ng/ml	Peanut samples	(Xu et al., 2013)
Aflatoxin M1 (AFM)	AFM-BSA conjugated AuNPs Anti-AFM modified magnetic beads	27.5 ng/L	Milk samples	(Zhang et al., 2013)
Melamine	Citrate-stabilised AuNPs	0.05 pM	Milk product	(Ma et al., 2014)
Melamine	Thymine containing DNA coated AuNPs	2 µg/L	Food simulants	(Wu et al., 2014)
Cholera toxin	Ab-conjugated AuNPs	10 nM	Tap/Lake water	(Khan et al., 2015)

1.4.3.2 Biological sensing

Relevant biological sensing papers are summarized in Table 1-2.

1.4.3.2.1 Proteins and biomarker

Liu and Huo (2009) conducted a systemic study of AuNP-DLS based methods using mouse IgG antibody as an analyte. The binding kinetics were investigated by measuring D_H as a function of time when mixing goat anti-mouse IgG Ab- and mouse IgG-conjugated AuNPs together in a 1:1 ratio. A linear response was observed and this suggested that the antibody-antigen interaction could crosslink the AuNPs leading to cluster formation, which is the key feature of the immunoaffinity NP aggregation assay. In addition to kinetics being tested, the temperature effect was also investigated. It was determined that at higher temperature (37 °C), aggregation occurred faster than at lower temperatures. For mouse IgG assay in solution, goat-anti mouse IgG was used as the bioreceptors and D_H was measured after incubation for 2 h at 37 °C. There was a linear response between the mean D_H and concentration of the IgG upto 5 µg/ml. After this point, the size dropped substantially forming a curve similarly to the Heidelberger-Kendall curve reported for immunoprecipitation assays. This phenomenon was explained as the 'hook effect'. It is a common situation observed in particle aggregation assays. This might be due to the large amount of antigen added to the system occupying all of the bioreceptors on the surface of AuNPs and thereby preventing crosslinking between AuNPs. This limits the upper range of detection of the assay.

To avoid this effect, it was suggested in the paper to adjust the NP concentration, dilute the analyte concentration or use a competitive assay format instead. The competitive platform was accomplished by forming an aggregate between goat anti-mouse IgG Ab- and mouse-IgG-conjugated AuNPs. Adding mouse IgG in solution competed with the mouse-IgG AuNPs in binding to the anti-mouse Ab conjugated AuNPs. A reduction in mean D_H was observed and the concentration of analyte could be quantified. Despite avoiding the hook effect, it should be noted that using competitive format provided a less sensitive assay system.

There is a large volume of published work describing the role of AuNP coupled with DLS in terms of molecular biomarker detection. The Qun Huo group was the first to demonstrate that the quantification of free prostate specific antigen (f-PSA) could be performed with this platform (Liu et al., 2008). The free to total PSA ratio is different in cancer patients and benign prostate hyperplasia patients. However, the range of PSA presented in blood is in ng/ml so very sensitive assays are required. The established methods are either time consuming, involve labelling or have low sensitivity. With the DLS method, the detection limit was 0.1 ng/ml. Ab conjugated AuNPs were used for detection while Ab conjugated AuNRs was used for analyte capture in this method. In the presence of f-PSA, there were two different sizes observed in the DLS size distribution; 20 – 60 nm representing the free AuNPs and AuNRs and 60 – 500 nm representing dimers/trimers/oligomers formed via antibody-antigen interaction. The ratio between the two size populations were plotted and a linear response proportional to the concentration of f-PSA added to the system was found. The selectivity was tested using a different cancer marker, CA125 and the technique showed no response.

There were reports of another cancer biomarker (alpha-fetoprotein - AFP), which significantly increases in liver cancer patients. Nietzold and Lisdat (2012) utilized anti-AFP monoclonal Ab (mAb)-conjugated AuNPs and were able to detect 0.1 – 0.4 µg/ml of AFP in serum samples with the direct assay format. They suggested that the bigger the particles, the larger the change in mean D_H would occur. In addition, small change in temperature, ionic strength and pH did not disturb the assay. Another study conducted by Chun et al., (2011) confirmed the principle of NP coupled DLS assay in detection of AFP. Anti-AFP IgG conjugated with gold-coated magnetic NPs were used as probes. Magnetic NPs were incorporated in the assay to ease AuNP functionalisation and orientation of anti-AFP IgG on the surface. Using this method an LOD of 0.01 ng/ml could be obtained. With regard to the detection probes, not only AuNPs were used in the DLS based assay, AuNRs or magnetic NPs were also used. In another paper published recently, silver NPs (AgNPs) were used as detection agents for carcinoembryonic antigen (CEA) – a tumour marker related to colorectal cancer (Miao et al., 2014). Anti-CEA IgG were conjugated to Ag-core Au-

shell nanoparticles (Ag@Au CSNPs) and used as probes. A linear response between mean D_H and concentration of CEA was observed. The incubation time was optimised to maximise the Ab-antigen interaction and 15 min was the optimum time reported. Also, pH effect was investigated and it was found out that at pH above pH 7.5, there was a decrease in mean D_H . It was concluded that this method provided a fast, convenient and sensitive (LOD = 35.6 pg/ml) method of detecting CEA with the volume of sample required for the assay being only 20 μ l.

In addition, there was a report regarding polypeptide detection. Qin et al., (2017) described a sandwich-type DLS assay for pancreatic polypeptide (PP). Two different aptamers that could bind to PP were immobilised on AuNPs. Crosslinking of the AuNPs followed addition of PP to the system as the two aptamers could bind to the PP at the same time, leading to cluster formation detected by DLS. The LOD was reported to be 56 pM.

1.4.3.2.2 Oligonucleotides

Various approaches established for quantifying DNA mainly involve fluorescent optical labelling. There are drawbacks apart from the process being time-consuming. With low DNA concentrations, the signal may not be strong enough to detect and fluorophores can photobleach or degrade with time, which results in inconsistent results. Thus, there are several studies conducted in searching for an alternative method for oligonucleotide detection and quantification.

Dai et al., (2008) was the first team to publish a paper in which they described the use of AuNPs coupled with DLS technique in detection of DNA sequences. Specific DNA sequences were detected via AuNPs conjugated to two different complementary DNAs. In the presence of target DNA, crosslinking between AuNPs occurred due to hybridization of the DNA and aggregation of the AuNPs was identified by DLS. The detection limit was approximated to be around 1 pM. Moreover, when the single base pair mismatched target DNA was added instead,

there was no AuNPs size shift, reflecting the possible application in differentiating intact and damaged or mutant DNA.

Consistently, Pylaev et al., (2011) reported a similar assay to detect cDNA sequences. They described the use of cetyltrimethylammonium bromide (CTAB)-coated positively charged AuNPs to detect a 21-mer single stranded DNA (ssDNA) from the human immunodeficiency virus type 1 (HIV-1 U5), a 23-mer ssDNA from the *Bacillus anthracis* cryptic protein and protective antigen precursor (pagA) genes. The results corresponded to the previous study in that the DLS method could discriminate single and three base pair mismatched sequences from the native sequence. Also, they compared the use of AuNRs as probes and suggested that AuNPs were more feasible for genome sensing. This concept was applied to double-stranded DNA and microRNA (miRNA) (Miao et al., 2011; Seow et al., 2014). Another paper reported by Zhang et al., (2012) confirmed the success of this technique for DNA detection. The paper described a slightly different method from that of Pylaev et al., (2011). Here, AuNPs were aggregated previously in the presence of dithiothreitol (DTT). By adding monothiol DNAs to the system, they could prevent the aggregation of the AuNPs, which led to the decrease in mean D_H proportionally.

The technique was not only reported for DNA or RNA detection, but also found application for transgenic product detection. In a paper published by Gao et al., (2011), sequence-specific nopaline synthase (NOS) gene produced in transgenic plants could be detected. Citrate-stabilised AuNPs were used to detect the transcripts in the presence of NaCl solution. The AuNPs were stabilised by the adsorption of NOS genes on the surface when the salt solution was added. However, in the presence of target sequence (sample), NOS genes were hybridized so the AuNPs were destabilized and aggregated when the salt solution was added. A linear relationship between the mean D_H and the target sequence concentrations was obtained with a detection limit of 0.3 fM.

1.4.3.2.3 *Bacteria, viruses and viral antigens*

There are a few reports applying AuNP-DLS based sensing platforms for large analytes such as viruses and bacteria.

Driskell et al., (2011) demonstrated that the technique could quantify human influenza A virus strain H1N1:PR8 by using mAb clone IC5-4F8 modified AuNPs as probes. The DLS assay successfully quantified the viruses with a LOD of 8.6×10^1 TCID₅₀/ml. The hook effect was observed similar to most DLS assays. The effect of NP concentration was also investigated and the data suggested that below the hook point, a greater D_H was observed at lower AuNP concentrations. So the dynamic range of assay could be adjusted by diluting or concentrating the AuNPs. However, it is worth noting that too dilute NP concentrations might result in too low scattering intensity signals, which would affect the signal to noise ratio.

In comparison to DLS assays for protein detection, the relationship of size-shift and concentration of the analyte was sigmoidal for virus detection. The possible explanation given by Driskell et al., (2011) was that the viruses are larger than proteins and a single virus could bind to more than one AuNP probes leading to a substantial change in size, in contrast, one molecule of a small protein would allow only a dimer to form and dimer would affect the D_H less than complexes-formed by larger analytes. Moreover, the effect of NP size was investigated and was expected to boost the sensitivity of the assay as seen in several studies already mentioned. Overall, a 30 nm core size of AuNPs provided the best detection limit compared with 60 and 80 nm. Steric hindrance could be the key explanation to this contradiction, as a virus is a large analyte and at low level of virus the 30 nm NPs could occupy the surface of viruses more than 60 and 80 nm NPs. This led to fewer unbound probes left over in the solution and resulted in larger mean D_H reported. In addition, the effect of AuNP concentration could be another reason as to why the effect of size contradicted the hypothesis and previous studies, because the DLS assay performed was based on the supplied concentration of each NP sizes, which had different number of particles/ml. Another point worth mentioning from this report by Driskell et al., (2011) is that AuNP stability was investigated. The functionalised AuNPs were

prepared and used in the DLS assay for four consecutive days and were stored at 4 °C between each assay. The results showed no reduction in performance.

Regarding virus detection, Wang et al., (2012) described a DLS assay for hepatitis B antigen (HBsAg). In this study, they used anti-HBsAg mAb-conjugated to 50 nm AuNPs as the detection agents coupled with anti-HBsAg polyclonal Ab (pAb)-conjugated to either 10 nm or 100 nm AuNPs. The ratio between those two probes were optimised. The system with AuNP100-AuNP50 particles showed considerably better response, with LOD at 0.005 IU/ml, as compared to the LOD at 0.01 IU/ml obtained from the AuNP10-AuNP50 system. This again corresponded to most studies in terms of AuNP size since 100 nm AuNPs scatter light more strongly than 10 nm AuNPs. The linear response between the mean D_H and concentration of analyte, conversely, was not observed in this experiment like in other DLS assay studies. The explanation given in the paper assumed that the clusters formed between two different sizes of AuNPs were not spherical in shape in which affects Brownian motion and the translational diffusion coefficient (D). This was confirmed with TEM images showing various shapes of aggregates. However, the assay was demonstrated to be selective against HBsAg, with a much faster data acquisition time and sensitivity compared with conventional ELISA method.

More recently, an AuNP-based DLS immunoassay has proved to be effective in detection of pathogenic bacteria. Huang et al., (2015) demonstrated the application of the assay for *Listeria monocytogenes*, a Gram positive bacteria causing food poisoning. The established method for this bacteria is culture-based, which takes approximately 7 days. The bacteria were extracted from lettuces using anti-*Listeria monocytogenes* monoclonal antibodies coated onto magnetic NPs (mAbs-MNPs). The quantitative assay was conducted by using anti-*Listeria monocytogenes* monoclonal antibodies coated onto AuNPs (mAbs-AuNPs) as detection agents similarly to most DLS-based methods. The mean D_H increased proportionally with increasing concentration of analyte. The reaction time between the mAbs-AuNPs and analytes was investigated and 30 min was reported to be optimum. They also tested the effect of antibody concentration coated onto the AuNPs and found out that 10 µg/ml of the antibodies gave a maximum response. The assay proved to be

selective to *Listeria monocytogenes* strains only and showed no significant response with 15 other bacterial strains. In addition, they revealed that the LOD of the assay could be enhanced by increasing of AuNP size, when optimal NP concentration was used. However, they suggested that the oversized NPs could block the antibody-antigen interaction because of steric hindrance.

Table 1-2 Biological sensing applications

Analyte	Probe	Detection limit	Source of sample	References
Proteins				
Free prostate specific antigen (f-PSA)	Detection Ab-conjugated AuNPs Capture Ab-conjugated AuNRs	0.1 ng/ml	Nanopure water	(Liu et al., 2008)
Mouse IgG Ab	Direct assay: Goat anti-mouse IgG Ab conjugated AuNPs Competitive assay The direct assay's probe and mouse IgG conjugated AuNPs	Direct: 0.5 ng/ml Competitive: 100 ng/ml	PBS buffer	(Liu and Huo, 2009)
Alpha-fetoprotein (AFP)	Anti-AFP conjugated gold-coated iron oxide magnetic NPs	0.01 ng/ml	Buffer solution	(Chun et al., 2011)
Alpha-fetoprotein (AFP)	Anti-AFP Ab-conjugated AuNPs	0.1 – 0.4 µg/ml	Serum sample	(Nietzold and Lisdat, 2012)
Carcinoembryonic antigen (CEA)	Anti-CEA Ab-conjugated silver core gold shell NPs (Ag@Au CSNPs)	35.6 pg/ml	Serum sample	(Miao et al., 2014)
Pancreatic polypeptide (PP)	Dual-aptamer immobilised AuNPs	56 pM	Buffer solution	(Qin et al., 2017)

Table 1-2: Biological sensing applications (continue)

Analyte	Probe	Detection limit	Source of sample	References
Oligonucleotides				
Target DNA	Single stranded DNA (ssDNA)-conjugated AuNPs (citrate-stabilised AuNPs)	1 pM	Buffer solution	(Dai et al., 2008)
Complementary DNA (cDNA) of	ssDNA-conjugated AuNPs ssDNA-conjugated AuNRs	AuNPs: 10 pM	Buffer solution	(Pylaev et al., 2011)
Double-stranded DNA (dsDNA)	dsDNA modified AuNPs	593 fM	Buffer solution	(Miao et al., 2011)
Nopaline synthase (NOS) gene	Citrate-stabilised AuNPs	3.0×10^{-14} M	Buffer solution	(Gao et al., 2011)
Let7 family microRNA (miRNA)	ssDNA-conjugated AuNPs	100 fmol	Buffer solution	(Seow et al., 2014)
Bacteria, Viruses and Virus antigens				
Human influenza A virus (H1N1:PR8)	mAb clone IC5-4F8 modified AuNPs	8.6×10^1 TCID ₅₀ /ml	PBS buffer (pH 7.4)	(Driskell et al., 2011)
Hepatitis B antigen (HBsAg)	Anti-HBsAg mAb-conjugated 50 nm AuNPs coupled with either anti-HBsAg polyclonal Ab (pAb)-conjugated 10 or 100 nm AuNPs	AuNP10-AuNP50: 0.01 IU/ml AuNP100-AuNP50: 0.005 IU/ml	Tris-HCl buffer (pH 7.4)	(Wang et al., 2012)
<i>Listeria Monocytogenes</i>	Anti- <i>Listeria monocytogenes</i> mAb conjugated AuNPs	3.5×10^1 CFU/ml 2.2×10^1 CFU/ml	PBS (pH 7.4) Lettuce sample	(Huang et al., 2015)

1.4.3.3 Other applications

There was a report by Zheng et al., (2015) on the potential of the NP-DLS coupled assay as a universal cancer screening test. The principle is based on the knowledge of tumour antigen-specific autoantibodies. It is a response of human body to tumour cells. Auto-antibodies are produced and secreted into our serum relatively early and before diagnosis of the disease. Therefore, they become one of the best biomarkers for cancer screening. The assay proposed utilized citrate-stabilised AuNPs as probes and contained two steps. The first involved mixing human serum sample with the AuNPs, which led to the adsorption of serum proteins on the AuNP surface, forming a complex with a 'protein corona'. After 5-20 min incubation, the mean D_H of AuNPs was measured (D_1). Following this, rabbit anti-human IgG Ab were added to the mixture and bound to the IgG present on the corona leading to NP crosslinking and cluster formation. Again, the mean D_H of AuNPs was measured (D_2). The ratio between D_2/D_1 were reported as a test score. So far, two pilot studies were conducted. The first study used prostate cancer versus non-cancer patient samples, whilst the second looked at prostate cancer versus benign prostate hyperplasia (BPH – a non-cancerous condition) samples. The specificities for both studies were 95% and 91%, respectively. It was concluded that this assay could be a fast, simple and reliable cancer screening test.

Another interesting applications of an NP aggregation assay coupled with DLS was to study protein-protein interaction. Conventional methods are mainly labelled techniques and true binding might be affected by fluorescence labels. Also, these assays are time-consuming and labour intensive. Recently, label-free techniques like SPR have become an option for protein-protein interaction monitoring. However, SPR requires a complex equipment and an expert to operate it. Furthermore, large protein aggregates cannot be studied with SPR. Bogdanovic et al., (2010) reported using DLS to examine the aggregation of glyceraldehyde 3-phosphate dehydrogenase (GAPDH). Anti-GAPDH Ab-conjugated AuNPs were used as detection probes. Previously, it was not possible to directly measure aggregation extent of GAPDH at low concentrations (<100 $\mu\text{g}/\text{ml}$), which are likely to be found under physiological conditions. Using the AbAuNP probes and DLS, it was revealed that

GAPDH tended to aggregate over a concentration range of 10 – 25 µg/ml. The study was conducted by measuring the average size of the AbAuNP probes and GAPDH complexes. Moreover, size distribution plots from DLS provided the characteristics of the aggregates formed too. It was reported that GAPDH aggregates were not uniform.

A different paper published by Qun Huo (2010) correspondingly revealed that this NP-DLS aggregation assay could be used for protein complex/aggregate detection. This potential to reveal the level of protein aggregation could be used to differentiate between normal and cancer patients. The study was focused on four different cancer biomarkers: CA125 (ovarian cancer), CEA (ovarian and colon cancer), CA19-9 (colon cancer) and prostatic acid phosphatase (PAP) (prostate cancer). Antibodies specific to each biomarker were conjugated to AuNPs. The assay was performed by comparing change in the average size of healthy and cancer assayed samples. It was shown that the levels of aggregated proteins in cancer patients samples were higher in healthy ones. The authors suggested that for cancer patients, the pattern of protein expression is different from normal cell function and when secreted out of the cells, the behaviour of proteins will be changed. Huo (2010) concluded that this might be an alternative method for cancer diagnosis. Correspondingly, it was also demonstrated recently that DLS assays could be used to screen antigen-antibody binding activity (Lai et al., 2015). Influenza virus (H1N1) was selected as an antigen of interest and four different mAbs (InA4, InA16, InA88 and InA97) were screened with the proposed technique. Data was compared to a gold standard ELISA. The results from the DLS assay was comparable to the results from ELISA but with only 30 min processing time.

A final application of a NP-coupled DLS technique is a tool for studying protein structure. Actually, DLS on itself can be used in protein size analysis, but there are some limitations. Small proteins (MW < 50 KDa) do not have enough scattering intensity and so the concentration of proteins has to be high (> 1 mg/ml) to be measured. In the paper published by Zheng et al., (2016), AuNPs were used in conjunction with DLS to determine the hydrodynamic size of protein disulphide

isomerase (PDI). The mean D_H of citrate-stabilised AuNPs was measured and compared with the average size after PDI was added to the AuNPs. Once more, the ability to form a protein corona on the AuNP surface was exploited. The difference in size before and after the corona formation could be calculated and reported as PDI hydrodynamic protein size. The study also compared the sizes of reduced and oxidised forms of PDI. The results were similar to X-ray diffraction analysis, which showed that the reduced form had a smaller hydrodynamic diameter. Relevant papers for other applications of NP-DLS based assay are summarised in Table 1-3.

Table 1-3 Other applications

Analytes	Probes	Proposed applications	References
Glyceraldehyde 3-phosphate dehydrogenase (GAPDH)	Anti-GAPDH Ab-conjugated AuNPs	Protein-protein interaction study	(Bogdanovic et al., 2010)
Cancer biomarkers	Ab-conjugated AuNPs	Cancer biomarker determination	(Huo, 2010)
Influenza virus (H1N1)	Ab-conjugated AuNPs	Antigen-antibody binding activity	(Lai et al., 2015)
Prostate cancer biomarker	Citrate-stabilised AuNPs	Cancer screening test	(Zheng et al., 2015)
Protein disulphide isomerase (PDI)	Citrate-stabilised AuNPs	Determine hydrodynamic size of protein	(Zheng et al., 2016)

1.4.4 Challenges in the development of nanoparticle-coupled dynamic light scattering detection

Initially, DLS was not an option for quantitative analysis for chemical and biological sensing because prior to the arrival of AuNPs it could not differentiate the light scattering from the polymer beads and background matrices so it could not meet the practical application at that time. However, it is now well-established from a variety of studies that NP-coupled DLS assays are capable of quantitative analysis for target analytes ranging from metal ions to proteins. Alternatively, the assay can be used in biomolecular interaction studies.

The main advantages of the size-shift assay over other methods is that it is a label-free technique with no labelling of the target or ligand needed. Therefore, true interactions can be obtained. Without labelling, the complexity of the technique is also reduced, removing the need for an expert to operate the DLS equipment and making the technique more available. In addition, homogeneous assays can be performed with this technique as there is no need to separate the NP probes and analytes before measurement takes place. DLS has a fast operation time and the assay results could be obtained within minutes. Furthermore, DLS has been commercialised in the form of plate reader. This opens up an opportunity to design high-throughput systems for screening or studying molecular interaction. In fact, there is the company Nano Discovery Inc. commercialises nanoparticle-coupled DLS technology as its core business. Their assays are sold in the form of AuNP ready-to-use conjugate kit; bioreceptors are provided by the customer.

To date, all applications of nanoparticle-coupled DLS assay have been established at the experimental stage and have not yet been widely accepted for industrial or field use. The remaining challenges for this technology are how to use the assay with various background matrices and how to maintain the stability of the nanoparticle reagents prepared for the assay. Regarding background matrices; it is necessary to make sure that the aggregation of AuNPs is specific to the target analyte and is not interfered with the background signal. In real world applications, there is a limited chance that the samples arrive in a pure solution and a complex matrix like

serum is more likely. Another challenge is the stability of the probes. This issue is critical to the technique because it is the key part of the aggregation control. The quality of AuNPs themselves should be maintained in order to avoid random aggregation. Moreover, the binding activity between the bioreceptor and target analyte is even more important to ensure the qualitative and quantitative efficacy of the assay.

1.5 Bioreceptors

The bioreceptor is an important element in any biosensing platform since the binding event between the target analyte and bioreceptor leads to generation of the signal, no matter which type of sensing application is concerned. Ideally, the receptor should bind specifically to the interested analyte, and the binding activity should produce a strong enough signal enable the development of a sensitive sensing system. In terms of NP-coupled DLS assays, several types of bioreceptor have been reported previously, especially oligonucleotides and antibodies. This section provides a brief summary of the bioreceptors used in optical sensing, together with the possible molecules that can be used to improve detection in NP- coupled DLS assays.

1.5.1 Oligonucleotides and aptamers

Oligonucleotides are commonly used coupled to AuNPs for DNA detection. The base pairing between complementary DNA has been exploited in sensing applications for a long time. The analytes for this type of bioreceptor are mainly DNA, RNA or their analogues (Luong et al., 2008; Jolly et al., 2016). Nevertheless, the stability of DNA is still a major problem as in some conditions (e.g. in acid solution) it can be depurinated (Brandt and Hoheisel, 2004). Hence, there has been an attempt to use an artificially synthesized nucleic acid or peptide nucleic acid (PNA) instead because it has the same characteristics as DNA or RNA but is far more stable at different temperatures or pHs. Also, it tolerates various enzymes (i.e. nuclease) (Demidov et al., 1994).

In recent time, protein-binding oligonucleotides, aptamers, have emerged. They are produced using the systematic evolution of ligands by exponential enrichment – known as SELEX and automated chemical solid-phase synthesis is used for production. The aptamers are single-stranded DNA (ssDNA) or RNA (ssRNA) sequences that can be produced to have a high specificity and affinity towards the target molecules. The binding mechanism of aptamers is based on conformational

change and not complementary base pairing. They are considered as antibody alternatives (Nimjee et al., 2005; Jolly et al., 2016).

Aptamers exhibit a reversible denaturation property with fully recovery of function which can be controlled by changing conditions such as pH, temperature, ionic strength. A variety of target analytes have been screened including proteins, small molecules, viruses, but the greatest advantage of aptamers is their ability to bind to small molecules. Although, the structure of theophylline and caffeine are almost identical (Figure 1-14), apart from one methyl group, aptamers against theophylline could specifically bind to the target with no cross reactivity. This was shown by Jiang et al., (2015). In the same way as oligonucleotides, aptamers are charged, which makes the binding responsive to solution they are in. This may restrict the use of aptamers in complex buffer solution like blood or biological samples (McKeague and DeRosa, 2012; Lakhin et al., 2013).

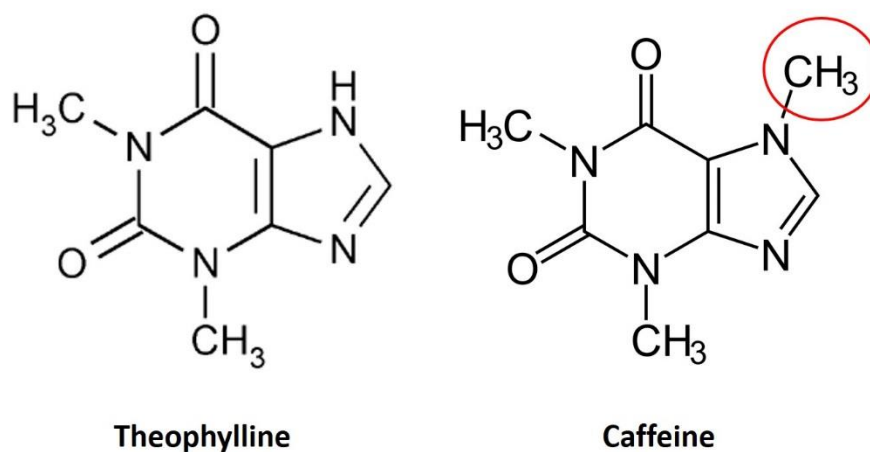


Figure 1-14 Structures of theophylline and caffeine. The red circle indicates a position of methyl group within caffeine structure that different from theophylline.

1.5.2 Antibodies and their alternatives

1.5.2.1 Antibodies

For decades, antibodies have been exploited by researchers in biological science. They have become one of the most frequently used tools in both therapeutic and diagnostic applications. Antibodies are used extensively in ELISA, protein blotting, immunohistochemistry, immunoprecipitation and flow cytometry analysis. Not only for research fields, antibodies are also used as therapeutic agents in treatment of cancer, autoimmune or inflammatory diseases. As bioreceptors, the specific interaction between antigen and the antibody is exploited in affinity based biosensors (Vo-Dinh and Cullum, 2000; Morrison et al., 2007).

Antibodies or immunoglobulins (Igs) are proteins produced by B cells to protect the body from invasion by foreign molecules. It is a very important element in the human immune system. Figure 1-15 shows a schematic of an antibody molecule. It has Y-shaped structure comprising of four polypeptide chains linked together with multiple disulphide bonds. Antibody basic structure comprises two identical 25 kDa light chains and two 50 kDa heavy chains. Both light and heavy chains contain variable regions at their N-termini whereas their C-termini are constant. The antigen binding site (Fab) is located at the N-terminus of each heavy chain and its adjacent light chain. There are three complementarity determining regions (CDRs) in the binding site that are actually involved in antigen binding. However, the remaining domains of both chains support the CDRs to aid binding specificity. Identical C-terminal parts of the two heavy chains form a region called Fc. It contains an effector site, which enables the antigen downstream destruction process.

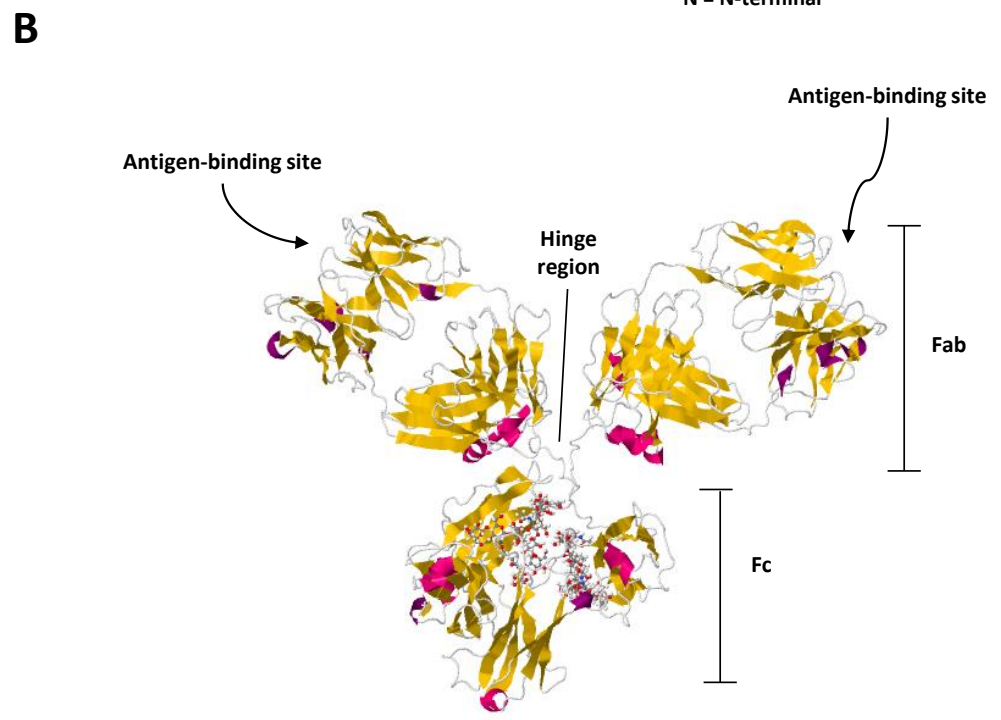
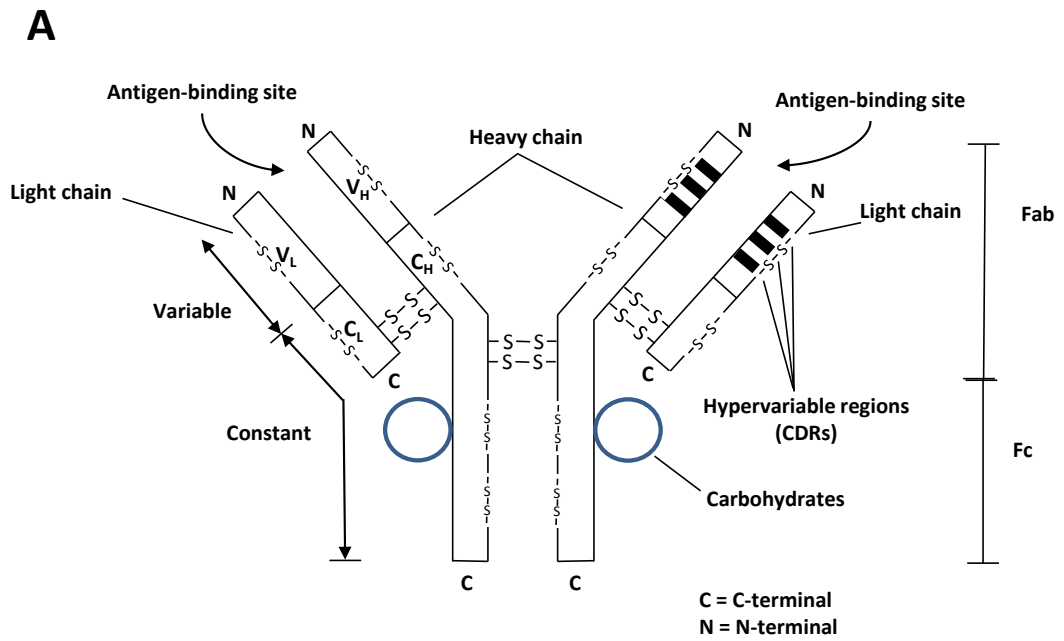


Figure 1-15 Antibody (IgG) molecular structure. (A), schematic of IgG structure comprising of two identical light chains and two identical heavy chains. Both light and heavy chains contain variable regions at their N-termini (V_L and V_H , respectively) whereas their C-termini are constant (C_L and C_H , respectively). The antigen binding site (Fab) is located at the N-terminus of each heavy chain and its adjacent light chain. There are three complementarity determining regions (CDRs) in the binding site that are actually involved in antigen binding. Identical C-terminal parts of the two heavy chains forms a region called Fc; (B), 3D structure of Ab from PDB file: 1IGY.

Antibodies are produced by immunizing animals such as mice, rabbits, chickens with the analyte of interest. Antibodies against the target are produced by the B cells, which can be isolated and utilized for monoclonal antibody production. However, antibodies produced in response to simple immunization are called 'polyclonal antibodies' and are made by multiple B cells. So essentially, they are a pool of antibodies that bind to the specific antigen at multiple epitopes. Monoclonal antibodies that bind to a single epitope are produced by isolating single antibody producing B cells from the animal, fusing the isolated cells with myeloma cells to produce hybridomas, and growing the hybridomas in the media that only allows the hybridomas to survive.

Antibodies have proven to be really useful tools for many applications. Yet, there are a number of disadvantages regarding antibodies. The production of antibodies involves animals, is time-consuming, requires expert labour and is expensive. Also, some target molecules antibody production is difficult. For example, toxic proteins in some cases cannot be injected to the animals as they may be harmful or even kill the animal. Also antibodies are large multimeric molecular structure containing multiple disulphide bonds and show limited stability.

Another major issue concerning antibody use is a batch-to-batch heterogeneity. This is a common problem with commercial antibodies. There was a report on this issue in 2015 (Baker, 2015; Bradbury and Plückthun, 2015) suggesting that antibody variation is a major cause of reproducibility problems in life sciences research because of batch-to-batch variability and poor characterisation. It was also reported that around 50% of globally invested funds on protein-binding reagents were wasted due to poorly characterised antibodies (Baker, 2015; Bradbury and Plückthun, 2015; O'Kennedy et al., 2017). With this downside, it is hard for diagnostic fields to rely on antibodies as it is difficult to maintain the quality on long-term supplies for assay. This drawback of antibodies can be solved by using monoclonal antibodies as they have no batch variability. However, monoclonal antibody production is complicated, time-consuming and very expensive. Therefore, several alternatives have been proposed to replace antibodies.

Antibody fragments have become a replacements for whole antibodies in solving the problems mentioned. It is the active fraction of the antibody, such as Fv, Fab and multivalent fragments, which participate in binding that are used. The fabrication of these fragments is fairly easy, including the removal the Fc region that sometimes provides unpleasant side effects for biopharmaceutical applications (Plückthun and Pack, 1997). By using synthetic or recombinant libraries from B cells, the specificity can be more controlled and production is also cheaper (Vaughan et al., 1996; Knappik et al., 2000). Nevertheless, the use of antibody fragments is not widespread because of their stability (Binz and Plückthun, 2005). For example, in the absence of the Fc region, some immobilization processes are not possible and thus several applications are restricted. A lot of attention has turned to non-antibody binding proteins and these will be discussed in the next section.

1.5.2.2 Non-antibody binding proteins

Non-antibody binding proteins are based on the concept of protein scaffold engineering. This refers to introduction of additional affinity function into a stable folded protein (Nygren and Skerra, 2004). The properties that protein scaffolds should have are to be strong, stable, compact and have a monomeric structure. These make for easy genetic engineering and expression in prokaryotic systems, which is inexpensive. In addition, their most significant property is their structurally rigid area, which means a region where the replacements, insertions or deletions of amino acids can take place at a primary structure level without disturbing overall protein structure, in order to generate new binding sites similar in those the antibody hypervariable loop (Skerra, 2003; Skerra, 2007).

With advancements in protein engineering and the latest library selection technologies, proteins that can replicate antibody function are already available. The procedure of generating synthetic non-antibody binding proteins usually starts with building a combinatorial library onto a preferred protein scaffold. The library is built by selective random mutagenesis of unprotected surface residues of the scaffold, typically unstructured loops. After this, a range of binding affinities are produced by

careful selection of variants using phage display. The degree of mutagenesis and the selection conditions are the two most important factors for determining biomolecular properties of the binding molecules. Ideally, the binding protein should have sufficient affinity and specificity to a target. Also, it should exhibit thermodynamic, chemical and enzymatic stabilities (Skerra, 2007; Hamzeh-Mivehroud et al., 2013).

In comparison with antibodies, non-antibody binding proteins possess better stability and their production is much cheaper. Most of them lack disulphide bonds, except where engineered in. This allow cysteine reduction to facilitate the orientation bioreceptor coupling and their use in intracellular assays and structural biology application (Helma et al., 2015). Additionally, without batch-to-batch variability, reproducibility is usually much higher. So far, there are more than 50 different non-antibody binding proteins reported. Broadly speaking, they can be classified into two groups. The first group is constrained peptides (2 – 4 kDa), while the second group comprises domain-sized scaffolds with ~ 6 – 20 kDa molecular weight. If we investigate further the mechanism of binding, they also can be divided into two subgroups (Table 1-4 and 1-5). The first binding mechanism is via surface-exposed side chains of secondary structural elements whilst the other is via the binding loop(s) on a protein scaffold. The latter mechanism mimics the binding by an antibody (Nygren and Skerra, 2004; Weidle et al., 2013).

Table 1-4 Examples of secondary structure based binding mechanism non-antibody (Ab) binding proteins. The list is intended to show a variety of non-Ab binding proteins that have been developed. PDB files were obtained from RCSB protein data bank (<http://www.rcsb.org/pdb/home/>).

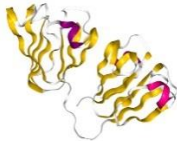
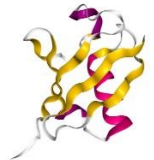
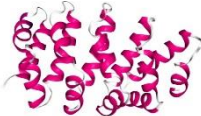
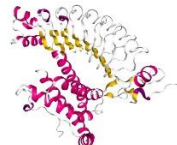
Name	Protein scaffolds	Species origin	Randomization	Structure	PDB	Ref
Darpin	Ankyrin repeat proteins	Human	7 residues in each <i>n</i> -repeat		4J7W	(Plückthun, 2015)
Affibody	Protein A	Bacteria (<i>Staphylococcus aureus</i>)	13 residues in 2 helices		1LP1	(Shishido et al., 2010)
Affilins (1)	γ -B-crystallin	Human	8 residues		2JDG	(Ebersbach et al., 2007)
Affilins (2)	Ubiquitin	Human	6 residues in the β -sheet		1UBI	(Hoffmann et al., 2012)
Armadillo repeats	Armadillo (homologous to b-catenin)	Consensus protein	6 residues in each internal repeat		4DB6	(Parmeggiani et al., 2008)
Repebody	Leucine-rich repeat (LRR) modules	Consensus protein	5 residues in each LRR		4J4L	(Lee et al., 2012)

Table 1-5 Examples of loop based binding mechanism non-antibody binding proteins. The list is intended to show a variety of non-Ab binding proteins that have been developed. PDB files were obtained from RCSB protein data bank (<http://www.rcsb.org/pdb/home/>).

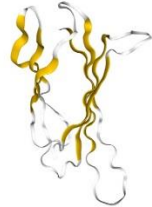
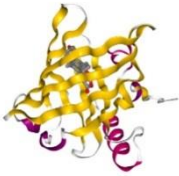
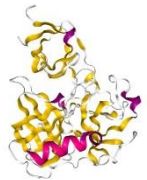
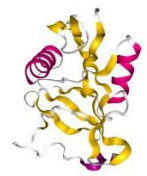
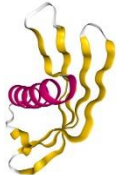
Name	Protein scaffolds	Species origin	Randomization	Structure	PDB	Ref
Adnectin	10 th domain of fibronectin type 3 (10Fn3)	Human extracellular matrix protein fibronectin	3 CDR regions total 20-25 residues		1TTG	(Lipovsek, 2011)
Anticalin	Lipocalins	Human body fluids	16-18 residues		1LNM	(Skerra, 2008)
Kunitz domain scaffold	Protease inhibitors	Human	1-2 loops		1KTH	(Dennis et al., 1995)
Avimer	Low-density lipoprotein receptor A domain	Human	28 residues		1AJJ	(Silverman et al., 2005)

Table 1-5 Examples of loop based binding mechanism non-antibody binding proteins (continue)

Name	Protein scaffolds	Species origin	Randomization	Structure	PDB	Ref
Knottin	Toxins	Spiders Scorpions Marine cone snails	3 disulfide bridges, the so-called cystine knot		2LZX	(Moore et al., 2012)
Fynomer	SH3 domain of human Fyn tyrosine kinase	Human	6 residues in 2 loops		4AFQ	(Schlatter et al., 2012)
Atrimer	Tetranectin	Human	6 – 9 amino acids between 5 loops		1TN3	(Zelensky and Gready, 2005)
Affimer	Protease inhibitor stefin A/phytolectin protein	Human/Plant	18 residues between 2 loops		4N6T	(Tiede et al., 2014)

In the field of non-antibody binding proteins, most research has focused on therapeutic applications to replace and overcome the drawbacks of monoclonal antibodies that have been used as therapeutic agents. However, some non-antibody binding proteins have been used in biosensing application too. Thioredoxins, Affibodies and Affimers are among the binding proteins that have been used in biosensing platforms (Ferrigno, 2016). Thioredoxin (TrxA), sometimes called a peptide aptamer, is an enzyme involving in the cytosolic thiol/disulfide equilibrium of bacteria *Escherichia coli* (*E.coli*). It is small, soluble and stable enzyme with short active site sequence forming accessible binding loops (LaVallie et al., 1993; Skerra, 2007). Regarding biosensing applications, Thioredoxin-based peptide aptamer microarrays were developed by Laurenson et al. (2011) for detection of endogenous cellular proteins; cyclin-dependent kinases 2 and 4 (CDK2 and CDK4) and virally encoded E6/E7 proteins from human papilloma virus (HPV) infected cells.

The Affibody is a non-antibody binding protein based on the protein A scaffold at the immunoglobulin G binding domain, called the Z domain. It consists of 58 amino acids with a binding loop mechanism. In 2005, Affibodies were successfully used in two different biosensing platforms. There were a real-time SPR biosensor and a microarray system (Renberg et al., 2005). It is interesting that the orientated Affibodies on the SPR sensor proved to significantly increase the sensitivity of the technique. However, it was not the case for the microarray system. In other work conducted by the same group, Affibody recognition ability was tested against IgA-, IgE-, IgG-antibodies, TNF- α , insulin and *Taq* DNA polymerase by using fluorescent-labeled analytes when the Affibodies were immobilized on microarray slides (Renberg et al., 2007). In addition, Affibody specific to human epidermal growth factor receptor type 2 (HER2) was used in combination with quantum dots (QDs) and iron oxide (IO) NPs for molecular imaging and diagnosis (Gao et al., 2011). Recently, Ravalli et al., (2015) reported the development of impedimetric biosensors using anti-HER2 Affibody as the bioreceptor. The limit of detection (LOD) of HER2 was around 6 $\mu\text{g/L}$.

1.5.2.3 Affimer (Adhiron)

Affimers are engineered protein scaffolds derived from the cystatin family commercialized under collaboration between the University of Leeds, the Leeds BioScreening Technology Group (BSTG) and Avacta Life Sciences Ltd. There are two scaffolds developed based around the human protease inhibitor stefin A and the plant phytocystatin protein, respectively.

In 2014, Tiede et al. successfully developed an engineered binding protein called the 'Adhiron', which now referred to as the Affimer. Its molecular weight is around 12-13 kDa and it contains 92 amino acids. The structure consists of four anti-parallel β -strands and one α -helix (Figure 1-16). The scaffold also contains two variable regions forming binding loops, similar to the CDR loops of antibodies. Randomization takes place within nine residues of each loop in generating the Affimer library. The generation of the Affimer library commenced with the preparation and modification of a consensus sequence derived from plant phytocystatins from many species. The coding region of the Affimer scaffold was cloned between NheI and NotI restriction sites in phagemid vector pBSTG1 to produce the Affimer/truncated pIII fusion protein in the ER2738 suppressor cells for phage display. Randomization was done by randomly introducing three base pairs at a time as a single codon for each of the 19 amino acids (excluding cysteine and stop codons). A high quality recombinant protein library could be generated with 3×10^{10} clones and 86% complexity.

The advantage of using non-antibody binding proteins in a biosensing platform is that a uniform protein can be produced by a cheaper and less complicated process, which enables long-term availability. In addition, because of their compact size, they can be packed on to the surface of biosensor more densely as compared to larger antibodies, which may enhance the sensitivity of the sensing platform. Due to their small size, the bioreceptors are immobilized closer to the surface of sensors than larger antibodies. Again, for some types of application this can help improve platform sensitivity (Tiede et al., 2014; Ferrigno, 2016).

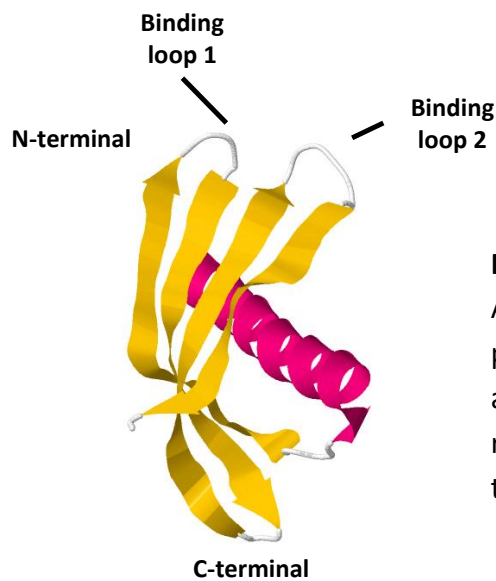


Figure 1-16 Molecular structure of an Affimer (PDB file 4N6T). Four anti-parallel β strands and one α helix strand are shown in yellow and pink, respectively. The two binding loops at the N-terminal are shown in grey.

So far, Affimers have proved to be as effective as antibodies in standard techniques such as Western blotting and ELISA (Tiede et al., 2014). In addition, Tiede et al., (2017) demonstrated further the use of Affimers in molecular and cell biology applications. For example, Affimers were used for *in vivo* imaging of the colorectal cancer marker Tenascin C. Affimers against Tenascin C were screened, characterised and used for tumour imaging compared to anti-Tenascin C antibody. The results were similar between the Affimer and antibody staining patterns. Moreover, Affimers have been used for super resolution microscopy, Affinity histochemistry, inhibiting extracellular receptor function and modulating ion channel activity (Tiede et al., 2017).

In terms of biosensing applications, Raina et al., (2015) successfully developed an Affimer-based impedimetric biosensor for detection of the anti-myc tag IgG. In this work, 34 Affimers against anti-myc tag IgG were screened from a phage library: 20 Affimers were selected via their affinities obtained by bio-layer interferometry (BLI). After ELISA was performed, anti-myc IgG Affimer clones 2 and 13 showed the highest responses, but clone 13 aggregated and therefore Affimer clone 2 was used in the sensor system. In addition, the thermal stability of the Affimer clone 2 was investigated using differential scanning calorimetry (DSC). No

degradation observed at temperature below 85 °C. The impedimetric biosensor was constructed via EDC/NHS amine coupling chemistry between amines of the Affimer and carboxylic group of monothiol-alkane-PEG-acid self-assembled monolayer (SAM) on a gold electrode. The sensor could detect 6.7 – 330 pM of anti-myc tag antibodies.

1.6 Project aims and impact statement: potential applications

The main objective of this project is to develop a NP size-shift assay coupling with DLS by using a non-antibody binding proteins, Affimers, as bioreceptors, Figure 1-17 shows a schematic of a proposed NP-coupled DLS assay. The Affimers are immobilized on AuNPs forming nanobiosensors. When the target analytes are added to the system, specific binding between the Affimers and the analytes will lead to crosslinking of the NPs and aggregates will form. Without needing separation of the excess AuNPs, the mean AuNP probe/aggregate size is determined via DLS. For complete quantitation, calibration curves can be obtained using standard solutions. Affimers will be screened and specifically characterized for use in the size-shift assay. In addition, the Affimer conjugated AuNPs will be investigated in terms of optimum concentration required for nanobiosensor preparation, the kinetics of the system as well as other related factors affecting the assay such as NP concentration or size. Finally, the reproducibility and stability of nanobiosensors are also examined.

As mentioned in section 1.4.4, the challenge remaining in the field of NP-coupled DLS assays is to produce bioreceptors-modified AuNPs with good stability, especially the maintenance of binding activity, because the binding event is the key in controlled aggregation and directly affects the sensitivity of the assay. Therefore, by replacing antibodies with more stable bioreceptors such as Affimers, the AuNPs obtained should give reproducible assay results and be stable for long term use. In comparison, antibodies used in the size shift assay are polyclonal and there have been several reports about the batch-to-batch variations of pAb. Hence, the binding activity should remain the same with the Affimers as they will not have the inhomogeneity problem. Additionally, there are also numerous reports using monoclonal antibodies for the size shift assay. However, at least two mAbs are required to crosslink AuNPs, which can restrict assay development in terms of production cost, so Affimers might be a solution to this problem as it is much cheaper to produce.

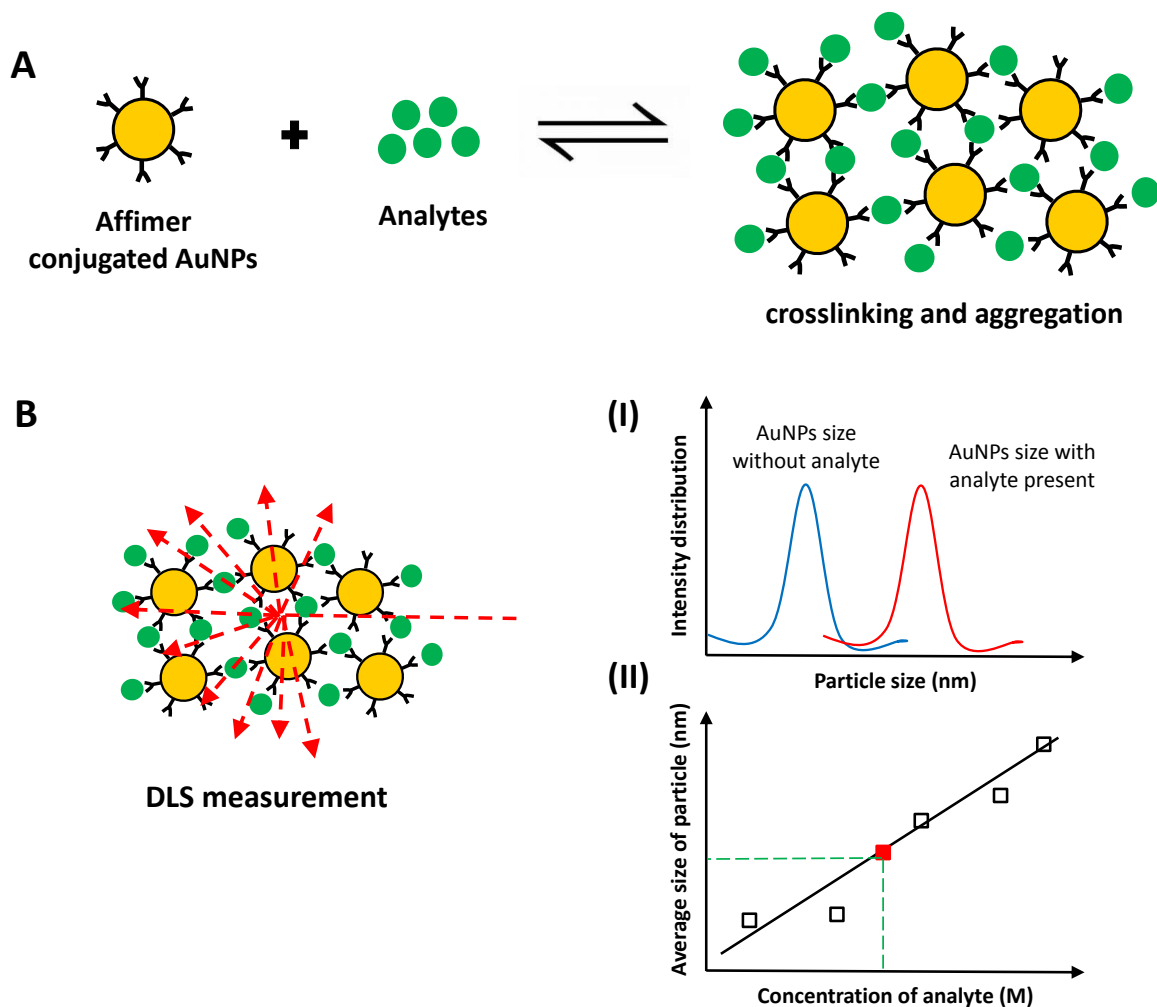
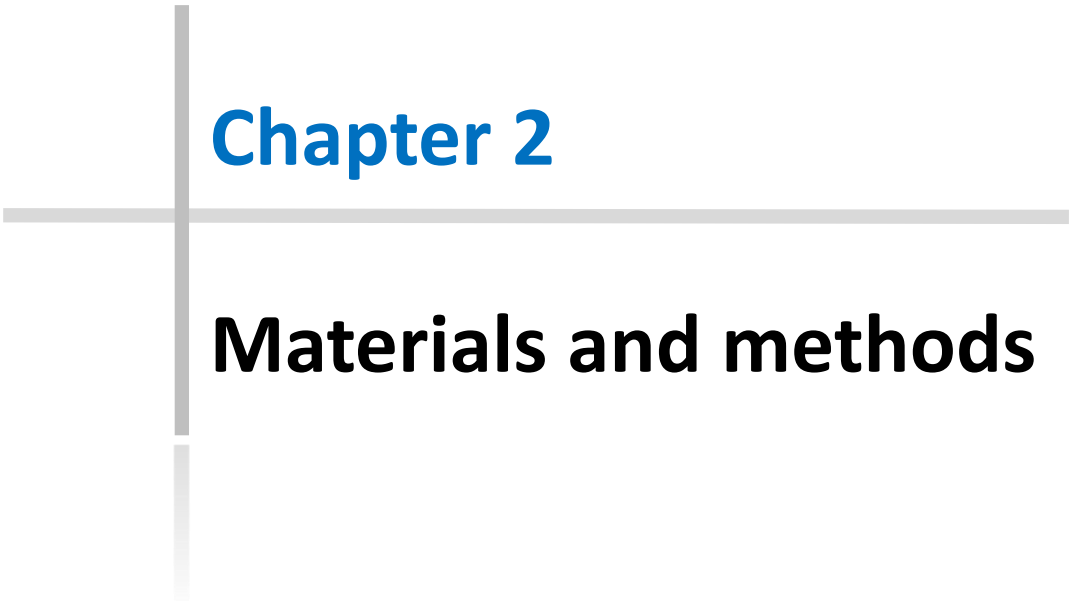


Figure 1-17 Schematic of NP-coupled DLS size shift assay. (A), Affimers for specific analyte are conjugated onto AuNPs and act as nanobiosensors. With the presence of analytes in the system, specific binding between the Affimer and analyte will lead to crosslinking and aggregation of the AuNPs. (B), DLS is used in detection of crosslinking and aggregation by measuring: (i), size shift of AuNPs before and after adding analytes to the system. The complete quantitation can be performed by generating a calibration curve, (ii).

The size shift assay using DLS is a label-free technique for which a wide variety of applications have been reported. By using a novel bioreceptor, the Affimer, the proposed assay could be an alternative technique with consistency of reagent quality and no interference from tagging molecules such as chromophores or fluorophores. A future aim is to develop a novel size-shift assay platform for screening purposes.

This would be useful for industries such as pharmaceuticals, food or agriculture. With more stable bioreceptors, there is potential to produce a ready-to-use kit for people in the field work to operate with only one instrument and one-step homogeneous assay. This particular assay will benefit developing countries particularly in terms of cost reduction, since DLS instruments are fairly common and not too expensive. In addition, if we can reduce the price of bioreceptors, the assay will be more accessible to most laboratories. Finally, a DLS plate readers are commercially available so there is an opportunity to develop a high-throughput system for detection and to study protein-protein interactions.



Chapter 2

Materials and methods

Chapter 2 Materials and Methods

2.1 Materials

2.1.1 Inorganic materials

Potassium iodide (KI), sodium chloride (NaCl) and sodium phosphate monobasic (NaH₂PO₄) were obtained from BDH laboratories and Fisher Scientific, respectively. Iodine (I₂) and sodium periodate (NaIO₄) were purchased from Sigma-Aldrich.

2.1.2 Organic materials

Myoglobin from equine heart, biotin maleimide, dimethyl sulfoxide (DMSO), imidazole and bovine serum albumin (BSA) were obtained from Sigma-Aldrich. Pierce® immobilized tris(2-carboxyethyl)phosphine (TCEP) gel, glycerol, EZ-link™ *N*-hydroxysuccinimide (NHS)-biotin, EZ-link™ hydrazide-biotin, high sensitivity streptavidin conjugated horseradish peroxidase (HRP), enhanced chemiluminescent (ECL) western blotting substrate and Glycolink™ coupling catalyst (containing GlycoLink coupling buffer; 0.1 M sodium acetate, 0.15 M NaCl, pH 5.5 and aniline) were purchased from Thermo Fisher Scientific. 3,3',5,5'-tetramethylbenzidine (TMB) substrate (Seramun® fast) was purchased from Seramun Diagnostica GmbH. *Clostridium difficile* toxin B and anti-*Clostridium difficile* toxin B Affimers (Clone 18C and 45C) were provided by the Leeds BioScreening Technology Group (BSTG).

2.1.3 Antibodies

All antibodies used in this project are summarised in Table 2-1.

Table 2-1 Summary of all antibodies used in this project

Antibody	Origin	Source
Anti-myoglobin	Rabbit polyclonal IgG	GenScript Ltd.
Anti-rabbit IgG-HRP	Goat polyclonal IgG	GenScript Ltd.
Anti-His ₆ -HRP	Rabbit polyclonal IgG	AbCam Plc.

2.1.4 Buffers and solutions

10X phosphate buffer saline (PBS) was purchased from Cambridge Bioscience and diluted with deionised water to 1X before used. 10X Tris-glycine SDS-PAGE running buffer and quick Coomassie stain were obtained from Bio-Rad Laboratories and Generon Ltd, respectively. Bradford dye reagent ready-to-use solution was purchased from Alfa Aesar. 10X blocking buffer and Tris were purchased from Sigma and Bio Basic Canada Inc, respectively. Glycine and acetic acid were purchased from BDH laboratory supplies. Tween-20[®] was obtained from Sigma-Aldrich. All other buffers were prepared in the laboratory and the summary of buffers used in this project is shown in Table 2-2.

Table 2-2 Summary of buffers used in this project

Name	Ingredients	pH	Application
1X PBS	137 mM NaCl; 10 mM phosphate; 2.7 mM KCl	7.4	General use
TE	10 mM Tris; 1 mM EDTA	8.0	Phage display
Glycine	0.2 M glycine	2.2	Phage display
Tris	1 M Tris-HCl	7.0 9.1	Phage display
1X TGS	25 mM Tris; 192 mM glycine; 0.1% (w/v) SDS	8.3	SDS-PAGE gel
PBS-T	1X PBS + 0.1% (v/v) Tween-20	7.4	Phage display ELISA
TAE	40 mM Tris; 20 mM acetate; 1 mM EDTA	8.6	Electrophoresis gel
Lysis buffer	50 mM NaH ₂ PO ₄ ; 300 mM NaCl; 30 mM imidazole; 10% (v/v) glycerol	7.4	Extraction and purification of Affimer
Wash buffer	50 mM NaH ₂ PO ₄ ; 500 mM NaCl; 30 mM imidazole; 10% (v/v) glycerol	7.4	
Elution buffer	50 mM NaH ₂ PO ₄ ; 500 mM NaCl; 300 mM imidazole; 20% (v/v) glycerol	7.4	

2.1.5 Kits and consumables

QIAGEN® Miniprep and plasmid Maxi kits were obtained from QIAGEN. NucleoSpin® Gel and PCR clean-up kit and 14 ml round-bottom polypropylene tubes were purchased from Macherey-Nagel and BD Falcon™, respectively. Millex®-GP filter unit (0.22 µm) and Mini-protein TGX precast protein gels (4-15% w/v, 12-well) for SDS-PAGE were purchased from Merck and Bio-rad laboratories, respectively. Nunc-Immuno™ Maxisorp™ 96-well solid plates and Eppendorf® protein LoBIND microcentrifuge tubes (1.5 ml) were purchased from Sigma-Aldrich. Zepa™ spin desalting columns (0.5 and 2 ml), small volume disposable cuvettes and NanoOrange™ protein quantitation kit were purchased from ThermoFisher Scientific. Corning® 15 and 50 ml centrifuge tubes and Pur-A-Lyzer™ Mini 6000 dialysing units were purchased from Sigma.

2.1.6 Growth media for bacteria and antibiotics

Carbenicillin disodium salt and kanamycin were obtained from Alfa Aesar in powder form and the stock solutions were prepared in sterile deionised water at 50 mg/ml and 25 mg/ml, respectively. Tryptone and agar were obtained from Sigma-Aldrich, whilst glucose and yeast extract were purchased from BDH laboratories and Oxoid respectively. All media used in this project are summarised in Table 2-3.

Table 2-3 Summary of all growth media for bacteria used in this project

Media	Ingredients
Luria-Bertani (LB)	Per 1 L: 10 g tryptone; 5 g yeast extract; 10 g NaCl
LB agar plate	Per 1 L: LB media + 15 g agar
2TY	Per 1 L: 16 g tryptone; 10 g yeast extract; 5 g NaCl
Super optimum broth (SOB)	Per 1 L: 20 g tryptone; 5 g yeast extract; 0.5 g NaCl; 10 ml of each 1 M MgCl ₂ and MgSO ₄
SOB with catabolite repression (SOC)	Per 100 ml: 2 ml of 20% (w/v) glucose + 98 ml of SOB media

2.1.7 Phage display and phage ELISA related materials

Nunc-Immuno™ Maxisorp™ strips, streptavidin coated (HBC) 8 –well strips, deep well 96 plate, KingFisher (200 µl) 96 plate, Neutravidin coated (HBC) 8-well strips were purchased from Thermo Scientific. Streptavidin beads (Dynabeads® MyOne™ Streptavidin T1, 10 mg/ml) were purchase from Invitrogen. Triethylamine and glycerol were purchased from Sigma-Aldrich. Anti-Fd-bacteriophage-HRP was obtained from Seramun Diagnostica GmbH. Tetracycline hydrochloride (1000x stock: 12 mg/ml in 70% (v/v) ethanol), ER2738 *E.coli* cells, M13K07 helper phage (titre ca. 10¹⁴/ml) and PEG-NaCl precipitation solution (20% (w/v) PEG 8000, 2.5 M NaCl) were prepared in the laboratory.

2.1.8 Subcloning Affimer DNA related materials

pET11a vector was provided by the BSTG. NotI-HF™ (20,000 units/ml), NheI-HF™ (20,000 units/ml), CutSmart™ buffer, 10X Antarctic phosphatase reaction buffer, Antarctic phosphatase (5,000 units/ml), DpnI, T4 DNA ligase (400,000 units/ml), 10X T4 DNA ligase reaction buffer and 6X orange G loading dye were purchased from New England Biolab® Inc. Phusion high-fidelity DNA polymerase containing phusion DNA polymerase (2 units/µl), 5X phusion HF buffer and DMSO were purchased from Thermo Scientific. dNTPs mix 25 mM was obtained from MB Biomedicals. XL1 blue supercompetent cells and agarose were obtained from Agilent technologies and Melford Laboratories Ltd, respectively. PCR primers; forward primer (Affimer short 5' – ATGGCTAGCGGTAACGAAAACCTCCCTG) and reverse primer (pDHis-C-rev 5' – TTACTAATGCGGCCGCACAAGCGTCACCAACCGGTTTG) were purchased from Sigma.

2.1.9 Expression and purification of Affimer related materials

BL21-Gold(DE3) competent cells and isopropyl β -D-1-thiogalactopyronoside (IPTG) were obtained from Agilent technologies and Promega, respectively. Pierce disposable column 2 ml and Halt protease inhibitor cocktail (100X) were purchased from Thermo Scientific. Bugbuster® 10X protein extraction reagent and Benzonase® nuclease, purity >99% were purchased from Novagen®. Amintra nickel-nitrilotriacetic acid (Ni^{2+} -NTA) resin was obtained from Expedeon. Lysis, wash and elution buffers were prepared in the laboratory using the ingredients summarised in Table 2-2.

2.1.10 Gold nanoparticles (AuNPs)

Streptavidin coated AuNPs (strep-AuNPs) with core diameter of 20 and 40 nm were purchased from BBI™ Solutions; whilst strep-AuNPs with core diameter of 60, 80 and 100 nm were obtained from Cytodiagnosics Inc.

2.2 Methods

2.2.1 Affimer production

2.2.1.1 Phage display

Biotinylation of target molecule; myoglobin (Mb) was biotinylated using biotin *N*-hydroxysuccinimide (NHS). First, Mb was dissolved in 1X PBS buffer (pH 7.4) at a concentration of 1 mg/ml, whereas biotin NHS was dissolved in DMSO (5 mg/ml). Next, 10 µl of 1 mg/ml Mb solution was added to 0.8 µl of biotin NHS and the total volume was adjusted to 100 µl using the PBS buffer. The mixture was incubated for 1 h at RT. Free biotin was removed by using a Zeba Spin Desalting Columns (7K MWCO). Then, 100 µl of 80% (v/v) glycerol was added to the mixture. The solution was stored at -20 °C.

ELISA was performed to check the success of biotinylation. Nunc-Immuno™ MaxiSorp™ strip was used for the ELISA. First, 50 µl of 1X PBS buffer (pH 7.4) were added to each well of the strip (four wells). The volumes of 1, 0.1 and 0.01 µl of biotinylated target were added to first three wells. After the strip was incubated overnight at 4 °C, 300 µl of 1X PBS (pH 7.4) + 0.1% (v/v) Tween-20 (PBS-T) were used to wash each well three times. Then, each well was blocked with 250 µl of 10x blocking buffer and incubated 3 h at 37 °C. PBS-T was used to wash three times before 50 µl of diluted high sensitivity streptavidin-HRP (1:1000 in 2x blocking buffer) were added to each well. The strip was incubated on a vibrating platform shaker for 1 h at RT and washed with PBS-T six times using the plate washer. Next, 50 µl of 3,3',5,5'-tetramethylbenzidine (TMB) substrate (SeramunBlau®) were aliquoted per well and colour allowed to develop for 3 min before measuring the absorbance at 620 nm.

Phage display screening; four panning rounds of phage display were performed in this experiment. For the first panning round, biotinylated Mb was bound to streptavidin-coated well for 2 h in the panning well, and then 5 µl of pre-panned phage library was added. The mixture was incubated for 2 h at RT on a vibrating platform shaker. After that, the panning well was washed 27 times with 300 µl of

PBS-T using a plate washer and eluted with 100 μ l of 0.2 M glycine (pH 2.2) for 10 min. Then, neutralisation was performed by adding 15 μ l of 1 M Tris-HCl (pH 9.1). The eluted phage was transferred immediately to an 8 ml aliquot of the ER2738 cells in a 50 ml Falcon tube. Second elution was performed by adding 100 μ l of the diluted triethylamine (14 μ l of triethylamine in 986 μ l of 1X PBS) and incubated for 6 min at RT. The neutralisation was done by adding 50 μ l of 1 M Tris-HCl (pH 7). The second eluted phage was transferred immediately to the ER2748 cells tube. The tube filled with ER2738 cells and eluted phage was incubated for 1 h at 37 °C without shaking and then plated onto LB agar plate with 100 μ g/ml carbenicillin (LB carb plate) and grown overnight (1 μ l of the phage-infected ER2738 cells was plated separately, to determine roughly the total number of cells per 8 ml). Colonies were scraped into 5 ml of 2TY media containing 100 μ g/ml carbenicillin and transferred to a 50 ml falcon tube. A further 2 ml of the 2TY media was added to scrape off any remaining cells. The cells were diluted to an 8 ml culture to obtain the absorbance at 600 nm around 0.2. The diluted cells were incubated for 1 h at 37 °C at 230 rpm. Then, they were infected with 0.32 μ l of M13K07 helper phage and incubated for 30 min at 37 °C at 90 rpm. Following this, 16 μ l of kanamycin (25 mg/ml) was added. The mixture was incubated overnight in an orbital incubator at 25 °C at 170 rpm. Next, the phage-infected cultures were centrifuged at 3500 xg for 10 min and the phage-containing supernatant was transferred to a fresh tube. Then, 2 ml of PEG-NaCl precipitation solution (20% (w/v) PEG 8000, 2.5 M NaCl) was added to the supernatant and the mixture was incubated overnight. The phage was centrifuged at 4,800 xg for 30 min to pellet the phage. This time the supernatant was removed and the pellet was resuspended with 320 μ l of buffer containing 10 mM Tris and 1 mM EDTA (TE buffer – pH 8) and transferred to a microcentrifuge tube to be centrifuged at 16,000 xg for 10 min. The phage-containing supernatant was recovered and stored at 4 °C.

For the second panning round of selection, streptavidin magnetic beads were used instead of the plate. Biotinylated Mb 15 μ l was added to 200 μ l of 2x blocking buffer with 50 μ l of the pre-blocked streptavidin beads and incubated for 1 h on a rotator. Meanwhile, 125 μ l aliquot of phage suspension from the first panning round was pre-panned by using pre-blocked streptavidin beads. Following this, the suspension

containing biotinylated Mb and the pre-panned phage suspension were centrifuged at 800 xg for 1 min and both tubes were placed on a magnet. The beads containing biotinylated Mb were washed three times with 500 µl of 2x blocking buffer and added to the supernatant containing the pre-panned phage. The beads were resuspended and transferred to the pre-blocked 96-deep-well plate. The plate was then put in the KingFisher Flex machine, which was set to run “Phage_display_pH_elution” protocol (Appendix 1). Similar to the first panning round, the bound phages were eluted and amplified in the same conditions.

For the third and fourth panning rounds, the method was exactly the same as the first panning round but using Neutravidin high binding capacity (HBC) and streptavidin coated plates instead, respectively. Also, 200 µl of phage-containing supernatant from the second and third panning rounds were used in the pre-panning steps, correspondingly. In the final panning round, the negative control with no Mb was also performed. Both panning and negative wells were washed three times with PBS-T, added with 100 µl of phage from the pre-pan well and incubated for 30 – 45 min at RT on a vibrating platform. After that, both wells were washed 27 times with 300 µl of PBS-T using a plate washer. The phage were eluted and amplified as mentioned above in the first panning round. But, this time the phage were plated with a range of volumes (0.1, 1, 10 and 100 µl) onto LB carb plates. For the negative controls, only 10 µl was plated in order to compare the result.

2.2.1.2 Phage ELISA

First, 48 individual ER2738 colonies from last panning round of phage display were picked and grown overnight in 200 µl 2TY media with 100 µg/ml carbenicillin in a 96-well V-bottom deep well plate at 37 °C with shaking 1050 rpm. A 25 µl of the overnight culture was transferred to new plate containing 200 µl of the 2TY and grown at 37 °C for 1 h at 1050 rpm in the incubating microplate shaker. After this, 10 µl of diluted M13K07 helper phage (titre ca. 10^{14} /ml) (1/1000) was added per well to a freshly grown culture using a multichannel pipette and incubated for 30 min at RT

in an incubating microplate shaker at 450 rpm. Following this, 10 µl of 1/20 diluted kanamycin stock (25 mg/ml) was added per well to the phage-infected cultures and incubated overnight at RT in the shaker at 750 rpm. Next, the phage infected-culture were centrifuged at 3500 xg for 10 min. The supernatant containing the phage was transferred to the ELISA plate to test for the binding to Mb.

A 50 µl aliquot of 5 mg/ml streptavidin was added into each well of a Nunc-Immuno™ Maxisorp™ 96-well plate and incubated overnight at 4 °C. After that, each well was blocked with 200 µl of 2x blocking buffer and incubated overnight at 37 °C. The plate was washed three times with 300 µl per well of PBS-T on a plate washer. Then, 50 µl per well of diluted biotinylated Mb (1/1000) were added into the first six columns of the streptavidin-coated 96-well plate. For the last six columns, 50 µl per well of 2x blocking buffer were added as negative control wells. The plate was incubated for 1 h at RT on a vibrating platform shaker. After that, it was washed three times with 300 µl per well of PBS-T and added with 10 µl per well of 10x blocking buffer. A 40 µl per well of phage-containing supernatant was added, each one was tested against the target and a negative control well (e.g. binder A1 was added to wells A1 and A7), and incubated for 1 h at RT on the shaker. The plate was washed six times with 300 µl per well of PBS-T before 50 µl per well of diluted anti-Fd-bacteriophage-HRP (1/1000) were added, incubated for 1 h at RT and washed ten times with PBS-T. Following washing, phage were visualised using TMB substrates with 3 min reaction time and the absorbance at 620 nm was measured.

2.2.1.3 DNA sequencing

Positive wells from the phage ELISA were selected for sequencing. 10 µl of the overnight culture plate from phage ELISA was grown in 3 ml of 2TY with 100 µg/ml of carbenicillin in the round bottom tube per well at 37 °C with 230 rpm in a shaking incubator. A QIAGEN® miniprep kit was used according to the instructions provided to extract the phagemid DNA. DNA concentrations were determined by measuring absorbance at 260 nm using a Nanodrop spectrometer. Then, 15 µl of each selected

phagemid DNAs were sent out to Beckman Coulter Genomics for sequencing at a DNA concentration < 100 ng/μl.

2.2.1.4 Subcloning Affimer DNA

Digestion of pET11a vector: initially, transformation of pET11a vector was carried out into XL-1 supercompetent cells. The competent cells were slowly thawed on ice; whilst 1 μl of pET11a DNA was aliquoted into a 1.5 ml low protein binding Eppendorf tube and pre-chilled on ice. Then, 10 μl of the competent cells were added to the pre-chilled DNA and incubated on ice for 30 min. The cells were heat shocked in a 42 °C water bath for 45 s before incubating on ice again for 2 min. Next, 180 μl of SOC media was added to the cells and incubated for 1 h at 37 °C with shaking at 230 rpm. The cells (100 μl) were then spread onto a LB carb plate and grown overnight at 37 °C. The vector was then multiplied using a QIAGEN® plasmid Maxi kit by following the instructions for low-copy plasmids and vector DNA was eluted in 400 μl sterile deionised water. The concentration of digested vector DNA was measured using a Nanodrop spectrometer at 260 nm.

Next, 5 μg of pET11a plasmid was digested with NheI and NotI restriction enzymes overnight at 37 °C. The following day, Antarctic phosphatase enzyme was added and incubated for 15 min at 37 °C. After that, it was inactivated by heating at 65 °C for 5 min. Then, 20 μl of 6X orange G loading dye was added and the digested vector was separated on a 0.7% (w/v) agarose gel. The gel was run in 1X TAE buffer at 100 V for 1 h. The digested vector was extracted from the gel using a NucleoSpin gel and PCR clean-up kit according to the manufacturer's instructions and eluted in 50 μl of sterile deionised water. The concentration of digested vector DNA was measured using a Nanodrop spectrometer and stored at -20 °C until ready for ligation process.

PCR amplification of the Affimer DNA sequences from the phagemid vector: the sequences of forward and reverse primers were provided by the BSTG. The C-terminal cysteine was added in this step by using the pDHis-C-rev reverse primer. A

25 µl PCR reaction was set up in a 0.2 ml PCR tube according to the following formula provided in Table 2-4.

Table 2-4 Summary of PCR 25 µl reaction set up for Affimer DNA amplification

Component	25 µl Reaction	Final Concentration
Sterile deionised water	13.8 µl	
5X Phusion HF buffer	5 µl	1X
dNTPs mix, 25 mM	0.2 µl	200 µM each
DMSO	0.75 µl	3%
Forward primer, 10 µM	2 µl	0.8 µM
Reverse primer, 10 µM	2 µl	0.8 µM
Phusion DNA polymerase	0.25 µl	0.02 units/µl
Template DNA (phagemid vector)	1 µl	

The PCR tube was transferred to a PCR machine thermocycled under conditions shown in Table 2-5. After that, the PCR product was cleaned up by using a NucleoSpin gel and PCR clean-up kit according to the manufacturer's instructions and eluted in 50 µl of sterile deionised water. Then, 50 µl of PCR product was digested with NheI and NotI restriction enzymes by incubating at 37 °C overnight. Finally, 0.5 µl of DpnI enzyme was added to remove methylated template DNA. Again, the product was purified using a NucleoSpin gel and PCR clean-up kit similar to previously performed. The concentration was measured using a Nanodrop spectrometer.

Table 2-5 Thermocycling conditions used for Affimer DNA amplification via PCR

Cycle Step	Temperature	Time	Cycles
Initial denaturation	98°C	30 seconds	1
Denaturation	98°C	20 seconds	30
Annealing	54°C	20 seconds	
Extension	72°C	20 seconds	
Final Extension	72°C	10 minutes	1
Hold	4°C	Hold	

Ligation of the NheI-NotI digested insert into the pET11a vector: ligation was carried out by mixing 40 ng of digested pET11a vector with 10 ng of insert DNA with the presence of DNA ligase (0.5 µl of T4 DNA ligase + 0.5 µl of 10X T4 DNA ligase buffer + sterile deionised water to make a total volume of 5 µl). The mixed solution was incubated overnight at RT. The negative control was also set up using the pET11a vector only. The ligation mix was transformed into XL-1 supercompetent cells by heat shock method as described earlier. The negative control plate should show no colonies.

Colonies from ligation mix plate were picked and grown in 3 ml of LB media containing carbenicillin (100 µg/ml) overnight at 37 °C with shaking 230 rpm. The plasmid DNA was extracted using a QIAGEN® miniprep kit according to the manufacturer's instruction but eluted in 50 µl sterile deionised water and sent out for sequencing to confirm the success of the subcloning process.

2.2.1.5 Expression of Affimer

Expression of Affimers was performed using the isopropyl β-D-1-thiogalactopyranoside (IPTG) induced expression method. First, the Affimer-pET11a plasmid was transformed into BL21-Gold (DE3) competent cells by using a heat shock protocol previously described in section 2.2.1.4. The start-up culture was prepared the following day by selecting and growing colonies overnight in 2 ml of 2TY containing carbenicillin (100 µg/ml) and 1% (w/v) glucose at 37 °C with shaking 230 rpm. Meanwhile, 50 ml of LB media was placed at 37 °C in a 250 ml flask overnight to warm the media. Next day, 100 µl of 50 mg/ml carbenicillin was added to the pre-warmed media, following by 625 µl of the overnight culture. The culture was grown until its optical density (OD) at 600 nm reached around 0.8 before adding IPTG to a final concentration of 0.1 mM. Then, the culture was incubated for an additional 18 h at 25 °C with shaking 150 rpm. The cells were harvested by centrifugation at 3,220 xg for 30 min using an Eppendorf centrifuge, model 5810R. The supernatant was removed and the cell pellet was stored at -20 °C until ready for purification.

2.2.1.6 Extraction and purification of Affimer

First, the cell pellet was thawed and resuspended in 1 ml of lysis buffer supplemented with Bugbuster® protein extraction reagent, Benzonase® nuclease and protease inhibitor cocktail (Table 2-6). The solution was transferred to a 2 ml microcentrifuge tube and incubated for 20 min on a rotator at RT. Next, the pellet was incubated at 50 °C in a water bath for 20 min to denature non-specific proteins (this step was optional for some Affimers). The solution was then centrifuged at 16,000 xg for 20 min to pellet the cell debris and insoluble proteins. Meanwhile, 300 µl of Ni²⁺-nitrilotriacetic acid (Ni²⁺-NTA) resin was resuspended in 1 ml lysis buffer in a 2 ml tube and washed one time by centrifugation at 1,000 xg for 1 min to sediment the resin and the buffer was carefully removed using a pipette.

Table 2-6 Showing the volume of supplement reagents in lysis buffer used for Affimer extraction

Reagents	Volume for 50 ml culture cell pellet
Bugbuster® 10X protein extraction reagent	100 µl (1X)
Benzonase® nuclease, purity > 99% (25 U/µl)	0.4 µl (10 U/ml)
Halt protease inhibitor cocktail (100X)	10 µl (1X)
Lysis buffer	to a total volume of 1 ml

The supernatant above the cell pellet containing soluble proteins was transferred to the washed resin and incubated for 2 h on a rotator at RT. After incubation, the mixed solution was centrifuged at 1,000 xg for 1 min to sediment the Affimer-bound resin. The supernatant was transferred to a fresh tube and kept at -20 °C to check whether there were unbound Affimers left or not. A Pierce disposable 2 ml column was used to facilitate the purification. The Affimer-bound resin was resuspended in 1 ml wash buffer and moved to the equilibrated column. The resin was washed with wash buffer several times until the absorbance at 280 nm of the wash buffer was consistently lower than 0.09. The Affimers were eluted with 500 µl of elution buffer.

The concentration of Affimers were determined using a Nanodrop spectrometer and biotinylation was performed immediately.

2.2.1.7 Biotinylation of Affimer

Affimers were biotinylated via maleimide coupling chemistry to the thiol group (-SH) of their C-terminal cysteine. Before starting the biotinylation process, immobilized TCEP reducing gel was used to reduce Affimer disulphide bonds to make sure that all -SH were available for labelling. First, 150 μ l of TCEP gel was washed with PBS containing 1 mM EDTA three times. Then, 4 μ l of PBS containing 50 mM EDTA, followed by adding of 150 μ l of 0.5 mg/ml Affimer. The mixture was incubated for 1 h at RT on a rotator (20 rpm) to keep the gel in suspension. After that, the mixture was centrifuged (1,000 \times g, 1 min) and the supernatant containing the reduced Affimer was recovered.

For biotin labelling, 5 mg biotin maleimide was dissolved in 1 ml of DMSO. Then, a 6 μ l aliquot was immediately added to the reduced Affimer. This was incubated at RT for 2 h. After that the free biotin maleimide was removed by using a Zepa spin desalting column (7K MWCO). The biotinylation was confirmed by ELISA (described in 2.2.1.1) and the samples were sent out to the Mass Spectrometry Facility (Faculty of Biological Science, University of Leeds) to confirm the success of biotinylation.

2.2.2 Characterisation of Affimers

2.2.2.1 Immunoprecipitation (pull-down assay)

All selected anti-Mb Affimers and Mb were dialysed in 1X PBS (pH 7.4) prior to the pull-down assay. First, 40 μ l of Ni²⁺-NTA resin was washed three times with wash buffer by centrifugation and resuspended in 40 μ l wash buffer. Then, 200 μ g of Affimer was added to the washed resin and incubated at 4 °C on a rotator for 90 min.

Next, the Affimer-loaded resin was centrifuged at 1,000 xg to remove unbound Affimers, following by a single wash with wash buffer. The same amount of Mb was added to the loaded resin and incubated overnight at 4 °C on a rotator. After that, the unbound Mb was removed by centrifugation at 1,000 xg, following by three washes with 1 ml wash buffer. After the final wash, the resin was resuspended in 60 µl of wash buffer and ready for confirmation. An SDS-PAGE gel was run with all fractions collected from the pull-down assay, which were unbound Affimer, washed Affimer, unbound Mb, all three washes to remove free Mb and the lysate.

First, 10 µl of each fraction was mixed with 10 µl of reducing dye and boiled at 95 °C for 5 min. Then, the mixed solutions were centrifuged at 16,000 xg for 5 min to sediment the resin. After that, 10 µl of the supernatants were loaded into the precast gel (4-15% (w/v)) along with 5 µl of protein ladder. The gel was run at 100V for 75 min with 1X Tris-glycine running buffer and developed with quick Coomassie stain dye for 1 h at RT.

2.2.2.2 Direct ELISA

First, Neutravidin-coated 96-well plate was prepared from Neutravidin in lyophilized form. The Neutravidin stock of 1 mg/ml was prepared using 100 mM PBS (store at -20 °C). Neutravidin at a concentration of 5 µg/ml in 100 mM PBS was added (50 µl/well) into a Nunc-Immuno™ Maxisorp™ 96-well plate. The plates were incubated overnight at 4 °C before used. The plate was blocked with 200 µl of 2x blocking buffer per well, overnight at 37 °C. The plate was then washed one time with PBS-T. Biotinylated Mb 1 mg/ml (prepared as mentioned in section 2.2.1.1) was diluted 1:1000 in 2x blocking buffer and aliquoted 50 µl per well and incubated at RT for 1 h on a plate shaker (400 rpm). Then, the plates were washed three times with PBS-T. Next, 10 µl of 10x blocking buffer was added into each well together with 40 µl of 0 – 100 µg/ml Affimers. Incubation was carried out at RT for 1 h on a shaking platform at 400 rpm. After three washing steps with PBS-T, 50 µl of anti-His₆-HRP (1:1000) in 2x blocking buffer were added as a secondary antibody and incubated at RT for 1 h

on a plate shaker (400 rpm). The washing was performed six times with PBS-T and TMB substrate was added 50 µl per well and colour allowed to develop for 5 min before measuring absorbance at 620 nm.

2.2.2.3 Surface plasmon resonance (SPR)

All Affimers were dialysed in filtered sterile 1X PBS containing 0.01% (v/v) Tween-20 (pH 7.4) before characterised with SPR.

Calibration free concentration analysis (CFCA): CFCA was carried out to quantify the active concentration of Affimers by using anti-His₆ Ab immobilised onto a carboxymethylated dextran (CM5) chip. The immobilisation was performed via 1-ethyl-3-(3-dimethylaminopropyl)carbodiimide/*N*-hydroxysuccinimide (EDC/NHS) linking of the functional group –COOH of the chip surface to the amine groups of the Ab. After this, ethanolamine was added to block the free –COOH groups on the surface. Next, an estimated 1 mg/ml of Affimer was diluted 1/5000 and injected to the flow cell with two different rates, 5 µl/min and 100 µl/min. The response was plotted against time and linear fitting was carried out. The concentration of Affimer could be calculated based on the diffusion coefficient and the differences in binding rates when injected at different rates.

Kinetics study: once the active concentration of Affimers was obtained, a streptavidin chip was used in kinetics analysis. Biotinylated Mb was first immobilised to the chip surface only on flow cell 2 and acted as the ‘receptor’; whilst flow cell 1 was used as a non-specific control cell (no Mb present). Next, Affimers (0 – 1000 nM) were flowed over both cells and acted as the ‘ligand’. Regeneration was implemented between each concentration of the Affimer using 10 mM glycine, pH 3 as regeneration buffer. Here, buffer only was used in the experiment as well to eliminate a non-specific binding on Mb immobilised surface. The sensorgram between response units and time was plotted using adjusted values by subtracting

both non-specific binding values obtained. The data were analysed using GraphPad Prism 7.

2.2.2.4 Affimer pair selection

To find a binding pair, five selected anti-Mb Affimers were screened by using a modified sandwich ELISA method. First, 50 µg/ml of Affimer was immobilised on a Nunc-Immuno™ Maxisorp™ 96-well plate 50 µl per well and incubated for 16 h at 4 °C. Wells were blocked with 250 µl of 10x blocking buffer for 3 h at 37 °C. Then, wells were washed with 200 µl of PBS-T three times and 50 µl of 50 µg/ml Mb was added per well and incubated 4 h on a plate shaker (400 rpm) at RT. After this the wells were washed six times with 200 µl of PBS-T to remove unbound Mb. The five selected biotinylated Affimers in 2x blocking buffer were added to the wells and left to incubate for 2 h on a shaking platform at RT, following by a ten washing steps with 200 µl of PBS-T. Biotinylated anti-Mb Ab and 1X PBS were used as positive and negative control, respectively. Finally, 1:1000 of streptavidin-HRP in 2x blocking buffer was added to the wells as a secondary antibody to detect biotinylated Affimer. The incubation was carried out for 1 h at RT on a shaker. Finally, the washing was performed ten times with PBS-T and TMB substrate was added 50 µl per well and allowed to develop for 25 min before measuring absorbance at 620 nm.

2.2.3 Preparation of nanobiosensors

2.2.3.1 Biotinylation of bioreceptors

Biotin maleimide was used to biotinylate Affimers as described in section 2.2.1.7; whilst anti-Mb IgGs were biotinylated using biotin hydrazide via the carbohydrate on the Fc region. First, 1 ml of 4.2 mg/ml sodium periodate was mixed with 2 mg/ml anti-Mb IgG in Glycolink coupling buffer and incubated for 30 min at RT protected from light. The excess sodium periodate was removed from the solution using a Zepa

spin desalting column (7K MWCO). Next, 200 μ l of 5 mM biotin hydrazide was added to 1.8 ml of the oxidized and purified solution. After this, 18 μ l of aniline was added to the mixture under a fume hood and incubated for 1 h at RT. Lastly, a new Zepha spin desalting column (7K MWCO) was used to remove the excess biotin hydrazide and aniline. The success of biotinylation for both IgGs and Affimers were confirmed by ELISA (see section 2.2.1.1). In addition, biotinylated Affimers were sent out for mass spectrometry at a concentration of 10 μ M.

2.2.3.2 Streptavidin-biotin coupling

To functionalise gold nanoparticles (AuNPs) via streptavidin-biotin coupling, 25 μ g of biotinylated bioreceptors were added to 1 ml of 40 nm core diameter streptavidin coated AuNPs (strep-AuNPs) (Optical density (OD) at 529 nm = 1) in a total volume of 1.5 ml. In terms of AuNPs, OD is often used as it is directly proportional to the concentration and is always given at the wavelength that shows peak absorbance. The ODs of 20, 40, 60, 80 and 100 nm core diameter streptavidin coated AuNPs were measured at 520, 529, 540, 553 and 572 nm, respectively.

Next, the mixed solutions were incubated for 2 h at RT on a rotator protected from light. After this, the mixture was centrifuged to remove unreacted biotinylated proteins. Table 2-7 shows the appropriate g forces used for different core diameter AuNPs. Following this, washing step was carried out by centrifugation, removal of supernatant and resuspending the AuNPs in PBS buffer. This step was repeated twice before the AuNPs were resuspended in 1 ml of the PBS buffer. The nanobiosensors were kept in a container protected from light at 4 $^{\circ}$ C.

Table 2-7 Appropriate g forces used for AuNPs with different core diameter

Core diameter of AuNPs (nm)	Speed (g)	Time (min)
20	6,500	30
40	4,500	30
60	1,200	30
80	600	30
100	400	30

2.2.4 Characterisation of nanobiosensors

2.2.4.1 Dot blotting

A 3 x 2 cm piece of nitrocellulose membrane was divided into two different areas for negative control and experiment. For both anti-Mb IgG and Affimers, strep-AuNPs was used as negative control. First, 6 μ l of each sample was spotted onto the membranes (by applying 2 μ l at a time, air-drying for 15 min and repeated again). The membranes were then blocked with a 3 ml blocking buffer comprising 5% (w/v) BSA in PBS-T for 1 h on a plate shaker to prevent non-specific binding. After that, the membranes were washed once with PBS-T and incubated with primary antibodies specific for each bioreceptor. For anti-Mb IgG, goat anti-rabbit HRP-conjugated IgG was used; while anti-His₆-HRP conjugated IgG was used for Affimer detection. Both secondary reagents were used at 1:1000 dilution in PBS-T. The incubation was performed for 1 h at RT on a shaker. Then, the membranes were washed by incubating in 5 ml of PBS-T for 5 min and this process was repeated two times. For the last washing step, PBS buffer was used instead of PBS-T as Tween-20 could interfere with the enhanced chemiluminescence (ECL) substrate. In the final step, ECL was applied for signal generation.

2.2.4.2 UV-spectrophotometry

The prepared anti-Mb IgG and Affimer conjugated AuNPs were diluted 1:1 with 1X PBS buffer (pH 7.4) then transferred to a 96-well plate (200 μ l) and scanned across the wavelength of 400 – 700 nm to obtain their UV spectra using a FLUOstar Omega plate reader.

2.2.4.3 Dynamic light scattering (DLS)

The DLS measurement on all sample solutions were made using a Zetasizer Nano series, Nano-ZS DLS system (Malvern Instruments Ltd). The instrument was equipped

with a red (633 nm) laser. The data were analysed using DTS Applications 5.10 software. For each sample, 10 measurement runs with 10 s/run were performed and the average value was reported. All measurements were performed at RT and a small volume disposable cuvette was used. For characterisation of functionalised AuNPs, 100 µl of each nanobiosensor was used in the measurement.

2.2.4.4 Quantification of bioreceptors on AuNP surface

First, 50 µg of anti-Mb IgG and Affimer were coupled to 2 ml of AuNPs with 40 nm core diameter ($OD_{529} = 1$) and incubated for 2 h at RT on a rotator. Following this, the mixtures were centrifuged at 4,500 xg for 30 min and the supernatants were transferred to low protein binding tubes for the indirect quantification method, whilst, the prepared AuNPs were used in the direct method. Then, multiple washing steps were carried out as previously described in section 2.2.3.2 and finally the functionalised AuNPs were resuspended in 2 ml of 1X PBS buffer (pH 7.4).

Indirect method: the Bradford assay was used to quantify the amount of biotinylated IgG and Affimer left in the supernatant after functionalisation. Standard solutions of IgG and Affimer (0 – 25 µg) were prepared in 1X PBS buffer (pH 7.4) to a final volume of 50 µl. The supernatants obtained from the preparation of anti-Mb IgG- and Affimer conjugated AuNPs (IgG-AuNPs and Affimer-AuNPs) were concentrated to 500 µl using Amicon 50K and 3K filters, respectively and 50 µl of the concentrated samples were used for quantification.

Next, 50 µl of standard and sample solution was mixed with 450 µl of Bradford dye reagent in 1.5 ml low protein binding tubes and incubated at RT for 5 min. Then, 200 µl of each solution was transferred to a 96-well plate, the absorbance was measured at 595 nm with a ThermoScientific Varioskan Flash 6.45 plate reader. The absorbance values of the standards and samples were subtracted from the value of reagent blank. The corrected values were used in generating calibration curves using OriginPro and linear fitting was performed.

Direct method: here, 1 ml of the prepared anti-Mb IgG- and Affimer-AuNPs were centrifuged at 4,500 xg for 30 min and the supernatants were transferred to fresh tubes. Both the sedimented AuNP pellets and supernatants were dissolved in 50 μ l of KI/I₂ solution containing 333 mM KI and 50 mM I₂ for 15 min. After this, all dissolved AuNPs and supernatants were diluted to a 10 ml volume with 1X PBS buffer (pH 7.4) and sent for quantification of gold by inductively coupled plasma-mass spectrometry (ICP-MS).

Another 1 ml of the IgG-AuNPs and Affimer-AuNPs were also centrifuged at 4,500 xg for 30 min. The supernatants were discarded; whilst the sedimented AuNP pellets were dissolved using KI/I₂ solution as above. The dissolved AuNPs were desalted using a Zepha spin desalting column (7K MWCO) to remove KI/I₂ that might interfere with a fluorescent dye (NanoOrange[®]). The released IgGs and Affimers were quantified using a NanoOrange[®] protein quantitation kit.

Standard solutions of IgG and Affimer (0 – 2.5 μ g) were prepared in 1X NanoOrange[®] reagent working solution from 10 μ g/ml stock solutions. For sample analysis, 10 μ l of each desalted solution was mixed with 240 μ l of 1X NanoOrange[®] working solution. All standard and sample solutions were prepared in 500 μ l tubes and incubated at 95 °C in a water bath for 10 min. All processes were carried out protected from light. The samples were allowed to cool down at RT for 20 min before 200 μ l of each solution was transferred to a 96-well plate for fluorescence intensity measurement as in the indirect method. The measurement was carried out with excitation and emission wavelengths of 485 nm and 590 nm, respectively. The fluorescence values of the standards and samples were subtracted from the value of reagent blank. The corrected values were used in generating calibration curves using OriginPro and linear fitting was performed.

2.2.5 Nanoparticle (NP)-coupled dynamic light scattering (DLS) size shift assay

All DLS measurement were performed as described in section 2.2.4.3.

2.2.5.1 Kinetics study

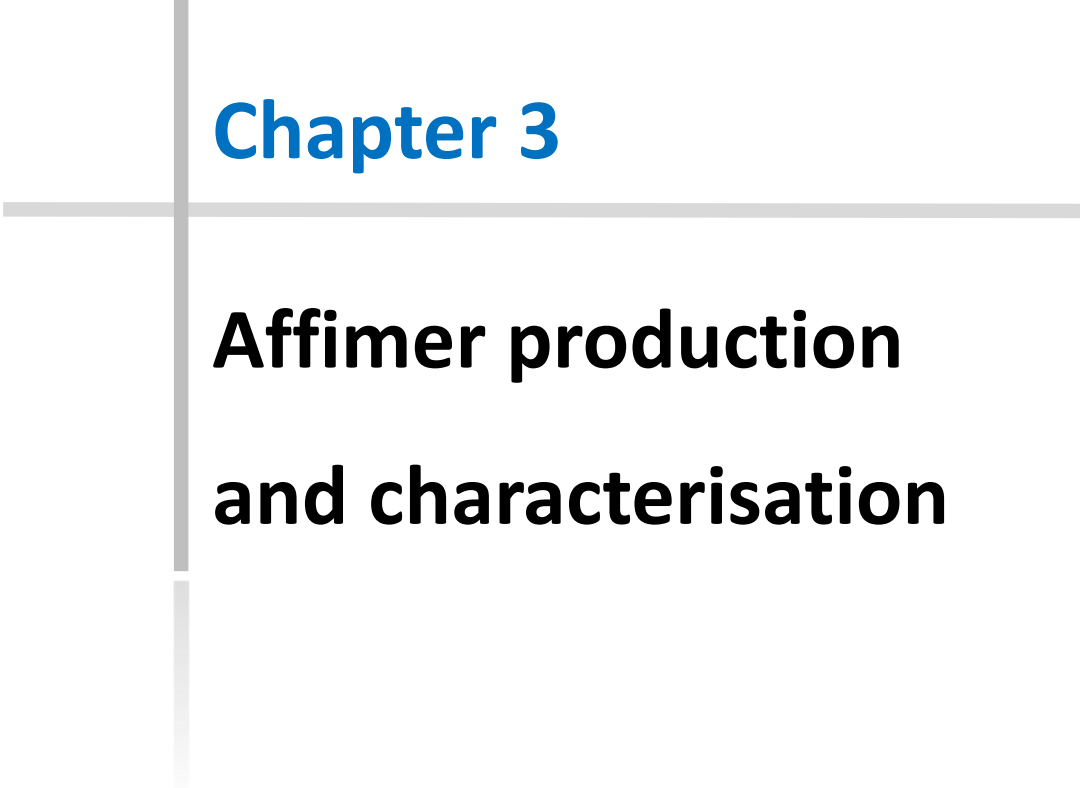
For kinetics study, four different functionalised AuNPs were used; myoglobin conjugated AuNPs (Mb-AuNPs), anti-myoglobin Affimer conjugated AuNPs (Affimer-AuNPs), anti-myoglobin IgG conjugated AuNPs (IgG-AuNPs) and strep-AuNPs. The functionalised AuNPs were prepared using methods described in section 2.2.3.2. Then, 100 μ l of Mb-AuNPs were mixed with 100 μ l Affimer-AuNPs and incubated at RT for 24 h. The average hydrodynamic diameters (D_H) were measured intermittently during this time. Positive and negative controls were performed by changing Affimer-AuNPs with IgG-AuNPs and strep-AuNPs, respectively. Triplicate experiments were carried out for each AuNP.

2.2.5.2 NP-coupled DLS size shift assay for myoglobin and Clostridium difficile toxin B detections

Mb stock solution with a concentration of 5 mg/ml was used to prepare Mb solutions at concentrations of 10 fM to 10 μ M by serial dilution using 1X PBS buffer (pH 7.4). Initially, 10 μ l of nanobiosensors was mixed thoroughly with 90 μ l of each Mb solution and incubated for 30 min at RT in a low binding protein tube prior to the measurements. Then, 80 μ l of the mixed solution was transferred to a small volume disposable cuvette for DLS measurements. For *Clostridium difficile* toxin B, similar process was carried out.

2.2.5.3 TEM

TEM images were captured using a JEM1400 model electron microscope (JEOL Ltd.). A beam voltage of 120 kV was used with a tungsten filament. Copper grids (3.05 mm diameter, 300 square meshes) coated with Formvar resin and carbon were used. For sample preparation, 5 μ l of each solution was dropped onto a grid and left to dry at RT for at least 30 min. Excess sample was removed using filter paper.

A decorative graphic consisting of a vertical grey line and a horizontal grey line intersecting at the center. The vertical line is positioned to the left of the text, and the horizontal line is positioned above the text.

Chapter 3

Affimer production and characterisation

Chapter 3 Affimer production and characterisation

3.1 Introduction

This chapter focuses on anti-myoglobin Affimer production and characterisation. Myoglobin (Mb) is a small globular protein with Mr 17 kDa (Figure 3-1). Its presence in blood indicates muscle injury and renal failure can also be indicated by detection of Mb in renal excretion. Formerly, Mb was an important cardiac marker for acute myocardial infarction (MI), but has been superseded by cardiac troponin, which is now the gold standard marker. Despite Mb appearing rapidly after acute MI, it is not specific to cardiac muscle like troponin as it can be released after injury of any muscle. Mb from equine heart was selected as a model analyte because it is an inexpensive protein with good availability. In addition, there are a lot of information regarding myoglobin structure or properties reported, which benefits laboratory investigations.

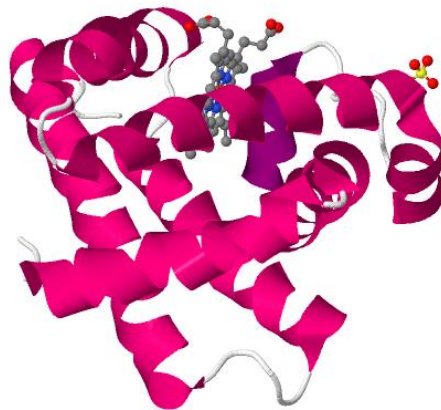


Figure 3-1 Molecular structure of myoglobin. This figure was derived from PDB file: 1WLA

Affimers are synthetic binding proteins that replicate antibody function. Previous work by Tiede et al. (2014) successfully generated a high quality Affimer based library. The size of the library was 3×10^{10} clones and 86% complexity after phage production (see Chapter 1). Phage display was used to select specific Affimers for analytes of interest.

3.2 Affimer production

3.2.1 Phage display screening

Phage display screening was performed to select anti-myoglobin Affimers from the library. Myoglobin was biotinylated via biotin NHS (see section 2.2.1.1) and used as a screening sample. ELISA was used to confirm the biotinylation process. Figure 3-2 shows that biotinylation of myoglobin was successful. Four panning rounds of screening were performed by immobilised biotinylated myoglobin onto a streptavidin plate, streptavidin magnetic beads, Neutraavidin plate and streptavidin plate, respectively. After the final panning round, the phage and negative control, which were the phage underwent panning but without biotinylated Mb immobilised on the streptavidin plate, were plated and 48 clones were randomly selected for phage ELISA.

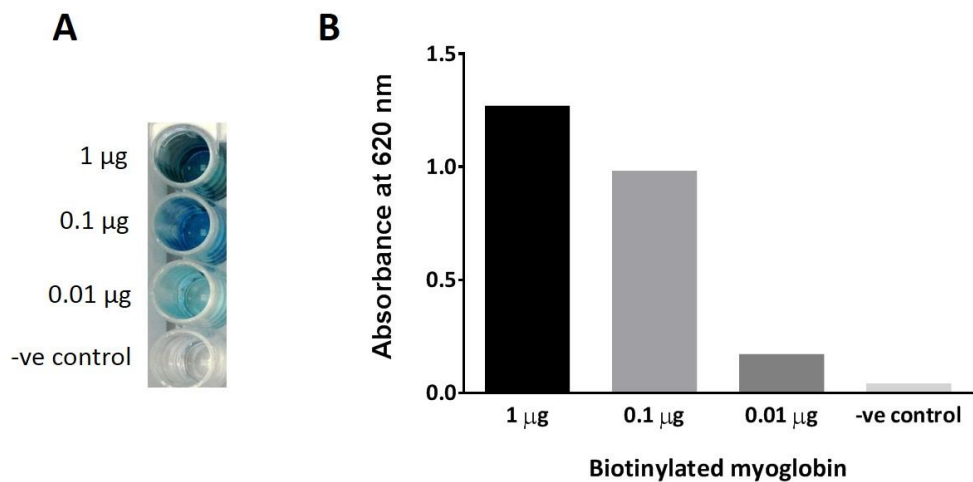


Figure 3-2 ELISA to validate biotinylation of myoglobin for phage display screening. (A), showing ELISA strip for three different dilutions of biotinylated myoglobin 1 mg/ml (1, 1/10 and 1/100) and negative control (PBS buffer) from top to bottom; (B), showing the absorbance at 620 nm of each tested sample.

3.2.2 Phage ELISA

Phage ELISA was conducted to confirm the binding of 48 selected clones to myoglobin. Biotinylated myoglobin was immobilised onto a streptavidin coated 96-well plate and then phage-containing supernatant was added to each well. Figure 3-3 shows the ELISA plate. As mentioned in Chapter 2, phage-containing supernatant was tested against the target in the first six columns (1 - 6), whereas 2x blocking buffer was used as a negative control in another six columns (7 - 12). For example, binder A1 was added to wells A1 and A7, therefore, the results were compared in the same manner. 3,3',5,5'-tetramethylbenzidine (TMB) substrate was used as detecting agent for HRP-conjugated anti-phage antibody by allowing 3 min reaction time. The absorbance at 620 nm for each well was measured and plotted as a histogram in Figure 3-4. It was observed that out of 48 clones, only 4 samples - E4, E5, F2 and G5 - showed no binding compared to their compared negative controls. Positive clones were designated by well number and sent for sequencing.

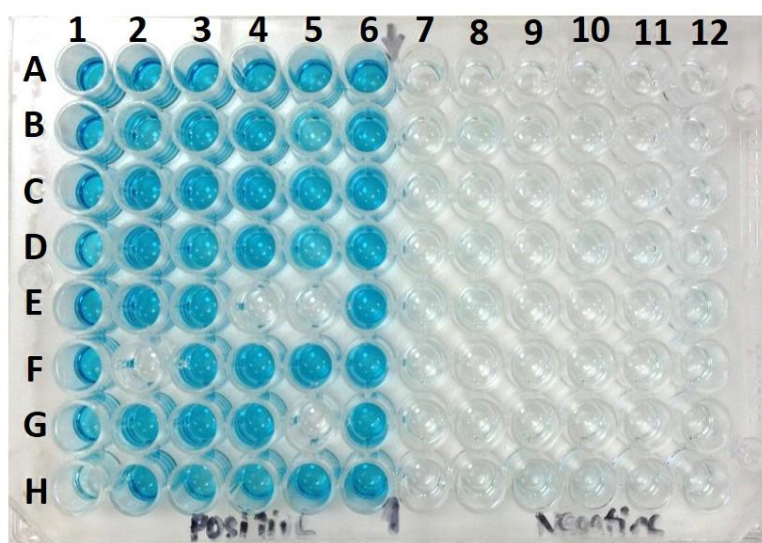


Figure 3-3 Phage ELISA to show binding of myoglobin Affimer binders. This ELISA plates was performed using randomly selected 48 Affimer clones, after four panning rounds of phage display screening. In column 1 to 6, the clones were tested against immobilised myoglobin via streptavidin-biotin reaction. Whereas, 2x blocking buffer were used as corresponding negative control in column 6 to 12 (e.g. A1 was compared with A7). The binder in wells E4, E5, F2 and G5 show no positive binding to myoglobin compared with their relative controls.

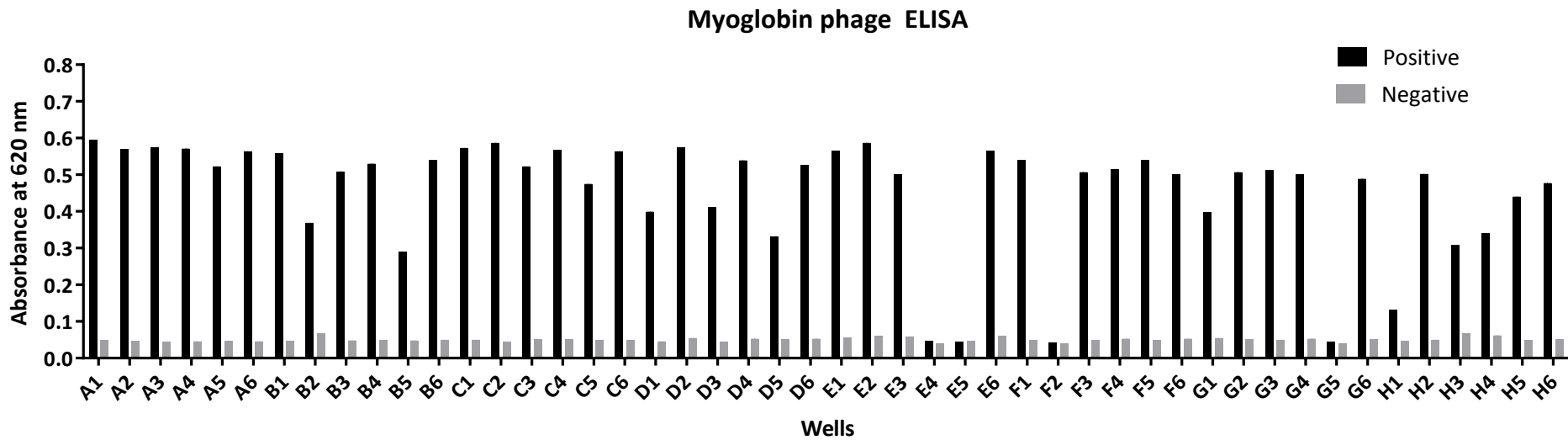


Figure 3-4 Phage ELISA histogram for anti-myoglobin Affimers. The histogram shows the comparison of absorbance at 620 nm of the tested wells with their corresponding negative wells. The binder in E4, E5, F2 and G5 show no significant absorbance difference.

3.2.3 DNA sequencing

DNA sequencing results for 44 binders is shown in Figure 3-5. To enable myoglobin-mediated inter-nanoparticle crosslinking, the nanoparticle size-shift assay requires at least two different binders that bind to different epitopes of the target in order to crosslink between the particles. Therefore, six binders were chosen based on the difference of binding loop sequences for this project.

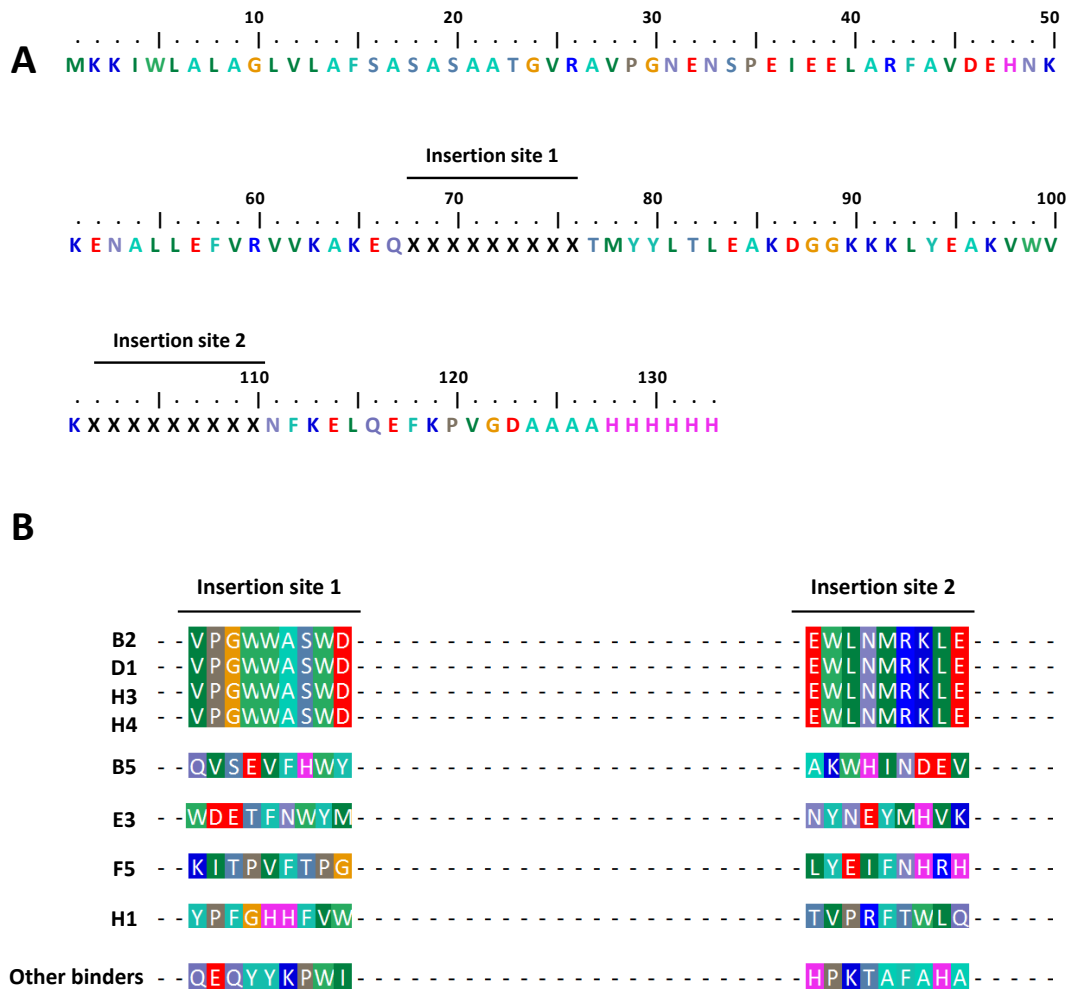


Figure 3-5 DNA sequencing results for anti-myoglobin Affimers. (A), showing Affimer scaffold sequence consisting of two insertion sites (9 amino acids in each site); (B), showing insertion sequences of each anti-Mb Affimer selected from a phage display library.

Table 3-1 shows six unique binders and their binding loop sequences (B5, C2, D1, E3, F5 and H1) from all 44 positive Affimer clones. Among all selected binders, the C2 sequence represents the majority; there were 36 clones with the same binding loops as C2, followed by D1 with four identical clones. The other binders are only present as one clone.

Table 3-1 Affimer insert sequences for six unique anti-myoglobin Affimers.

Name	Insertion site 1	Insertion site 2
B5	QVSEVFHWY	AKWHINDEV
C2	QEQYYPWI	HPKTAFABA
D1	VPGWWASWD	EWLNMRKLE
E3	WDETFNWYM	NYNEYMHVK
F5	KITPVFTPG	LYEIFNHRH
H1	YFPGHHFVW	TVPRFTWLQ

3.2.4 Subcloning

Selected coding sequence of phagemids containing anti-myoglobin Affimers were cloned into pET11a vector in order to increase their expression. According to the protocol optimized by the BSTG, PCR was used to amplify the DNA coding sequence. At this stage, a cysteine residue was inserted at the C-terminal region by incorporating the codon sequence in the reverse primer. PCR gel purification kit was used to purify the product prior to digestion with DpnI to get rid of the methylated template plasmid DNA according to the manufacturer's protocol. Figure 3-6 shows the bands of the purified PCR product after the digestion of DpnI on 1% (w/v) agarose gel. The purified product's size was around 300 base pairs, which corresponds to the theoretical size of Affimer clone. However, when using the concentrated DNA templates, the PCR products after the second clean-up show that there was some original template DNA left in the samples (Figure 3-6A). Compared to the 1/30 dilution DNA templates in Figure 3-6B, the obtained PCR products were cleaner. Therefore, these suggested that the phagemid DNA templates should be diluted down to minimize the amount of original template DNA left in the purified product.

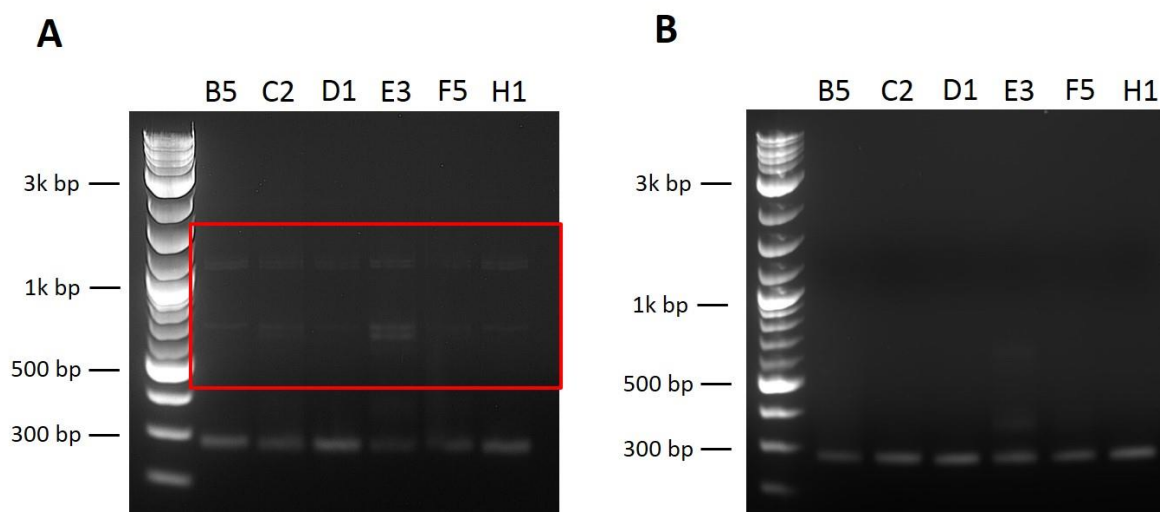


Figure 3-6 Gel electrophoresis for anti-myoglobin Affimer inserts. The 1% (w/v) agarose gel shows the bands migrated at around 300 base pairs. (A), concentrated DNA templates were used and there were some original template fragment left (shown in red box area); (B), 1/30 dilution of DNA templates were used and much cleaner products were observed.

The purified PCR products were then digested with *NheI* and *NotI* restriction enzymes and cloned into pET11a vector containing the Affimer scaffold similarly digested. The schematic of incorporating Affimers into pET11a vector is shown in Figure 3-7 and Figure 3-8 shows the map of pET11a vector used in the experiment. The vector was provided by the BSTG.

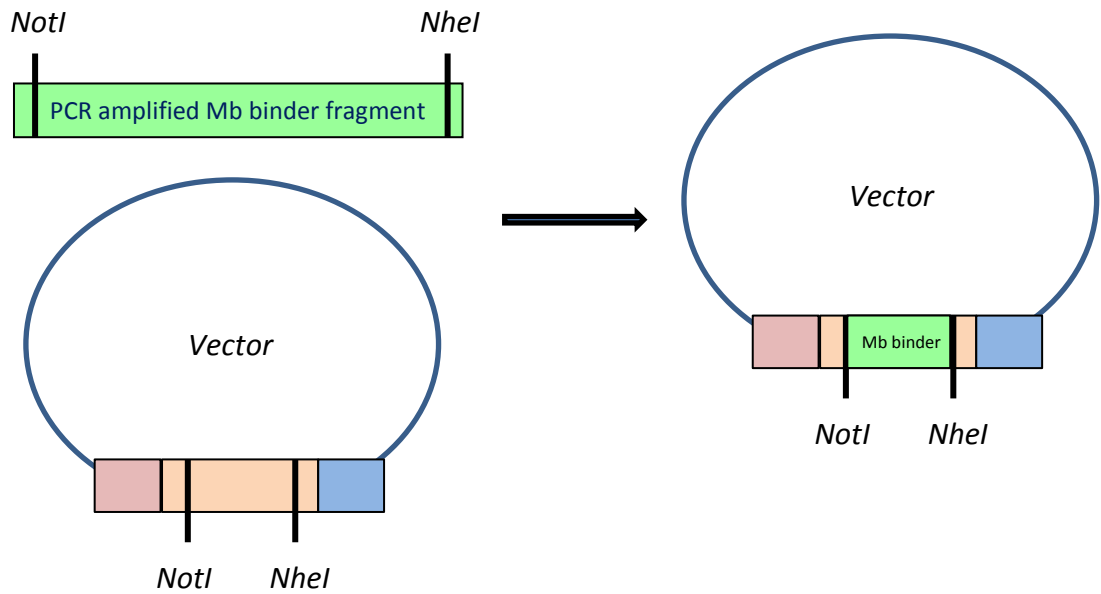


Figure 3-7 Schematic of incorporating Affimers into pET11a vector. The vector and PCR amplified fragment containing anti-myoglobin Affimer coding sequence are cut with the same restriction enzymes. The ligation process is done using T7 ligase enzyme.

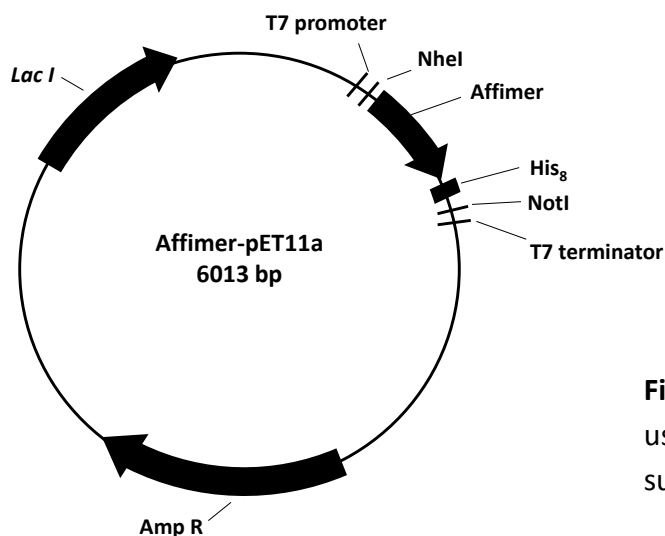


Figure 3-8 pET11a vector map used in anti-myoglobin Affimer subcloning process

The linearised pET11a fragment was run on 1% (w/v) agarose gel, shown in Figure 3-9 and a gel extraction kit was used to extract the linear pET11a. Ligation was performed overnight by mixing the PCR and pET11a fragments together and then the mixture binder was transformed into XL-1 competent cells using the heat shock technique. The negative control was carried out by transformation of only pET11a fragment with no PCR products. Plasmid DNA of each binder was extracted from positive colonies by miniprep kit. Those DNAs were sent out for sequencing again to confirm the success of the subcloning process. The sequences are shown in Figure 3-10. All plasmids with the right sequences were used for expression and purification.

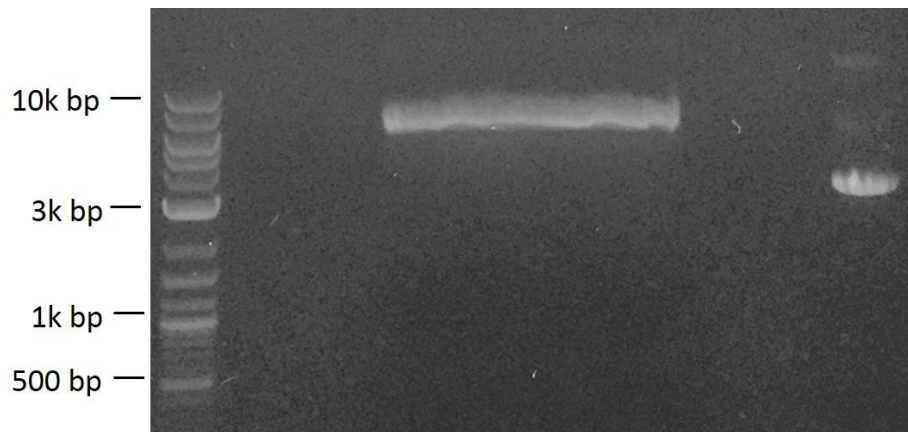


Figure 3-9 Gel electrophoresis for linearised pETT11a vector. The 1% (w/v) agarose gel showing the linearised pET11a vector migrated at a slower rate compared to uncut pET11a vector that moves much faster as it is in supercoiled form.

3.2.5 Expression and purification

A protocol for expression of Affimers was established previously using an IPTG induction method by BSTG. The expression was based on the pET expression system for recombinant protein. Some optimization was carried out in order to increase the yield for each Affimer, after plasmid DNA containing anti-Mb Affimers were transformed into BL21-Gold (DE3) competent cells. Originally, single colonies from each binder were picked and a start-up culture was inoculated in 2 ml LB media + 1% (w/v) glucose. However, it was found out that using 2TY media as a start-up culture instead could increase the yield by 0.5 - 1 mg/50 ml culture. Also, a final IPTG concentration of 0.1 mM with a longer incubation time (16 h) provided a better yield when compared with 0.5 mM incubated for 6 h was used. The optimisation was effective for three binders (B5, C2 and F5 with a yield of 3-4 mg/50 ml culture), whilst, the other binders' yields were limited to around 0.1 mg/50 ml culture.

Purification of Affimer was performed using Ni²⁺-NTA resin as the Affimer structure contained a His₈ tag, after the 50 ml culture of transformed BL21-Gold (DE3) had been harvested. The cells were lysed using lysis buffer and heated at 50 °C for 20 min. The cell lysates were subsequently centrifuged to remove insoluble protein. Only the soluble fraction was transferred to the tubes containing the Ni²⁺-NTA resin and incubated for 2 h. After that, the mixture was applied to the equilibrated column and the flow-through fractions were collected (section 2.2.1.6). The resins were centrifuged and supernatants were kept to check if there were Affimers left. The bound-resin was washed with wash buffer to eliminate unbound proteins before the elution buffer containing 300 mM imidazole was added. Then, 4-15% (w/v) gradient SDS-PAGE gels were used to confirm the expression of Affimer (Figure 3-11). All six elutions of each binder were run on the gels alongside with the lysate, insoluble and soluble fractions, as well as the supernatants from the bound-resin. For all six anti-Mb Affimer (B5, C2, D1, E3, F5 and H1), the elution bands migrated in the range between 10 and 15 kDa, which is around the theoretical Mr of Affimers (12 – 13 kDa). It is clear that the Affimer D1, E3 and H1 showed a limited protein expression compared with B5, C2 and F5 despite using the same volume of eluant.

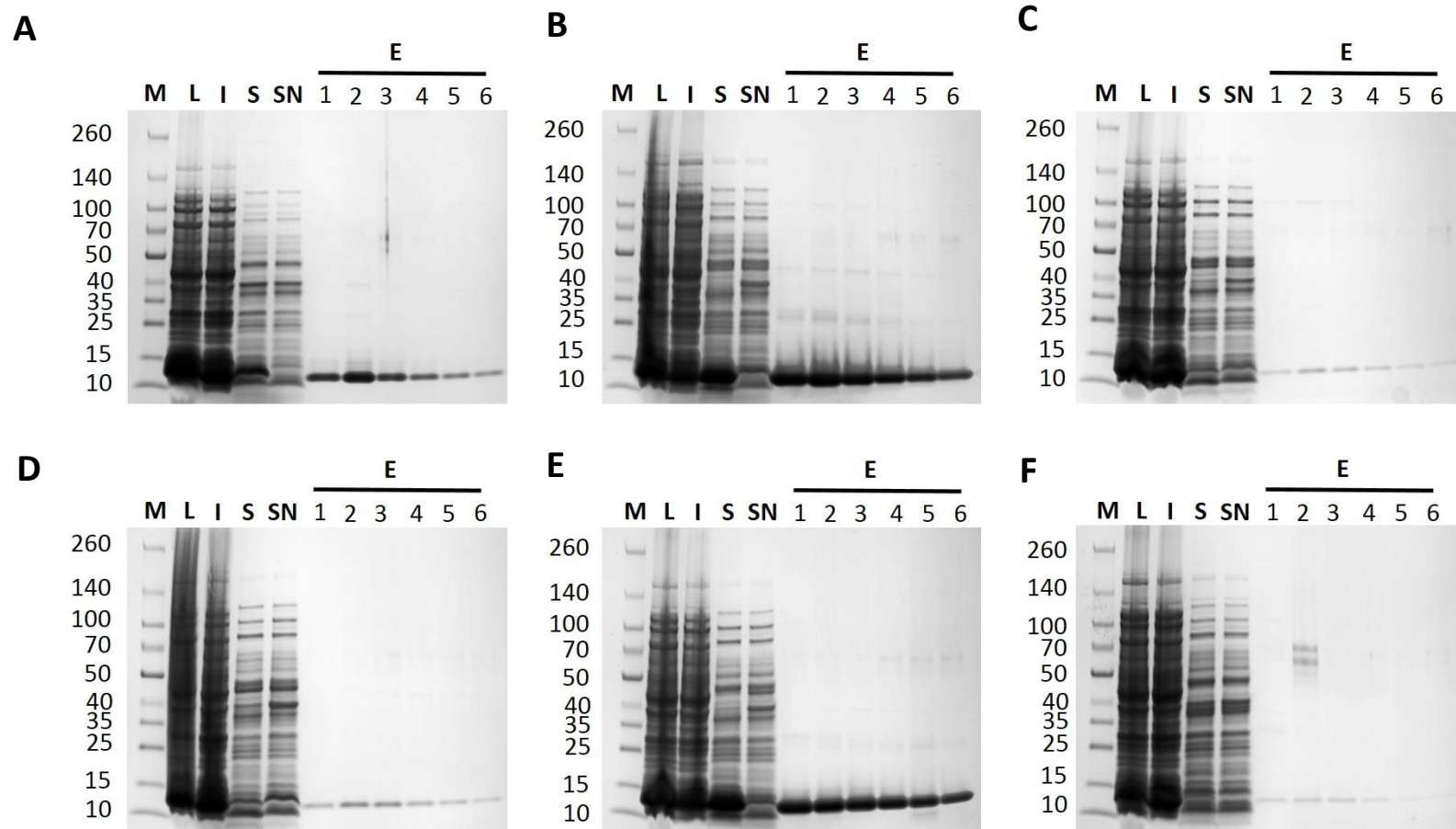


Figure 3-11 SDS-PAGE gel of purified anti-Mb Affimers. (A) – (F) showing gels of Affimers B5, C2, D1, E3, F5 and H1, respectively. The 4-15% (w/v) gradient gel was used to confirm the expression of the binders. The lanes denote: (M), protein ladder (kDa); (L), lysate fraction; (I), insoluble protein fraction; (S), soluble protein fraction; (SN), supernatant fraction for unbound Affimers; (E), imidazole eluted fractions 1 – 6. The Affimers were eluted using elution buffer containing 50 mM NaH_2PO_4 , 500 mM NaCl; 300 mM imidazole; 20% (v/v) glycerol; pH 7.4. 10 μl of sample was loaded in each well.

In a typical protein purification process, there is no heating at 50 °C step, which was used in the original protocol provided by the BSTG. The heating was introduced in order to remove non-specific proteins based on the property of Affimers that they are stable at higher temperature compared to other proteins. However, not all of the anti-Mb Affimers could tolerate temperatures over 50 °C and so processing the lysates without the 50 °C heating step was tested. The SDS-PAGE gels in Figure 3-12 show gels of non-heated lysate expression batch. In Figure 3-11, the supernatant containing soluble proteins after the centrifugation to remove insoluble protein (Lane S) of D1, E3 and H1 gels show a limited amount of Affimers at the bands migrating between 10 – 15 kDa. Whereas in the gels of non-heated lysates in Figure 3-12, there were intense bands at the same position in Lane S. Optimisation of the purification method increased the expression yield of D1, E3 and H1 substantially to around 2 – 2.5 mg/50 ml culture but the yield of B5, C2 and F5 only showed slight increase. This suggested that anti-Mb Affimers with different loop sequences have unique properties.

The purified Affimers were biotinylated using biotin maleimide at the C-terminal cysteine immediately after the purification process to avoid aggregation, which was experienced with all binders at high concentrations. This may be due to disulphide bond formation from the thiol groups of cysteine residue. Also, some Affimers were kept in elution buffer by snap freezing in liquid nitrogen.

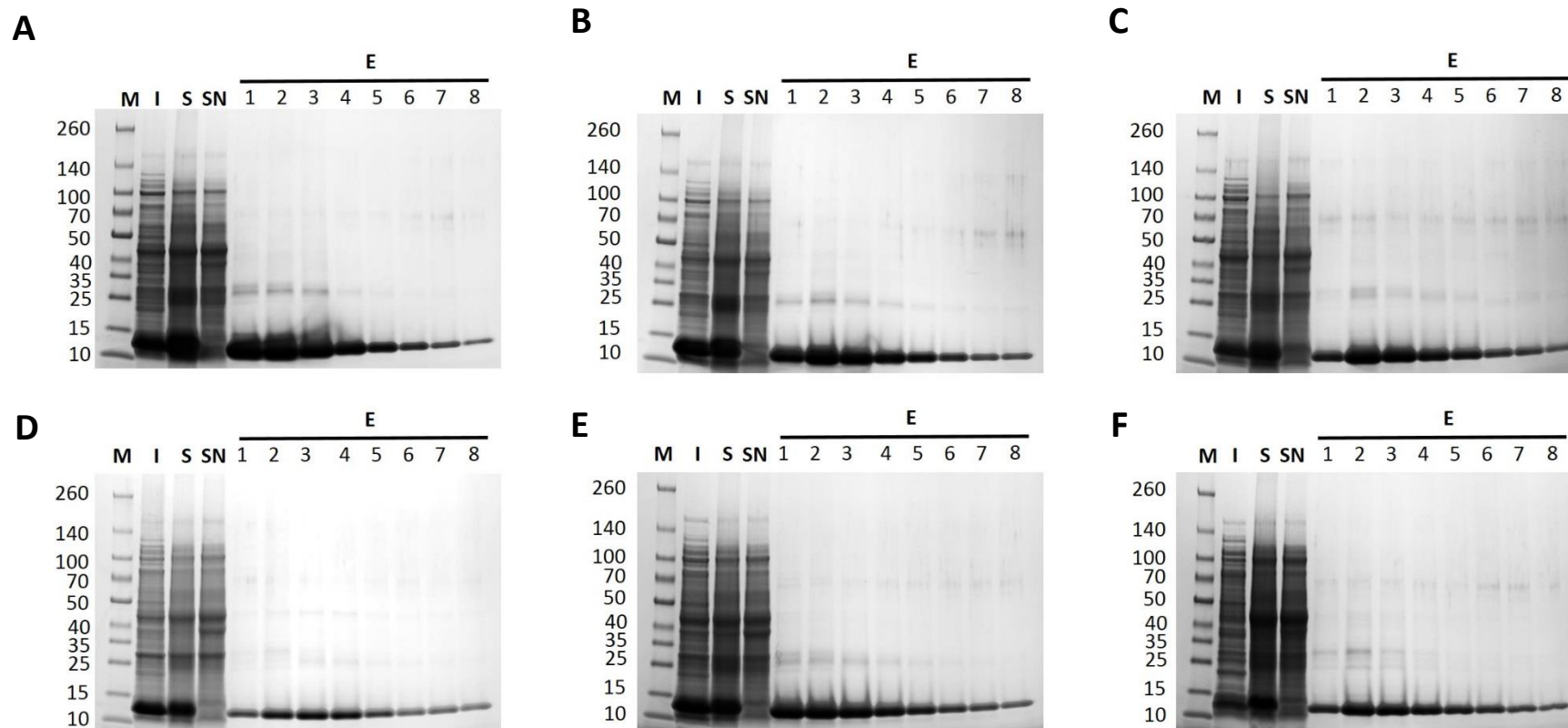


Figure 3-12 SDS-PAGE gel of purified anti-Mb Affimers without heating step to the cell lysates. (A) – (F) showing gels of Affimers B5, C2, D1, E3, F5 and H1, respectively. The 4-15% (w/v) gradient gel was used to confirm the expression of the binders. The lanes denote: (M), protein ladder (kDa); (I), insoluble protein fraction; (S), soluble protein fraction; (SN), supernatant fraction for unbound Affimers; (E), imidazole eluted fractions 1 – 8. The Affimers were eluted in elution buffer containing 50 mM NaH_2PO_4 , 500 mM NaCl; 300 mM imidazole; 20% (v/v) glycerol; pH 7.4. 10 μl of sample was loaded in each well.

3.3 Affimer characterisations

As anti-myoglobin Affimers were selected from phage display screening, the binding of each occurred when protein was expressed on the phage's surface. Therefore, it is very important to confirm the binding properties of Affimers selected from the phage library and check they can still adequately bind the target when independent from the phage.

3.3.1 Immunoprecipitation (pull-down assay)

The immunoprecipitation or pull-down assay is a well-known technique used to isolate a particular protein out of solution by relying on antigen-antibody binding activity. In this experiment, anti-Mb Affimers were used instead of antibody to pull down the analyte. Figure 3-13A – F shows the SDS-PAGE gels resulting for anti-Mb Affimers B5, C2, D1, E3, F5 and H1, respectively. The Affimers were immobilised onto Ni²⁺-NTA resin via their His₆-tag residues and excess Affimers were removed by centrifugation. The supernatant was kept and run on an SDS-PAGE gel. In the lane of unbound Affimer (UB AF), there were bands migrating between 10 – 15 kDa, suggesting the Affimers were in this fraction. This confirmed that the resins were saturated with the binders before moving to the next step. The Affimer loaded resins were then incubated with myoglobin solution overnight and the supernatants containing unbound myoglobin were kept to run on an SDS-PAGE gel. Unbound Mb was removed by several washing steps; after three washes, no Mb was observed in the flow-through fractions.

The lysates of each Affimer were then boiled for 5 min at 95 °C to break the binding and centrifuged down to sediment the resin. The supernatants were loaded on 4-15% (w/v) SDS-PAGE gel (section 2.2.2.1). However, western blotting was not performed as in usual immunoprecipitations because Mb used was a recombinant purified protein. All Affimers showed that they bound specifically to myoglobin and removed it from solution. As seen in the last lane, the bands migrated to two different components, Mb (~ 17 kDa) and the Affimer (12-13 kDa). Also, the washing steps 1 – 3 showed no proteins in the flow-through fractions, which means there were no non-specifically bound proteins to the resins as well as other contaminants.

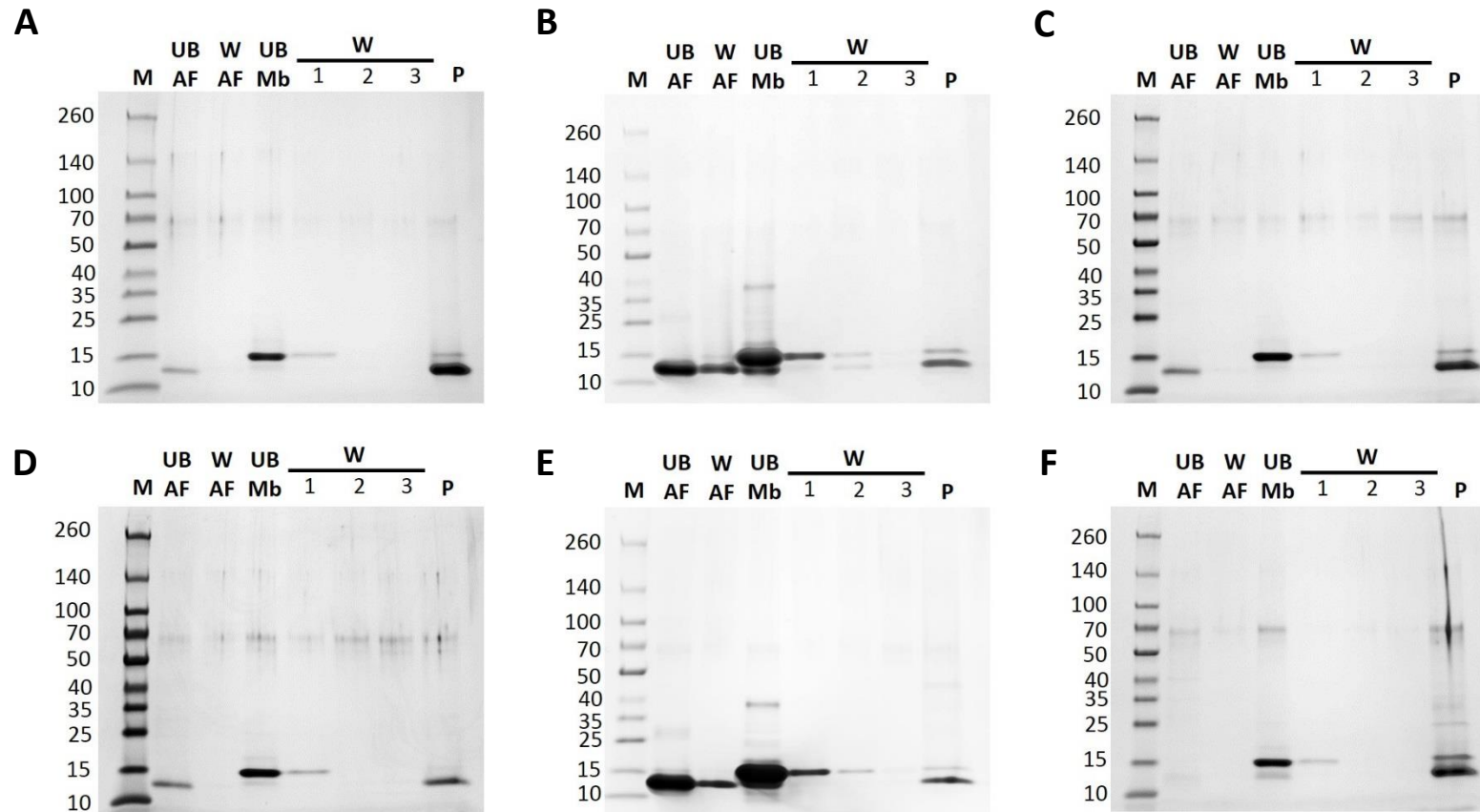


Figure 3-13 SDS-PAGE gel for pull-down Mb using Affimers. (A) – (F) showing gels of Affimers B5, C2, D1, E3, F5 and H1, respectively. The lanes denote: (M), Mr marker protein ladder (10 – 260 kDa); (UB AF) and (UB Mb), unbound fractions of Affimer and Mb, respectively; (W), washed fraction 1 - 3; (P), mixture pull down lysate. All Affimers pulled Mb from solution as the bands in Lane P show both Affimer (12 – 13 kDa) and Mb (17 kDa).

3.3.2 ELISA analysis with purified Affimers

To evaluate the binding characteristics of Affimers as proteins, the anti-myoglobin Affimers were used in an ELISA (Figure 3-14). Myoglobin was biotinylated and immobilized onto streptavidin coated Nunc-Immuno™ Maxisorp™ 96-well plate and each Affimer was used as a primary detection agent at varying concentrations. Anti-His₆-HRP was used as secondary antibody at 1:1000 dilution.

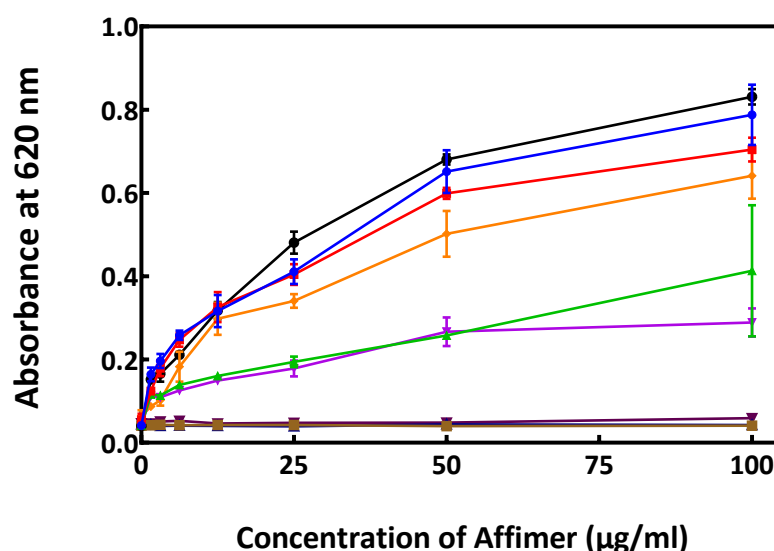


Figure 3-14 Direct ELISA results for six anti-Mb Affimers together with negative controls. Anti-His₆-HRP conjugate was used as the secondary reagent at 1/1000 and TMB was used as substrate by allowing 5 min reaction time. (♦), anti-Mb Affimer B5; (■), anti-Mb Affimer C2; (▲), anti-Mb Affimer D1; (✕), anti-Mb Affimer E3; (+), anti-Mb Affimer F5; (●), anti-Mb Affimer H1 and the negative controls (■), anti-yeast SUMO Affimer, (★), anti-calprotectin Affimer 4 and (✕), anti-calprotectin Affimer 15.

All six anti-Mb Affimers showed binding to Mb in proportion to the concentration of Affimers. Among selected binders, D1 and E3 showed the least response compared with the other four binders that had similar levels of binding. To prevent non-specific binding of secondary antibody to the Affimers, one anti-yeast-SUMO and two anti-calprotection Affimers (4 and 15) were used as negative controls in the experiment. They showed minimum response suggesting that the binding of anti-Mb Affimers was genuine.

3.3.3 Binding kinetics

To investigate the binding parameters (K_a , K_b) of selected anti-Mb Affimers that have been expressed, SPR was used. Biotinylated Mb was immobilised onto a streptavidin (SA) chip and acted as a receptor in this context. Conventionally, the immobilized component is the 'receptor' and the flowing component is the 'ligand'. The Affimers were used as analyte flowing in solution over surface. With this design, accurate concentration of analyte is very important for determining the binding parameters. Therefore, calibration free concentration analysis (CFCA) was used to measure the active concentration of each Affimer prior to the kinetics study using a carboxymethylated dextran (CM5) chip onto which anti-His₆-antibodies were immobilised.

The SPR experiment was set up by using two flow cells (cell 1 and 2) on an SA chip. The first cell (flow cell 1) was used to eliminate non-specific binding by flowing the Affimers over the sensor surface without any Mb immobilised. So the real binding data could be corrected non-specific binding of Affimers to the chip itself by subtraction. Another control to prevent non-specific binding was to flow buffer only over flow cell 2, onto which had previously immobilised biotinylated Mb. This again was used to subtract from the binding data. A multicycle kinetic study was performed with concentration of Affimers ranging from 0 – 1000 nM with 120 and 480 seconds of association and dissociation time, respectively. Anti-yeast-SUMO was used as a negative control and 10 mM glycine pH 3 was selected as the regeneration buffer after each concentration cycle ended. Real time binding data from the experiment is shown in Figure 3-15.

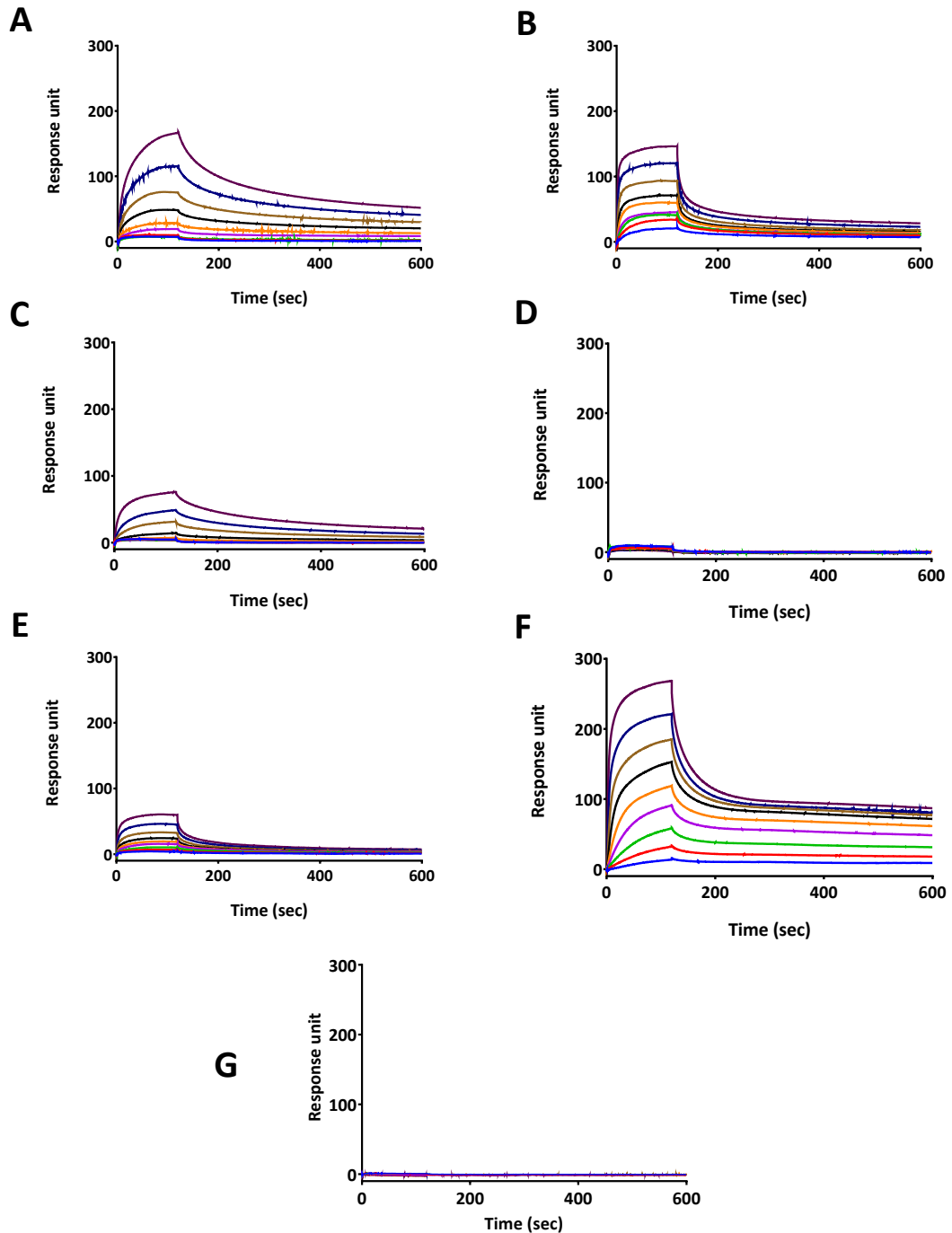


Figure 3-15 Real time binding data of SPR experiment on anti-Mb Affimers and its negative control. The graphs (A-G) show real time binding data of anti-Mb B5, C2, D1, E3, F5, H1 and anti-yeast SUMO Affimer systems, respectively. All Affimers except E3 and anti-yeast-SUMO showed binding activity to Mb immobilised on a streptavidin (SA) chip. Concentrations of Affimer used were: (—), 3.91 nM; (—), 7.81 nM; (—), 15.62 nM; (—), 31.25 nM; (—), 62.5 nM; (—), 125 nM; (—), 250 nM; (—), 500 nM; (—), 1 μ M.

From these data, we can see the binding responses with all anti-Mb Affimers except E3. All response binding curve showed the steep association characteristic and followed by a much shallower dissociation curve, which could not be seen in Affimer E3 (Figure 3-15D). Similar to the negative control, there was no binding responses of anti-yeast-SUMO Affimer to Mb at any of concentrations used (Figure 3-15G). Despite Affimer E3 being successfully used in ELISA and pull down assay, it showed no response in the SPR system. A possible explanation could be that it aggregated during the experiment as we can see a slight increase of a noisy line in the association curve (Figure 3-16A) compared with anti-yeast-SUMO that showed no binding at all (Figure 3-16B). This could mean that some Affimer E3 could bind to Mb but insufficient to generate a proper binding curve as seen in others. As a result, Affimer E3 was excluded from subsequent analyses as the other Affimers proved to be better in terms of binding kinetics.

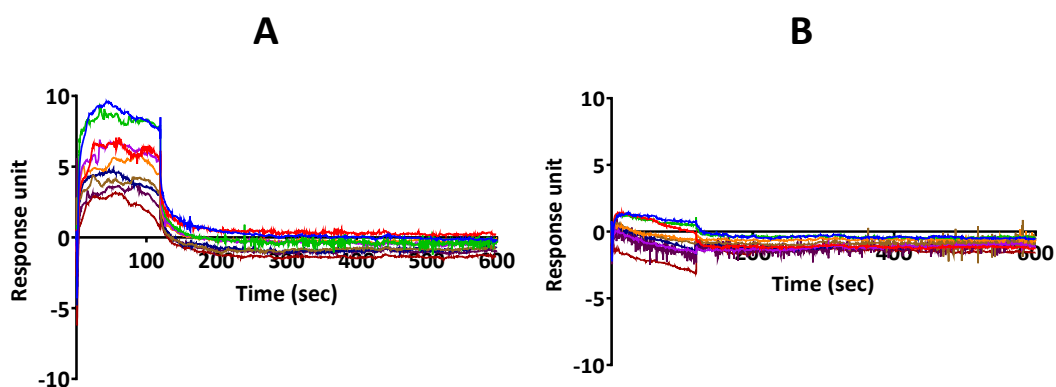


Figure 3-16 Real time binding data of anti-Mb Affimer E3 and anti-yeast-SUMO Affimer on an expanded scale. (A), Affimer E3 binding data with some degree of binding, but binding curves were non-smooth indicating aggregation problems; (B), anti-yeast-SUMO Affimer binding data with no binding activity at all.

To compare the remaining five anti-Mb Affimers, the association and dissociation half-time of the highest concentration (1000 nM) of each Affimer were plotted (Figure 3-17). If we draw an arbitrary line to divide the graph in Figure 3-17 into four sections representing four different characteristics of bioreceptor, the ideal binder should fall into the bottom right section, which means it takes less time to reach 50% maximum responses and take long time to half dissociate to a plateau phase as known as “fast on – slow off” binders. However, there was no anti-Mb Affimers that met the criteria of an ideal binder. The best Affimers from this graph would be B5 and D1 that both fell into “slow on – slow off” binders, although it must be admitted that the designation ‘fast’ and ‘slow’ are somewhat arbitrary. As well as C2 and F5 that fell in the “fast on – fast off” binder segment. In addition, if we look deeply into the size of maximum response, represented by the size of the circles, B5 might be a better binder as compared to D1 at the same concentration as it gave more SPR response units. H1 gave the largest maximum response compared to others but with its “slow on – fast off” property made it less desirable.

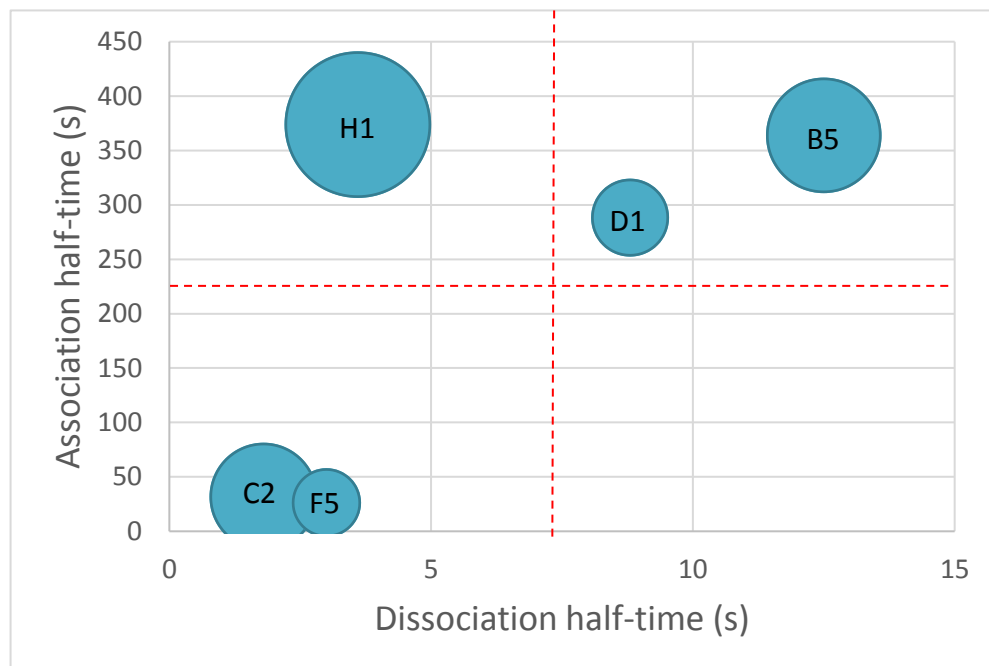


Figure 3-17 Comparison graph of five anti-Mb Affimers SPR binding data. The graph was plotted using the real time binding data of the maximum concentration of each Affimer (1000 μ M). The X-axis represents how fast the dissociation happened. Y-axis is how fast the association happened. Area of circle is the total association maximum (B_{max}). The ideal binders should be on the bottom-right of the graph.

Figure 3-18 shows typical SPR binding curve containing association and dissociation phases.

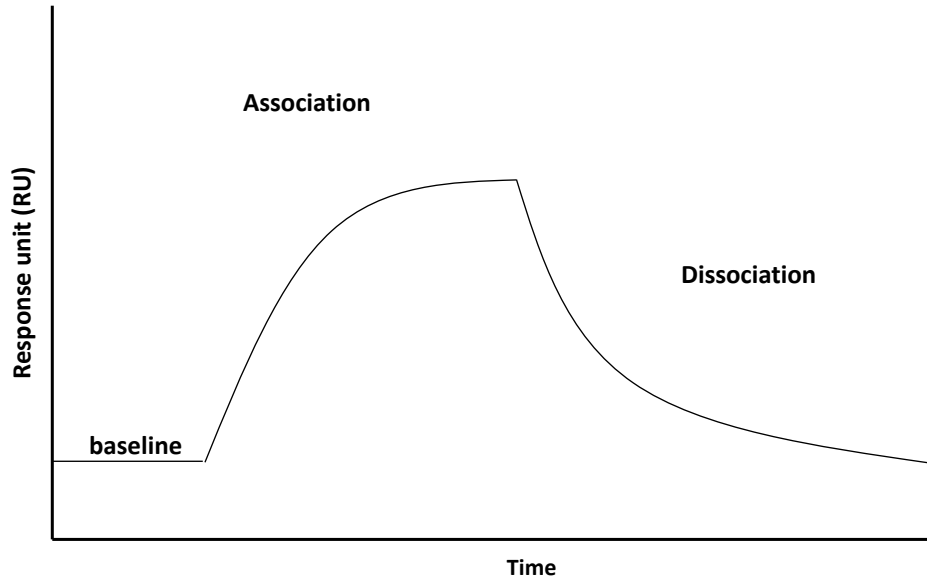


Figure 3-18 Typical SPR binding curve containing association and dissociation phases.

The time-dependent rate equations for association phase is described as:

$$\frac{dn}{dt} = k_{on} (N - n)C - k_{off} \cdot n \quad (3-1)$$

where n is concentration of analyte-ligand complex, N is concentration of immobilised ligands, k_{on} is association rate constant ($M^{-1}s^{-1}$), k_{off} is dissociation rate constant (M) and C is concentration of analyte in solution (M). In a real experiment, n approaches its terminal value n_{max} in an exponential manner with a time constant, τ . Equation governs this interaction is:

$$n = n_{max} [1 - \exp(-\frac{t}{\tau_{on}})] \quad (3-2)$$

where t is time (s), n_{max} is equal to $N \cdot \frac{k_{on}C}{k_{on}C + k_{off}}$ and τ_{on} is described as $\frac{1}{k_{on}C + k_{off}}$.

In terms of dissociation phase, it is measured by removing the analyte solution and exchanging it with running buffer, which means C is set to zero. It can be described as:

$$\frac{dn}{dt} = -k_{off} \cdot n \quad (3-3)$$

This time the conditions during the association phase are changed and the dissociation rate solely depends on time and the concentration of the analyte-ligand complex at the start of dissociation. Therefore, a different equation is used, where τ_{off} is described as $\frac{1}{k_{off}}$ (equation 3-4).

$$n = n_{max} \exp\left(-\frac{t}{\tau_{off}}\right) \quad (3-4)$$

These equations (3-1 to 3-4) can then be used to calculate the overall affinity constant (K_D) (M) using equation 3-5:

$$K_D = \frac{k_{off}}{k_{on}} \quad (3-5)$$

According to these data, binding parameters (K_a , K_b and apparent K_D) could be calculated. The ideal binding between a bioreceptor to an analyte should follow a one-site or 1:1 binding saturation model like an antibody to its analyte. Initially, a one-site specific binding analysis was performed. It was found that the data fitting for all five binders did not follow a one-site binding model (Figure 3-19, Table 3-2), whilst fitting a two-site specific binding model fitted the data much better (Figure 3-20) and the χ^2 and R^2 were improved substantially (Table 3-3). The two site model assumes two distinct and non-interacting binding sites within the Affimer population.

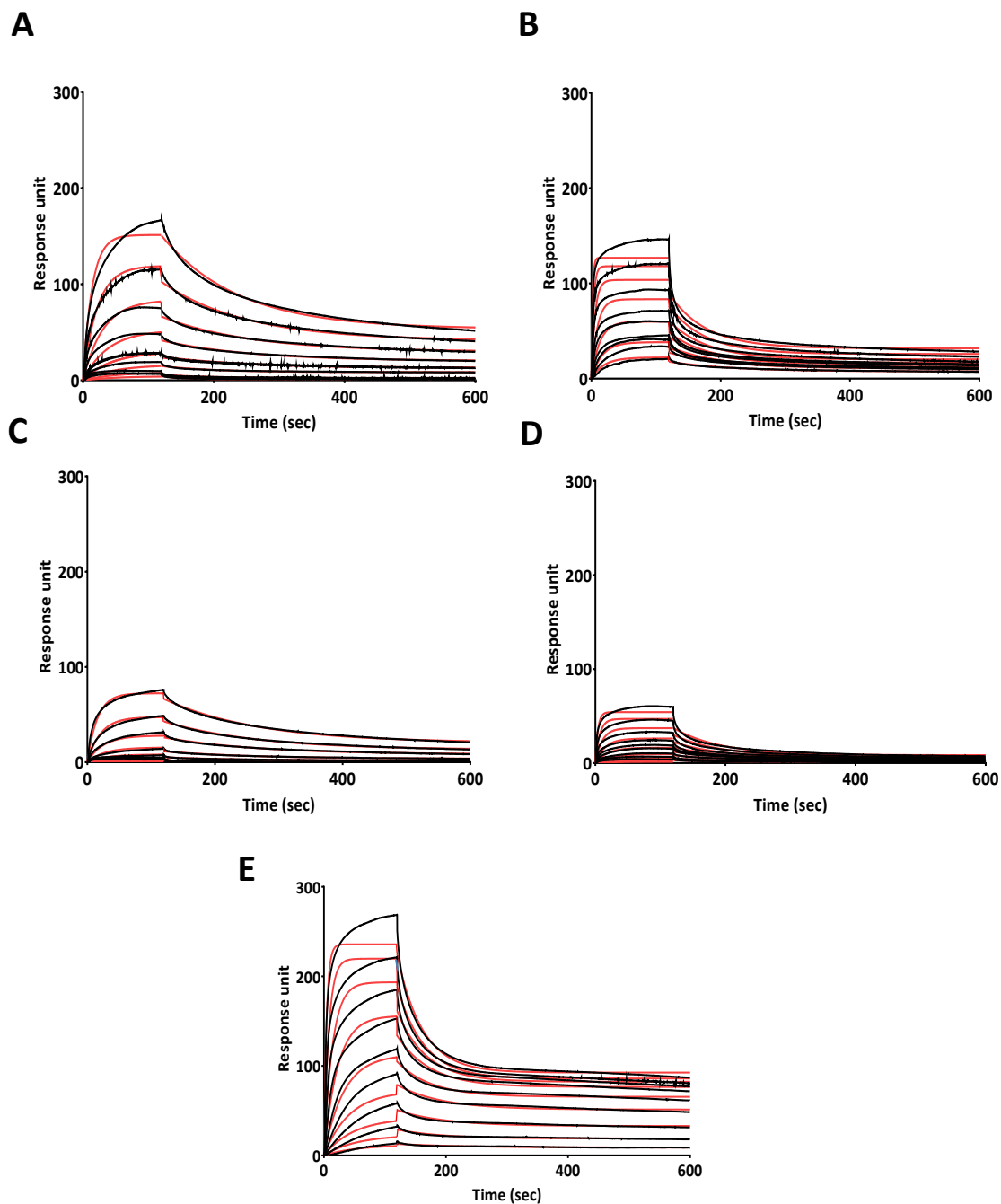


Figure 3-19 One-site binding model data fitting. The graphs show (—) raw data obtained from SPR Data, whilst, (—) fitted data is shown overlaid. Data modelled (A-E) were from anti-Mb Affimers B5, C2, D1, F5 and H1, respectively.

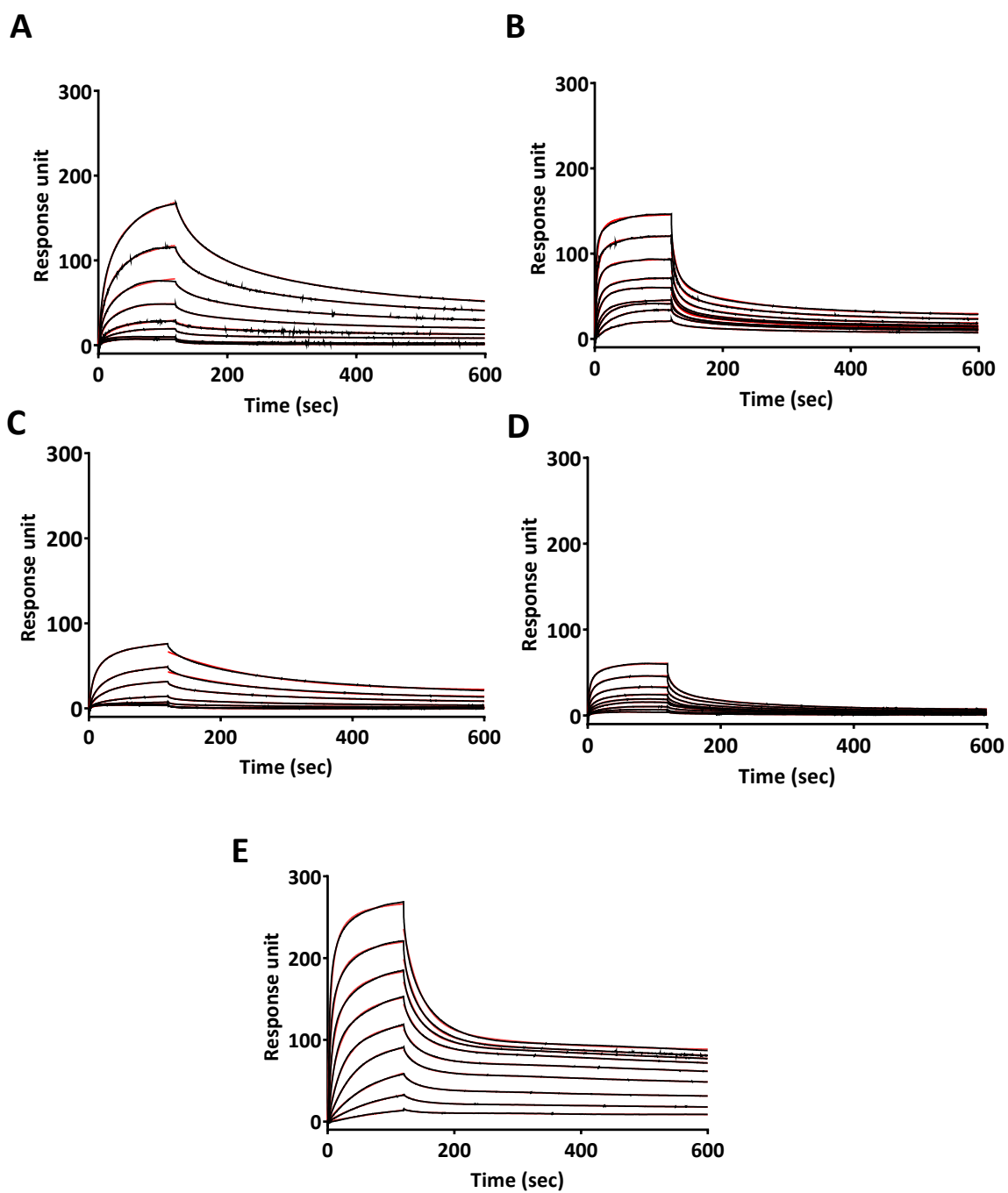


Figure 3-20 Two-site binding model data fitting. The graphs show (—) raw data obtained from SPR Data, whilst, (—) fitted data is shown overlaid. Data modelled (A-E) were from anti-Mb Affimers B5, C2, D1, F5 and H1, respectively.

Table 3-2 Data from one-site binding model. Using the one-site binding model, the χ^2 and R^2 values reflected the poor fit seen in Figure 3-19.

Binder	K_{on} (1/Ms)	K_{off} (1/s)	K_D (M)	R^2	χ^2
B5	5.31×10^4	1.96×10^{-2}	3.69×10^{-7}	0.781	5.816
C2	5.41×10^5	4.36×10^{-2}	8.05×10^{-8}	0.598	12.5
D1	3.01×10^4	3.36×10^{-2}	1.12×10^{-6}	0.793	2.516
F5	2.21×10^5	3.98×10^{-2}	1.80×10^{-7}	0.676	3.994
H1	2.18×10^5	1.71×10^{-2}	7.87×10^{-8}	0.868	13.18

Table 3-3 Data from two-site binding model. Using this model both χ^2 and R^2 values were improved compared with one-site model (Figure 3-20). The parameters for population 1 and population 2 binding are shown with the percentage describing the weighting of each site towards the overall K_D value.

Binder	Binding site 1			Binding site 2			Global parameters				
	K_{on1} (1/Ms)	K_{on1} (1/s)	K_{D1} (M)	K_{on2} (1/Ms)	K_{off2} (1/s)	K_{D2} (M)	%site 1	%site 2	K_D Total	R^2	χ^2
B5	1.75×10^8	6.69×10^{-3}	3.82×10^{-11}	1.14×10^8	6.84×10^{-2}	6.00×10^{-10}	60.7	39.3	4.68×10^{-10}	0.975	0.805
C2	1.12×10^7	8.83×10^{-2}	7.89×10^{-9}	1.28×10^7	7.42×10^{-3}	5.79×10^{-10}	53.0	47.0	5.06×10^{-9}	0.992	0.829
D1	9.53×10^8	1.99×10^{-2}	2.09×10^{-11}	3.28×10^8	8.67×10^{-2}	2.64×10^{-10}	50.8	49.2	1.45×10^{-10}	0.916	0.267
F5	9.48×10^6	6.66×10^{-2}	7.03×10^{-9}	4.11×10^7	8.20×10^{-3}	2.00×10^{-10}	65.7	34.3	6.11×10^{-9}	0.986	0.329
H1	1.13×10^7	2.00×10^{-3}	1.76×10^{-10}	2.83×10^7	4.06×10^{-2}	1.44×10^{-9}	49.6	50.4	9.55×10^{-10}	0.996	1.336

By using the two-site specific binding model, the overall affinity constant was then calculated with Equation 3-5. Parameters calculated from the two-site binding process were given in two figures. For the association parameter, two K_{on} s were given as in K_{on1} and K_{on2} , representing high and low affinity. Also, dissociation parameters (K_{off}) were given as K_{off1} and K_{off2} , which represent fast and slow dissociation rate. In order to select the right K_{on} and K_{off} to use, the considerations were based on the description of binding property given to each binder in Figure 3-17. B5 and D1 were described as ‘slow on – slow off’ binders. While, C2 and F5 were foreseen as ‘fast on – fast off’ binders. In terms of H1, a ‘slow on – fast off’ model was described. Table 3-4 reports the binding parameters (K_{on} , K_{off} and K_D) derived from the two-site specific binding model including a percentage function describing the weighting of each site towards the overall K_D value.

Surprisingly, the proportion between two populations were similar (around 50%). It might be that anti-Mb Affimers might experience stability issues, as with biological samples, especially proteins, there is always a certain level of heterogeneity. This is because in real world applications, proteins are labile and can contain a small proportional of “damaged” proteins within the whole population. In addition, myoglobin immobilised on the SPR chip itself might be altered as it is also a protein. This might alter the context of epitope presentation on its surface, so that binding kinetics become affected. Another possible explanation could be that the Affimers contains cysteine and dimerisation might occur, which later affects the binding kinetics by an increased avidity effect. Further experiments could be conducted to prove this hypothesis. For example, the addition of a protecting group, such as an alkane-maleimide, could prevent the formation of dimers before the SPR experiment was run.

The overall K_D denotes the apparent K_D of the whole population. In terms of reporting kinetic parameters, it might be better to report the optimal K_D for the whole population than the overall K_D . However, in real applications, the ideal system is rarely found. Therefore, it is more desirable to report the overall value (Figure 3-21), especially when the proportions of each population were close.

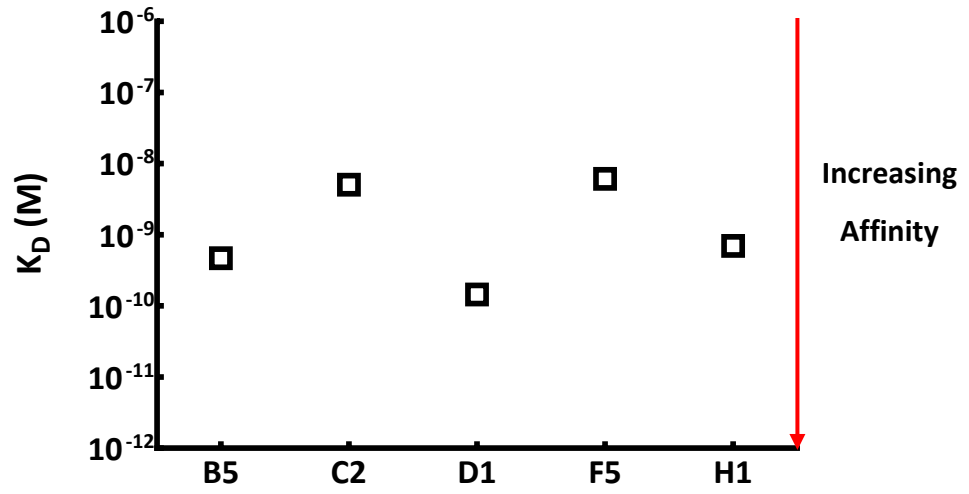


Figure 3-21 Summary of overall K_D values for anti-myoglobin Affimers.

3.3.4 Affimer pair selection

For nanoparticle size shift assay in this project, the main principle is based on the crosslinking of nanoparticle probes as discussed in Chapter 1. Bioreceptors immobilised on a nanobiosensor should act as crosslinkers, in other words, bind to two or more epitopes like a polyclonal antibody. Therefore Affimer pair ELISA was conducted to identify among the five selected binders whether they bind to different epitopes or not. The schematic in Figure 3-22 shows the Affimer pair ELISA used in the experiment. One Affimer was fixed onto the plate and followed by Mb as the analyte. Then, another biotinylated Affimer was used as the primary detection agent and detected with streptavidin-HRP as a secondary agent. Each Affimer was fixed onto the plate and tested against four different Affimers with and without Mb in order to quantify non-specific binding. In addition, each Affimer was tested against themselves to identify whether the Affimer itself can bind to more than one epitope. Biotinylated anti-Mb polyclonal antibody and PBS buffer were used as positive and negative controls for the ELISA, whilst biotinylated anti-calprotectin Affimer was used as non-specific binding control, respectively.

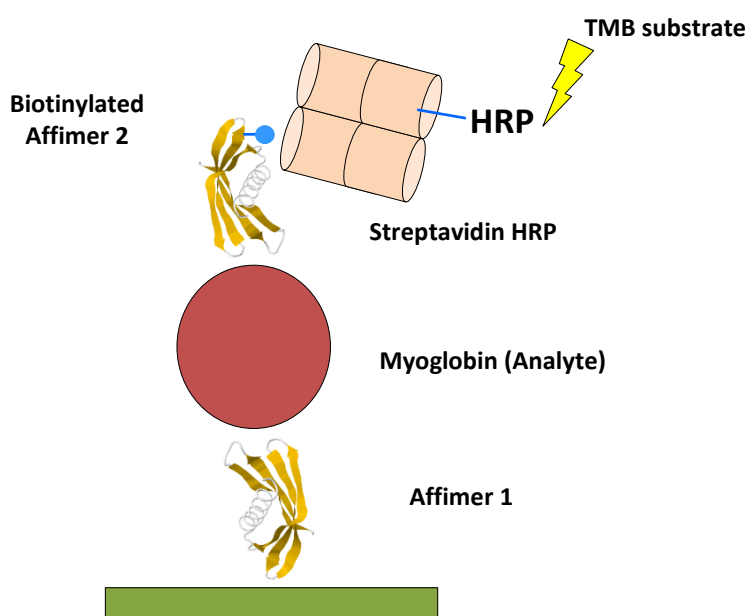


Figure 3-22 Schematic of Affimer pair ELISA. One Affimer is fixed to the Nunc-Immuno™ Maxisorp™ 96-well plate, following by myoglobin. The second Affimer is used in a form of biotinylated protein as a sandwich primary detection agent. Streptavidin-HRP is used as secondary quantification agent and TMB substrate is used for detection.

The histograms in Figure 3-23 (A-E) show the pair ELISA data comparing the absorbance at 620 nm in the presence and absence of Mb (black and grey column, respectively). First, the positive controls for every Affimer showed significant binding signals ($p < 0.05$). Also, both negative and non-specific controls showed insignificant signal, which indicated that the systems were working properly. Figure 3-23A shows that when B5 was fixed to the plate, only F5 could access to its epitope and bind to Mb. Whereas, when F5 was fixed (Figure 3-23D), B5 could not bind to the analyte. This might due to the location of the B5 epitope close to the F5 epitope so when F5 bound to myoglobin first, the position of Affimer F5 prevented Affimer B5 from binding to Mb. Similarly, when C2 was fixed to the plate, three binders (D1, F5 and H1) could bind to Mb as shown in Figure 3-23B. On the contrary, there were no positive data showing that C2 or other binders could bind to Mb when D1 and H1 were fixed (Figure 3-23C and E). The possible explanations for this case is that when C2 binds first, the position of C2 allowed D1 and H1 to access their epitopes. But when D1 and H1 bound first, they hindered the C2 epitope and prevented C2 from binding. However, only when F5 was fixed, C2 could significantly bind to myoglobin. Taken together, these results suggest that among all five binders C2 and F5 are most likely to bind to different epitopes that are not close together or hinder each other.

What stands out in this experiment is that when each binder was fixed and tested against themselves, only C2 that gave a significant binding signal ($p < 0.05$), which suggests among the five selected binders C2 might bind to more than one epitope. That might be the reason why when C2 bound to Mb first, it allowed other binders to bind more. Furthermore, this might be the reason why C2 is the most frequently found Affimer when screened from the library as reported earlier in section 3.2.3.

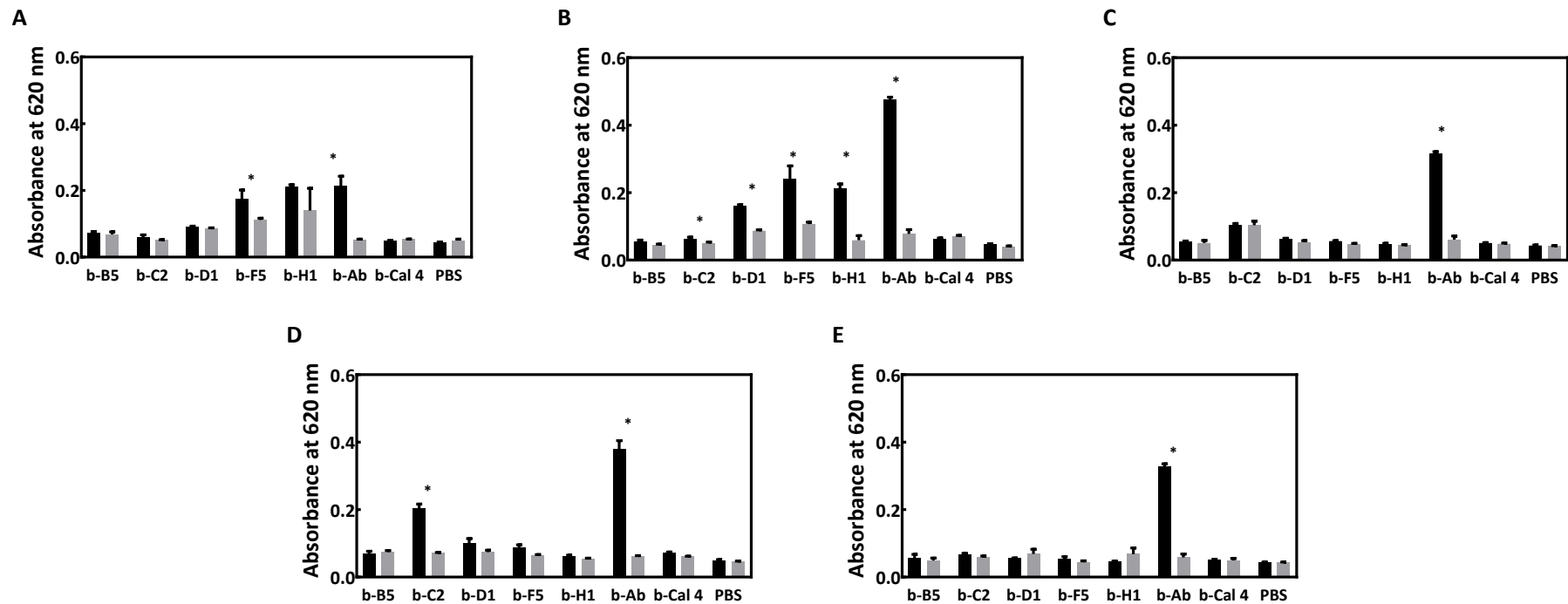


Figure 3-23 Affimer pair ELISA data for anti-Mb Affimers. (A-E) showing histograms of five different fixed Affimer– B5, C2, D1, F5 and H1, respectively on a Nunc-Immuno™ Maxisorp™ 96-well plate. X-axis shows the biotinylated Affimer used to test against the fixed Affimer. Y-axis shows the absorbance value at 620 nm. The black column represents the experiment well with Mb present. The grey column represents the negative control well without Mb. (*) indicates significant values tested with independent t-test between the well with Mb present and the well without Mb ($p < 0.05$).

3.4 Discussion

This chapter has focused mainly about the screening and production of anti-Mb Affimers. The screening was successfully done with six different anti-Mb Affimers, which seems to be small number compared with the size of library of 3×10^{10} clones. This might be due to the compact size of Mb itself that restricted the binding of Affimer. Mb is a globular monomer with Mr 17 kDa and is around 3.5 nm dimension. This is pretty similar to the Affimer (12 - 13 kDa, 2 - 3 nm). The process of subcloning and expression were optimised and established previously; nevertheless, it was found out that D1, E3 and H1 gave less yield compared with B5, C2 and F5 as mentioned earlier. By skipping the heating step during the purification process, the yield of those three binders could be increased, suggesting that changes in the 2 x 9 amino acids binding loop affects Affimer properties as they represent ~ 20% of total sequence. Also, the purified anti-myoglobin Affimers were forming aggregates that might due to the formation of dimers because of the inclusion of the C-terminal cysteine residue for conjugation purpose. This phenomenon is normal for free thiols as the formation of disulphide bond provides more thermodynamically stable state. However, this phenomenon may also affect their thermal stability or other properties. Therefore, it is necessary to reduce the disulphide bond before using the Affimers. The selection of reducing agents was not a problem as Affimers contain only one cysteine. A more detailed account of this issue is given in the following chapter.

Regarding selection of characterisation methods, it would be ideal to perform full characterisation on all the selected binders. Though, the main aim of this work is to identify the suitable binders for nanoparticle size-shift assay. Thus, various characterisations were performed to validate the Affimers for specific purposes. First, immunoprecipitation and direct ELISA were conducted to confirm the specific binding of six selected binders to Mb when they were in a form of purified proteins, not phage expressed proteins. All purified anti-Mb Affimers proved to bind specifically to Mb. With respect to direct ELISA results, Affimer E3 seemed to be binding with lowest response over the same concentration range.

SPR was selected to identify their binding kinetic parameters. The K_D obtained for the five selected Affimers were between pM to nM range excepting Affimer E3 that experienced aggregation and showed no binding. This result was in accordance with direct ELISA data proposing that Affimer E3 might be the worst of the Affimers, so Affimer E3 was excluded from further analysis. As previously stated, the binding kinetics of the binders were not fitted well using a one-site binding model but they were fitted better with two-site binding model. It seems like the K_D (s) obtained were overestimated compared with other Affimers selected from the library. The work presented in this chapter would have been more complete if it had included the results from other experiments that could identify the equilibrium K_D as a comparison, for example, radioisotope ligand binding assay or fluorescence polarisation. Still, the SPR data provides comparative information about the five-selected anti-Mb Affimers, which lead to appropriate selection of binders for the project together with other specific characterisations.

Additionally, sandwich ELISA was adapted to use as a tool to find an Affimer pair for the project. As was pointed out in the Introduction (Chapter 1), the main mechanism of the size-shift assay is crosslinking between gold nanoparticles (AuNPs) and for this to happen, more than one binder is required. The method might not be able to give specific location concerning the epitope of each binder but it was enough for the project to move forward. According to the Affimer pair ELISA results, C2 and F5 were most likely to bind to different epitopes among all the selected Affimers despite the fact that their affinities were not the best. It was hypothesized that when using these two Affimers, Mb-mediated crosslinking could be occur, which lead to aggregation of nanoparticles that is a key feature of the assay mechanism discussed in Chapter 5.

Chapter 4

Functionalisation of gold nanoparticles (AuNPs)

Chapter 4 Functionalisation of gold nanoparticles (AuNPs)

4.1 Introduction

Work in this chapter focuses on gold nanoparticle (AuNP) functionalisation for the dynamic light scattering (DLS) assay. As mentioned in Chapter 1, AuNPs possess a modifiable surface which makes them a candidate materials for biosensing applications. There are several methods for bioreceptor functionalisation onto the AuNP surface. Physical interaction is a simple method but requires a large amount of bioreceptor and is susceptible to the surrounding environment. A chemical coupling method, conversely, is more complicated for processing but preferable as it requires less bioreceptor and is more durable. Moreover, the method provides orientated immobilization, allowing ready access to the bioreceptor binding site(s). This is very important to maximise the bioreceptor binding function and assay performance (Ma et al., 2010; Jazayeri et al., 2016).

In this project, conjugation was achieved by using the streptavidin-biotin interaction. It is a well-known non-covalent interaction, which is very strong with a $K_D \sim 10^{-15}$ M. Also, biotin is versatile for linking bioreceptors as it can be easily obtained with a number of functional moieties including maleimide, hydrazide or *N*-hydroxysuccinimide (NHS) to couple to –SH, carbohydrate or –NH₂ groups. Linking streptavidin coated AuNPs (strep-AuNPs) to biotinylated bioreceptors is an efficient way to produce stable nanobiosensors for DLS assays. Here, the anti-myoglobin (Mb) C2 Affimer was used to optimise functionalisation as it had the best expression yield. Findings were then applied to other Affimers.

Another conjugation pathway is to use biotin maleimide to target thiol groups. Reduction of IgG is required to make its thiol groups available for conjugation. Whilst the whole IgG has multiple disulphide bonds linking light and heavy chains together, the disulphide bridge can be cleaved only at the hinge region by certain reductants and yields two –SH groups for coupling. However, half-IgG generation is a complex process and the conditions used depend on variations in the IgG structure. Makaraviciute et al. (2016) suggested that 35 mM TCEP reducing agent at pH 4.5 gave the best half-IgG yield for rabbit anti-Mb IgG. However, the acidic condition might not be an appropriate for AuNP stability and therefore, this method was not considered here.

In addition to these two biotinylation reagents, biotin hydrazide is another linker used in IgG biotinylation. The oxidation of carbohydrates by sodium periodate (NaIO_4) at Fc region of IgG yields reactive aldehydes, which reacts with biotin hydrazide forming a stable hydrazone linkage (Figure 4-2). This reaction was successfully used in linking hydrazide terminated liposomes (Wagh and Law, 2013) and PEG-dithiol linker (Kumar et al., 2008) to IgGs. To enable orientation of the IgG and assure that the binding site faces outwards, here, biotin hydrazide was selected for the biotinylation process.

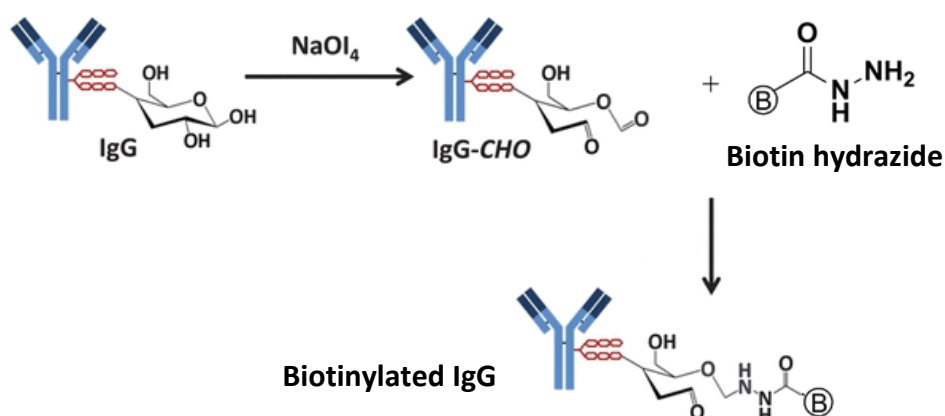


Figure 4-2 Biotin hydrazide reaction. Carbohydrates at the Fc region of IgG was oxidized by sodium periodate (NaIO_4) and immediately reacted with biotin hydrazide to form a stable hydrazone linkage.

Biotinylation of anti-Mb IgG was performed by the method described in section 2.2.3.1. ELISA was carried out to confirm the success of biotinylation after unbound biotin hydrazide was removed by desalting. Figure 4-3 shows that biotinylation of anti-Mb IgG was successful.

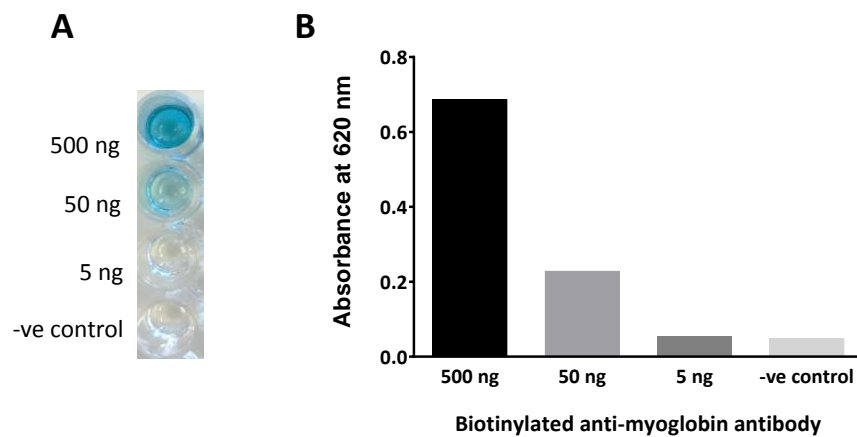


Figure 4-3 ELISA to show biotinylation of anti-myoglobin IgG (anti-Mb IgG) for AuNP functionalisation. (A), showing ELISA strip for three different dilutions of biotinylation of anti-Mb IgG 0.5 mg/ml (1, 1/10, 1/100) and negative control (PBS buffer) from top to bottom; (B), showing the absorbance at 620 nm of each tested samples.

4.2.2 Affimers

For Affimers, biotin maleimide was selected for biotinylation since they contain one cysteine at their C-terminus. However, the -SH groups are likely to form disulphide bridges so reduction of the Affimer disulphide bonds was conducted by using TCEP gel. The use of TCEP as reductant avoids the needs to remove it, as would be the case for mild thiol reductants such as 2-mercaptoethylamine (2-MEA) (Goode et al., 2016). Immediately after the reduction, biotin maleimide was added and incubated for 2 h at RT. The reaction scheme is shown in Figure 4-4. After free biotin maleimide was removed by desalting, ELISA and mass spectrometry were used to confirm biotinylation. Figure 4-5 and 4-6 show ELISA and mass spectrometry results of C2 Affimers biotinylation; other Affimers results are shown in Appendix 2 – 6.

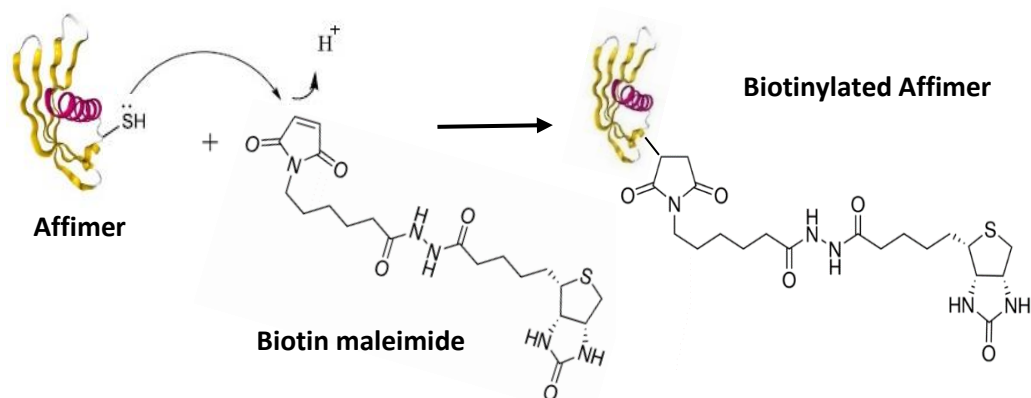


Figure 4-4 Schematic of biotin maleimide interaction to Affimer.

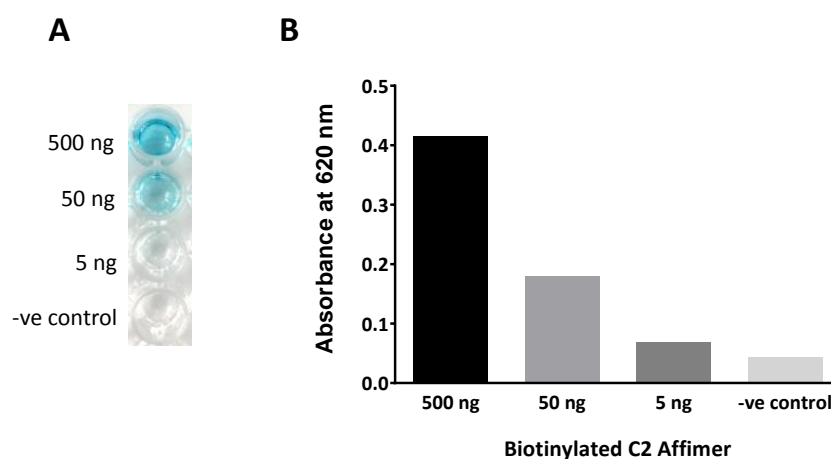


Figure 4-5 ELISA to show biotinylation of C2 Affimer for AuNP functionalisation. (A), showing ELISA strip for three different dilutions of biotinylated C2 Affimer 0.5 mg/ml (1, 1/10 and 1/100) and negative control (PBS buffer) from top to bottom; (B), showing the absorbance at 620 nm of each tested samples.

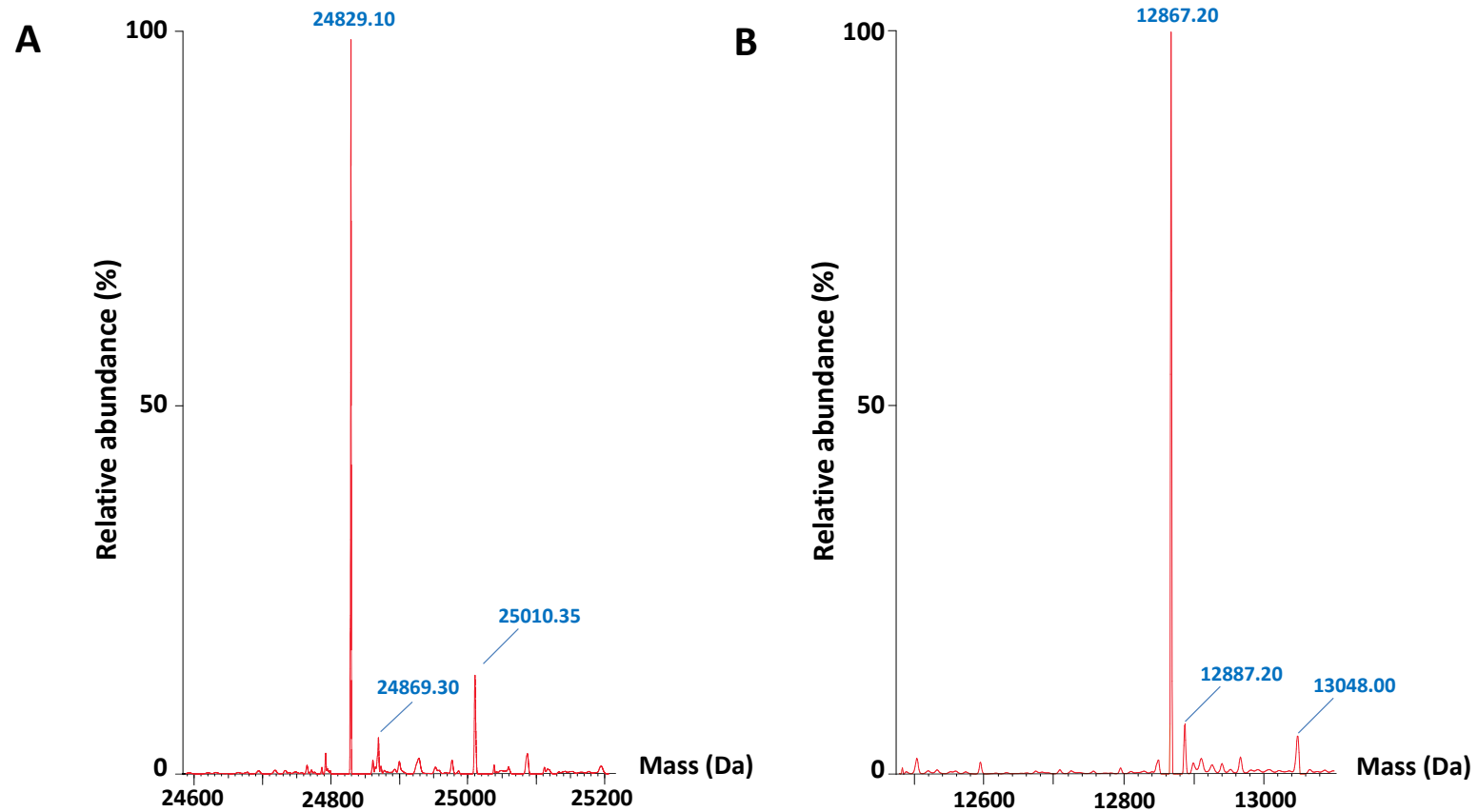


Figure 4-6 Mass spectra of C2 Affimer. (A), showing C2 Affimer before biotinylation, the highest mass peak at 24829.10 Da corresponded to Mr of dimeric C2 Affimer; (B), showing after biotinylation, the highest mass peak at 12867.20 Da corresponded to Mr of C2 Affimer monomer plus biotin maleimide (Mr 451.54 Da).

Mass spectra of C2 Affimers shown in Figure 4-6A shows the highest mass peak at 24829.10 Da, which is twice the estimated Mr of an Affimer monomer (12 – 13 kDa). This result supports the idea of dimerization of the Affimers due to their thiol group at the C-terminal cysteine. Based on the assumption that the dimer form presented in solution, the mass of C2 Affimer monomer form would equal to 12414.55 Da. The mass was lower than expected Mr of C2 Affimer obtained from its sequence via ProtParam tool (12547.2 Da) by around 132-136 Da. This phenomenon was observed in other four selected Affimer mass spectrum results. Table 4-1 gives a summary of mass from selected Affimers obtained by mass spectrometry. The missing mass corresponds to the mass spectrum peak of methionine (around 132-133 Da). In addition, it was reported that in most recombinant proteins, removal of the translation initiator N-terminal methionine (Met) is crucial for its function and stability (Liao et al., 2004). A likely explanation is that the sequence obtained from subcloned DNA containing Met but in the actual expressed protein, N-terminal Met was cleaved off.

Table 4-1 Summary of all selected anti-myoglobin Affimers masses obtained by mass spectrometry.

Affimer	Mass obtained by mass spectrometry (Da)		ProtParam calculated mass from DNA sequence (Da)	Missing mass (Da)
	<i>Dimer</i>	<i>Calculated monomer</i>		
B5	24967.55	12483.78	12619.30	135.52
C2	24829.10	12414.55	12547.20	132.65
D1	25003.60	12501.80	12635.40	133.60
F5	24733.55	12366.78	12501.30	134.52
H1	25037.30	12518.65	12650.40	131.75

In Figure 4-6B, the mass spectrum shows the highest mass peak at 12867.2 Da for the C2 Affimer and no peak was found at the same position in its dimer form, which suggested that all C2 Affimers were reduced. This confirmed the success of biotinylation as the mass difference from the monomer form of C2 Affimer alone was within the range of biotin maleimide Mr (451.54 Da). Table 4-2 presents the biotinylated masses of all selected Affimers.

Table 4-2 Summary of all selected biotinylated anti-myoglobin Affimers masses obtained by mass spectrometry.

Affimer	Calculated monomer mass (Da)	Biotinylated mass (Da)	Mass difference (Da)
B5	12483.78	12939.08	455.30
C2	12414.55	12867.20	452.65
D1	12501.80	12955.14	453.34
F5	12366.78	12821.08	454.30
H1	12518.65	12970.40	451.75

4.3 Preparation of AuNP nanobiosensors

4.3.1 Streptavidin coated AuNPs

In this project, streptavidin coated AuNPs with different core diameters (20, 40, 60, 80 and 100 nm) were used, so their sizes were measured by DLS as baseline before any functionalisation. Before the measurement, the AuNP storage buffers were removed by centrifugation and 10 mM PBS buffer (pH 7.4) was used to resuspend the pellets. All strep-AuNPs used were maintained at an optical density (OD) of 1.0. The ODs of 20, 40, 60, 80 and 100 nm core diameter AuNPs were measured at 520, 529, 540, 553 and 572 nm, respectively. In addition, DLS laser power was adjusted for each size of AuNPs via attenuation in order to prevent saturation of the detector as different sizes of AuNPs provide different scattering intensities. AuNPs with core diameter of 20, 40 and 60 nm used attenuation numbers 11, 10 and 9, respectively; whilst 80 and 100 nm used the same attenuation number 8.

Here, DLS was used as the main characterisation technique because it has proved to be an effective tool in studying protein-protein interaction as explained earlier in Chapter 1. The diameter of a streptavidin molecule is around 11.3 nm with a height of 2.04 nm; this was reported by Neish et al. (2002), who studied the dimensions using atomic force microscopy (AFM). When proteins fully adsorb onto the AuNP surface, the diameter of the AuNPs is expected to increase at least by twice the diameter of the protein molecule. Proteins have weak intrinsic light scattering properties that can only be detected by DLS when a high concentration is used. However, binding of proteins on the AuNP surface makes them measurable by DLS (Jans et al., 2009; James and Driskell, 2013). Therefore, it was estimated that when streptavidin fully coated onto AuNPs with different core diameter, the mean D_H should increase around 22 nm. Nevertheless, it was observed from Table 4-3 that the size shift observed varies over the range 15 – 30 nm.

Table 4-3 Mean D_H of streptavidin coated AuNPs (strep-AuNPs) obtained from DLS. Concentrations of each strep-AuNPs were kept the same as $OD_x^* = 1$ and 100 μ l of each AuNPs were measured in a small volume cuvette. For each sample, 10 runs with 10 s/run were performed and the average value were reported. Standard deviation was derived from triplicate measurements. (Note * The ODs of 20, 40, 60, 80 and 100 nm core diameter streptavidin coated AuNPs were measured at 520, 529, 540, 553 and 572 nm, respectively).

<i>Core diameter (nm)</i>	<i>Mean D_H (nm)</i>	<i>SD (n=3)</i>	<i>Size shift from core diameter (nm)</i>
20	38.74	0.50	18.74
40	54.98	1.22	14.98
60	84.16	1.28	24.16
80	105.39	1.68	25.39
100	130.21	1.67	30.21

A possible explanation is due to the possible orientations of streptavidin on the AuNP surface. Figure 4-7 shows a graphic of possible orientations of streptavidin on AuNPs. Figure 4-7A represents streptavidin vertically adsorbing onto the AuNP surface. In this case, the size increases should be around 22 nm as expected. But there is also a possibility of streptavidin adsorbing at different angles as shown in Figure 4-7B. This might be the reason why various size shifts were witnessed in DLS measurements. Another possibility is when streptavidin adsorbs flat onto AuNP surface (Figure 4-7C), the size increases should be around 4 nm. However, this was not observed here. It should be noted that there was a chance of having mixed orientations of streptavidin on the AuNPs as well and that DLS is a technique that measures whole population of samples.

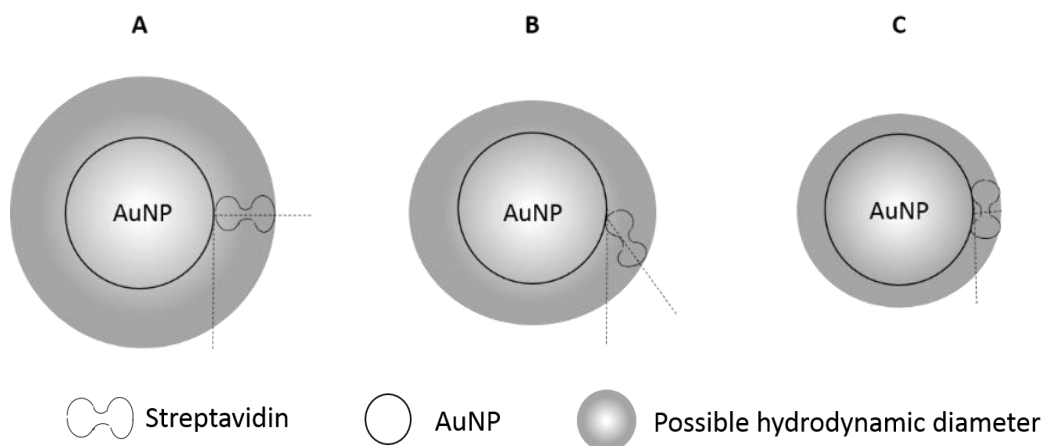


Figure 4-7 Graphics illustrate the possible orientations of streptavidin on AuNP surface. (A), vertical; (B), angled; and (C), flat orientations.

Furthermore, to confirm that the size increases of strep-AuNPs are not from aggregation before functionalisation, size distributions plots of each AuNP are shown in Figure 4-8. It is apparent from the plots that all strep-AuNPs had a narrow distribution, suggesting no pre-aggregation had occurred when the storage buffers were removed and 10 mM PBS buffer (pH 7.4) was used for resuspension.

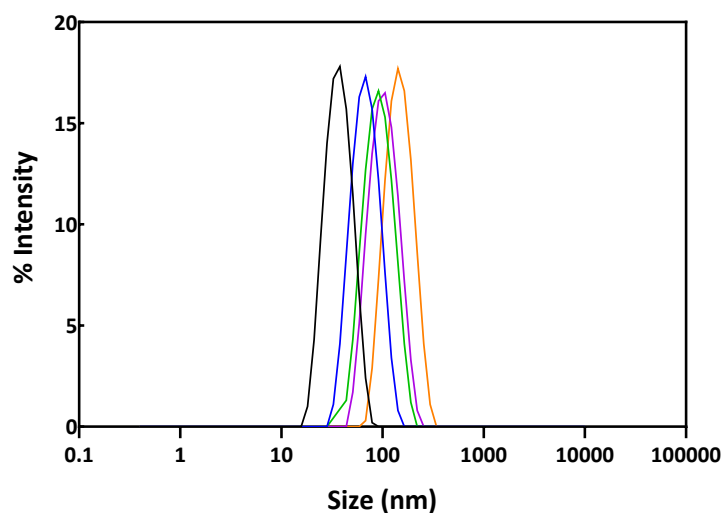


Figure 4-8 Size distribution plots of all streptavidin coated AuNPs (strep-AuNPs) with different core diameters. The AuNPs were centrifuged and replaced the storage buffer with 1 ml of 10 mM PBS buffer (pH 7.4) before DLS measurement was made; The core diameter of strep-AuNPs are (—), 20 nm; (—), 40 nm; (—), 60 nm; (—), 80 nm; (—), 100 nm. Data are obtained as described in Table 4-3. SD were omitted for clarity.

4.3.2 Conjugation of bioreceptors onto the AuNP surface

To test the conjugation method, initially, 1 ml of streptavidin coated AuNPs (strep-AuNPs) with 40 nm core diameter ($OD_{529} = 1$) in 10 mM PBS buffer (pH 7.4) were mixed with 25 μ g of each biotinylated IgG and C2 Affimer. The mixed solutions were incubated for 2 h at RT and free biotinylated bioreceptors were removed by centrifugation. Multiple wash steps were carried out to ensure that there was no unbound biotinylated IgG or Affimer left. Dot blotting, UV-spectrometry and DLS were used to confirm the conjugation. Figure 4-9 shows dot blotting results confirming that there were IgGs and C2 Affimers present on the AuNP surfaces.

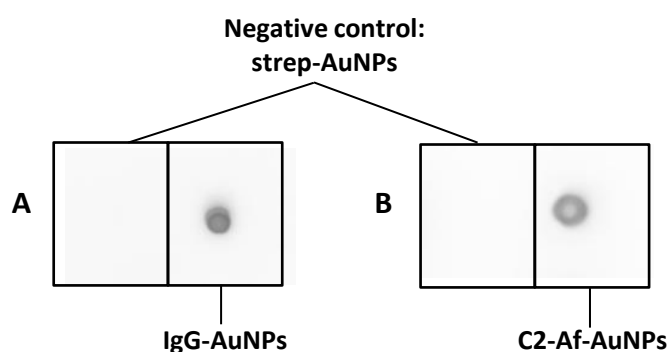


Figure 4-9 ECL dot blot immunoassay to check bioreceptors conjugation onto AuNPs. (A), left and right panels contained streptavidin coated AuNPs (strep-AuNPs) and IgG-conjugated AuNPs (IgG-AuNPs), respectively; (B), left and right panels contained strep-AuNPs and C2 Affimer-conjugated AuNPs (C2-Affimer-AuNPs), respectively. The blots were tested for the presence of bioreceptors through an ECL immunoassay with goat anti-rabbit IgG HRP-conjugated and anti-His₆-HRP-conjugated as primary antibodies (1:1000) for IgG and C2 Affimer, respectively.

Additionally, UV-spectrometry was used to confirm the conjugation process. The absorbance spectra of strep-AuNPs before and after functionalisation were measured. As shown in Figure 4-10, strep-AuNPs with 40 nm core diameter exhibited localised surface plasmon resonance (LSPR) peak at 529 nm. After conjugation with IgGs and C2 Affimers, the LSPR peak shifted to 538 and 534 nm, respectively. The shift to longer wavelengths after the conjugation was expected because modification of the NP surface could affect the local refractive index of the NPs, leading to LSPR changing.

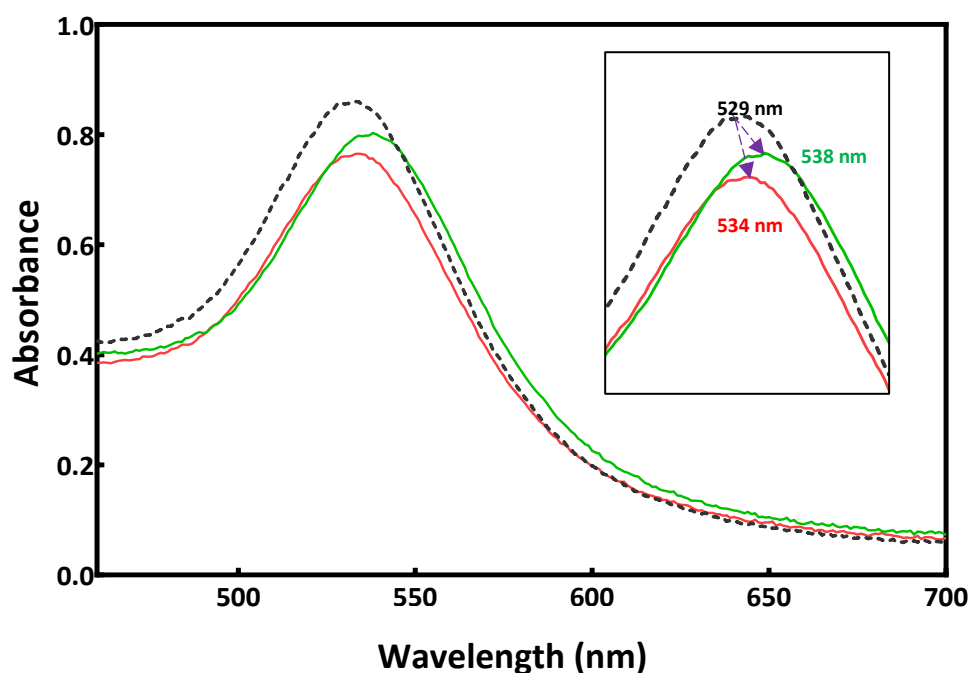


Figure 4-10 The absorbance spectra of strep-AuNPs before and after conjugation with IgG or C2 Affimer. (---), strep-AuNPs without bioreceptors; (—), IgG conjugated AuNPs (IgG-AuNPs); (—), C2 Affimer conjugated AuNPs (C2-Affimer-AuNPs); the expanded spectrum inset shows the shift of LSPR peaks after conjugation. The AuNPs were diluted 1:1 with 1X PBS buffer (pH 7.4) then 200 μ l of each AuNPs were transferred to a 96-well plate and scanned across the wavelength of 400 – 700 nm using a FLUOstar Omega plate reader.

Furthermore, DLS was another technique used to confirm the functionalisation. The average sizes of the strep-AuNPs before and after the conjugation were measured and are reported in Table 4-4. The mean D_H of strep-AuNPs was 54.97 ± 1.31 nm, which was consistent as previously reported in section 4.3.1. Upon conjugation of bioreceptors to the AuNPs, the sizes shifted to different extents depending on whether IgG or Affimer were coupled. For IgG, it was observed that the size increased by around 18.83 nm. This increase in particle size was expected as the mean D_H of IgG was reported to be 7 – 10 nm, so an increase of 15 – 20 nm would be expected (Driskell et al., 2011). For C2 Affimer, the size shifted by around 7.8 nm. Again, this corresponded to around twice its diameter (~ 3 nm). Besides the mean D_H , DLS provides size distribution data. Figure 4-11 presents the size distribution plots of IgG- and C2-Affimer-AuNPs compared to strep-AuNPs. A

narrow distribution was observed in both systems indicating no aggregation occurred. These data further confirm the success of functionalisation via the streptavidin-biotin interaction.

Table 4-4 Mean D_H of strep-AuNPs (40 nm core diameter) before and after conjugation with IgGs and C2 Affimers via the streptavidin-biotin interaction. Triplicate measurements were carried out as described in Table 4-3.

Nanobiosensors	Mean D_H (nm)	SD (n = 3)
strep-AuNPs	54.97	1.31
C2-Affimer-AuNPs	62.72	1.16
IgG-AuNPs	73.80	1.96

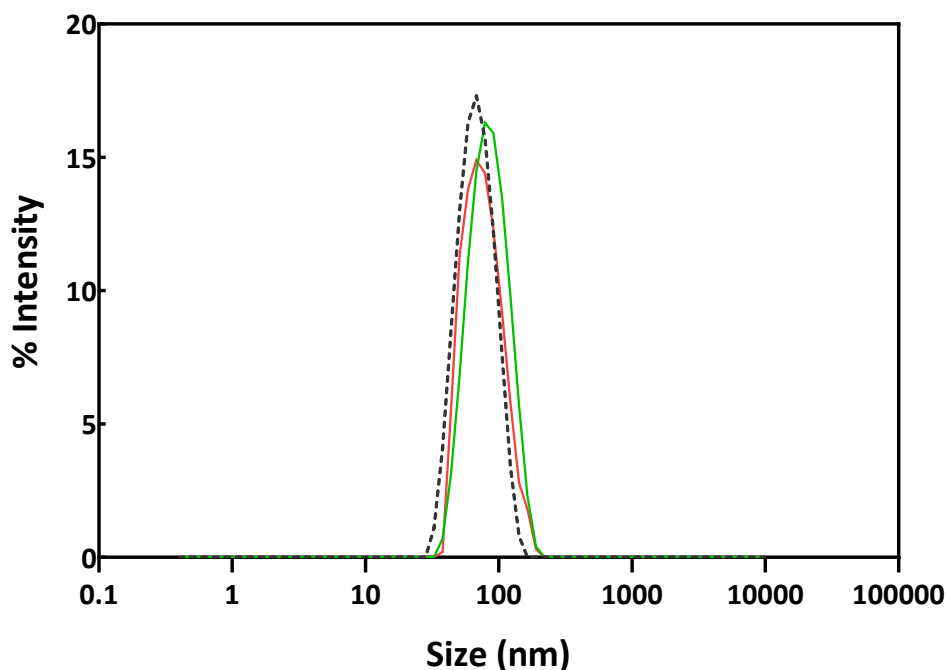


Figure 4-11 Size distribution plots of streptavidin coated AuNPs before and after functionalisation with IgGs and C2 Affimers. The lines represent streptavidin coated AuNPs: (---), without bioreceptors; (—), functionalised with IgGs; (—), functionalised with C2 Affimers. Data are obtained as described in Table 4-3. SD were excluded for clarity.

4.3.3 Optimising functionalisation

Optimisation was carried out to investigate factors affecting the functionalisation and thereby to maximise the binding activity of the nanobiosensors. In this section, the time of incubation and concentration of bioreceptors were investigated using DLS.

4.3.3.1 Time of incubation

Incubation time between biotinylated binding proteins (IgG and C2 Affimer) and strep-AuNPs was studied using strep-AuNPs with 40 nm core diameter and DLS. The experiments were performed by mixing 50 μg of each bioreceptors with the AuNPs at a concentration of $\text{OD}_{529} = 1$. The mean D_{HS} of each AuNP were recorded over a 2 h time period to optimise the functionalisation time. As shown in Figure 4-12, after strep-AuNPs were mixed and incubated with the biotinylated proteins, there was a gradual increases of both IgG-AuNP and Affimer-AuNP sizes over time. For IgG-AuNPs, the size shift started to reach a maximum at around 20 nm and leveled off after about 1 h of incubation; whilst the Affimer system took slightly longer to reach its maximum shift of around 10 - 11 nm after around 1.30 h. The incubation time was investigated with other AuNP core diameters (20, 60, 80 and 100 nm) as well and the data are shown in Figure 4-13.

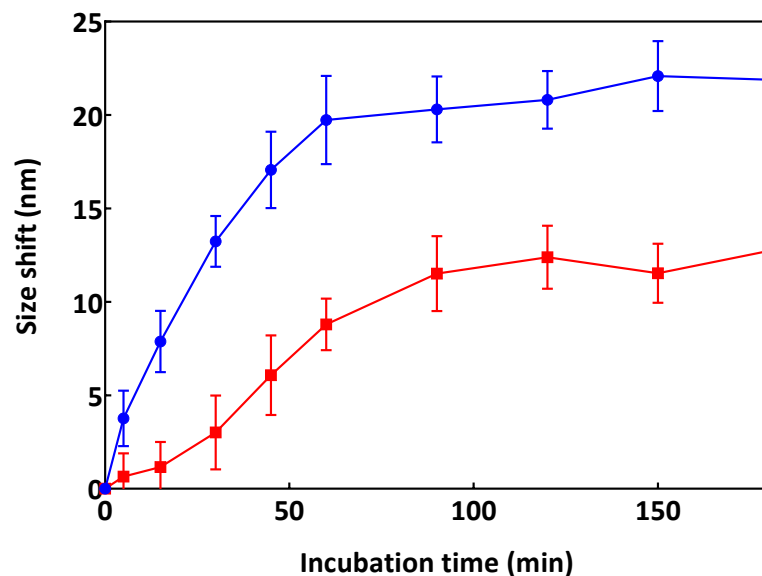


Figure 4-12 Effect of incubation time on AuNP functionalisation via the streptavidin-biotin interaction for AuNPs with 40 nm core diameter. Size shifts of streptavidin coated AuNPs (1 ml of AuNPs concentration at $OD_{529} = 1$) mixed with 50 μg in a 500 μl volume of (●), biotinylated IgG; and (■), biotinylated C2 Affimer were recorded over 3 h of incubation time. Data are mean \pm SD ($n = 3$).

The data from 20 and 60 nm AuNPs support the observation on 40 nm AuNPs that after 1 h and 1.30 h respectively, the IgGs and C2 Affimers size had shifted the maximum. This might be due to the thermodynamics of molecules trying to align themselves into the lowest energy conformation. Also, C2 Affimers are much smaller than IgGs so it is likely that more Affimers were attached to strep-AuNPs and required more time to orientate on the AuNP surface. However, with 80 and 100 nm AuNPs, it was observed that both IgG- and C2-Affimer-AuNPs size shifts had reached their maximum shifts faster, at 45 min and 1 h for IgG and C2 Affimer, respectively. Overall, these data suggested that an optimum incubation time is more than 1 and 1.30 h for IgG and Affimer, respectively. To generalise the protocol for DLS assay, 2 h of incubation time was used throughout the experiment in preparation of AuNP nanobiosensors.

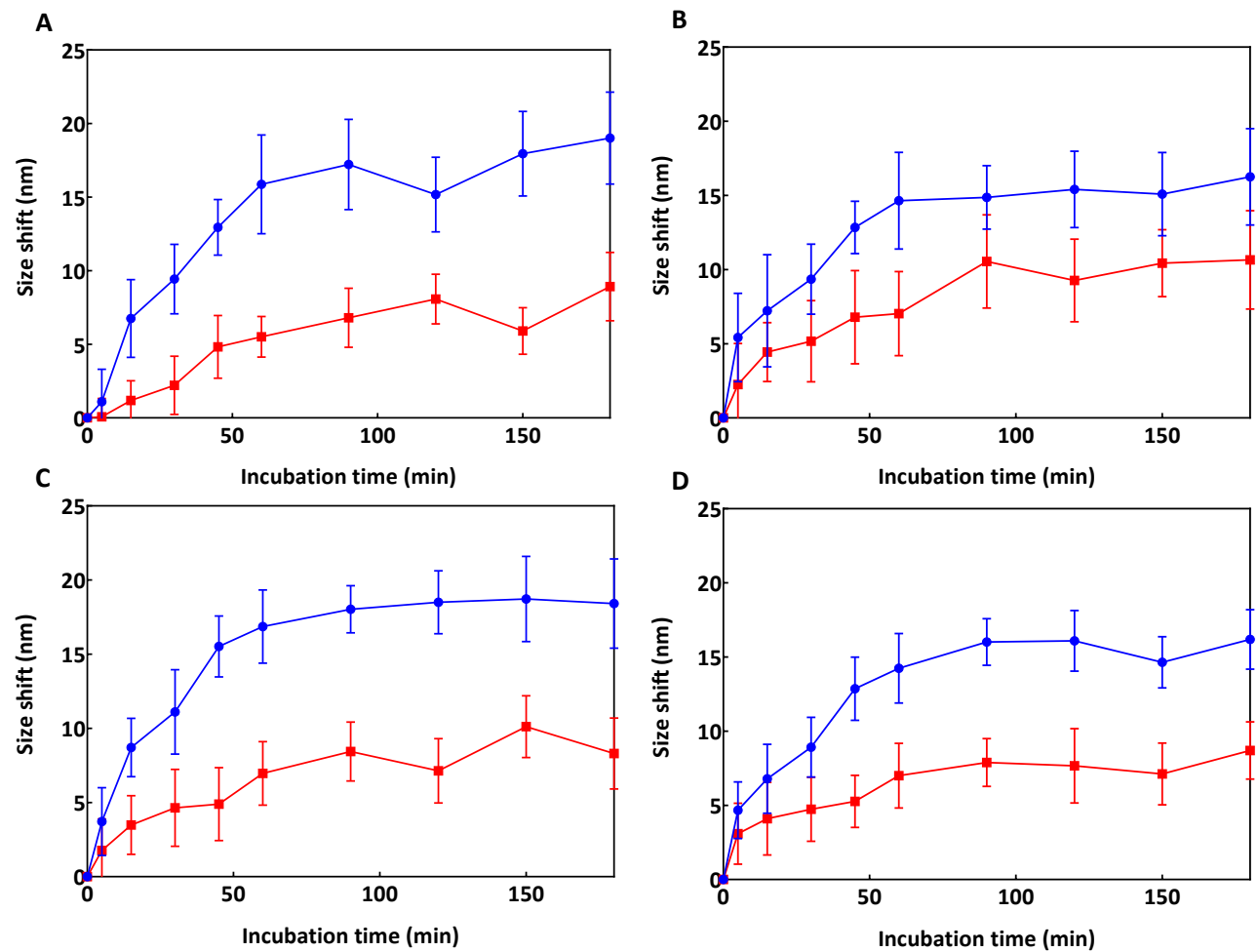


Figure 4-13 Effect of incubation time on AuNP functionalisation via the streptavidin-biotin interaction for different sizes of AuNPs. Experiments were performed as described in Figure 4-12 with AuNPs size of (A), 20 nm; (B), 60 nm; (C), 80 nm; and (D), 100 nm. Size shifts of streptavidin coated AuNPs mixed with 50 μ g in a 500 μ l volume of (\bullet), biotinylated IgG; and (\blacksquare), biotinylated C2 Affimer. Data are mean \pm SD (n = 3).

4.3.3.2 Concentration of biotinylated bioreceptors

The concentration of biotinylated bioreceptors used in functionalisation is also another important factor to be considered. Too few bioreceptors may lead to unsaturated surfaces regions on the AuNPs whilst excess protein may result in free bioreceptor in the system. In both cases an assay performance would possibly be affected. Figure 4-14 shows the size shift of strep-AuNPs with 40 nm core diameter ($OD_{529} = 1$) after incubation for 2 h with different amounts of biotinylated IgG and C2 Affimer. Their maximum shifts reached ~ 16 and 8 nm for IgG and C2 Affimer, respectively at amounts above 25 μg . The effect of bioreceptor concentration was also explored with other AuNP core diameters (20, 60, 80 and 100 nm). The data are shown in Figure 4-15.

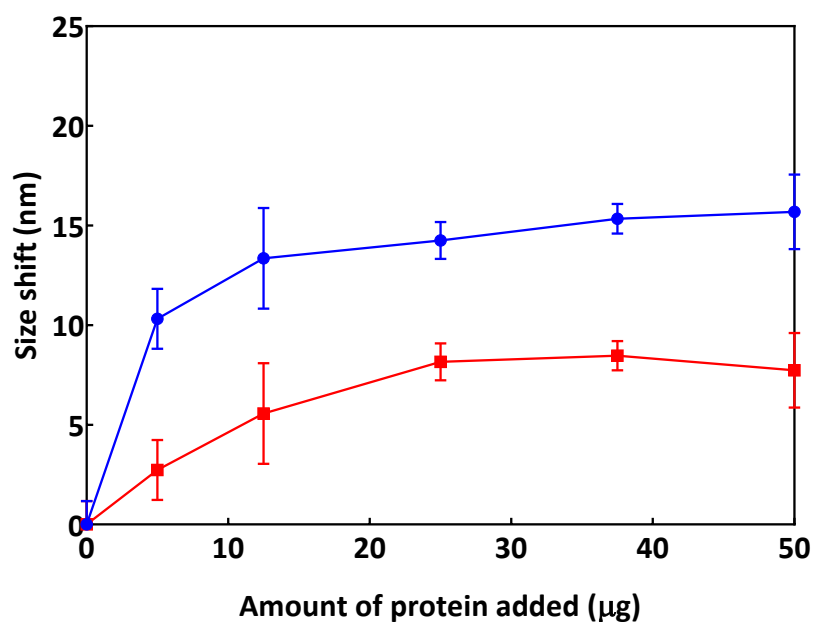


Figure 4-14 Effect of bioreceptor concentration used in AuNP functionalisation via the streptavidin-biotin interaction for AuNPs with 40 nm core diameter. Size shifts of streptavidin coated AuNPs (1 ml of AuNPs concentration at $OD_{529} = 1$) after conjugation with different amount of biotinylated IgG and C2 Affimer in a total volume of 1.5 ml. (●), represents IgG-AuNPs; and (■), represents C2-Affimer-AuNPs. Data are mean \pm SD (n=3).

The data of 60, 80 and 100 nm show similar trends as the 40 nm AuNPs as above the amount of 25 μg ; maximum shifts had reached and levelled off. Whereas for 20 nm AuNPs, the maximum shifts of IgG- and C2-Affimer-AuNPs started to level off at an amount above 15 μg . This might be due to their smaller size in which required less bioreceptor to fully cover the surface. Based on these experiments, surface coverage of bioreceptors was not increased by the addition of more than 25 μg biotinylated IgG or C2 Affimer. Therefore, the amount of 25 μg biotinylated IgG and C2 Affimer was used in subsequent functionalisations as being the most suitable for a generalised protocol.

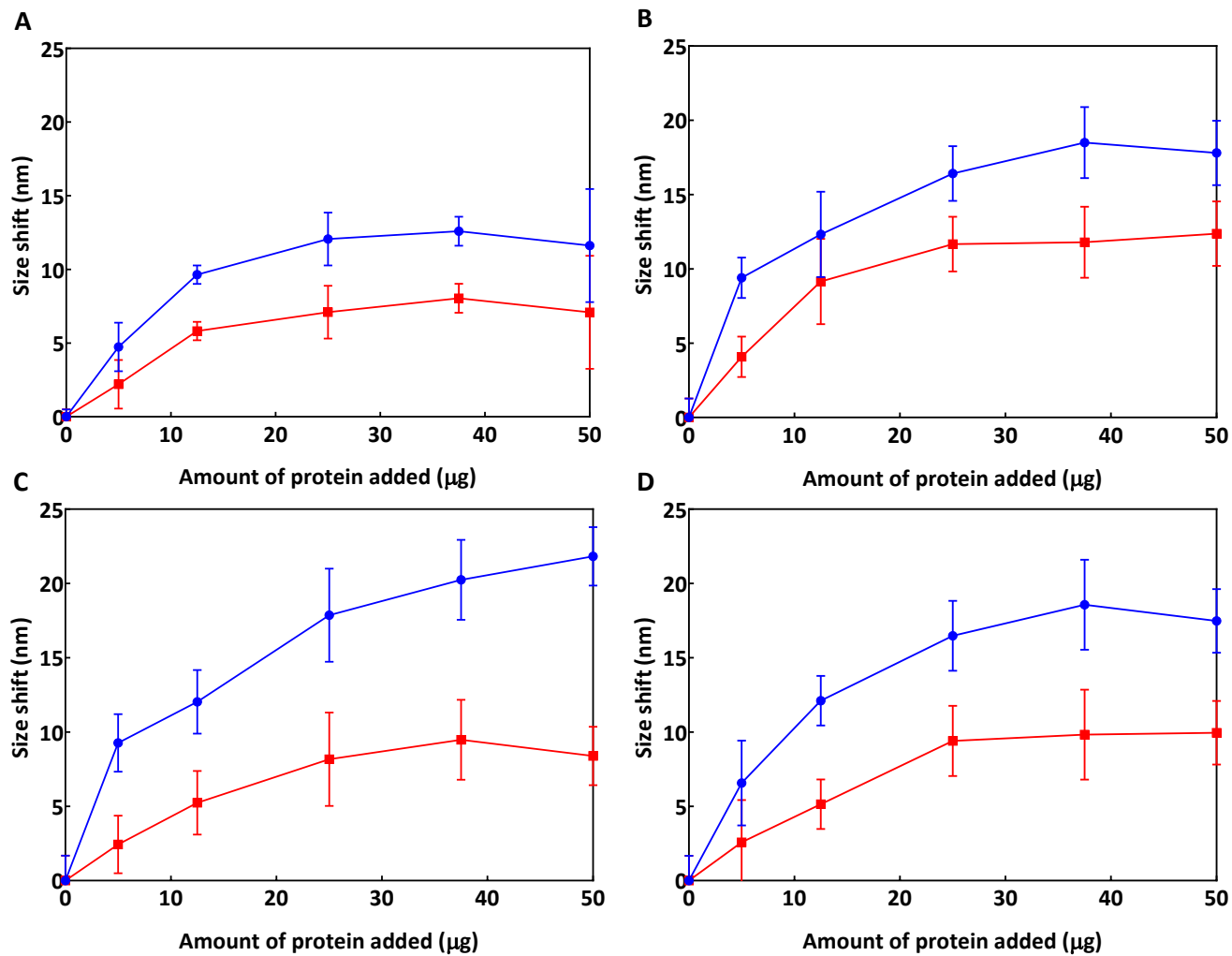


Figure 4-15 Effect of bioreceptor concentration used in AuNP functionalisation via the streptavidin-biotin interaction for different sizes of AuNPs. Experiments were performed as described in Figure 4-14 with AuNPs size of (A), 20 nm; (B), 60 nm; (C), 80 nm; and (D), 100 nm. Size shifts of streptavidin coated AuNPs after conjugation with different amount of biotinylated IgG and C2 Affimer. (●), shows IgG-AuNPs; and (■), shows C2-Affimer-AuNPs. Data are mean \pm SD (n = 3).

4.4 Quantification of bioreceptors on the AuNP surface

The characterisations of nanobiosensors carried out in the previous section are all indirect methods and these methods could not provide the actual amount of binding proteins conjugated onto the AuNP surface. One, indirect way to quantify the amount of attached bioreceptors is to quantify bioreceptors left in the supernatant after conjugation using the Bradford or BCA protein assays. However, overestimation of attached bioreceptors is commonly found when using this indirect method as proteins are sticky and stick to container, e.g. Eppendorf, used for manipulation. Therefore, a direct method is preferable despite it being a more complicated protocol.

In this section, a direct method was used to quantify bioreceptors (IgGs or Affimers) attached to the AuNPs. This method was adapted from a study by Filbrun and Driskell (2016). This direct method comprises two main parts; (i), dissolution of AuNPs and (ii), quantification of gold and the bioreceptors. First, the IgG- and C2-Affimer-AuNPs were prepared with 40 nm core diameter AuNPs under optimised conditions. Then, KI/I₂ etchant solution was used to dissolve the AuNPs. Here, complete dissolution of gold was confirmed by ICP-MS instead of AAS, which provided the amount of gold in solution. IgG- and C2-Affimer-AuNPs were centrifuged at 4,500 xg for 30 min after the last wash step, the supernatants obtained were kept and sent for gold quantification by ICP-MS in order to confirm that all AuNPs were completely pelleted. Figure 4-16 shows the concentration of gold in 1 ml samples measured with ICP-MS for both IgG- and C2-Affimer-AuNPs.

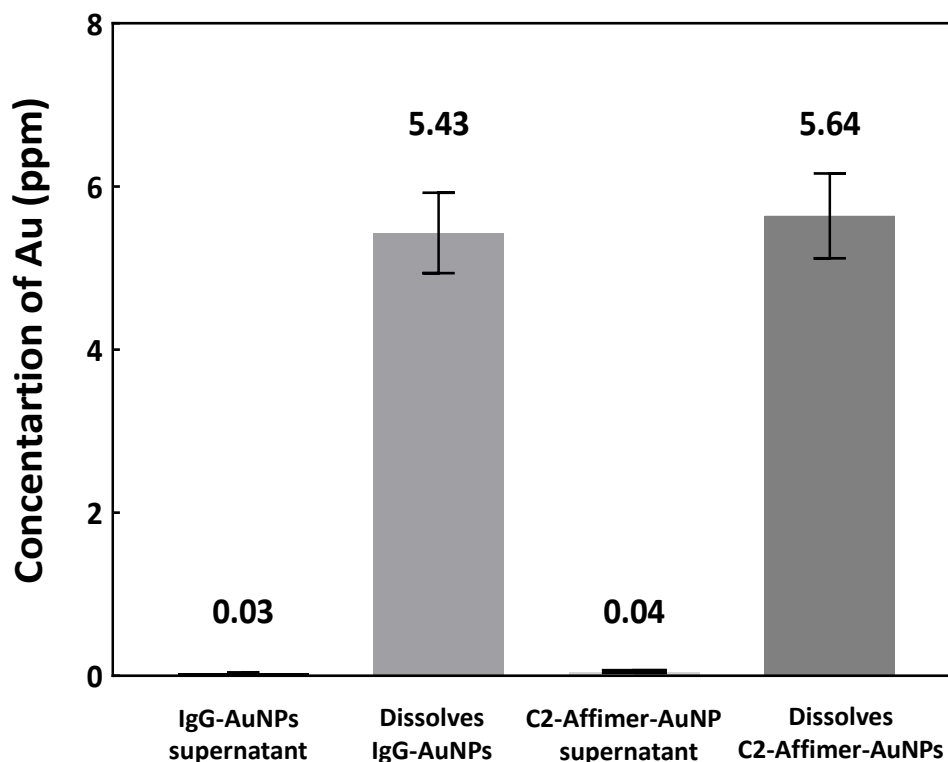


Figure 4-16 Concentration of gold from 1 ml AuNP nanobiosensors obtained by ICP-MS analysis. Data are mean \pm SD (n = 3).

The concentrations obtained by ICP-MS indicated that all AuNPs in both IgG- and C2 Affimer systems were fully dissolved because there was no gold left in the supernatants. The number of AuNPs in the solutions was calculated using an information provided by the manufacturer that one nanoparticle of 40 nm core diameter has a gold mass of 6.47×10^{-16} g. Therefore, each IgG- and C2-Affimer-AuNP contained 8.39×10^{10} and 8.72×10^{10} NP/ml, respectively which were comparable to the manufacturer's information which gave 8.99×10^{10} NP/ml. The number of AuNPs obtained from ICP-MS were less than the information given in the data sheet. This might be due to the loss of some AuNPs during multiple washing steps. A summary of all gold concentrations obtained by ICP-MS for other AuNPs are reported in Table 4-5. The AuNPs with 20 and 60 core diameters showed a similar trend to the 40 nm AuNPs. The 80 and 100 nm AuNPs data, conversely, showed more AuNPs obtained from the experiment. A likely explanation is that there were batch-to-batch variations of AuNP production and the reported numbers from the manufacturer were estimates.

Table 4-5 Comparison of theoretical and ICP-MS measured AuNP concentrations.

<i>Core diameter (nm)</i>	<i>Theoretical AuNP concentration (NP/ml)</i>	<i>AuNP concentration (NP/ml)</i>	
		IgG-AuNPs	C2-Affimer-AuNPs
20	7.00×10^{11}	6.44×10^{11}	6.21×10^{11}
40	8.99×10^{10}	8.39×10^{10}	8.72×10^{10}
60	1.96×10^{10}	1.11×10^{10}	1.40×10^{10}
80	7.82×10^9	9.23×10^9	9.42×10^9
100	3.84×10^9	5.95×10^9	6.00×10^9

After dissolution of the AuNPs, the IgGs and Affimers conjugated onto the AuNP surface were released into the solution and the concentrations of these proteins was measured using a fluorescent dye NanoOrange. Two sets of IgG and C2 Affimer standard solutions were prepared to generate accurate calibration curves for both nanobiosensors. The calibration curves are shown in Appendix 7. Also, before quantification of proteins, the interferents (e.g. KI/I₂) were removed by using a 7K MWCO spin desalting column. In this project, strep-AuNPs were used, therefore they were used as a baseline in the fluorescent quantification method to ensure that streptavidin did not interfere with the actual amount of binding protein estimated. The indirect method was also carried out by using the Bradford assay to determine the biotinylated IgG or C2 Affimers left in the supernatant. Again, two sets of calibration curves were generated using IgG and C2 Affimer standard solutions (the calibration curves are reported in Appendix 8).

Figure 4-17 compares numbers of IgG and C2 Affimers conjugated to AuNP obtained by direct and indirect quantification methods. These results correlated with the previous study by Filbrun and Driskell (2016) in that the indirect method overestimated the amount of the molecules attached onto AuNP surface. For IgG-AuNPs, the direct method estimated 280 ± 49 IgGs/NP, compared to 509 ± 91 IgGs/NP obtained using the Bradford assay. Similar to C2-Affimer-AuNPs, the indirect method estimated 1014 ± 274 Affimers/NP, which was double the amount quantified by the direct method (565 ± 115 Affimers/NP).

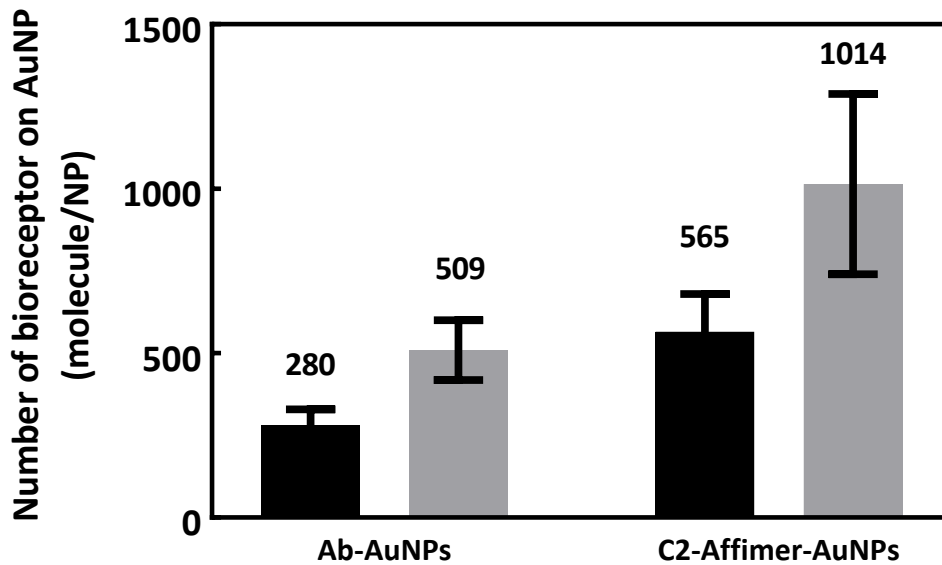


Figure 4-17 The number of bioreceptor molecules conjugated onto AuNP surface compared between the direct and indirect quantification methods. (■), shows the quantification using the direct method; (▒), shows the indirect method using the Bradford assay to quantify left over bioreceptors in supernatants. Data are mean \pm SD (n = 3).

One interesting finding is that the number of C2 Affimer molecules conjugated per AuNP were more than the IgG for both methods. This may be explained by the fact that Affimers are 3 - 4 times smaller than IgGs, so more molecules could fit on to the surface. However, the conjugation method used here was via the interaction of biotin and previously adsorbed streptavidin on the AuNP surface. So attachment of biotinylated molecules may be restricted by the number of streptavidins present.

The number of streptavidins was quantified using the fluorescence method. Figure 4-18 shows the comparison between the quantified streptavidin molecules on the AuNP surface, compared with the theoretical number of molecules calculated¹. The theoretical number of streptavidins was calculated based on the surface area of spherical NPs of a given diameter ($4\pi r^2$) and dimension of

¹ This was calculated by Dr.Lewis Mackenzie

streptavidin ($2 \times 11.3 = 22.6 \text{ nm}^2$) (Neish et al., 2002). Also, it was assumed that the proteins take up a square footprint on the surface of NPs and are perfectly packed so there is no surface area left to waste. The experimental data shows slightly more of streptavidins coated onto the NPs than the calculated data. A possible explanation might be that the curvature of NPs was not included in the assumption of the theory. It is likely that with the curvature of NPs, less steric hindrance was present and lead to underestimated theoretical data for streptavidin molecules packing.

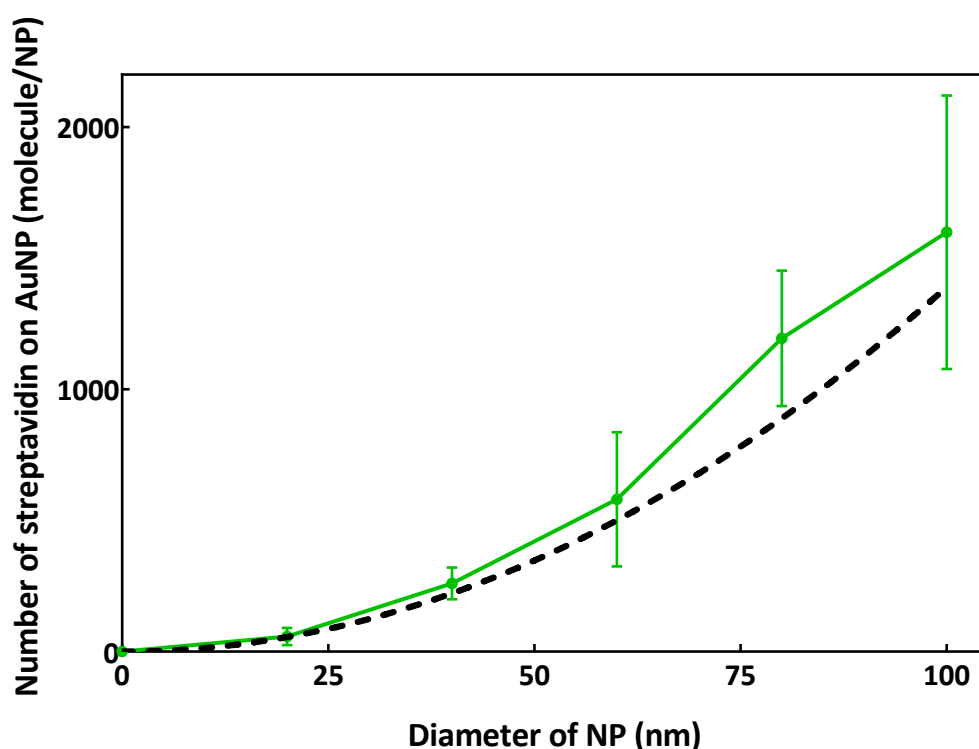


Figure 4-18 Number of streptavidin on AuNP (molecule/NP). Comparison between (—•—), the calculated data based on NP surface area and (—●—), measured data obtained by the direct fluorescence method. Measured data are mean \pm SD ($n = 3$).

In addition, when plotting the numbers of IgG and C2 Affimer obtained from the direct quantification method for 20, 40, 60, 80 and 100 nm core diameters AuNP nanobiosensors (Figure 4-19), it was apparent that for every core diameter AuNP, C2 Affimer numbers were higher than the IgG numbers. These results are in line with Ferrigno (2016) who suggested that the compact size of Affimers could increase the density of bioreceptors aligned on a sensor surface. Streptavidin is tetrameric and

contains four identical subunits each with a binding site for biotin. However, around 1 – 2 binding pockets were estimated to be available for binding after coupling to the AuNPs.

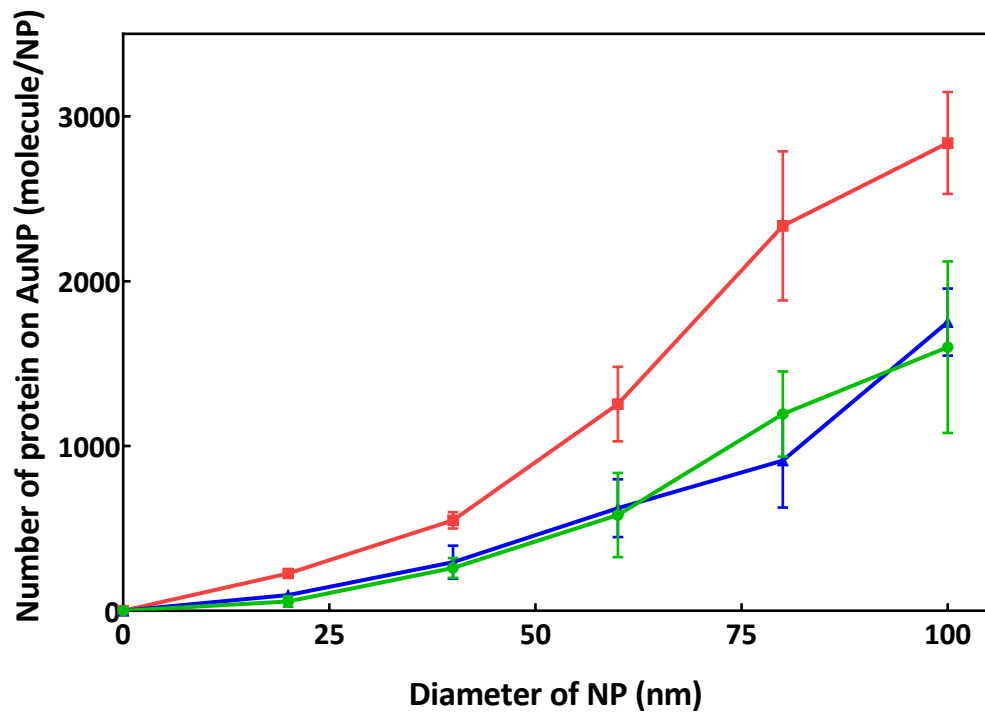


Figure 4-19 Number of bioreceptors on AuNP (molecule/NP). The measured data were obtained by the direct fluorescence method and are presented with (●), streptavidin; (▲) IgG; (■), C2 Affimer. Data are mean \pm SD (n = 3).

4.5 Discussion

In this section, the preparation of AuNP nanobiosensors has been explained together with their characterisation. Streptavidin-biotin coupling was selected as a main mechanism for attaching bioreceptors onto the AuNP surface. It is a very strong non-covalent bonding that has been successfully used for many conjugation processes (e.g. Aslan et al., 2004; Liu and Huo, 2009; D'Agata et al., 2017). Among a variety of biotin linkers, biotin hydrazide was selected for biotinylation of IgG as it interacts with oxidized carbohydrates at the Fc region and leads to an orientated IgG on the AuNPs. Whereas biotin maleimide was used with Affimers as they contain a single cysteine at the C-terminus. The success of biotinylation was confirmed by ELISA. Mass spectrometry was carried out in the case of C2 Affimer; using this approach for IgG was not possible as it was a polyclonal reagent. However, in principle it could be used with a monoclonal IgG. Both techniques confirmed the biotinylation of IgGs and Affimers. In addition, the obtained mass spectra confirmed that the aggregates formed after purification of Affimers were due to their dimerization.

For the functionalisation process, strep-AuNPs were mixed with biotinylated IgGs and Affimers and interaction allowed to occur. Dot blotting, UV-spectrophotometry and DLS were used to confirm the functionalisation. These techniques are not quantitative analyses that provide the actual number of bioreceptors on each AuNP. However, they were rapid, easy to perform and provided quick characterisation of the nanobiosensors. The shift to longer wavelength in LSPR of IgG coated AuNPs corresponded to previous studies (Kumar et al., 2008; Zhang et al., 2015; D'Agata et al., 2017). In addition, C2 Affimers tagged AuNPs showed a similar, but smaller shift. This is probably due to the size of Affimers which are smaller than IgGs. DLS provided size distribution data in order to check whether there was no pre-aggregation occurring during the functionalisation process. The DLS data are in line with previous studies that when proteins are fully coated onto the AuNP surfaces, the mean D_H increases by at least twice the diameter of protein used. However, orientation of proteins might affect the D_H obtained and

therefore, a combination of techniques should be used to characterise the nanobiosensors produced.

A direct quantitation method was also conducted to further study the AuNP functionalisation. The method was based on the dissolution of the AuNPs and direct quantitation of the dissolved gold by ICP-MS and released bioreceptors by a fluorescent method using NanoOrange dye. It proved to be more effective in comparison to the indirect method used which tended to overestimate the amount of bioreceptor conjugated onto the AuNP surface, as it mainly determined the free biotinylated bioreceptors left in the supernatant. However, proteins are sticky and could stick to the container and not just the AuNP. The data obtained from the direct method showed that C2 Affimers were packed more densely onto AuNPs (565 Affimers/NP) compared to IgGs (280 IgGs/NP). This was predicted as the Affimers are 3 - 4 times smaller in size than IgG, despite there being a similar number of streptavidin molecules on the AuNP surface. This might occur due to streptavidin's four binding pockets per molecule for biotin, even if being coated on AuNPs, it was estimated that at least two binding positions were free for interaction. An implication of this is the possibility that the Affimer nanobiosensors may provide better sensitivity in size shift assay since there are more of them attached to the AuNP surface.

Various factors related to the AuNPs functionalisation were investigated as well. It was found out that after 1 h and 1.30 h, there was no increase in mean D_H with longer incubations for IgGs and C2 Affimers, respectively. This might be due to thermodynamic of molecules trying to align themselves into the lowest energy conformation. This idea was supported by the quantitation of IgGs and C2 Affimers. With more molecules conjugated onto AuNP surface, a longer time is required in arranging them into their most suitable positions. Regarding the amount of biotinylated bioreceptor used, there was no difference between IgG and C2 Affimer in that the amounts higher than 25 μg of the proteins provided a stable size shift except with 20 nm AuNPs where at the amounts above 15 μg , the maximum shifts were observed in both IgG and C2 Affimer. However, it should be noted that the molar concentrations of IgGs and C2 Affimers used in the conjugation process were

different since an Affimer is about 1/12th Mr of an IgG (Mr = 12.5 kDa and 150 kDa for Affimer and IgG, respectively). So, a 25 µg IgG is equal to 0.16 nmol, whereas 25 µg of C2 Affimer is equal to 2 nmol in a total volume of 1.5 ml. This might be another reason why C2 Affimers attached more to the surface and required more time to align themselves on the AuNP surface. Nevertheless, the data obtained from DLS showed saturation of IgG on the AuNP surface at 25 µg as well as C2 Affimer.

Here, the optimised functionalisation was successfully established by incubating 25 µg of biotinylated bioreceptors with strep-AuNPs for 2 h. Dot blotting, UV-spectrophotometry or DLS can be used in semi-quantitative characterisation of the nanobiosensors. The Chapter that follows moves on to consider the design of NP size shift assay using the nanobiosensors prepared and DLS.

Chapter 5

**Nanoparticle-coupled
dynamic light scattering
size shift assay**

Chapter 5 NP-coupled DLS size shift assay

5.1 Introduction

Once the functionalisation of AuNPs had been successfully optimised (Chapter 4), the nanobiosensors were prepared and used in the NP-coupled DLS assay for detecting our model analyte, myoglobin (Mb). In this Chapter, anti-Mb Affimers (Chapter 3) were used in a systemic study on Mb detection. Various factors related to the size shift assay have been investigated such as kinetics of aggregation, avidity effects of the bioreceptors, effect of NP size and concentration, stability of nanobiosensors and Affimers-based system compared to IgG-based system. In addition, the optimised method was used with other protein analytes to test the versatility of the assay. To avoid confusion throughout this chapter, the 'analyte' will refer to Mb unless otherwise stated. Also, 'antibody (IgG)' and 'Affimer' will refer as specific binding reagents for Mb. Moreover, the streptavidin coated AuNPs (strep-AuNPs) with 40 nm core diameter were used except when the effect of size was tested.

5.2 Kinetics study

Regarding the NP size shift assay, it is important to understand the kinetics of the NP aggregation assay to properly design the assay format. The kinetics study was conducted by mixing Mb conjugated AuNPs (Mb-AuNPs) and Affimer conjugated AuNPs (Affimer-AuNPs) in a 1:1 volume ratio. Crosslinking of the AuNPs should occur due to the binding between Mb and Affimers (mixed C2 and F5 Affimers), leading to a shift in size. Streptavidin coated AuNPs (strep-AuNPs) and IgG conjugated AuNPs (IgG-AuNPs) were used as negative and positive controls respectively. Monitoring the change in size intermittently during 24 h provides an overview of the kinetics as well as the ability of DLS in detecting the aggregation events.

All the nanobiosensors were prepared via streptavidin-biotin coupling, with Mb, Affimers and IgGs being biotinylated using biotin NHS, biotin maleimide and biotin hydrazide, respectively. Then, 25 µg of each biotinylated protein was

incubated with 40 nm core size strep-AuNPs for 2 h at RT. More details of conjugation process are detailed in Chapter 4. Table 5-1 shows the original sizes of all functionalised AuNPs used in the kinetics study.

Table 5-1 Original sizes of all functionalised AuNPs used in the kinetics study measured by DLS. 100 μ l of each AuNPs was transferred to a small volume cuvette and measured three times with 10 runs at 10 s/run. Data were obtained from triplicate measurements.

Functionalised AuNPs	Mean D_H (nm)	SD (n=3)
Streptavidin coated AuNPs	55.28	1.17
Myoglobin conjugated AuNPs	64.08	1.38
IgG conjugated AuNPs	67.06	1.67
Affimer conjugated AuNPs	61.88	1.47

The mean D_H after the conjugation of all functionalised AuNPs indicated that each protein were fully coupled to the AuNP surfaces. As described in the earlier chapters, when proteins were fully coating the AuNPs, the mean D_H of the particles is expected to increase at least by twice the diameter of that protein molecule. For Mb-AuNPs the size increased from 55.28 ± 1.17 to 64.08 ± 1.38 nm, which corresponded roughly to twice the diameter of Mb ($D \sim 3.5$ nm). Similarly, Affimer AuNPs sizes increased by around 6.6 nm, the shift in size was correlated with its diameter ($\sim 2 - 3$ nm). However, the IgG-AuNP size shifted only by around 11.78 nm, which was slightly lower than expected, as the D_H of an IgG is around 7 – 10 nm. This is probably due to the orientation of IgG on the AuNP surface. Still, the size distribution plots confirmed that the size distributions were narrow and there were no signs of aggregates presented (Figure 5-1).

The mean D_H values of the 1:1 volume ratio mixed solutions between Mb-AuNPs and three different nanobiosensors are illustrated in Figure 5-2. When Mb-AuNPs were mixed with strep-AuNPs, the mean D_H remained the same and there was no significant increase in size even after 24 h incubation. Conversely, the size increased linearly in both IgG and Affimer systems during the incubation time. After 24 h, the size of Affimer-AuNPs increased from 61.88 ± 1.47 to 118.67 ± 4.11 nm. Whilst, the size of IgG-AuNPs increased from 67.06 ± 1.67 to 131.90 ± 4.32 nm. The

increases in size of the AuNPs were due to specific binding events between IgG/Affimer and Mb on the AuNPs and eventually led to crosslinking of the particles.

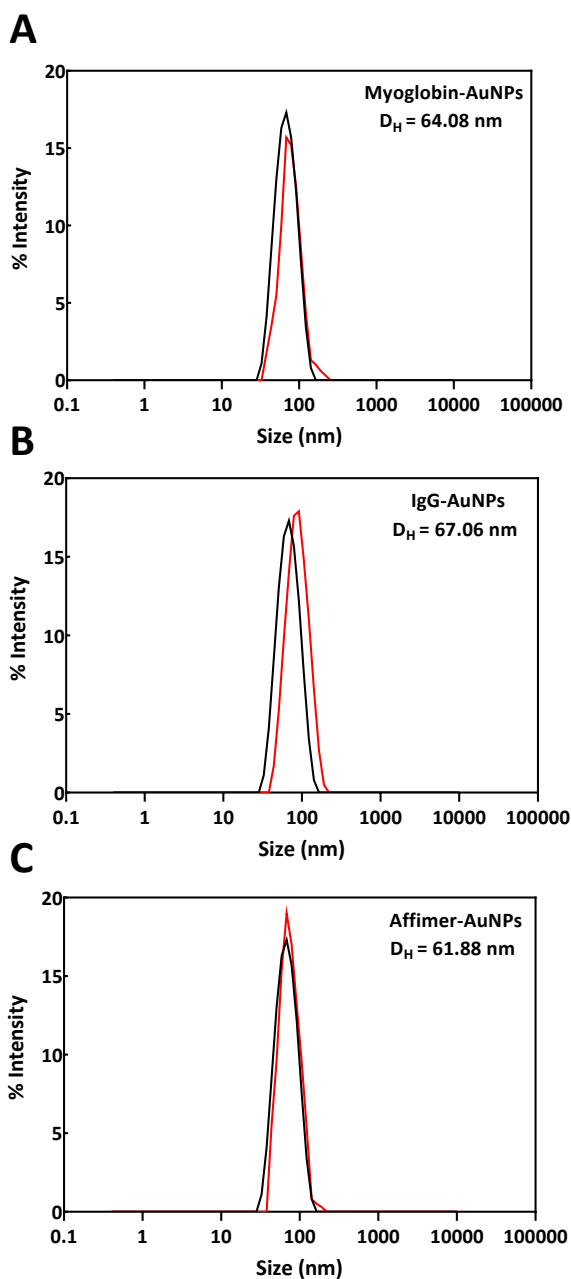


Figure 5-1 Size distribution plots of all functionalised AuNPs used in the kinetics study. The measurements were performed as described in Table 5-1. SD were excluded for clarity. (A), myoglobin conjugated AuNPs (Mb-AuNPs); (B), anti-myoglobin IgG conjugated AuNPs (IgG-AuNPs); (C), anti-myoglobin Affimer conjugated AuNPs (Affimer-AuNPs); The size and size distribution of streptavidin-AuNPs before, (—) and after, (—) conjugation process.

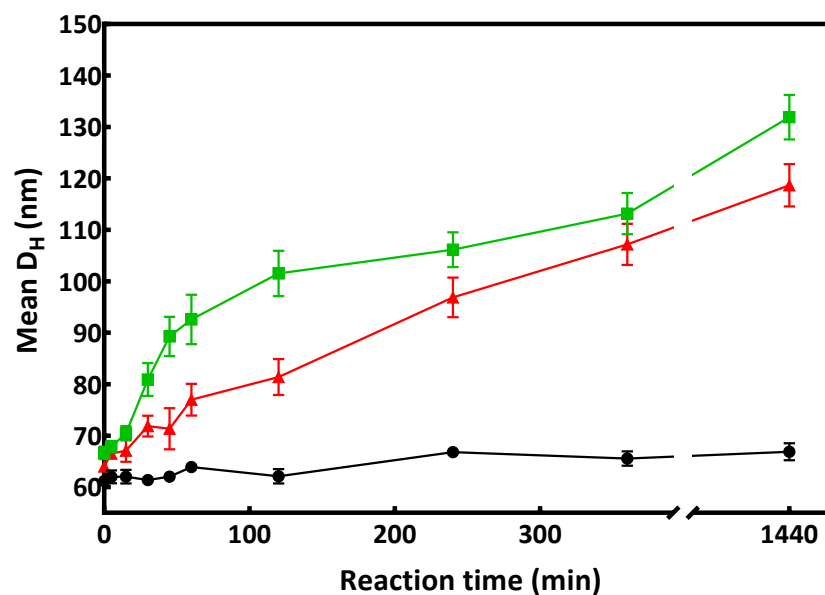


Figure 5-2 The average hydrodynamic diameter (D_H) of a 1:1 volume ratio mixture of myoglobin conjugated AuNPs (Mb-AuNPs) and three different nanobiosensors over 24 h. 50 μ l of Mb-AuNPs was mixed with 50 μ l streptavidin coated AuNPs, (\bullet); anti-myoglobin IgG conjugated AuNPs, (\blacksquare); and anti-myoglobin Affimer conjugated AuNPs, (\blacktriangle). Data are mean values \pm SD (n=3).

Closer inspection of data shows that the size-shift rate was much faster in the first 100 min of incubation. After that the size still increased but at a much slower rate. A possible explanation would be that dispersed AuNPs move at a certain rate and once dimers and trimers formed, these larger AuNPs move slowly than monomers, which led to a slower interaction rate. Figure 5-3 shows the mean D_H of each mixed solution in the first hour of incubation. After 30 min, it was obvious that the mean D_H had shifted from the baseline for both IgG and Affimer based systems.

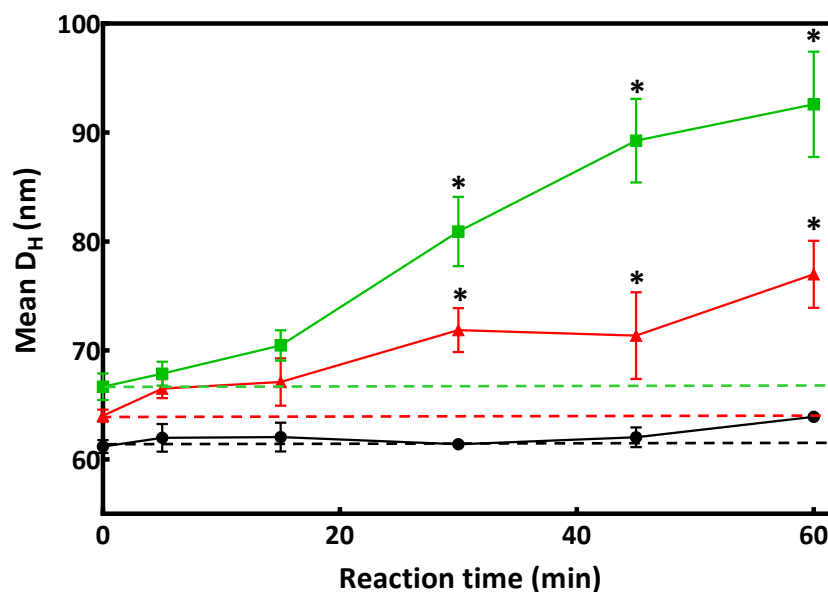


Figure 5-3 The average hydrodynamic diameter (D_H) of a 1:1 volume ratio mixture of myoglobin conjugated AuNPs (Mb-AuNPs) and three different nanobiosensors in an expanded scale. 50 μ l of Mb-AuNPs was mixed with 50 μ l streptavidin coated AuNPs, (●); anti-myoglobin IgG conjugated AuNPs, (■); and anti-myoglobin Affimer conjugated AuNPs, (▲). The dashed lines represent the baseline D_H in 0 min of each system. Data are mean values \pm SD ($n=3$). (*) indicates significant values tested with independent t-test between experiment and their baseline D_H ($p < 0.05$).

In addition, Figure 5-4 shows the size distributions of all three mixed solutions compared at incubation times of 1 min and 24 h. It can be seen from the size distribution plots from Figure 5-4A that after 24 h, there was no significant shift in size for the negative control system, whilst, there were substantial shifts in size in the other two systems (Figure 5-4B and C). The size distribution plots obtained from DLS also provided details of the aggregates forming. In the case of the positive control using IgG-AuNPs, at 1 min most of NP population (> 90%) had a size < 100 nm. At 24 h, however, a broader size distribution curve was observed with almost all of the population shifted to > 100 nm. This supported the idea that at 1 min the binding between Mb-AuNPs and IgG-AuNPs occurred to a limited extent, resulting in only a few dimers presence in the solution. However, after 24 h, more dimers, trimers and larger multimers formed, leading to a broader size distribution curve. The Affimer based system showed a similar trends compared to the IgG based nanobiosensors.

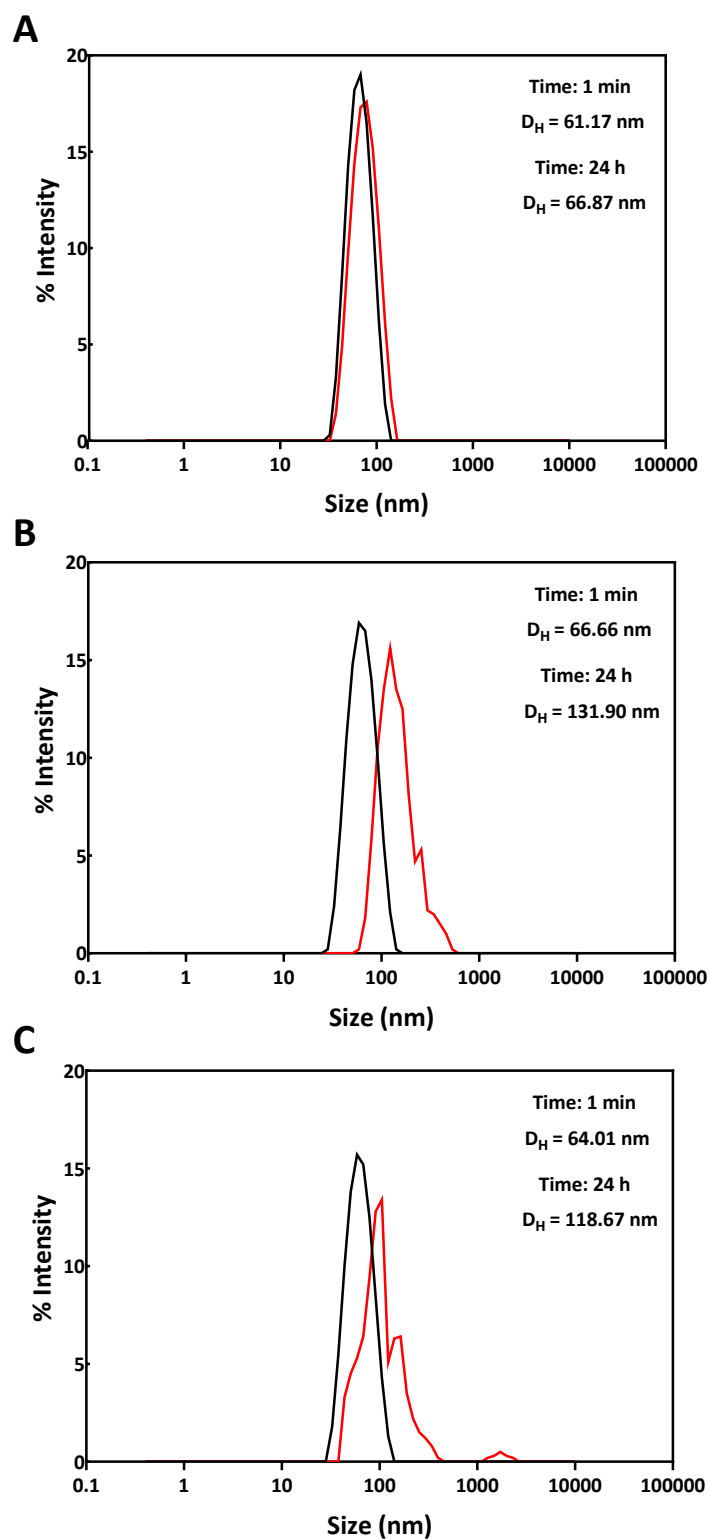


Figure 5-4 The size distributions of all three mixed solutions comparing at incubation times of 1 min, (—); and 24 h, (—). (A), Mb-AuNPs + strep-AuNPs; (B), Mb-AuNPs + IgG-AuNPs; and (C), Mb-AuNPs + Affimer-AuNPs. Data obtained as described in Figure 5-2.

5.3 Detection of myoglobin using NP-coupled DLS size shift assay

5.3.1 Antibody (IgG) based assay

IgG conjugated AuNPs (IgG-AuNPs) have been successfully used in various affinity assays using DLS. Therefore, as a comparator, polyclonal Ab (IgG) functionalised AuNPs were prepared and used to detect Mb. To enable comparison between different nanobiosensors, the shift in size from the original AuNP size will be plotted instead of the absolute mean D_H . Biotinylated IgG via biotin-hydrazide were linked to strep-AuNPs according to the method optimised in Chapter 4. The IgG-AuNPs prepared were characterised with DLS before used. The mean D_H was 71.08 ± 1.37 nm and the size distribution plot also showed no aggregation during the conjugation (Appendix 9A). The mean D_H of IgG-AuNPs before and after mixing with the analyte over the concentration range 10 fM to 10 μ M was measured by DLS after incubation at RT for 30 min. Strep-AuNPs were used instead of IgG-AuNPs as negative control. The results are shown in Figure 5-5.

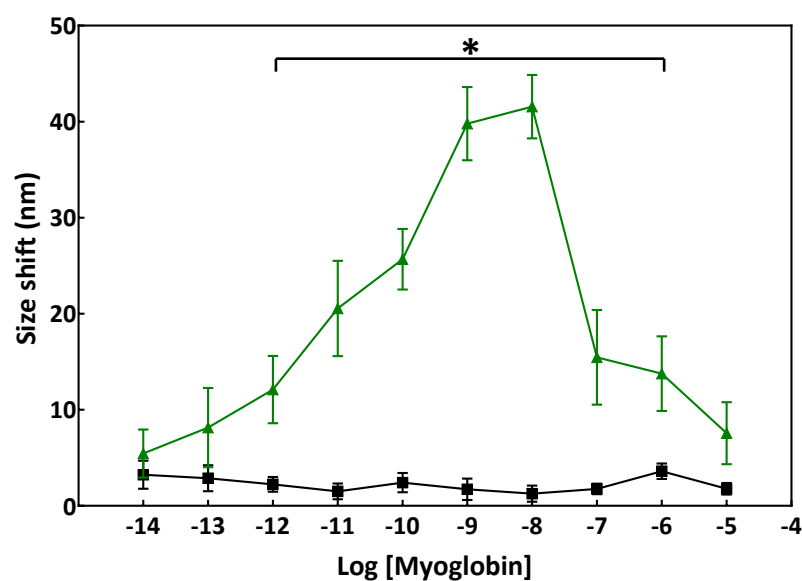


Figure 5-5 Size shift of Mb (90 μ l) mixed with IgG nanobiosensors (10 μ l) after incubating at RT for 30 min. IgG conjugated AuNPs, (\blacktriangle); streptavidin coated AuNPs as a negative control, (\blacksquare); each DLS measurement was performed at 10 s/run for 10 runs, data are mean values \pm SD (n=3). (*) indicates significant values tested with independent t-test between experiment and negative control ($p < 0.05$).

It is apparent from the data that the size of strep-AuNPs remained almost the same with a < 5 nm shift, whilst, for IgG-AuNPs the size shifted gradually when the concentration of Mb increased from 10 fM to around 10 nM in a linear response. Above concentrations of 10 nM, the size shift dropped substantially and showed a non-linear response. The data obtained from IgG-AuNPs is similar to that formerly reported regarding particle aggregation assays (Liu and Huo, 2009; Driskell et al., 2011; Khan et al., 2015). A possible explanation for this might be that all the nanobiosensors were saturated with analytes so there were no free bioreceptors to crosslink between NPs. This resulted in increasing of size due to the binding of analytes to nanobiosensors but there was no crosslinking between AuNPs so there was no aggregation observed by DLS. This type of response is known as the 'hook effect' (previously explained in section 1.4.3.2.1, Chapter 1). The upper detection limit was restricted by the concentration at which the hook point started, in this case over 10 nM.

Data was initially fitted using a one-site binding profile to derive initial values for the binding parameters for the system. The equation governing the one site model is shown as:

$$B = \frac{B_{max}*[L]}{K_D+[L]} + c \quad (5-1)$$

where B and B_{max} is size shift and maximum size shift (nm), respectively, $[L]$ is concentration of analyte (M), K_D is binding constant (M) and c is a constant value. However, the one-site model might not be the right choice considering the fact that a pAb was used in the system, which means there would be more than one population of receptors affecting the binding. For this reason, a multiple-site binding model was implemented for polyclonal reagents such as the anti-Mb IgG used. The equation represents the multiple-site binding kinetics is shown as:

$$B = \left\{ D * \left(\frac{B_{max1} * [L]}{K_{D1} + [L]} \right) \right\} + \left\{ E * \left(\frac{B_{max2} * [L]}{K_{D2} + [L]} \right) \right\} + \dots + \left\{ Z * \left(\frac{B_{maxn} * [L]}{K_{Dn} + [L]} \right) \right\} + c \quad (5-2)$$

The multiple-site binding model allows all different populations in the system accountable for the binding constants (D, E, Z) to be calculated. By substituting a one-site binding model with a two-site binding model (in which equal populations of binders were assumed), the R^2 and χ^2 were improved from 0.9384 and 4.438 to 0.9953 and 1.739, respectively. The fitting curves of both models are shown in Figure 5-6. When trying to fit with more than a two-site model (e.g. three or more), however, there was no difference in terms of the binding parameters. This is probably due to the fact that the difference in affinity was too small so they could not be mathematically differentiated. Therefore, two-site binding model best represented the data.

Regarding the limit of detection (LOD) of the assay, it is calculated as the minimum concentration of analyte which provides a signal that is greater than the maximum signal of the negative control plus three standard deviations. According to the data in Figure 5-6, the maximum mean plus three SDs of strep-AuNPs was 7.62 nm. Hence, by using equation 5-2 and parameters derived from the fitting model (Table 5-2), an LOD of 148 fM could be obtained for the assay.

Table 5-2 Binding parameters derived from one- and two-site fitting models of myoglobin assay using IgG-AuNP nanobiosensors. K_D values obtained are apparent K_D s as they are made up of a population of IgGs. Data was analysed using GraphPad Prism 7.0.

Parameters	One-site model	Two-site model
B_{max1}	31.25	14.4
K_{D1}	6.05×10^{-11}	1.22×10^{-12}
B_{max2}	-	22.48
K_{D2}	-	2.47×10^{-10}
R^2	0.9384	0.9953
χ^2	4.438	1.739
c	9.756	6.047

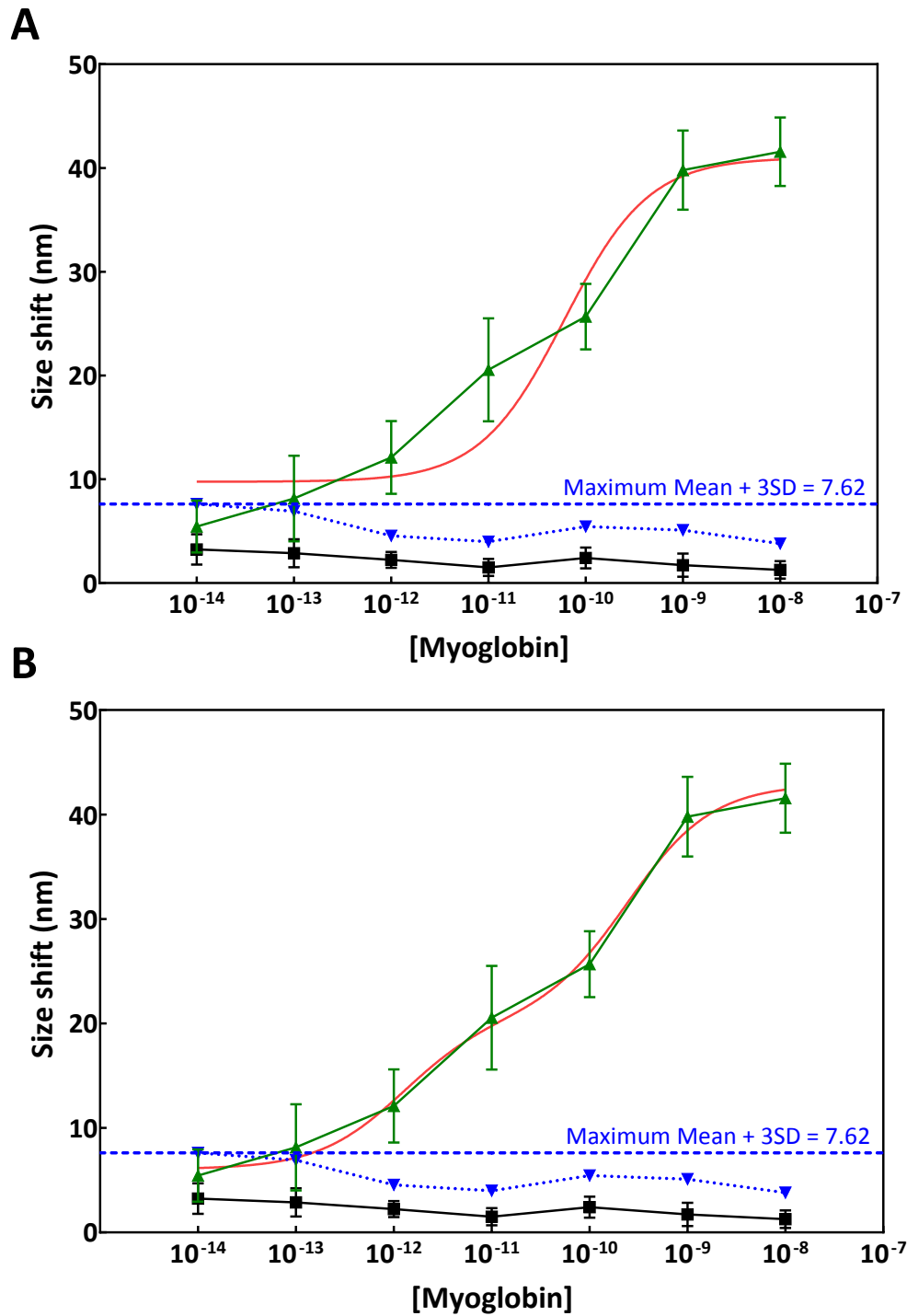


Figure 5-6 One-site, (A); and two-site, (B) model fittings of an assay for Mb using IgG conjugated AuNPs in the concentration range of 10 fM – 10 nM. Measured data was illustrated by (▲), for IgG-AuNPs; (■), negative control using strep-AuNPs; (—), fitted data; (▼), negative control mean values plus their three SDs (n=3); (---), maximum negative control mean value plus three SD (n=3).

5.3.2 Paired Affimer based assay

Here, C2 and F5 anti-myoglobin Affimers were used as bioreceptors in NP-coupled DLS assay, since Affimer pair ELISA performed previously suggested that they are most likely to bind to different epitopes (see Chapter 3). Both Affimers were biotinylated with biotin maleimide according to the optimised method in Chapter 4. Then, the same amount of each Affimer was conjugated onto strep-AuNPs. The pair of Affimer conjugated AuNPs (paired-AuNPs) prepared were characterised with DLS before use. The mean D_H was 62.36 ± 2.01 nm and their size distribution plots showed no aggregation (Appendix 9B). Detection of Mb was performed using the paired-AuNPs in the same way as for the IgG based system. Figure 5-7 shows the size shift of paired-AuNPs in the presence of 10 fM to 10 μ M Mb as compared to IgG-AuNPs and strep-AuNPs.

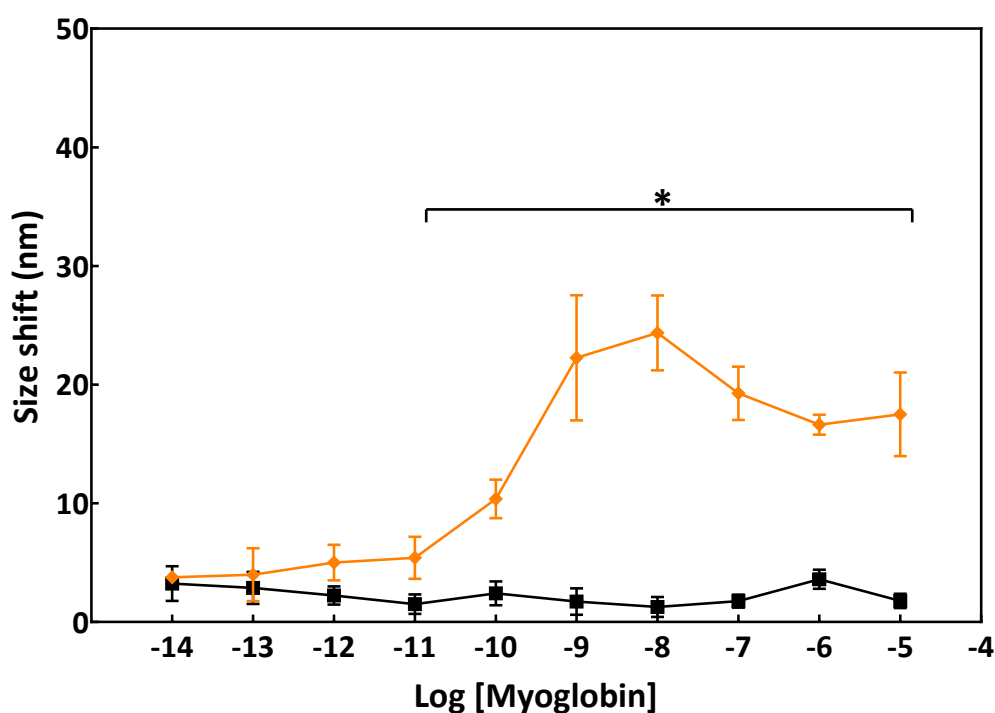


Figure 5-7 Size shift of Mb (90 μ l) mixed with paired Affimer nanobiosensors (10 μ l) after incubating at RT for 30 min in comparison with negative control. Paired Affimer conjugated AuNPs, (\blacklozenge); streptavidin coated AuNPs as a negative control, (\blacksquare); each DLS measurement was performed at 10 s/run for 10 runs, data are mean values \pm SD (n=3). (*) indicates significant values tested with independent t-test between experiment and negative control ($p < 0.05$).

From this data, there was a proportional response between the paired-AuNPs size shift and concentration of Mb added until at a certain point when the size shift dropped and was no longer related to the concentration. This phenomenon again could be explained by the hook effect. In comparison to IgG-AuNPs, the size shift of paired-AuNPs showed a similar trend. The hook point started at the same concentration, which was 10 nM. However, the size shift of the paired Affimer system was less than with IgG-AuNPs at the same concentration of Mb. The maximum shift of IgG-AuNPs was 41.57 ± 3.31 nm, whereas paired-AuNPs maximum size-shift was only 24.36 ± 3.16 nm.

Because two different Affimers were used in this experiment, it was first assumed that a two-site binding model would be more suitable than a one-site binding model. Nevertheless, when a two-site model was used, there was no difference in terms of parameters derived, only slight change in χ^2 from 0.675 to 0.954 (Table 5-3 and Figure 5-8). This is almost certainly due to the fact that the affinities of both C2 and F5 Affimers are similar and could not be distinguished from each other. Apparent K_D s from SPR data reported earlier (see Chapter 3) are 5.06 and 6.11 nM for C2 and F5, respectively. The LOD of paired-AuNPs in detection of Mb was 41.6 pM, which means the sensitivity of the assay was less than IgG-AuNPs that possessed an LOD of 148 fM.

Table 5-3 Binding parameters derived from one- and two-site fitting models of myoglobin assay using paired-AuNP nanobiosensors. Data was analysed using GraphPad Prism 7.

Parameters	One-site model	Two-site model
B_{max1}	21.05	10.52
K_{D1}	2.16×10^{-10}	2.16×10^{-10}
B_{max2}	-	10.52
K_{D2}	-	2.16×10^{-10}
R^2	0.9962	0.9962
χ^2	0.675	0.954
c	4.219	4.219

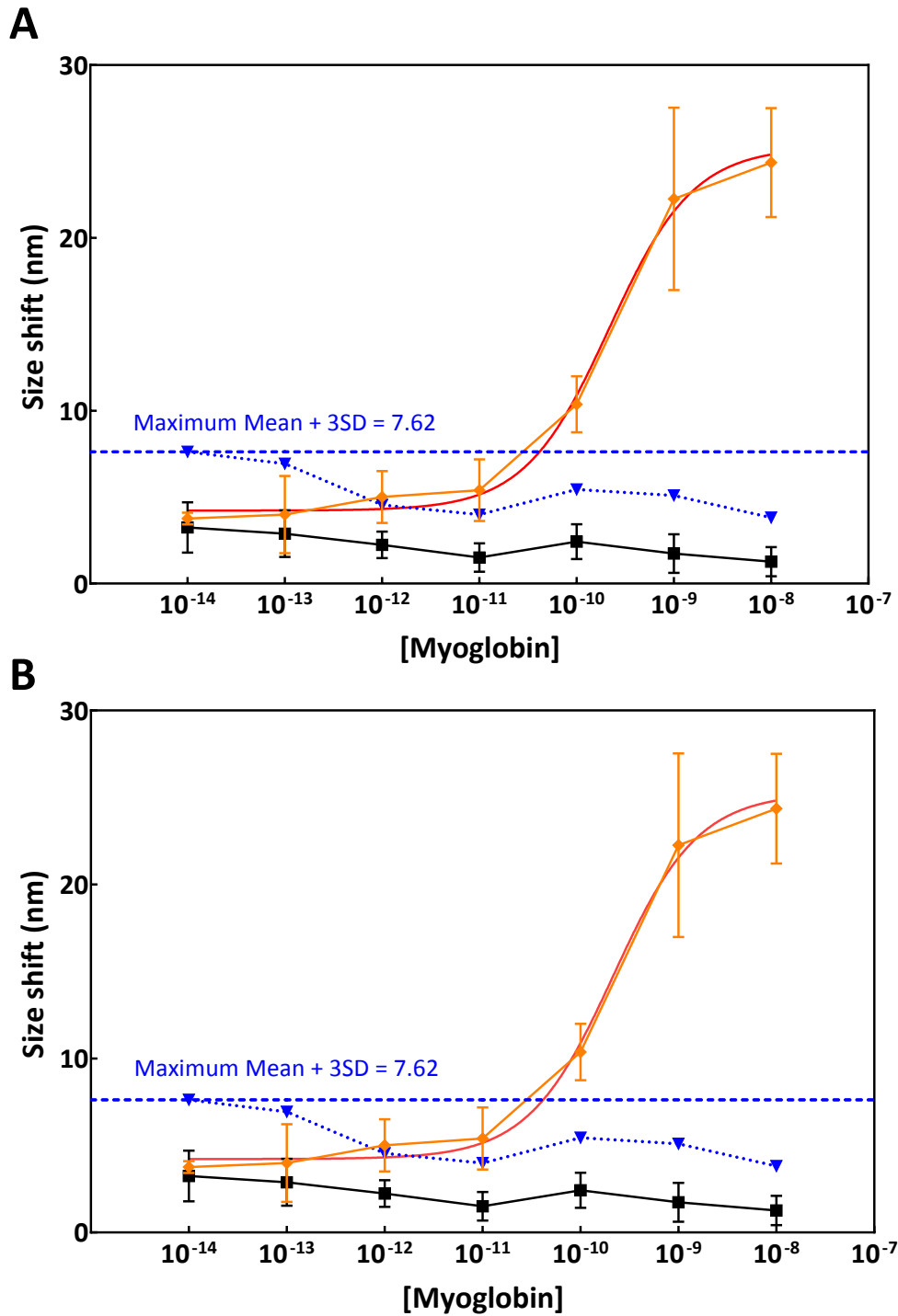


Figure 5-8 One-site, (A); and two-site, (B) model fittings of an assay for Mb using paired Affimers conjugated AuNPs in the concentration range of 10 fM – 10 nM. Measured data was illustrated by (◆), paired-AuNPs; (■), negative control using strep-AuNPs; (—), fitted data; (▼), negative control mean values plus their three SDs (n=3); (---), maximum negative control mean value plus three SD (n=3).

5.3.3 Multiple Affimer based assay

To increase the sensitivity of the Affimer based assay, a multiple Affimer based approach was investigated. Antibodies used in the positive control were polyclonal, which were selective to the analyte but bound at multiple binding sites. The high sensitivity of the antibody based system might result from this factor. A key aspect of using more than two Affimers as bioreceptors in NP-coupled DLS assay is to replicate the binding characteristics of a pAb. Therefore, all five Affimers available (see Chapter 3) were conjugated onto AuNPs using the same methods and used for Mb detection. The mean D_H of multiple Affimer-functionalised AuNPs was 63.14 ± 1.98 nm and the size distribution plot showed no aggregation before use (Appendix 9C). The same assay format as IgG and paired-Affimer nanobiosensors was carried out. The size shifts of multiple-AuNPs in the presence of 10 fM to 10 μ M Mb along with paired-AuNPs, IgG-AuNPs and strep-AuNPs are presented in Figure 5-9.

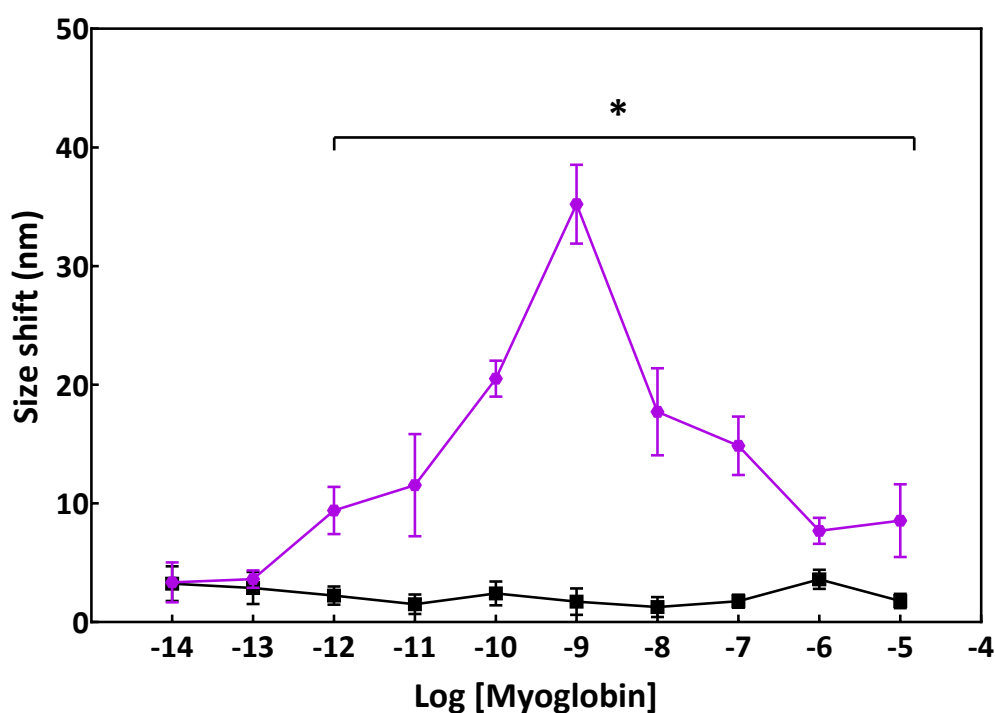


Figure 5-9 Size shift of Mb (90 μ l) mixed with multiple Affimer nanobiosensors (10 μ l) after incubating at RT for 30 min in comparison with negative control. Multiple Affimer conjugated AuNPs, (\bullet); streptavidin coated AuNPs as a negative control, (\blacksquare); each DLS measurement was performed at 10 s/run for 10 runs, data are mean values \pm SD (n=3). (*) indicates significant values tested with independent t-test between experiment and negative control ($p < 0.05$).

As expected, multiple-AuNPs detected Mb when compared to strep-AuNPs. The data for multiple-AuNPs had the same trend as IgG-AuNPs and paired-AuNPs presented previously. However, the hook effect of multiple Affimer system occurred at a lower concentration of 1 nM. This might be because pAbs have many IgG clones that can bind to different epitopes and facilitate crosslinking between NPs before the hook effect occurred, whilst with five different Affimers, there were more limited opportunities for this effect. However, the paired Affimer nanobiosensor with only two different clones also showed the hook point at concentration above 10 nM. Therefore it is more likely that the AuNP concentration might affect the hook point as suggested by Driskell et al. (2011). In the preparation of the nanobiosensors, multiple washing steps were involved which could alter the NP concentration in multiple Affimer based system. Nevertheless, multiple-AuNPs showed a larger size shift as compared to paired-AuNPs. The maximum size-shift was 35.21 ± 3.32 nm, which is around 10 nm more than the paired-AuNPs. However, the response was still less than for IgG based systems.

Again, the measured data of multiple-AuNPs were fitted with both one- and two-site fitting models. When changing from a one-site to a two-site model, the R^2 and χ^2 were improved from 0.9577 and 3.231 to 0.9981 and 1.179, respectively (Table 5-4). The fitting curves of both models are shown in Figure 5-10. The result corresponded to the IgG based assay system. The LOD of the multiple Affimer based system was 554 fM.

Table 5-4 Binding parameters derived from one- and two-site fitting models of myoglobin assay using multiple Affimer-AuNP nanobiosensors. Data was analysed using GraphPad Prism 7.

Parameters	One-site model	Two-site model
B_{max1}	31.95	8.20
K_{D1}	1.05×10^{-10}	3.18×10^{-13}
B_{max2}	-	29.36
K_{D2}	-	2.06×10^{-10}
R^2	0.9577	0.9981
χ^2	3.231	1.179
c	6.005	2.681

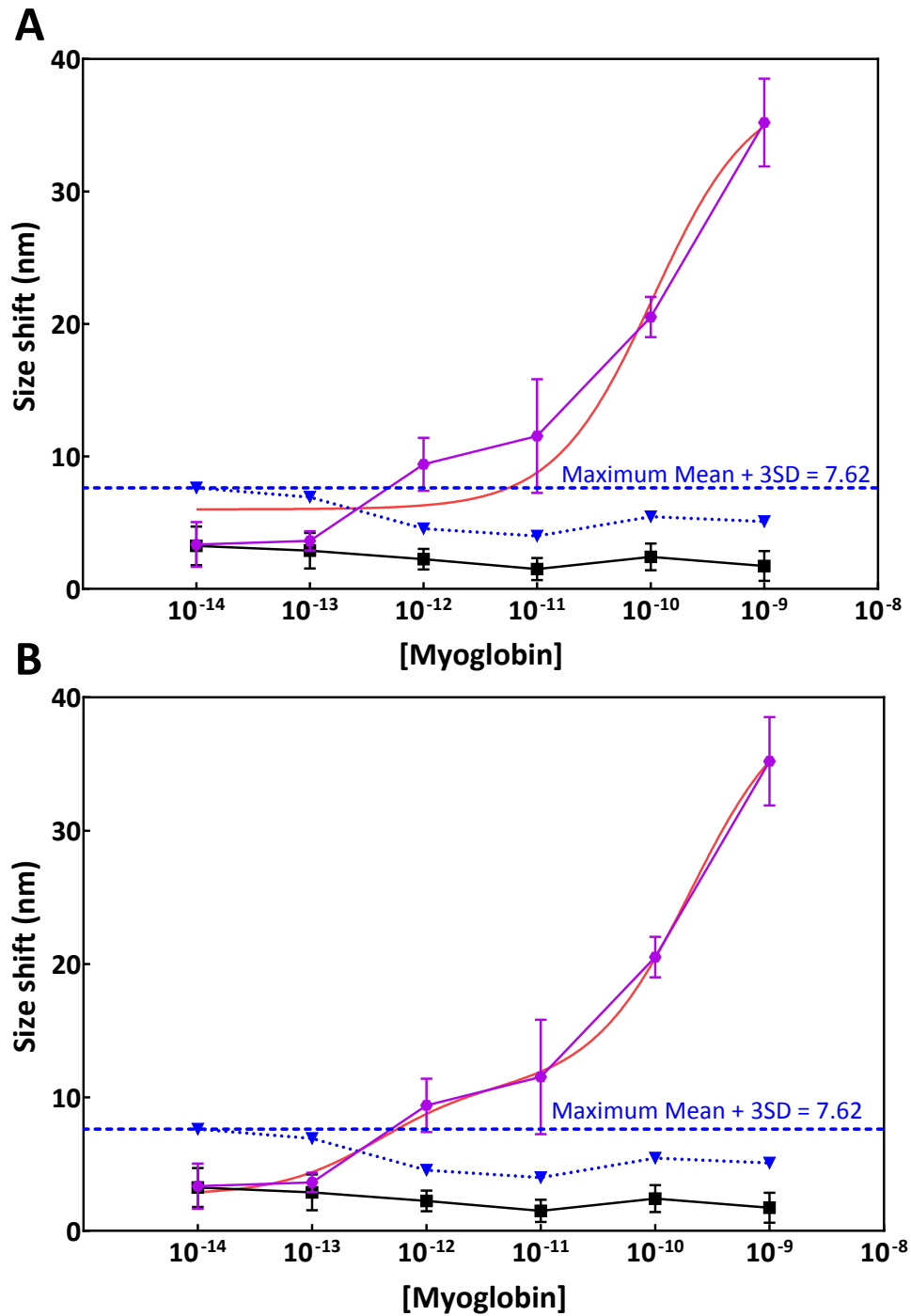


Figure 5-10 One-site, (A); and two-site, (B) model fittings of an assay for Mb using multiple Affimer conjugated AuNPs in the concentration range of 10 fM – 10 nM. Measured data was illustrated by (●), multiple-AuNPs; (■), negative control using strep-AuNPs; (—), fitted data; (▼), negative control mean values plus their three SDs (n=3); (---), maximum negative control mean value plus three SD (n=3).

Once more, more than two-site fitting models were also tested as there were five Affimers present in the system. However, there was no significant difference when more than a two-site fitting model was used. This result is explained by their apparent K_D s from SPR data. The K_D s are reported in Table 5-5. The Affimers can be grouped into two subgroups according to their K_D s; (i), B5, D1 and H1 with the K_D of around 0.1 – 0.7 nM and (ii), C2 and F5 with the K_D of around 5 – 6 nM. The two subgroups have a maximum 40 times K_D difference between extremes (i.e. D1 vs F5). It is possible, therefore, that the overall binding characteristic of multiple-AuNPs could be explained by these two populations of Affimers. Interestingly, the parameters obtained from multiple-AuNPs fitting was correlated with the paired-AuNPs. According to the data in Table 5-4, one of the apparent K_D s obtained from the multiple-AuNPs was almost equal to the one obtained from paired Affimer based system; 2.06×10^{-10} and 2.16×10^{-10} M, respectively. These results further support the idea that if the difference in affinities are small, they cannot be mathematically differentiated.

Table 5-5 Apparent K_D s of five selected anti-myoglobin Affimers from SPR data.

Affimer	K_D (M)
B5	4.68×10^{-10}
C2	5.06×10^{-9}
D1	1.45×10^{-10}
F5	6.11×10^{-9}
H1	6.95×10^{-10}

5.3.4 TEM images

To understand the assay further, size distribution plots of Mb mixed with multiple Affimer nanobiosensors at different concentrations were obtained (Figure 5-11A-D). TEM were introduced in order to visualise the AuNPs undergoing aggregation. Representative TEM images at each Mb concentration together with their size distribution plots except for with 1 pM of Mb as there were no good quality images obtained (Figure 5-11E-H).

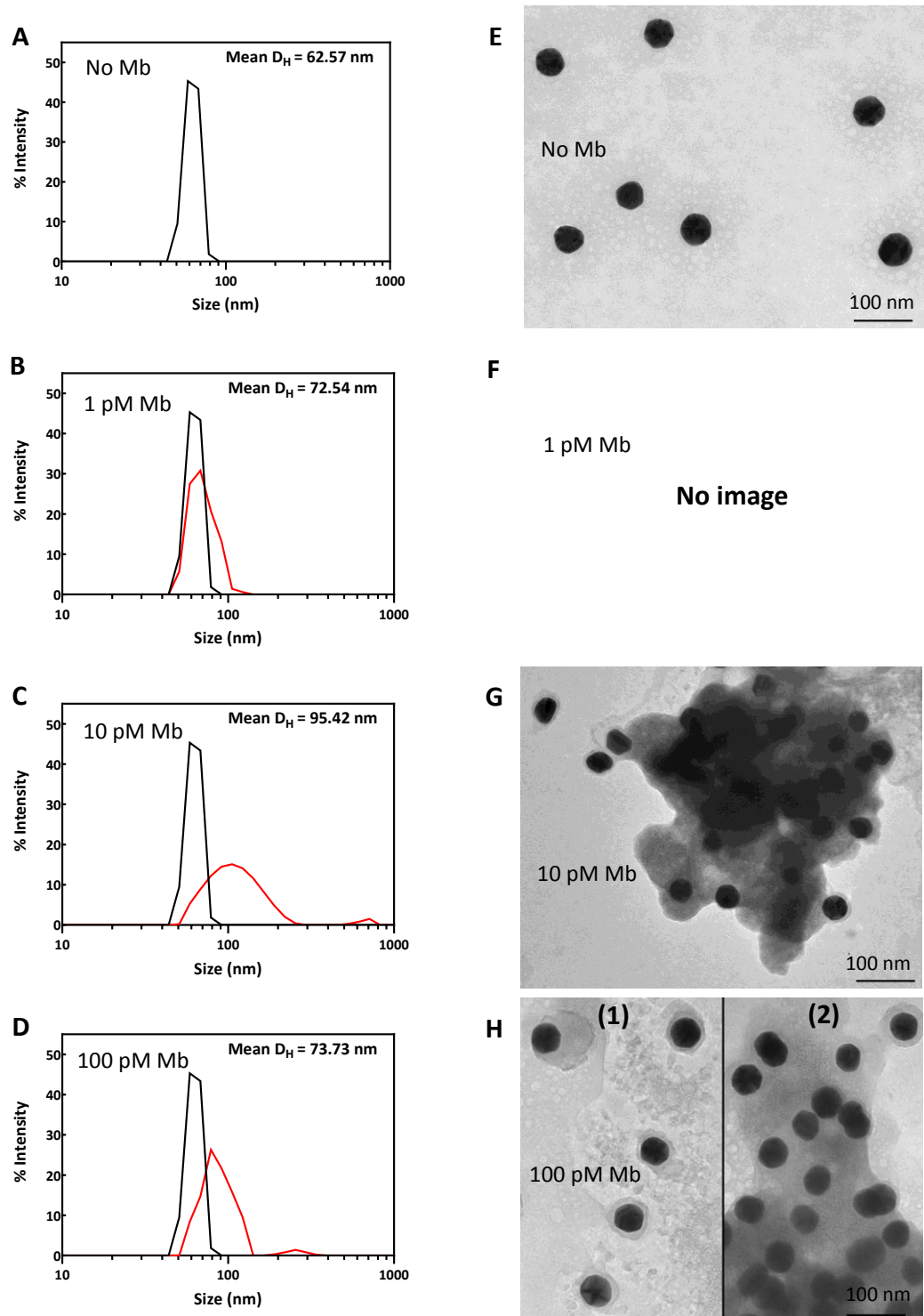


Figure 5-11 Size distribution plots of multiple Affimer nanobiosensors with and without Mb and their corresponded TEM images. Panels (A-D) shows the size distribution plots of multiple-AuNPs without Mb and with 1 pM Mb, 1 nM Mb and 100 nM Mb, respectively; panels (E-H) shows representative TEM images for no Mb, 1 nM Mb and 100 nM, respectively; multiple-AuNPs without Mb, (—); with Mb present, (—); H(1) and H(2) were from the same TEM grid but from different areas.

The size distribution of multiple-AuNPs was characteristically narrow, suggesting that there was no aggregation prior to the addition of Mb. Accordingly, there were no clusters observed in the corresponding TEM image as well (Figure 5-11A and E). When a low concentration of Mb (1 pM) was added, the size distribution became broader and shifted slightly to the right, indicating a binding event between the nanobiosensors and the analyte (Figure 5-11B). Still, the binding was not enough to crosslink the NPs into clusters and the shift in size observed might be due to some formation of dimers or trimers. At 1 nM Mb, which was equal to the hook point of multiple-AuNPs reported in the last section, the size distribution curves extensively shifted to the right (Figure 5-11C), suggesting there were aggregates forming. A TEM image of the sample confirmed this speculation (Figure 5-11G) where clusters were seen.

Another concentration tested was in the region above the hook point (100 nM). The size distribution curve obtained from this region (Figure 5-11D) was similar to the one obtained from mixed solution of the nanobiosensors and 1 pM Mb (Figure 5-11B). Also, their mean D_{HS} were almost equivalent, 73.73 and 72.54 nm for 100 nM and 1 pM, respectively. It is likely that the abundance of Mb in the system fully saturated all Affimers on the AuNP surfaces and left no bioreceptor to enable AuNP-crosslinking. This result was confirmed by the TEM image in Figure 5-11H(1), showing single AuNP coated with a thick protein layer. Closer inspection of the curve in Figure 5-11D, however, shows that there was a small peak around 200 – 300 nm, indicating the formation of some larger AuNP clusters in the system. This result suggested that at above the hook point concentration, crosslinking might be able to occur but to a lesser extent as compared to the lower concentrations. This result corresponded to another area of the same TEM grid (Figure 5-11H(2)) where dimers, trimers or clusters were seen.

5.4 Non-specific control

To investigate the selectivity of the assay, bovine serum albumin (BSA) was used as an analyte instead of Mb. Multiple-AuNPs and strep-AuNPs were used to detect BSA over 10 fM – 10 μ M. The size-shifts of both nanobiosensors are shown in Figure 5-12. Both systems show similar trends, there was a slight shift in AuNP size in the presence of BSA after 30 min incubation. However, the shifts were less than 10 nm and only above BSA concentration present > 10 nM, where the size shifts greater. At these concentrations was the range where the hook effect started when multiple-AuNPs were incubated with Mb. These results suggest that the system selective for Mb.

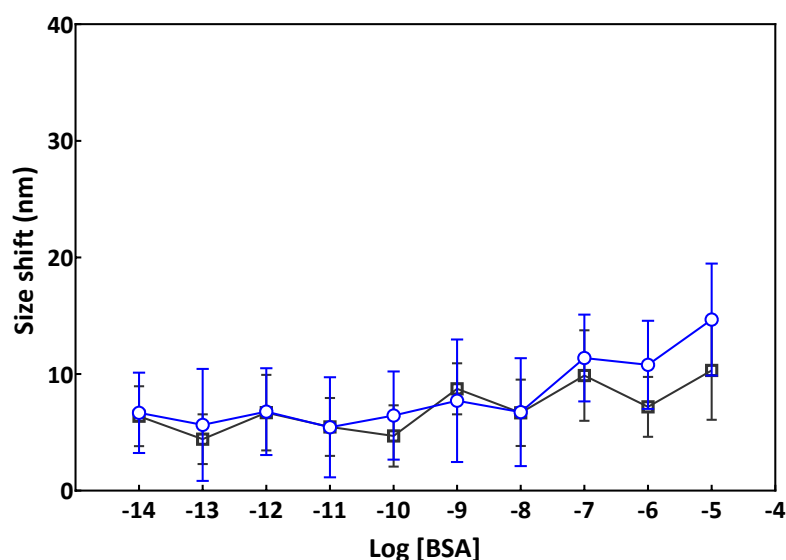


Figure 5-12 Size shift of BSA (90 μ l) mixed with multiple anti-myoglobin Affimer nanobiosensors (10 μ l) after incubating at RT for 30 min. Multiple Affimers conjugated AuNPs, (\oplus); streptavidin coated AuNPs as a negative control, (\boxplus); each DLS measurement was performed at 10 s/run for 10 runs, data are mean values \pm SD (n=3). No significant difference ($p < 0.05$) found between experiment and negative control.

Previously, different protein analytes were used with the anti-Mb Affimer AuNPs to eliminate non-specific binding of the nanobiosensors to Mb. Here, anti-calprotectin Affimers instead of anti-Mb Affimers were conjugated to AuNPs to

exclude non-specific binding of Mb itself. The anti-calprotectin Affimers 4 and 15 were tested using direct ELISA (see Chapter 3) and showed no binding to Mb. Anti-calprotectin Affimers conjugated AuNPs (cal-Affimer-AuNPs) were prepared and characterised. The mean D_H of cal-Affimer-AuNPs was 62.91 ± 2.14 nm and the size distribution plot showed no aggregation before use (Appendix 9D). The cal-Affimer-AuNPs were used as nanobiosensors in the presence of 10 fM to 10 μ M Mb in the same manner as IgG and anti-Mb Affimer nanobiosensors. The results are shown in Figure 5-13.

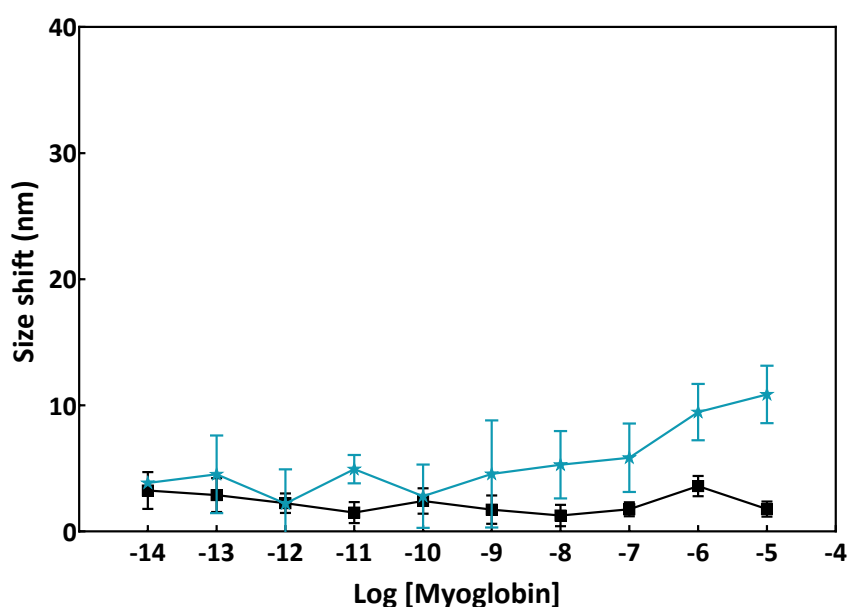


Figure 5-13 Size shift of Mb (90 μ l) mixed with anti-calprotectin Affimer nanobiosensors (10 μ l) after incubating at RT for 30 min. Anti-calprotectin Affimer conjugated AuNPs, (★); streptavidin coated AuNPs as a negative control, (■); each DLS measurement was performed at 10 s/run for 10 runs, data are mean values \pm SD (n=3). No significant difference ($p < 0.05$) found between experiment and negative control.

It is apparent from the data that there was a slight increase in size (around 5-6 nm). However, there was no significant difference found between the cal-Affimer-AuNP and strep-AuNP response in terms of size shift after Mb was added to the system. Again, the size slightly shifted further when the concentration of Mb was > 10 nM. This may be due to the fact that proteins such as BSA or Mb themselves have intrinsic scattering property and could be detected by DLS at high concentrations.

5.5 Effect of NP size

According to the Mie theory, light scattering intensity is proportional to the 6th power of the radius of the particle (Yguerabide and Yguerabide, 1998). Hence, it is hypothesized that with larger NPs, a larger scattering intensity could be detected. This might enhance the sensitivity of a size shift assay using DLS. Strep-AuNPs with a gold core diameter of 20, 40, 60, 80 and 100 nm were used to investigate the effect. To understand the effect of size better, IgG-AuNP nanobiosensors were prepared and tested along with the Affimers. The nanobiosensors were prepared and characterized according to the optimized method developed (Chapter 4). All of the nanobiosensors were used at 1x concentration as received. Figure 5-14 shows the size shift response curves from IgG- and multiple Affimer nanobiosensors.

According to the data, the assay performance improved when the AuNP core diameter was changed from 20 to 40 nm in both systems. Nevertheless, when the core sizes of AuNPd were further increased to 60, 80 and 100 nm, there was no significant further effect. In addition, there was also no difference in the concentration where the hook effect started for multiple-AuNPs, but for IgG nanobiosensors, 20 nm AuNPs, the hook point was shifted slightly higher, from 10 nM to 100 nM. In 80 and 100 nm core diameters AuNP, conversely, the hook points were decreased from 10 nM to 1 nM. These shifts were also reported in the size study by Driskell et al. (2011), which suggested that it might be due to different AuNP concentrations used. Further details about NP concentration will be discussed in the next section.

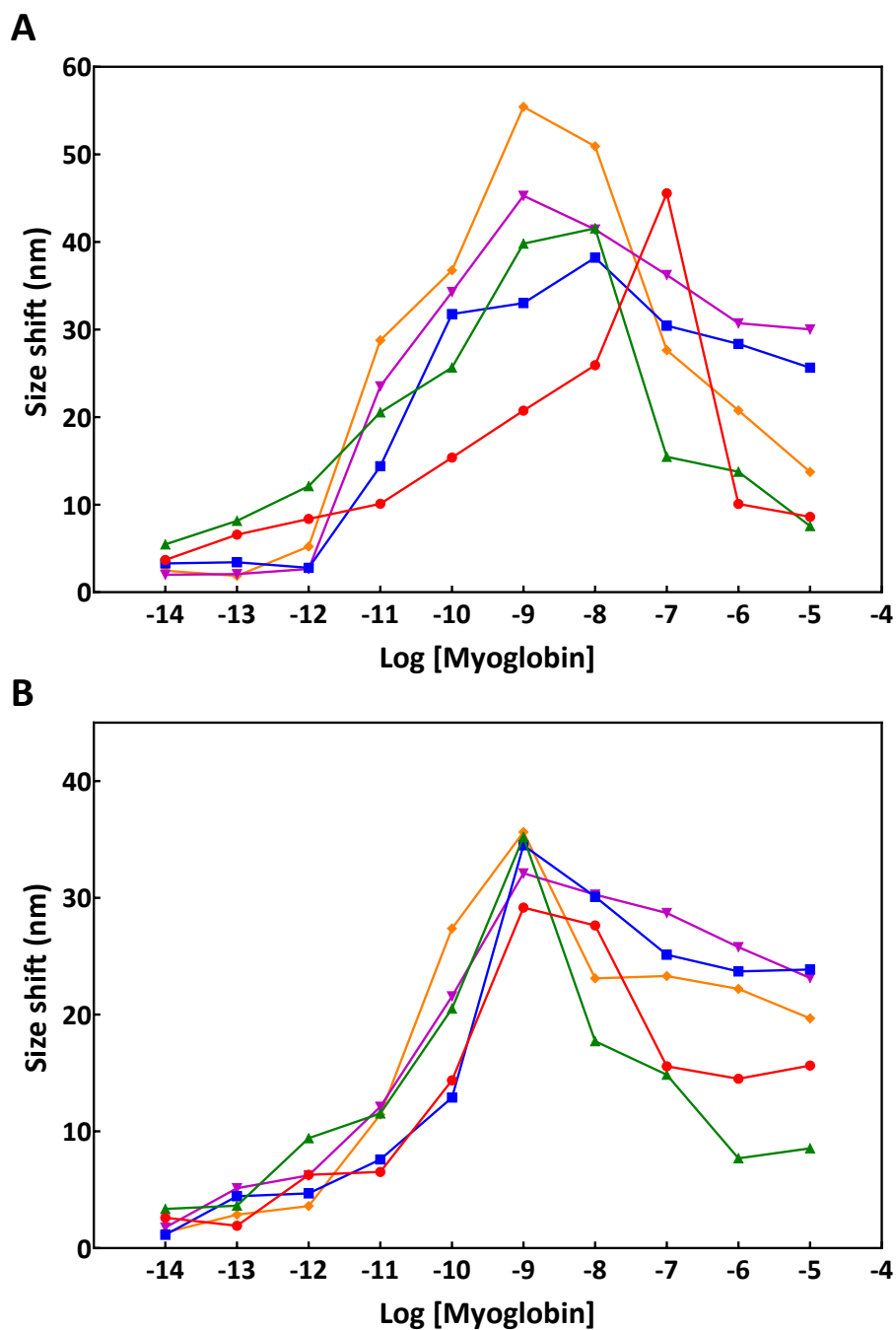


Figure 5-14 Effect of AuNP size on the DLS assay for Mb detection. The experiments were performed by mixing different concentration of Mb (90 μ l) with 10 μ l of each AuNP and incubated for 30 min before DLS measurement. (A) and (B) represents IgG- and multiple-AuNPs, respectively; line graph represents AuNP core diameters of (●), 20 nm; (▲), 40 nm; (■), 60 nm; (▼), 80 nm and (◆), 100 nm. The mean responses of triplicate experiments were reported but SD bars were omitted for clarity. Full data are shown in Appendix 10.

The LODs for each nanobiosensor preparation (20 to 100 nm AuNPs) were calculated by fitting a two-site binding model in the same manner as previous. Figure 5-15 shows the LODs comparing between IgG and multiple Affimer based systems. The data confirm what was observed from the response curves earlier in that 40 nm core diameter provided a better sensitivity than 20 nm. The LODs were improved from 49.1 pM to 148 fM and 34.2 pM to 554 fM for IgG and Affimer AuNPs, respectively, whilst the LODs of 60, 80 and 100 nm AuNPs were slight better than 20 nm AuNPs, still the sensitivities of both IgG- and multiple-AuNPs were not superior to the 40 nm AuNP nanobiosensors.

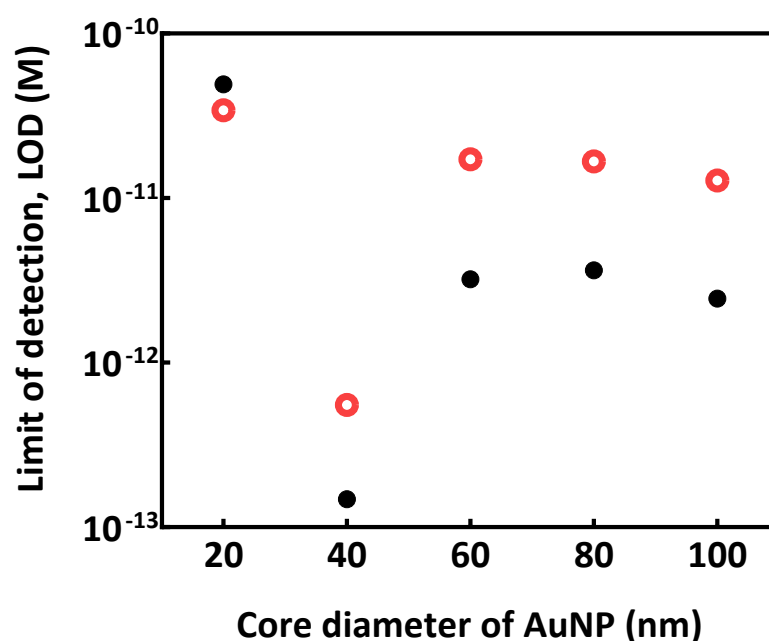


Figure 5-15 Limit of detections (LODs) of DLS assay for Mb detection using different AuNP core diameters. (●), IgG-based; and (○), multiple-based nanobiosensors.

This finding is contrary to most previous studies, which have suggested that increasing AuNP size could improve the sensitivity of the assay (Nietzold and Lisdat, 2012; Wang et al., 2012). However, these data are in line with two studies by Driskell et al. (2011) and Huang et al. (2015). The first study compared influenza virus detection by 30, 60 and 80 nm AuNP core diameter sensors; anti-virus IgGs were used as bioreceptors. It was reported that the best sensitivity was obtained from the

30 nm AuNPs. There were two explanations; the concentration of NPs used were different and the steric hindrance of larger probes could restrict binding between bioreceptors and analytes, which lead to less aggregation. This particular reason was also used to explain of the results found by Huang et al. (2015) when they used AuNP core diameters of 30, 70 and 100 nm to detect the bacteria *Listeria monocytogenes*. The 30 nm AuNPs showed better responses in terms of size shift. In this case, Mb is a globular protein with the size of 3.5 nm, therefore, it could be that when large NPs like 60, 80 or 100 nm AuNP nanobiosensors were used, access to the binding epitope was restricted by steric hindrance which affects the binding stoichiometry. It is possible that using a linker to distance the Affimer from the AuNP surface may help here. Another interesting observation from this data is that when 20 nm core diameter AuNPs were used, the Affimer nanobiosensors provided better sensitivity compared to IgG-AuNPs. It is possible that since Affimers are smaller than IgGs, when larger AuNPs were used, there was a restrictions in binding to the Mb, leading to less sensitivity observed.

5.6 Effect of NP concentration

NP concentration is expected to be one of the important factors affecting a DLS assay as DLS measures the whole population of particles. When concentrated nanobiosensors are used, a higher concentration of analyte is required to crosslink all of the nanobiosensors and it is likely to have individual AuNPs in the system. Conversely, it is estimated that a greater shift in size could be obtained from dilute nanobiosensors as there are fewer single AuNPs left in the system and lead to better sensitive assay. To investigate the effect of NP concentration, the DLS assay was conducted using four different concentrations of IgG- and multiple Affimer-AuNPs. The data are shown in Figure 5-16.

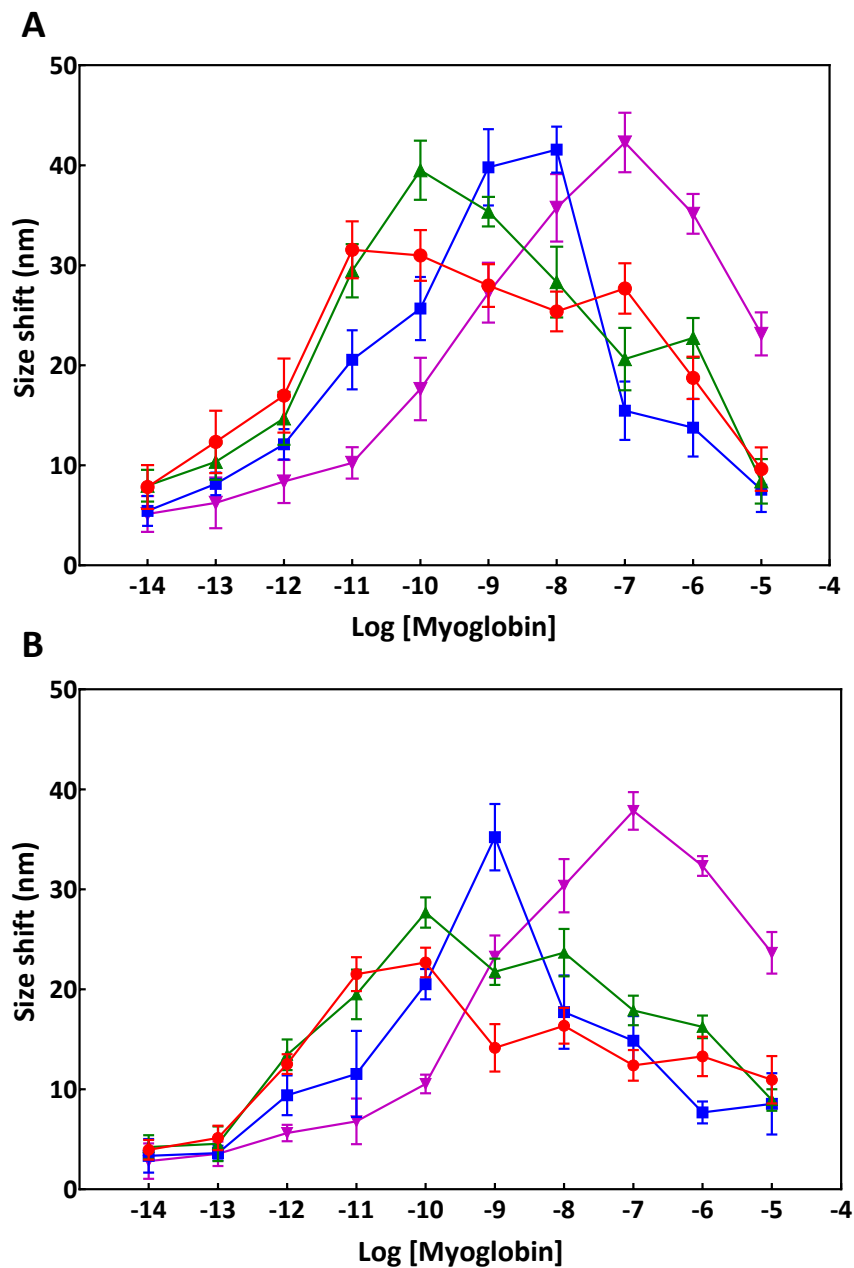


Figure 5-16 Effect of AuNP nanobiosensor concentration on the DLS assay for Mb detection. The experiments were performed by mixing different concentration of Mb (90 μ l) with 10 μ l of each nanobiosensor and incubated for 30 min before DLS measurement. (A) and (B) represents IgG- and multiple-AuNPs, respectively; line graphs represents four different concentrations of AuNPs used in Mb detection; (—●—), 0.01x AuNP (8×10^8 NP/ml); (—▲—), 0.1x AuNP (8×10^9 NP/ml); (—■—), 1x AuNP (8×10^{10} NP/ml); (—▼—), 10x AuNP (8×10^{11} NP/ml). The experiments were performed by mixing 10 Data are mean values \pm SD (n=3).

To obtain more dilute nanobiosensors, PBS was used to dilute the stock; whilst concentrated nanobiosensors were obtained by centrifugation and redispersion in a smaller volume of the same buffer. In Figure 5-16A, the data were in accordance with the hypothesis that a larger size shift could be obtained with more dilute AuNP nanobiosensors at concentrations below the hook point. For the Affimer based system, however, when the nanobiosensors were further diluted to 0.01x (8×10^8 NP/ml), there was no difference in sensitivity as compared to 0.1x (8×10^9 NP/ml). In terms of hook effect, the concentrations at which hook point occurred decreased with diluted nanobiosensors. These data provide support for the explanation of the hook effect given in Chapter 1. With less AuNPs in the solution, there will be less bioreceptors present and saturation can occur at lower concentration of analyte.

Figure 5-17 shows the dynamic range of each nanobiosensor concentration for both IgG- and Affimer system. Again, the LODs of each nanobiosensor were calculated by fitting with a two-site binding model, whilst the maximum detection point could be obtained from the hook point. As expected, different dynamic ranges could be obtained by changing the AuNP nanobiosensor concentration. Surprisingly, the LODs were contradict the prediction that better sensitive should be achieved from the most dilute concentration. A likely explanation is that when further diluting the AuNPs, scattering intensities may be reduced as there was too much.

When the dynamic range of both nanobiosensor systems are compared, IgG-AuNPs provided a wider detection range, especially with more concentrated nanobiosensors (Figure 5-17A). It is possible that these data may be due to steric hindrance. As Affimers are small, they were attached closer to the AuNP surface than IgGs would be, so when there were too many nanobiosensors in the solution, these AuNPs could block each other from binding Mb.

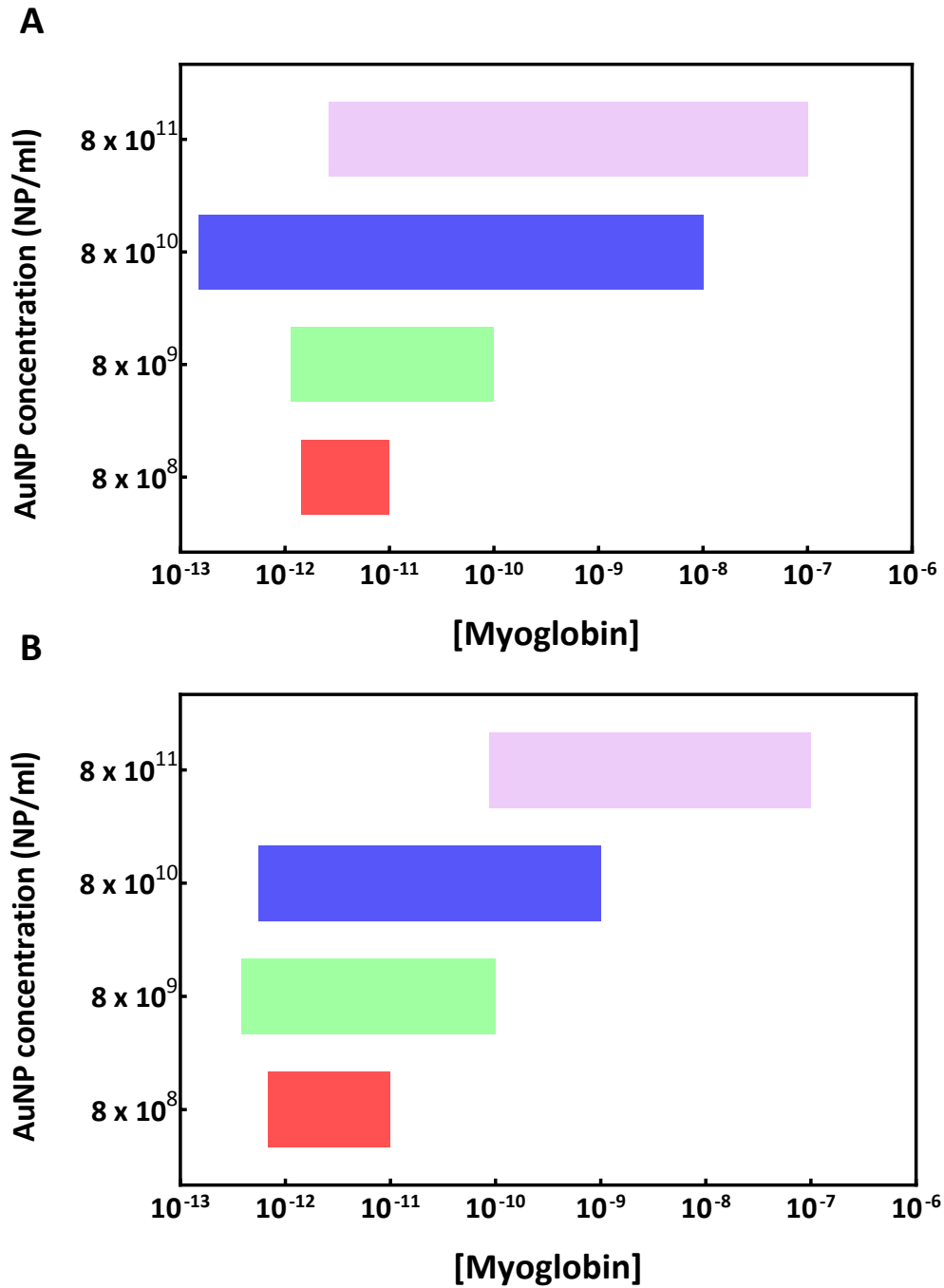


Figure 5-17 Dynamic ranges of DLS assay for Mb detection using four different nanobiosensor concentrations. (A) and (B) represents IgG- and multiple Affimer-AuNPs, respectively; The nanobiosensor concentrations were: (■), 8×10^8 NP/ml; (■), 8×10^9 NP/ml; (■), 8×10^{10} NP/ml; (■), 8×10^{11} NP/ml.

5.7 Stability of nanobiosensors

To study the stability of nanobiosensors used in DLS assay, IgG- and multiple Affimer-AuNPs were prepared on day 1 and were used for Mb detection on days 1, 3, 7 and 35. The sensors were kept at 4 °C protected from light between uses. The AuNP sizes were determined before every use and the results are shown in Figure 5-18; whilst the size shift response curves are shown in Figure 5-19.

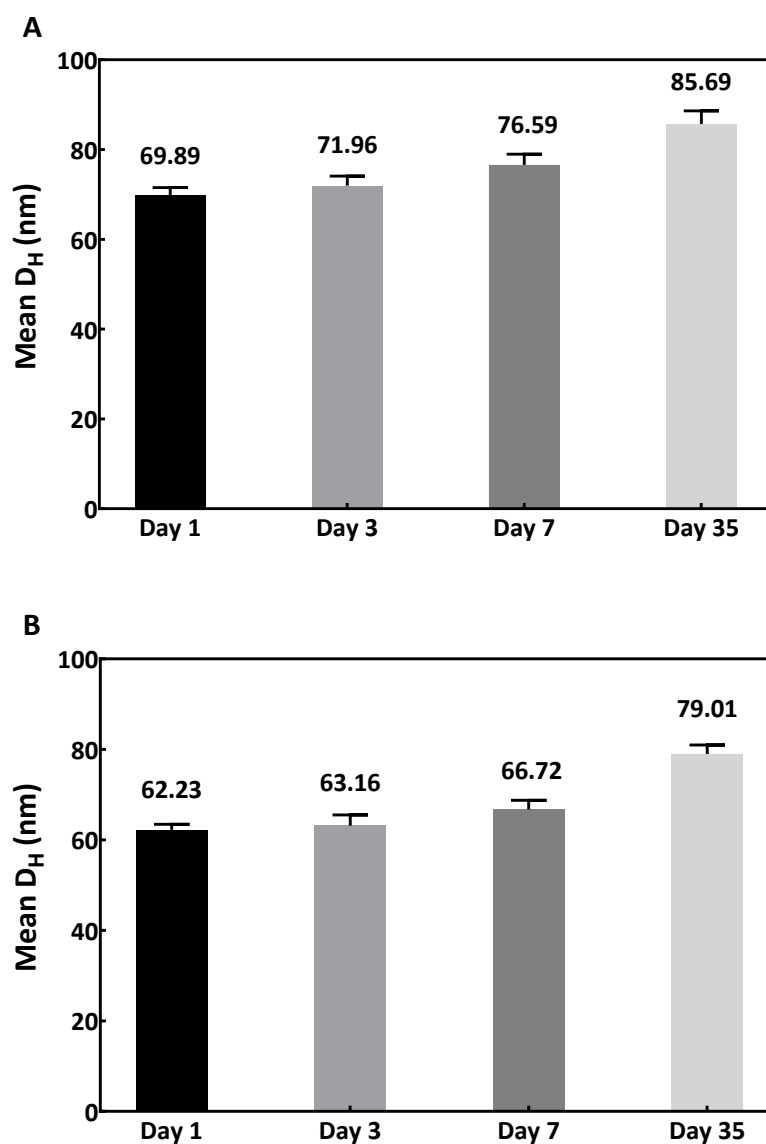


Figure 5-18 Mean D_H of AuNP probes used in stability study. Mean D_H of (A) IgG-AuNPs and (B) multiple Affimer-AuNPs before assay day 1, (■); day 3, (■); day 7, (■); day 35, (■).

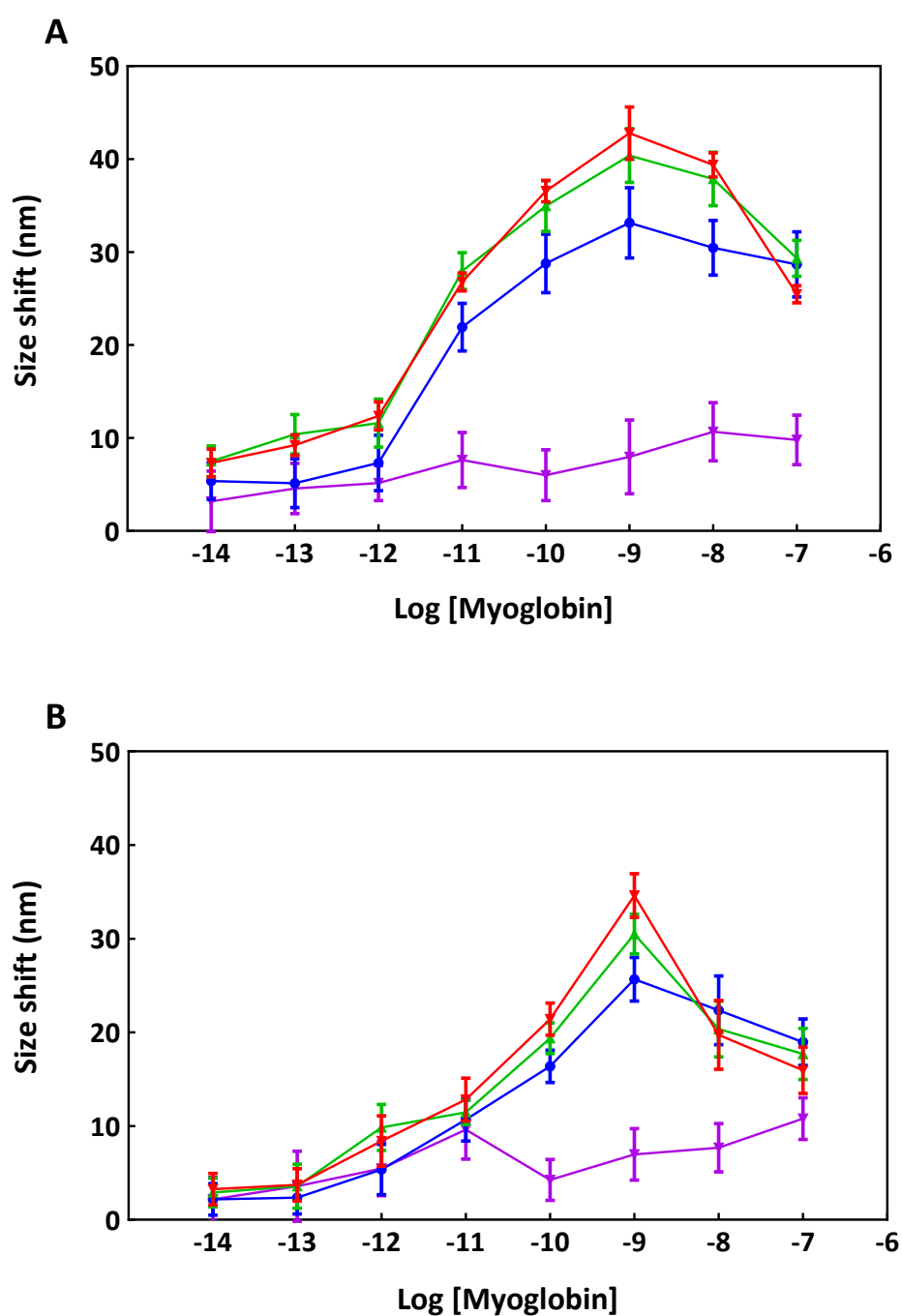


Figure 5-19 DLS assay for Mb detection performed on day 1, 3, 7 and 35 to study the stability of nanobiosensors. The calibration curves obtained from (A), IgG-AuNPs; and (B), multiple Affimer-AuNPs performed on day 1, ($\color{red}\blacktriangle$); day 3, ($\color{green}\blacktriangle$); day 7, ($\color{blue}\blacktriangle$); and day 35, ($\color{purple}\blacktriangle$); The experiments were performed as described in Figure 5-9 and Mb solution were prepared freshly each day from stock solution. AuNP nanobiosensors were stored at 4 °C protected from light between uses. Data are mean values \pm SD (n=3).

There was slight increase of AuNP sizes at day 3 and day 7 for both systems. However, these changes were not significant compared with day 1 AuNP sizes. The performance curves of day 1, 3 and 7 showed the same characteristics for both systems, suggested that the assays were reproducible. Moreover, the hook points of day 1, 3 and 7 assays also occurred at the same concentration. However, it is apparent from Figure 5-19 that when the nanobiosensors were kept longer, to day 35, calibration curves could not be obtained from both IgG and Affimer AuNPs. At day 35, the mean D_H of both IgG and Affimer nanobiosensors shifted around 15 – 16 nm from day 1 sizes. This indicated some aggregation of the AuNPs, suggesting that both nanobiosensors were not stable up to 35 days. It may be that the nanobiosensors were stable up to some intermediate point, between 7 and 35 days but this experiment suggested that both IgG and Affimer nanobiosensors were stable and could be used within 1 week without any preservatives added.

5.8 Versatility of NP-coupled DLS size shift assay using Affimers

Here, the optimised assay was used with *Clostridium difficile* toxin B. In comparison to Mb, it is a much larger protein (Mr 270 kDa) so it is a good analyte to investigate the versatility of the assay platform. Also, anti-toxin B Affimers have been screened, well-characterised and were ready to use. However, there were only two Affimers provided, which were Affimer 18C and 45C. These two Affimers were confirmed as a binding pair, binding to different epitopes. Therefore, toxin B assay was performed as paired Affimer assay. In this section, the term “Affimer” will refer as anti-toxin B Affimer, unless stated otherwise.

To begin the process, both 18C and 45C Affimers were biotinylated using biotin maleimide to couple to the C-terminal Cys –SH. The prepared anti-toxin B Affimer AuNPs (txB-Affimer-AuNPs) were characterised with DLS. The mean D_H of the nanobiosensors was 63.31 ± 1.69 nm, confirming the success of functionalisation as the size shift was around 8 nm which corresponds to around twice the diameter of an Affimer (~ 3 nm). Also, the size distribution plot showed no aggregation during the conjugation (Appendix 9E). Detection of toxin B was performed as for the Mb assay. The mean D_H of txB-Affimer-AuNPs before and after mixing with toxin B over the range 10 fM to 10 μ M was measured by DLS after incubation at RT for 30 min. Strep-AuNPs were used as negative control.

Figure 5-20 shows the size shift of txB-Affimer-AuNPs in the presence of 10 fM to 10 μ M toxin B compared with strep-AuNPs. There was a proportional response between txB-Affimer nanobiosensors size shift over the concentration range 10 pM to 10 nM before the hook effect started. Within this range, there was no responses observed in the negative control system but after the hook point, there was an increased shift for strep-AuNPs. This may be due to the large size of toxin B, which will have a greater intrinsic scattering property than Mb.

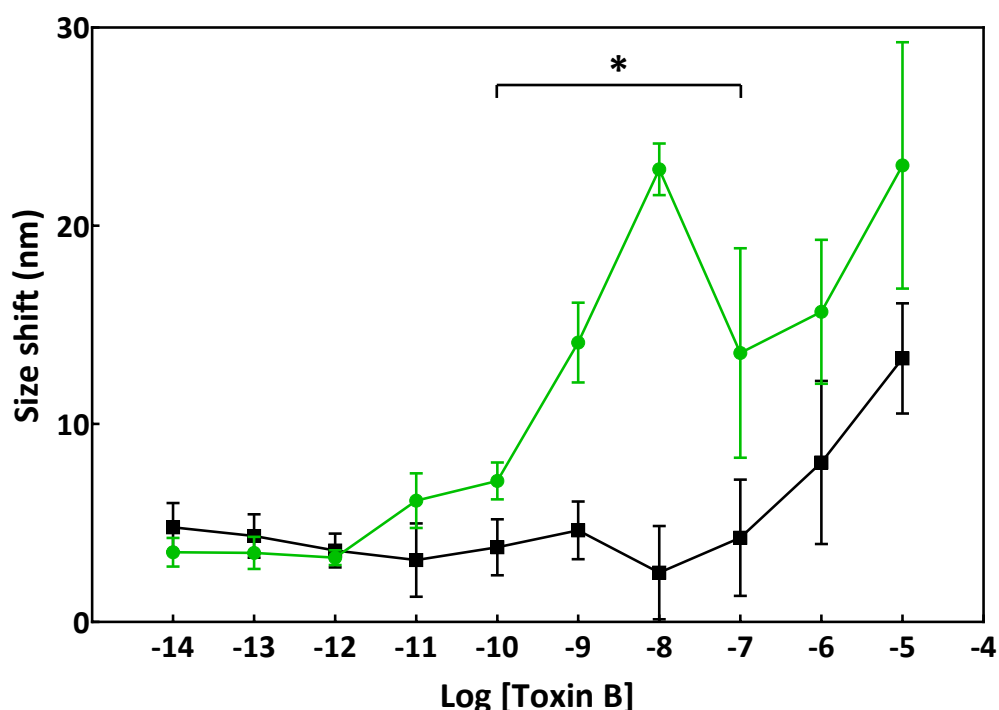


Figure 5-20 Size shift of toxin B (90 μ l) mixed with anti-toxin B paired Affimer nanobiosensors (10 μ l) after incubating at RT for 30 min. Anti-toxin B paired Affimers conjugated AuNPs, (\bullet); streptavidin coated AuNPs as negative control, (\blacksquare); each DLS measurement was performed at 10 s/run for 10 runs, data are mean values \pm SD (n=2). (*) indicates significant values tested with independent t-test between experiment and negative control ($p < 0.05$).

The measured data was fitted with a two-site binding model since two different Affimers were used and the R^2 and χ^2 are reported in Table 5-6. The fitting curves of this model is shown in Figure 5-21. The LOD of txB-Affimer-AuNPs in detection of toxin B was around 30 nM, which was less sensitive as compared to the Mb assay. A likely explanation is that with larger analyte protein present in the DLS system, the scattering property of the protein will affect the size shift response. This was observed from the negative control system in which the size increased with higher concentration of toxin B in the solution.

Table 5-6 Binding parameters derived from a two-site fitting model of toxin B assay using anti-toxin B paired Affimer nanobiosensors. Data was analysed using GraphPad Prism 7.

Parameters	Two-site model
B_{max1}	18.93
K_{D1}	1.46×10^{-9}
B_{max2}	3.08
K_{D2}	4.09×10^{-12}
R^2	0.9973
χ^2	0.6651
c	3.273

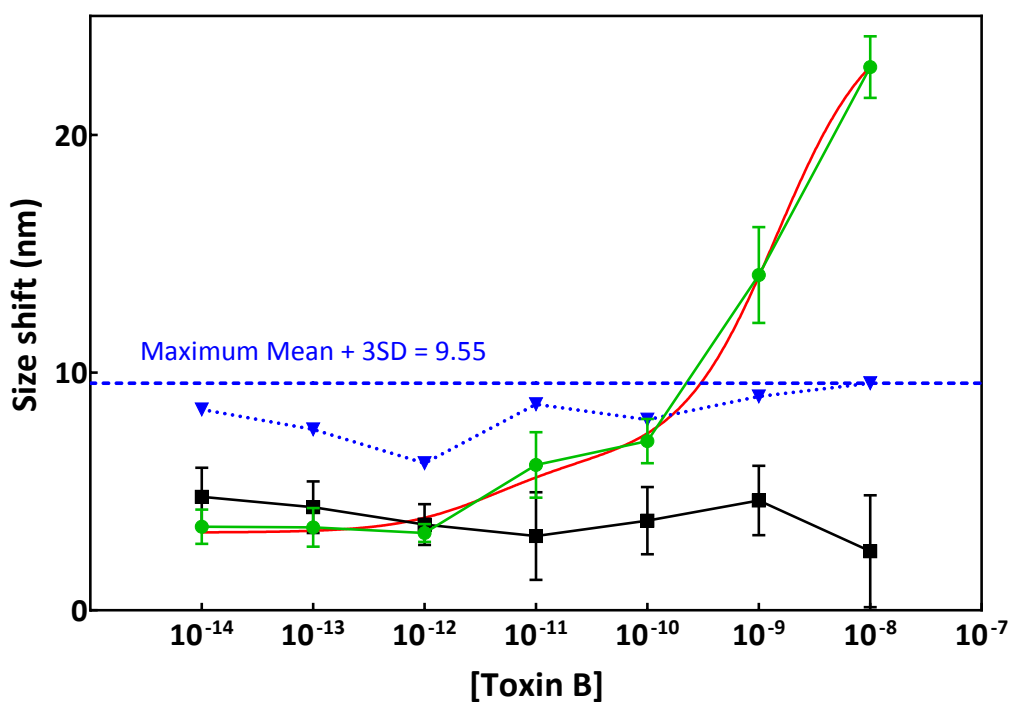


Figure 5-21 Two-site model fitting of an assay for toxin B using anti-toxin B paired Affimer conjugated AuNPs in the concentration range of 10 fM - 10 nM. Measured data was illustrated by (●), anti-toxin B paired Affimer-AuNPs; (■), negative control using strep-AuNPs; (—), fitted data; (▼), negative control mean values plus their three SDs (n=2); (---), maximum negative control value plus three SD (n=2).

5.9 Discussion

Data presented in this chapter has highlighted the ability of Affimers to act as bioreceptors for a NP-coupled DLS size shift assay. It was demonstrated in the kinetics study that Affimer-AuNPs could bind to Mb-AuNPs and exhibited similar kinetics to IgG-AuNPs. This result corresponded to that presented in a kinetic study by Liu and Huo (2009) who studied the capability of DLS to monitor aggregation caused by immunoaffinity induced-interaction. DLS provided not only the average D_H size but it could provide details regarding the aggregation state. These preliminary data have shown that aggregation was affected by the incubation time and suggest that a minimum of 30 min incubation time should be applied in designing the assay format.

In Mb detection assay using nanobiosensors, IgGs were used as a positive control in order to understand the mechanism of the assay before moving on to use the Affimers. There was a linear relationship observed between the size shift responses and increased Mb concentrations. IgG nanobiosensors were able to detect Mb with a detection range of 148 fM – 10 nM. The most important information achieved from the positive control system is that the NP-coupled DLS assay also showed the hook effect in reduced response and no relationship found with Mb concentrations. This hook point will determine the assay's upper limit of detection. In addition, a two-site binding model was proved to be best representing the parameter calculation.

The paired Affimer based system proved to be selective for Mb compared to negative controls (strep-AuNPs) and the size shift response curve showed a similar trend to IgG based system and had the same hook point. However, the sensitivity of the paired Affimer-AuNPs was much lower as compared to IgG system (LOD = 41.6 pM). To increase the sensitivity of the Affimer system, all five selected Affimers were used to "replicate" a polyclonal IgG on the AuNP surface. It was shown here that the sensitivity was improved to 554 fM. A possible explanation would be that the multiple Affimer based system may benefit from the avidity effect. Also, previous studies on the size shift assays using DLS for monomeric analytes mostly used pAbs

(Liu and Huo, 2009; Wang et al., 2012). Therefore the finding of this study suggest that a number of selective clones of a particular binding reagent on an AuNP, i.e. for the same target protein but to different epitope, may be the key factor to enhance the sensitivity of the assay for monomeric analytes. Moreover, the selectivity of the assay was also examined by using different analytes with anti-Mb Affimer nanobiosensors and using different Affimer nanobiosensors with Mb. These results show that the assay was selective to Mb.

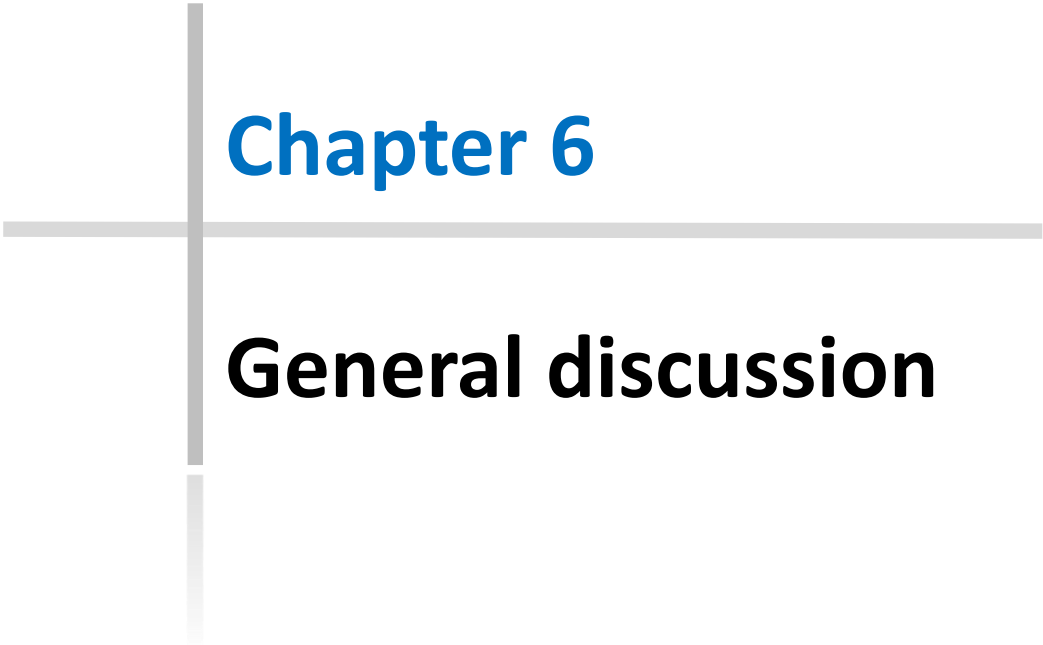
Furthermore, factors related with AuNP were investigated. Regarding the effect of NP size; when changing the AuNP core diameter from 20 to 40 nm, the results are in line with the hypothesis that a larger size NP could provide a stronger scattering intensity and therefore better sensitivity. However, when the size of NPs was further increased, the outcome was contrary to this hypothesis and some previous findings (Nietzold and Lisdat, 2012; Wang et al., 2012). A possible explanation may be due to the steric effect of the nanobiosensor and analyte. Mb is a compact protein with a size around 3.5 nm, with larger AuNPs, there might be some blocking effects. This outcome was shown for IgG-AuNPs too. It can therefore be assumed that steric hindrance plays an important role in the binding activity and assay performance which also depends on the analyte itself.

Another factor investigated was the NP concentration, as DLS measures the whole population of NPs. The results obtained from IgG-AuNPs were in accordance with previous studies that a larger size shift could be obtained with more dilute AuNP nanobiosensor at concentrations below the hook point. However, with Affimer-AuNPs, when diluted the concentration to around 0.01x of stock concentration, there was no difference seen and LODs were not lowered. This may be due to scattering intensities being reduced. These data are consistent with those of Driskell et al. (2011) who studied the effect of AuNP concentration in their DLS assay for influenza virus detection. By adjusting the concentration of NPs, different detection range could be obtained.

The objective of this project is to improve the stability of nanobiosensors in aggregation assay using DLS, so the stability of Affimer and IgG nanobiosensors were

tested and compared. Both systems were stable for one week but not when kept for 35 days; similar findings were reported by Driskell et al. (2011) who also focused on functionalised AuNP stability. In their study, the IgG conjugated AuNPs were prepared on day 1 and used on day 2, 3 and 4, consecutively. All three assays showed a high level of reproducibility and had the same hook point concentration. It was suggested that the functionalised AuNPs should be prepared and used within one week. Nevertheless, there was no report of functionalised AuNP stability in other studies. It would have been better if measurements were done at day 10, 15 for better understanding of the stability characteristics. In addition, a biocide such as sodium azide (NaN_3) should be added to the system to prevent degradation of proteins by microbial attack.

Overall, these results show that Affimers can be used in a NP size shift assay using DLS with Mb and show the same range of sensitivity compared with a IgG based system. In addition, the assay platform was tested against a much larger analyte, toxin B. The LOD of the assay was 30 nM, which was inferior to that Mb. Nonetheless, these results showed that the platform could be used with different analytes apart from Mb.

A decorative graphic consisting of a vertical grey line and a horizontal grey line intersecting at the center. The vertical line is slightly thicker than the horizontal line.

Chapter 6

General discussion

Chapter 6 General discussion

6.1 General discussion

In recent years, there have been several reports evidencing the potential of nanoparticle (NP) coupled dynamic light scattering (DLS) size shift assays in detecting a wide variety of analytes. These are summarised in Chapter 1 of this thesis. The challenge in this assay field is to produce nanobiosensors whose binding activity can be maintained under various conditions and over a longer term since the key mechanism of the assay is based on a specific binding event between bioreceptor and analyte. To date, the bioreceptors used in the assays were antibodies, oligonucleotides or DNA-aptamers; whereas synthetic binding proteins have not been investigated.

The main objective of this project was to develop a NP size shift assay coupling to DLS by using non-antibody binding proteins, Affimers, as bioreceptors. Most synthetic binding proteins have been investigated as therapeutic agents as an alternative to monoclonal antibody, or have been explored for *in vivo* imaging. However, the work in this thesis has been focused on using the Affimers as bioreceptors for sensing purposes. A previous study by Raina et al. (2015) showed that an Affimer could be used as a bioreceptor on an electrochemical impedimetric biosensor for detection of an anti-myc tag antibody. In addition, Xie et al., (2017) reported the use of an Affimer together with a monoclonal Ab in a chemiluminescent assay for detection of glypican-3 (GPC3), which is a protein biomarker for hepatocellular carcinoma. Therefore, it was hypothesized that Affimers could be used as bioreceptors in a NP-based DLS size shift assay. Here, the Affimers were immobilised onto the AuNP surface which were then used as nanobiosensors to detect specific proteins. Fundamental parameters affecting the NP-coupled DLS size shift assay were explored.

6.2 Affimer production and characterisation

Myoglobin (Mb) was selected as a model analyte in this project as it is an inexpensive protein with good availability and has well understood structure and properties. It should be stressed here that the use of Mb was not for a final application since biosensing platform development requires extensive investigation before moving on to practical use. Six different Affimers against Mb were successfully selected by biopanning of a phage display library. The selected Affimers were subcloned from phagemid DNA into a bacterial expression vector for protein expression. Although the Affimers could be easily produced by prokaryotic expression system, the work carried out in this thesis demonstrated that amongst the six anti-Mb Affimers, their physicochemical properties are differed. These properties included level of expression, thermal stability, association and dissociation constants.

The general protocol for Affimer production included a 20 min heating step to eliminate non-specific proteins based on finding that the Affimer scaffold can tolerated temperatures over 70 °C (Raina et al., 2015; Tiede et al., 2014; Tiede et al., 2017). However, it was found out that three of the anti-Mb Affimers (D1, E3 and H1) were not tolerant to this temperature as without heating step, expression yields were higher. This result corresponded to the suggestion by Nygren and Skerra (2004) that property of the wild-type scaffold may be affected by changes within the structure, such as in the binding loops. With Affimers, around 20 % of the total sequence is contributed by the two, nine residue binding loops.

In addition, a single cysteine was successfully inserted to the C-terminus of the Affimers to facilitate the immobilization of the Affimer onto a sensor surface. However, the thiol side chain (-SH) of the cysteine residue tended to form a disulphide bridge between two Affimers and caused aggregation, as observed after the purification of the proteins. This was proved by mass spectroscopy of anti-Mb Affimers (Figure 4-6 and Appendix 3 - 6) and the fact that the aggregates could be redispersed with reducing agents such as TCEP. For characterisation of Affimers, immunoprecipitation (pull-down assay), ELISA and SPR methods were used for all of

the anti-Mb Affimers, except Affimer E3 that aggregated out of solution when SPR was performed and so it was excluded from the project. The aggregation issue was similar to that reported by Raina et al. (2015) who screened the Affimer library for anti-myc tag antibodies; they also found that some Affimer clones aggregated and had to be excluded. In this project, a modified sandwich ELISA was also used to identify pairs of Affimers for crosslinking AuNPs in the size shift assay.

Overall, the production of Affimers is similar to monoclonal antibody since once Affimer DNA is obtained the protein can be expressed, although Affimers use much simpler prokaryotic systems. Protein could then be produced without the batch-to-batch variation found in pAbs. In addition, no animals were used as well as special cell culture media or complex equipment. There may be some issues regarding Affimer production, such as low expression yield, aggregation, but in general, it seems that the limiting process for Affimer production is screening for the best binders suitable for a particular application. Therefore, combinations of characterisation methods should be implemented earlier in screening stages to distinguish the best Affimers.

6.3 Nanoparticle (NP) coupled dynamic light scattering (DLS) size shift assay using synthetic binding proteins

Functionalisation of bioreceptors onto the AuNP surface was an important process for generating nanobiosensors for the NP-coupled size shift assay. Coupling via the streptavidin-biotin interaction was selected as it is more durable than physical adsorption and requires fewer bioreceptors in the process. It was previously used by Gestwicki et al. (2000) and Liu and Huo (2009) for AuNP functionalisation. After the Affimers were produced and tested, functionalisation of the AuNP surface with Affimers was carried out to generate Affimer nanobiosensors. Biotin maleimide was used to biotinylate Affimers via the thiol group on the Affimer C-terminus that was provided by an engineered cysteine. In contrast, biotin hydrazide was used for biotinylation of IgG at the oxidized Fc region carbohydrate. Streptavidin coated

AuNPs (strep-AuNPs) were then mixed with the biotinylated bioreceptors. Factors related to the functionalisation were examined which were time of incubation and concentration of the biotinylated IgGs and Affimers (Chapter 4).

Once the nanobiosensors had been successfully fabricated, a combination of techniques was used to confirm the presence of the bioreceptors on the AuNPs. Conventional methods such as UV-spectrophotometry, dot blotting and DLS were used in combination to verify the success of functionalisation. However, these methods could not quantify the number of Affimers or antibodies attached to each AuNP. Therefore, the direct fluorescence method proposed by Filbrun and Driskell, (2016) was adapted and used to quantify IgGs and Affimers attached to the AuNPs. The experimental data showed that Affimers packed more densely onto the AuNP surface (565 Affimers/NP) compared to IgGs (280 IgGs/NP). This supports the idea that the smaller size of Affimers allows them to be immobilised more densely, which leads to the enhancement of the sensing system sensitivity (Ferrigno, 2016).

The kinetics study between Affimers conjugated AuNPs (Affimer-AuNPs) and myoglobin conjugated AuNPs (Mb-AuNPs) was conducted in order to understand the overall aggregation process compared to established IgG nanobiosensors (IgG-AuNPs). The data showed that Affimer-AuNPs had similar kinetics to IgG-AuNPs. The binding event required at least 30 min to reach equilibrium but the maximum size shift response of Affimer nanobiosensors was typically less than IgG system. This data helped in designing an appropriate assay protocol.

The NP-coupled DLS size shift assay using the Affimers as bioreceptors was successfully developed and used to detect Mb to prove the principle. The response curves obtained from Affimer- and IgG-AuNPs showed similar trends. A linear response was observed with an increase concentrations of Mb until the hook point was reached. The hook effect was found in both systems. It is a phenomenon that occurs when larger amounts of analyte is present in the system at the same time and all bioreceptors on the AuNPs are occupied. This leads to decrease in crosslinking. The effect has been reported in previous NP-coupled DLS assays and the hook point determines the upper limit of detection (Liu and Huo, 2009; Driskell et al., 2011;

Huang et al., 2015). The hook effect is seen in a number of different binding assays including the ELISA. The Affimer nanobiosensors prepared were selective for Mb and showed no response when BSA added. Also, the size shift responses were due to specific binding between the Affimers and Mb: when non-specific (control) Affimers were used, there was no significant response.

Initially, two Affimer clones were used as bioreceptors as they should be able to crosslink between AuNPs. It was proved that paired Affimer nanobiosensors could be used for Mb detection but the sensitivity (LOD = 41.6 pM) was lower as compared to IgG-nanobiosensors (LOD = 148 fM) even when there were more molecules of Affimer attached on the AuNPs. Nevertheless, it should be noted that the IgG used was a polyclonal antibody. The Affimers are monoclonal and bind to a single epitope. Therefore, multiple Affimers were used as bioreceptors in the assay to mimic the polyclonal characteristics of IgG used. The sensitivity of the assay was improved substantially from 41.6 pM to 554 fM LOD, which was in the same range of IgG-AuNPs for Mb detection.

The effect of NP size was also examined since the Mie theory predicts that light scattering intensity is proportional to the 6th power of the radius of the particle (Yguerabide and Yguerabide, 1998) and previous studies have shown the sensitivity of the assay could be improved by using larger AuNPs (Nietzold and Lisdat, 2012; Wang et al., 2012). The findings of our study suggested that it was not always the case that larger AuNPs provide better sensitivity. The data corresponded to two previous studies by Driskell et al. (2011) and Huang et al. (2015), who reported that sensitivity was not necessarily improved with increasing AuNP size. The explanations given in both studies were pretty similar that this might be due to different concentration of AuNPs being used and steric hindrance between larger AuNPs and the analytes may have prevented binding. The analytes from both researches were influenza virus and bacteria *Listeria monocytogenes*, respectively, which are large biomolecules. Here, conversely, Mb is a small protein with around 3.5 nm diameter. However, the steric effect that blocked the binding might come from the AuNPs themselves. Larger particles could prevent each other from binding to Mb and

changing the binding stoichiometry. Also, it is worth pointing out that with small AuNPs (20 nm), the LOD of the Affimer based system was slightly better than for IgG-AuNPs (Figure 5-15). This data further supported the idea that steric hindrance is an important factor to consider as Affimers are smaller than IgGs. With smaller AuNPs the Affimers were not restricted by the size of the NPs in binding to Mb.

AuNP concentration was another factor investigated in this thesis, as DLS measures the whole population of the samples. It was expected that more dilute AuNPs suspension could provide better sensitivity because all the AuNPs should be involved in crosslinking and forming aggregates. As a result, there should be less unbound nanobiosensors left in solution, giving a larger shift in size (Driskell et al., 2011; Zheng et al., 2016). The experimental data for both IgG and Affimer nanobiosensors corresponded to the theory except when very dilute AuNPs (8×10^8 NP/ml) was used. This is likely because the scattering intensities reduced due to limited scattering material. These results are consistent with the report by Driskell et al. (2011). These findings suggest that the detection range of the size shift assay can be adjusted by varying the AuNP concentration. This factor should be considered alongside the size of AuNPs used.

Additionally, Affimer nanobiosensors for *Clostridium difficile* toxin B were prepared and used in the same assay format to investigate the versatility of the Affimer size shift assay. Toxin B was selected as it is a large biomolecules ($M_r \sim 270$ kDa) and there were anti-toxin B Affimers available and well-characterised. However, the sensitivity of the toxin B detection was in the nM range and the hook point occurred at a higher concentration compared to the detection of Mb. Also, it should be noted that only two anti-toxin B Affimers were used and the sensitivity might be improved if multiple Affimers are used. Another interesting point from this work is that with toxin B present in the control system (strep-AuNPs) larger size shift responses were seen, especially at higher concentrations, as compared to the changes seen with Mb. This might be related to the fact that the analyte itself can be measured directly by DLS because proteins possess a weak light scattering property.

Taken together, these findings suggest that in general the NP-coupled DLS size shift assay works optimally with bioreceptors that can bind to multiple epitopes of the analyte. The current data highlight the potential importance of avidity effects on the DLS size shift assay over the number of bioreceptors on the AuNP surface. In addition, the detection range of the assay can be tailored to each analyte by selecting appropriate AuNP size and concentration. With large biomolecules, their intrinsic light scattering property could interfere with the size shift assay. Therefore, it is best to conduct a DLS measurement for the large biomolecules alone without the AuNPs to determine the concentrations at which the weak scattering effect does not interfere. For smaller biomolecules, the steric effect is the main factor to be considered as binding between Affimers and analytes can be hindered by the size of AuNPs used. These observations are based on experiments carried out in PBS buffer and the buffer used and matrix in which the analyte is presented (e.g. serum, urine) should also be considered.

Regarding the stability of nanobiosensors, previous work in NP-coupled DLS size shift assays have not dealt with the long term stability of the nanobiosensors used. Only one study examined the stability of their antibody functionalised AuNPs (Driskell et al., 2011). In this thesis, the stability test was conducted for around five weeks. Both IgG-AuNPs and Affimer-AuNPs showed no significant difference and were stable over a week when kept at 4 °C protected from light (Figure 5-19). It may be that they were stable beyond this, however, the next time point assayed was 35 days at which their performance had deteriorated. The data here correlated with the stability data of Driskell et al. (2011). A limitation of the stability test was that it could not differentiate the cause of instability; whether coming from AuNP functionalisation or bioreceptor damage. For instance, if sodium azide was added to the storage buffer it might help prevent degradation of proteins by microbial action. This should be carried out as part of any future assay development.

6.4 Future work and opportunities

This study has demonstrated that synthetic binding proteins, Affimers, could be used in NP-coupled DLS size shift assays. The findings of this research provide insights for assay development and show its versatility for various bioreceptors. We have also shown that Affimers can be used in optical sensing systems in addition to their applications in molecular and cell biology, as reported by Tiede et al. (2017). Additionally, NP-coupled DLS size shift assays are not restricted to proteins but can be designed for other analytes. At present, Tiede et al. (2017) have been able to screen Affimers against small organic compounds, such as 2,4,6-trinitrobenzene (TNT). This opens up another opportunity to develop NP-coupled DLS size shift assays in a competitive assay format for detection of small molecules (e.g. drugs, pesticides). Therefore, future work needs to be carried out to establish whether the Affimer based nanobiosensors are effective in a competitive format.

The opportunity to develop the NP-coupled DLS size shift assays further, lies in two key areas; the feasibility of using the assays with samples in various matrices (e.g. serum) and stability of the nanobiosensors (Pierre-Pierre and Huo, 2015). In terms of background signal, the assay has mostly been reported for laboratory rather than “real world” applications. It was suggested by Jans and Huo (2012) that to overcome the matrix scattering intensities from blood samples, at least 100 nm diameter AuNPs should be used. It would be interesting to assess the effects of background matrices on the Affimer based NP-system. Affimers might also be a solution to the stability of the nanobiosensors since they are much more thermally stable than IgG (Tiede et al., 2014; Tiede et al., 2017).

It is very important that the binding activity between the bioreceptor and target analyte is maintained to ensure the qualitative and quantitative efficiency of the assay over time. Also, the assay requires the use of polyclonal reagents in crosslinking AuNPs. Polyclonal antibodies, although easily available suffer from batch-to-batch variability, whereas using multiple monoclonal antibodies would be too expensive for assay development. The production of Affimers is easier and cheaper with no batch-to-batch variation as they are clonal reagents. Further

research might explore the screening process for multiple Affimers that bind to different epitopes on the target protein in order to replicate polyclonal reagents. In addition, more research is needed to better understand the stability of the Affimer-nanobiosensors and whether the functionalisation alters the binding efficacy or stability in long term use. The company Nano Discovery Inc.² in the US is currently commercializing the NP-coupled DLS size shift technology under the name D2Dx™. However, the AuNP sensors are sold in the form of conjugation kits for antibody immobilization. The antibodies are not provided and the conjugation has to be performed before the assay. With Affimers, that are stable thermodynamically and chemically, development of ready-to-use assay kits might be easier to make without the extra conjugation steps.

In summary, the analytical science and specifically biosensing fields have increasingly shifted towards label-free systems. The main advantages of these assays over others is that no labelling of the target or ligand is needed. Therefore, the assay is less complicated and true interactions can be obtained. The NP-coupled DLS size shift assay is another optical label-free technique that proved useful for many applications such as biomarker detection and studies on protein-protein interaction. In comparison to conventional optical label-free techniques such as SPR, DLS is rapid and assay results can be obtained within minutes. Additionally, homogeneous assays can be performed as there is no need to separate the nanobiosensors and analytes before measurement take place. The equipment itself is cheaper as well as the consumables required for measurements. DLS can be operated with cuvettes or 96-well plates, which cost less than SPR chip. Glass cuvettes are also available for reuse if needed. Although the use of AuNPs might be costly as the nanobiosensors are single-use for each measurement, the NP-coupled DLS size shift assay only requires a small volume of AuNPs per sample (around 20 µl/sample). Overall, in a long-term consideration for small laboratories or industries with limited budget, DLS might be a better option for protein-protein interaction as DLS can be used for protein and

² <http://www.nanodiscoveryinc.com/>

particle size analysis as well. This technique also has a potential to be developed into a high-throughput format as DLS plate readers are now available.

References

- Ahmed, A., Rushworth, J.V., Wright, J.D. and Millner, P.A. 2013. Novel Impedimetric Immunosensor for Detection of Pathogenic Bacteria *Streptococcus pyogenes* in Human Saliva. *Analytical Chemistry*. **85**(24),pp.12118–12125.
- Ahmed, F.E., Wiley, J.E., Weidner, D.A., Bonnerup, C. and Mota, H. 2010. Surface plasmon resonance (SPR) spectrometry as a tool to analyze nucleic acid-protein interactions in crude cellular extracts. *Cancer Genomics & Proteomics*. **7**(6),pp.303–309.
- Aslan, K., Lakowicz, J.R. and Geddes, C.D. 2004. Nanogold-plasmon-resonance-based glucose sensing. *Analytical Biochemistry*. **330**(1),pp.145–155.
- Aslan, K., Luhrs, C.C. and Pérez-Luna, V.H. 2004. Controlled and Reversible Aggregation of Biotinylated Gold Nanoparticles with Streptavidin. *The Journal of Physical Chemistry B*. **108**(40),pp.15631–15639.
- Bain, C.D., Troughton, E.B., Tao, Y.T., Evall, J., Whitesides, G.M. and Nuzzo, R.G. 1989. Formation of monolayer films by the spontaneous assembly of organic thiols from solution onto gold. *Journal of the American Chemical Society*. **111**(1),pp.321–335.
- Baker, M. 2015. Reproducibility crisis: Blame it on the antibodies. *Nature*. **521**(7552),pp.274–276.
- Bell, N.C., Minelli, C. and Shard, A.G. 2013. Quantitation of IgG protein adsorption to gold nanoparticles using particle size measurement. *Analytical Methods*. **5**(18),p.4591.
- Beqa, L., Singh, A.K., Khan, S.A., Senapati, D., Arumugam, S.R. and Ray, P.C. 2011. Gold Nanoparticle-Based Simple Colorimetric and Ultrasensitive Dynamic Light Scattering Assay for the Selective Detection of Pb(II) from Paints, Plastics, and Water Samples. *ACS Applied Materials & Interfaces*. **3**(3),pp.668–673.
- Bertero, M. and Pike, E.R. 1991. Exponential-sampling method for Laplace and other dilationally invariant transforms: I. Singular-system analysis. *Inverse Problems*. **7**(1),p.1.
- Binz, H.K. and Plückthun, A. 2005. Engineered proteins as specific binding reagents. *Current Opinion in Biotechnology*. **16**(4),pp.459–469.
- Bogdanovic, J., Colon, J., Baker, C. and Huo, Q. 2010. A label-free nanoparticle aggregation assay for protein complex/aggregate detection and study. *Analytical Biochemistry*. **405**(1),pp.96–102.

- Bombarová, K., Chlpík, J. and Cirák, J. 2015. Surface Plasmon Resonance Ellipsometry Based Biosensor for the Investigation of Biomolecular Interactions. *Materials Today: Proceedings*. **2**(1),pp.70–76.
- Bradbury, A. and Plückthun, A. 2015. Reproducibility: Standardize antibodies used in research. *Nature*. **518**(7537),pp.27–29.
- Brandt, O. and Hoheisel, J.D. 2004. Peptide nucleic acids on microarrays and other biosensors. *Trends in Biotechnology*. **22**(12),pp.617–622.
- Brar, S.K. and Verma, M. 2011. Measurement of nanoparticles by light-scattering techniques. *TrAC Trends in Analytical Chemistry*. **30**(1),pp.4–17.
- Brown, K.R., Fox, A.P. and Natan, M.J. 1996. Morphology-Dependent Electrochemistry of Cytochrome *c* at Au Colloid-Modified SnO₂ Electrodes. *Journal of the American Chemical Society*. **118**(5),pp.1154–1157.
- Brust, M., Walker, M., Bethell, D., Schiffrin, D.J. and Whyman, R. 1994. Synthesis of thiol-derivatised gold nanoparticles in a two-phase Liquid–Liquid system. *J. Chem. Soc., Chem. Commun.* **0**(7),pp.801–802.
- Chambers, J.P., Arulanandam, B.P., Matta, L.L., Weis, A. and Valdes, J.J. 2008. Biosensor recognition elements. *Current Issues in Molecular Biology*. **10**(1–2),pp.1–12.
- Chen, Q., Wu, X., Wang, D., Tang, W., Li, N. and Liu, F. 2011. Oligonucleotide-functionalized gold nanoparticles-enhanced QCM-D sensor for mercury(II) ions with high sensitivity and tunable dynamic range. *The Analyst*. **136**(12),p.2572.
- Chu, P.-T., Lin, C.-S., Chen, W.-J., Chen, C.-F. and Wen, H.-W. 2012. Detection of Gliadin in Foods Using a Quartz Crystal Microbalance Biosensor That Incorporates Gold Nanoparticles. *Journal of Agricultural and Food Chemistry*. **60**(26),pp.6483–6492.
- Chun, C., Joo, J., Kwon, D., Kim, C.S., Cha, H.J., Chung, M.-S. and Jeon, S. 2011. A facile and sensitive immunoassay for the detection of alpha-fetoprotein using gold-coated magnetic nanoparticle clusters and dynamic light scattering. *Chemical Communications*. **47**(39),p.11047.
- Clark, L.C. and Lyons, C. 1962. ELECTRODE SYSTEMS FOR CONTINUOUS MONITORING IN CARDIOVASCULAR SURGERY. *Annals of the New York Academy of Sciences*. **102**(1),pp.29–45.
- Cohen, R.J. and Benedek, G.B. 1975. Immunoassay by light scattering spectroscopy. *Immunochemistry*. **12**(4),pp.349–351.
- Cooper, M.A. 2006. Optical biosensors: where next and how soon? *Drug Discovery Today*. **11**(23–24),pp.1061–1067.

- D'Agata, R., Palladino, P. and Spoto, G. 2017. Streptavidin-coated gold nanoparticles: critical role of oligonucleotides on stability and fractal aggregation. *Beilstein Journal of Nanotechnology*. **8**,pp.1–11.
- Dai, Q., Liu, X., Coutts, J., Austin, L. and Huo, Q. 2008. A One-Step Highly Sensitive Method for DNA Detection Using Dynamic Light Scattering. *Journal of the American Chemical Society*. **130**(26),pp.8138–8139.
- Damborsky, P., vitel, J. and Katrlík, J. 2016. Optical biosensors. *Essays In Biochemistry*. **60**(1),pp.91–100.
- Dasary, S.S.R., Senapati, D., Singh, A.K., Anjaneyulu, Y., Yu, H. and Ray, P.C. 2010. Highly Sensitive and Selective Dynamic Light-Scattering Assay for TNT Detection Using *p*-ATP Attached Gold Nanoparticle. *ACS Applied Materials & Interfaces*. **2**(12),pp.3455–3460.
- Demidov, V.V., Potaman, V.N., Frank-Kamenetskii, M.D., Egholm, M., Buchard, O., Sönnichsen, S.H. and Nielsen, P.E. 1994. Stability of peptide nucleic acids in human serum and cellular extracts. *Biochemical Pharmacology*. **48**(6),pp.1310–1313.
- Dennis, M.S., Herzka, A. and Lazarus, R.A. 1995. Potent and Selective Kunitz Domain Inhibitors of Plasma Kallikrein Designed by Phage Display. *Journal of Biological Chemistry*. **270**(43),pp.25411–25417.
- Di Pasqua, A.J., Mishler, R.E., Ship, Y.-L., Dabrowiak, J.C. and Asefa, T. 2009. Preparation of antibody-conjugated gold nanoparticles. *Materials Letters*. **63**(21),pp.1876–1879.
- Dixon, M.C. 2008. Quartz Crystal Microbalance with Dissipation Monitoring: Enabling Real-Time Characterization of Biological Materials and Their Interactions. *Journal of Biomolecular Techniques : JBT*. **19**(3),pp.151–158.
- Dreaden, E.C., Alkilany, A.M., Huang, X., Murphy, C.J. and El-Sayed, M.A. 2012. The golden age: gold nanoparticles for biomedicine. *Chem. Soc. Rev.* **41**(7),pp.2740–2779.
- Driskell, J.D., Jones, C.A., Tompkins, S.M. and Tripp, R.A. 2011. One-step assay for detecting influenza virus using dynamic light scattering and gold nanoparticles. *The Analyst*. **136**(15),p.3083.
- Dunn, A.S. 1986. Polymeric stabilization of colloidal dispersions. By D. H. Napper, Academic Press, London, 1984. pp. xviii + 428, price £39.50, \$65.00. ISBN 0-12-513980-2. *British Polymer Journal*. **18**(4),pp.278–278.
- Durgadas, C.V., Lakshmi, V.N., Sharma, C.P. and Sreenivasan, K. 2011. Sensing of lead ions using glutathione mediated end to end assembled gold nanorod chains. *Sensors and Actuators B: Chemical*. **156**(2),pp.791–797.

- Ebersbach, H., Fiedler, E., Scheuermann, T., Fiedler, M., Stubbs, M.T., Reimann, C., Proetzel, G., Rudolph, R. and Fiedler, U. 2007. Affilin—Novel Binding Molecules Based on Human γ -B-Crystallin, an All β -Sheet Protein. *Journal of Molecular Biology*. **372**(1),pp.172–185.
- Evans, S.D. and Ulman, A. 1990. Surface potential studies of alkyl-thiol monolayers adsorbed on gold. *Chemical Physics Letters*. **170**(5–6),pp.462–466.
- Faraday, M. 1857. The Bakerian Lecture: Experimental Relations of Gold (and Other Metals) to Light. *Philosophical Transactions of the Royal Society of London*. **147**(0),pp.145–181.
- Fei, Y., Sun, Y.-S., Li, Y., Yu, H., Lau, K., Landry, J., Luo, Z., Baumgarth, N., Chen, X. and Zhu, X. 2015. Characterization of Receptor Binding Profiles of Influenza A Viruses Using An Ellipsometry-Based Label-Free Glycan Microarray Assay Platform. *Biomolecules*. **5**(3),pp.1480–1498.
- Ferrigno, P.K. 2016. Non-antibody protein-based biosensors. *Essays In Biochemistry*. **60**(1),pp.19–25.
- Filbrun, S.L. and Driskell, J.D. 2016. A fluorescence-based method to directly quantify antibodies immobilized on gold nanoparticles. *The Analyst*. **141**(12),pp.3851–3857.
- Frens, G. 1973. Controlled Nucleation for the Regulation of the Particle Size in Monodisperse Gold Suspensions. *Nature Physical Science*. **241**(105),pp.20–22.
- Gao, D., Sheng, Z. and Han, H. 2011. An ultrasensitive method for the detection of gene fragment from transgenics using label-free gold nanoparticle probe and dynamic light scattering. *Analytica Chimica Acta*. **696**(1–2),pp.1–5.
- Gao, J., Chen, K., Miao, Z., Ren, G., Chen, X., Gambhir, S.S. and Cheng, Z. 2011. Affibody-based nanoprobe for HER2-expressing cell and tumor imaging. *Biomaterials*. **32**(8),pp.2141–2148.
- Garipcan, B., Caglayan, M. and Demirel, G. 2011. New Generation Biosensors based on Ellipsometry In: P. A. Serra, ed. *New Perspectives in Biosensors Technology and Applications* [Online]. InTech. [Accessed 13 September 2017]. Available from: <http://www.intechopen.com/books/new-perspectives-in-biosensors-technology-and-applications/new-generation-biosensors-based-on-ellipsometry>.
- Gestwicki, J.E., Strong, L.E. and Kiessling, L.L. 2000. Visualization of Single Multivalent Receptor-Ligand Complexes by Transmission Electron Microscopy The authors thank Colleen Lavin (UW Madison, Microscopy Resource) and Kim Dickson for experimental support. This work was supported in part by the NIH (GM 55984). J.E.G. acknowledges the NIH Biotechnology Training Grant for support (T32GM08349). L.E.S. was supported by an NIH predoctoral

fellowship (GM 18750). *Angewandte Chemie (International Ed. in English)*. **39**(24),pp.4567–4570.

- Goode, J., Dillon, G. and Millner, P.A. 2016. The development and optimisation of nanobody based electrochemical immunosensors for IgG. *Sensors and Actuators B: Chemical*. **234**,pp.478–484.
- Green, T.A. 2014. Gold etching for microfabrication. *Gold Bulletin*. **47**(3),pp.205–216.
- Häkkinen, H. 2012. The gold–sulfur interface at the nanoscale. *Nature Chemistry*. **4**(6),pp.443–455.
- Hamzeh-Mivehroud, M., Alizadeh, A.A., Morris, M.B., Bret Church, W. and Dastmalchi, S. 2013. Phage display as a technology delivering on the promise of peptide drug discovery. *Drug Discovery Today*. **18**(23–24),pp.1144–1157.
- Hao, R.-Z., Song, H.-B., Zuo, G.-M., Yang, R.-F., Wei, H.-P., Wang, D.-B., Cui, Z.-Q., Zhang, Z., Cheng, Z.-X. and Zhang, X.-E. 2011. DNA probe functionalized QCM biosensor based on gold nanoparticle amplification for *Bacillus anthracis* detection. *Biosensors and Bioelectronics*. **26**(8),pp.3398–3404.
- Hassan, P.A., Rana, S. and Verma, G. 2015. Making Sense of Brownian Motion: Colloid Characterization by Dynamic Light Scattering. *Langmuir*. **31**(1),pp.3–12.
- Helma, J., Cardoso, M.C., Muyldermans, S. and Leonhardt, H. 2015. Nanobodies and recombinant binders in cell biology. *The Journal of Cell Biology*. **209**(5),pp.633–644.
- Hermanson, G.T. 2008. *Bioconjugate techniques* 2nd edition. San Diego: Academic Press.
- Hoffmann, A., Kovermann, M., Lilie, H., Fiedler, M., Balbach, J., Rudolph, R. and Pfeifer, S. 2012. New Binding Mode to TNF-Alpha Revealed by Ubiquitin-Based Artificial Binding Protein A. Pastore, ed. *PLoS ONE*. **7**(2),p.e31298.
- Huang, C.-C. and Chang, H.-T. 2006. Selective Gold-Nanoparticle-Based ‘Turn-On’ Fluorescent Sensors for Detection of Mercury(II) in Aqueous Solution. *Analytical Chemistry*. **78**(24),pp.8332–8338.
- Huang, S.-H. 2007. Gold nanoparticle-based immunochromatographic assay for the detection of *Staphylococcus aureus*. *Sensors and Actuators B: Chemical*. **127**(2),pp.335–340.
- Huang, X., Xu, Z., Mao, Y., Ji, Y., Xu, H., Xiong, Y. and Li, Y. 2015. Gold nanoparticle-based dynamic light scattering immunoassay for ultrasensitive detection of *Listeria monocytogenes* in lettuces. *Biosensors and Bioelectronics*. **66**,pp.184–190.

- Huo, Q. 2010. Protein complexes/aggregates as potential cancer biomarkers revealed by a nanoparticle aggregation immunoassay. *Colloids and Surfaces B: Biointerfaces*. **78**(2),pp.259–265.
- James, A.E. and Driskell, J.D. 2013. Monitoring gold nanoparticle conjugation and analysis of biomolecular binding with nanoparticle tracking analysis (NTA) and dynamic light scattering (DLS). *The Analyst*. **138**(4),p.1212.
- Jans, H. and Huo, Q. 2012. Gold nanoparticle-enabled biological and chemical detection and analysis. *Chem. Soc. Rev.* **41**(7),pp.2849–2866.
- Jans, H., Liu, X., Austin, L., Maes, G. and Huo, Q. 2009. Dynamic Light Scattering as a Powerful Tool for Gold Nanoparticle Bioconjugation and Biomolecular Binding Studies. *Analytical Chemistry*. **81**(22),pp.9425–9432.
- Jazayeri, M.H., Amani, H., Pourfatollah, A.A., Pazoki-Toroudi, H. and Sedighimoghaddam, B. 2016. Various methods of gold nanoparticles (GNPs) conjugation to antibodies. *Sensing and Bio-Sensing Research*. **9**,pp.17–22.
- Jiang, H., Ling, K., Tao, X. and Zhang, Q. 2015. Theophylline detection in serum using a self-assembling RNA aptamer-based gold nanoparticle sensor. *Biosensors and Bioelectronics*. **70**,pp.299–303.
- Johnson, S. and Krauss, T.F. 2017. Label-free affinity biosensor arrays: novel technology for molecular diagnostics. *Expert Review of Medical Devices*. **14**(3),pp.177–179.
- Jolly, P., Estrela, P. and Ladomery, M. 2016. Oligonucleotide-based systems: DNA, microRNAs, DNA/RNA aptamers. *Essays In Biochemistry*. **60**(1),pp.27–35.
- Ju, R.T.C., Frank, C.W. and Gast, A.P. 1992. CONTIN analysis of colloidal aggregates. *Langmuir*. **8**(9),pp.2165–2171.
- Kaittanis, C., Santra, S. and Perez, J.M. 2010. Emerging nanotechnology-based strategies for the identification of microbial pathogenesis. *Advanced Drug Delivery Reviews*. **62**(4–5),pp.408–423.
- Kalluri, J.R., Arbnesi, T., Afrin Khan, S., Neely, A., Candice, P., Varisli, B., Washington, M., McAfee, S., Robinson, B., Banerjee, S., Singh, A.K., Senapati, D. and Ray, P.C. 2009. Use of Gold Nanoparticles in a Simple Colorimetric and Ultrasensitive Dynamic Light Scattering Assay: Selective Detection of Arsenic in Groundwater. *Angewandte Chemie International Edition*. **48**(51),pp.9668–9671.
- Khan, S.A., DeGrasse, J.A., Yakes, B.J. and Croley, T.R. 2015. Rapid and sensitive detection of cholera toxin using gold nanoparticle-based simple colorimetric and dynamic light scattering assay. *Analytica Chimica Acta*. **892**,pp.167–174.
- Kim, N.H., Baek, T.J., Park, H.G. and Seong, G.H. 2007. Highly sensitive biomolecule detection on a quartz crystal microbalance using gold nanoparticles as signal

amplification probes. *Analytical Sciences: The International Journal of the Japan Society for Analytical Chemistry*. **23**(2),pp.177–181.

Kim, Y., Johnson, R.C. and Hupp, J.T. 2001. Gold Nanoparticle-Based Sensing of 'Spectroscopically Silent' Heavy Metal Ions. *Nano Letters*. **1**(4),pp.165–167.

Knappik, A., Ge, L., Honegger, A., Pack, P., Fischer, M., Wellnhofer, G., Hoess, A., Wölle, J., Plückthun, A. and Virnekäs, B. 2000. Fully synthetic human combinatorial antibody libraries (HuCAL) based on modular consensus frameworks and CDRs randomized with trinucleotides 1 Edited by I. A. Wilson. *Journal of Molecular Biology*. **296**(1),pp.57–86.

Kumar, S., Aaron, J. and Sokolov, K. 2008. Directional conjugation of antibodies to nanoparticles for synthesis of multiplexed optical contrast agents with both delivery and targeting moieties. *Nature Protocols*. **3**(2),pp.314–320.

Lai, Y.H., Koo, S., Oh, S.H., Driskell, E.A. and Driskell, J.D. 2015. Rapid screening of antibody–antigen binding using dynamic light scattering (DLS) and gold nanoparticles. *Anal. Methods*. **7**(17),pp.7249–7255.

Lakhin, A., Tarantul, V. and Gening, L. 2013. Aptamers: Problems, Solutions and Prospects. *Acta Naturae*. **5**(4),pp.34–43.

Laurenson, S., Pett, M.R., Hoppe-Seyler, K., Denk, C., Hoppe-Seyler, F., Coleman, N. and Ko Ferrigno, P. 2011. Development of peptide aptamer microarrays for detection of HPV16 oncoproteins in cell extracts. *Analytical Biochemistry*. **410**(2),pp.161–170.

LaVallie, E.R., DiBlasio, E.A., Kovacic, S., Grant, K.L., Schendel, P.F. and McCoy, J.M. 1993. A Thioredoxin Gene Fusion Expression System That Circumvents Inclusion Body Formation in the E. coli Cytoplasm. *Nature Biotechnology*. **11**(2),pp.187–193.

Lee, S.-C., Park, K., Han, J., Lee, J. -j., Kim, H.J., Hong, S., Heu, W., Kim, Y.J., Ha, J.-S., Lee, S.-G., Cheong, H.-K., Jeon, Y.H., Kim, D. and Kim, H.-S. 2012. Design of a binding scaffold based on variable lymphocyte receptors of jawless vertebrates by module engineering. *Proceedings of the National Academy of Sciences*. **109**(9),pp.3299–3304.

Lee, T.M.-H. 2008. Over-the-Counter Biosensors: Past, Present, and Future. *Sensors*. **8**(9),pp.5535–5559.

Liao, Y.-D., Jeng, J.-C., Wang, C.-F., Wang, S.-C. and Chang, S.-T. 2004. Removal of N-terminal methionine from recombinant proteins by engineered *E. coli* methionine aminopeptidase. *Protein Science*. **13**(7),pp.1802–1810.

Lin, D., Liu, H., Qian, K., Zhou, X., Yang, L. and Liu, J. 2012. Ultrasensitive optical detection of trinitrotoluene by ethylenediamine-capped gold nanoparticles. *Analytica Chimica Acta*. **744**,pp.92–98.

- Lipovsek, D. 2011. Adnectins: engineered target-binding protein therapeutics. *Protein Engineering Design and Selection*. **24**(1–2),pp.3–9.
- Liu, X., Dai, Q., Austin, L., Coutts, J., Knowles, G., Zou, J., Chen, H. and Huo, Q. 2008. A One-Step Homogeneous Immunoassay for Cancer Biomarker Detection Using Gold Nanoparticle Probes Coupled with Dynamic Light Scattering. *Journal of the American Chemical Society*. **130**(9),pp.2780–2782.
- Liu, X. and Huo, Q. 2009. A washing-free and amplification-free one-step homogeneous assay for protein detection using gold nanoparticle probes and dynamic light scattering. *Journal of Immunological Methods*. **349**(1–2),pp.38–44.
- Love, J.C., Estroff, L.A., Kriebel, J.K., Nuzzo, R.G. and Whitesides, G.M. 2005. Self-Assembled Monolayers of Thiolates on Metals as a Form of Nanotechnology. *Chemical Reviews*. **105**(4),pp.1103–1170.
- Luong, J.H.T., Male, K.B. and Glennon, J.D. 2008. Biosensor technology: Technology push versus market pull. *Biotechnology Advances*. **26**(5),pp.492–500.
- Ma, H., Wu, B., Huang, C. and Jia, N. 2014. One-step highly sensitive detection of melamine using gold nanoparticle-based dynamic light scattering. *Anal. Methods*. **6**(1),pp.67–72.
- Ma, L.-N., Liu, D.-J. and Wang, Z.-X. 2014. Gold Nanoparticle-Based Dynamic Light Scattering Assay for Mercury Ion Detection. *Chinese Journal of Analytical Chemistry*. **42**(3),pp.332–336.
- Ma, L.-N., Liu, D.-J. and Wang, Z.-X. 2010. Synthesis and Applications of Gold Nanoparticle Probes. *Chinese Journal of Analytical Chemistry*. **38**(1),pp.1–7.
- Makaraviciute, A., Jackson, C.D., Millner, P.A. and Ramanaviciene, A. 2016. Considerations in producing preferentially reduced half-antibody fragments. *Journal of Immunological Methods*. **429**,pp.50–56.
- Marks, R.S. (ed.). 2007. *Handbook of biosensors and biochips*. Chichester: Wiley.
- McKeague, M. and DeRosa, M.C. 2012. Challenges and Opportunities for Small Molecule Aptamer Development. *Journal of Nucleic Acids*. **2012**,pp.1–20.
- Miao, XiangMin, Feng, Z., Tian, J. and Peng, X. 2014. Glucose detection at attomole levels using dynamic light scattering and gold nanoparticles. *Science China Chemistry*. **57**(7),pp.1026–1031.
- Miao, X., Ling, L., Cheng, D. and Shuai, X. 2012. A highly sensitive sensor for Cu²⁺ with unmodified gold nanoparticles and DNAzyme by using the dynamic light scattering technique. *The Analyst*. **137**(13),p.3064.

- Miao, X., Ling, L. and Shuai, X. 2013. Sensitive detection of glucose in human serum with oligonucleotide modified gold nanoparticles by using dynamic light scattering technique. *Biosensors and Bioelectronics*. **41**,pp.880–883.
- Miao, X., Ling, L. and Shuai, X. 2011. Ultrasensitive detection of lead(ii) with DNzyme and gold nanoparticles probes by using a dynamic light scattering technique. *Chemical Communications*. **47**(14),p.4192.
- Miao, Xiangmin, Zou, S., Zhang, H. and Ling, L. 2014. Highly sensitive carcinoembryonic antigen detection using Ag@Au core–shell nanoparticles and dynamic light scattering. *Sensors and Actuators B: Chemical*. **191**,pp.396–400.
- Miao, X.-M., Xiong, C., Wang, W.-W., Ling, L.-S. and Shuai, X.-T. 2011. Dynamic-Light-Scattering-Based Sequence-Specific Recognition of Double-Stranded DNA with Oligonucleotide-Functionalized Gold Nanoparticles. *Chemistry - A European Journal*. **17**(40),pp.11230–11236.
- Mirkin, C.A., Letsinger, R.L., Mucic, R.C. and Storhoff, J.J. 1996. A DNA-based method for rationally assembling nanoparticles into macroscopic materials. *Nature*. **382**(6592),pp.607–609.
- Moore, S.J., Leung, C.L. and Cochran, J.R. 2012. Knottins: disulfide-bonded therapeutic and diagnostic peptides. *Drug Discovery Today: Technologies*. **9**(1),pp.e3–e11.
- Morrison, D.W.G., Dokmeci, M.R., Demirci, U. and Khademhosseini, A. 2007. Clinical Applications of Micro- and Nanoscale Biosensors *In*: K. E. Gonsalves, C. R. Halberstadt, C. T. Laurencin and L. S. Nair, eds. *Biomedical Nanostructures* [Online]. Hoboken, NJ, USA: John Wiley & Sons, Inc., pp. 439–460. [Accessed 24 July 2017]. Available from: <http://doi.wiley.com/10.1002/9780470185834.ch17>.
- Morrison, I.D., Grabowski, E.F. and Herb, C.A. 1985. Improved techniques for particle size determination by quasi-elastic light scattering. *Langmuir*. **1**(4),pp.496–501.
- Nabok, A., Tsargorodskaya, A., Mustafa, M.K., Székács, I., Starodub, N.F. and Székács, A. 2011. Detection of low molecular weight toxins using an optical phase method of ellipsometry. *Sensors and Actuators B: Chemical*. **154**(2),pp.232–237.
- Nam, J.-M. 2003. Nanoparticle-Based Bio-Bar Codes for the Ultrasensitive Detection of Proteins. *Science*. **301**(5641),pp.1884–1886.
- Nam, J.-M., Stoeva, S.I. and Mirkin, C.A. 2004. Bio-Bar-Code-Based DNA Detection with PCR-like Sensitivity. *Journal of the American Chemical Society*. **126**(19),pp.5932–5933.

- Neish, C.S., Martin, I.L., Henderson, R.M. and Edwardson, J.M. 2002. Direct visualization of ligand-protein interactions using atomic force microscopy. *British Journal of Pharmacology*. **135**(8),pp.1943–1950.
- Nietzold, C. and Lisdat, F. 2012. Fast protein detection using absorption properties of gold nanoparticles. *The Analyst*. **137**(12),p.2821.
- Nimjee, S.M., Rusconi, C.P. and Sullenger, B.A. 2005. Aptamers: An Emerging Class of Therapeutics. *Annual Review of Medicine*. **56**(1),pp.555–583.
- Nygren, P.-Å. and Skerra, A. 2004. Binding proteins from alternative scaffolds. *Journal of Immunological Methods*. **290**(1–2),pp.3–28.
- O’Kennedy, R., Fitzgerald, S. and Murphy, C. 2017. Don’t blame it all on antibodies – The need for exhaustive characterisation, appropriate handling, and addressing the issues that affect specificity. *TrAC Trends in Analytical Chemistry*. **89**,pp.53–59.
- Parmeggiani, F., Pellarin, R., Larsen, A.P., Varadamsetty, G., Stumpp, M.T., Zerbe, O., Caflisch, A. and Plückthun, A. 2008. Designed Armadillo Repeat Proteins as General Peptide-Binding Scaffolds: Consensus Design and Computational Optimization of the Hydrophobic Core. *Journal of Molecular Biology*. **376**(5),pp.1282–1304.
- Pavesi, L. and Fauchet, P.M. (eds.). 2008. *Biophotonics*. Berlin: Springer.
- Peng, G., Hakim, M., Broza, Y.Y., Billan, S., Abdah-Bortnyak, R., Kuten, A., Tisch, U. and Haick, H. 2010. Detection of lung, breast, colorectal, and prostate cancers from exhaled breath using a single array of nanosensors. *British Journal of Cancer*. **103**(4),pp.542–551.
- Pierre-Pierre, N. and Huo, Q. 2015. Dynamic Light Scattering Coupled with Gold Nanoparticle Probes as a Powerful Sensing Technique for Chemical and Biological Target Detection *In*: C. Wang and R. M. Leblanc, eds. *Recent Progress in Colloid and Surface Chemistry with Biological Applications* [Online]. Washington, DC: American Chemical Society, pp. 157–179. [Accessed 18 July 2017]. Available from: <http://pubs.acs.org/doi/10.1021/bk-2015-1215.ch009>.
- Pissuwan, D., Cortie, C.H., Valenzuela, S.M. and Cortie, M.B. 2010. Functionalised gold nanoparticles for controlling pathogenic bacteria. *Trends in Biotechnology*. **28**(4),pp.207–213.
- Plückthun, A. 2015. Designed Ankyrin Repeat Proteins (DARPs): Binding Proteins for Research, Diagnostics, and Therapy. *Annual Review of Pharmacology and Toxicology*. **55**(1),pp.489–511.
- Plückthun, A. and Pack, P. 1997. New protein engineering approaches to multivalent and bispecific antibody fragments. *Immunotechnology*. **3**(2),pp.83–105.

- Pollitt, M.J., Buckton, G., Piper, R. and Brocchini, S. 2015. Measuring antibody coatings on gold nanoparticles by optical spectroscopy. *RSC Adv.* **5**(31),pp.24521–24527.
- Pylaev, T.E., Khanadeev, V.A., Khlebtsov, B.N., Dykman, L.A., Bogatyrev, V.A. and Khlebtsov, N.G. 2011. Colorimetric and dynamic light scattering detection of DNA sequences by using positively charged gold nanospheres: a comparative study with gold nanorods. *Nanotechnology.* **22**(28),p.285501.
- Qi, C., Tian, X.-S., Chen, S., Yan, J.-H., Cao, Z., Tian, K.-G., Gao, G.F. and Jin, G. 2010. Detection of avian influenza virus subtype H5 using a biosensor based on imaging ellipsometry. *Biosensors and Bioelectronics.* **25**(6),pp.1530–1534.
- Qin, S., Chen, N., Yang, X., Wang, Q., Wang, K., Huang, J., Liu, J. and Zhou, M. 2017. Development of Dual-Aptamers for Constructing Sandwich-Type Pancreatic Polypeptide Assay. *ACS Sensors.* **2**(2),pp.308–315.
- Raina, M., Sharma, R., Deacon, S.E., Tiede, C., Tomlinson, D., Davies, A.G., McPherson, M.J. and Wälti, C. 2015. Antibody mimetic receptor proteins for label-free biosensors. *The Analyst.* **140**(3),pp.803–810.
- Ravalli, A., da Rocha, C.G., Yamanaka, H. and Marrazza, G. 2015. A label-free electrochemical affisensor for cancer marker detection: The case of HER2. *Bioelectrochemistry.* **106**,pp.268–275.
- Renberg, B., Nordin, J., Merca, A., Uhlén, M., Feldwisch, J., Nygren, P.-Å. and Eriksson Karlström, A. 2007. Affibody Molecules in Protein Capture Microarrays: Evaluation of Multidomain Ligands and Different Detection Formats. *Journal of Proteome Research.* **6**(1),pp.171–179.
- Renberg, B., Shiroyama, I., Engfeldt, T., Nygren, P.-Å. and Karlström, A.E. 2005. Affibody protein capture microarrays: Synthesis and evaluation of random and directed immobilization of affibody molecules. *Analytical Biochemistry.* **341**(2),pp.334–343.
- Rushworth, J.V., Hirst, N.A., Goode, J.A., Pike, D.J., Ahmed, A. and Millner, P. 2013. *Impedimetric biosensors for medical applications: current progress and challenges.* New York, NY: ASME Press : Momentum Press.
- Saha, K., Agasti, S.S., Kim, C., Li, X. and Rotello, V.M. 2012. Gold Nanoparticles in Chemical and Biological Sensing. *Chemical Reviews.* **112**(5),pp.2739–2779.
- Sato, K., Hosokawa, K. and Maeda, M. 2003. Rapid Aggregation of Gold Nanoparticles Induced by Non-Cross-Linking DNA Hybridization. *Journal of the American Chemical Society.* **125**(27),pp.8102–8103.
- Schlatter, D., Brack, S., Banner, D.W., Batey, S., Benz, J., Bertschinger, J., Huber, W., Joseph, C., Rufer, A.C., van der Klooster, A., Weber, M., Grabulovski, D. and Hennig, M. 2012. Generation, characterization and structural data of

chymase binding proteins based on the human Fyn kinase SH3 domain. *mAbs*. **4**(4),pp.497–508.

- Seow, N., Tan, Y.N. and Yung, L.-Y.L. 2014. Gold Nanoparticle-Dynamic Light Scattering Tandem for the Rapid and Quantitative Detection of the let7 MicroRNA Family. *Particle & Particle Systems Characterization*. **31**(12),pp.1260–1268.
- Shinde, S.B., Fernandes, C.B. and Patravale, V.B. 2012. Recent trends in in-vitro nanodiagnosics for detection of pathogens. *Journal of Controlled Release*. **159**(2),pp.164–180.
- Shishido, T., Mieda, H., Hwang, S.Y., Nishimura, Y., Tanaka, T., Ogino, C., Fukuda, H. and Kondo, A. 2010. Affibody-displaying bionanocapsules for specific drug delivery to HER2-expressing cancer cells. *Bioorganic & Medicinal Chemistry Letters*. **20**(19),pp.5726–5731.
- Si, S., Kotal, A. and Mandal, T.K. 2007. One-Dimensional Assembly of Peptide-Functionalized Gold Nanoparticles: An Approach Toward Mercury Ion Sensing. *The Journal of Physical Chemistry C*. **111**(3),pp.1248–1255.
- Silverman, J., Lu, Q., Bakker, A., To, W., Duguay, A., Alba, B.M., Smith, R., Rivas, A., Li, P., Le, H., Whitehorn, E., Moore, K.W., Swimmer, C., Perlroth, V., Vogt, M., Kolkman, J. and Stemmer, W.P.C. 2005. Multivalent avimer proteins evolved by exon shuffling of a family of human receptor domains. *Nature Biotechnology*. **23**(12),pp.1556–1561.
- Singh, V., Nair, S.P.N. and Aradhyam, G.K. 2013. Chemistry of conjugation to gold nanoparticles affects G-protein activity differently. *Journal of Nanobiotechnology*. **11**(1),p.7.
- Skerra, A. 2008. Alternative binding proteins: Anticalins - harnessing the structural plasticity of the lipocalin ligand pocket to engineer novel binding activities: Anticalins. *FEBS Journal*. **275**(11),pp.2677–2683.
- Skerra, A. 2007. Alternative non-antibody scaffolds for molecular recognition. *Current Opinion in Biotechnology*. **18**(4),pp.295–304.
- Skerra, A. 2003. Imitating the humoral immune response. *Current Opinion in Chemical Biology*. **7**(6),pp.683–693.
- Storhoff, J.J., Lucas, A.D., Garimella, V., Bao, Y.P. and Müller, U.R. 2004. Homogeneous detection of unamplified genomic DNA sequences based on colorimetric scatter of gold nanoparticle probes. *Nature Biotechnology*. **22**(7),pp.883–887.
- Sun, L., Yu, C. and Irudayaraj, J. 2007. Surface-Enhanced Raman Scattering Based Nonfluorescent Probe for Multiplex DNA Detection. *Analytical Chemistry*. **79**(11),pp.3981–3988.

- Tamayo, J., Kosaka, P.M., Ruz, J.J., San Paulo, Á. and Calleja, M. 2013. Biosensors based on nanomechanical systems. *Chem. Soc. Rev.* **42**(3),pp.1287–1311.
- Tiede, C., Bedford, R., Heseltine, S.J., Smith, G., Wijetunga, I., Ross, R., AlQallaf, D., Roberts, A.P., Balls, A., Curd, A., Hughes, R.E., Martin, H., Needham, S.R., Zanetti-Domingues, L.C., Sadigh, Y., Peacock, T.P., Tang, A.A., Gibson, N., Kyle, H., Platt, G.W., Ingram, N., Taylor, T., Coletta, L.P., Manfield, I., Knowles, M., Bell, S., Esteves, F., Maqbool, A., Prasad, R.K., Drinkhill, M., Bon, R.S., Patel, V., Goodchild, S.A., Martin-Fernandez, M., Owens, R.J., Nettleship, J.E., Webb, M.E., Harrison, M., Lippiat, J.D., Ponnambalam, S., Peckham, M., Smith, A., Ferrigno, P.K., Johnson, M., McPherson, M.J. and Tomlinson, D.C. 2017. Affimer proteins are versatile and renewable affinity reagents. *eLife*. [Online]. **6**. [Accessed 28 July 2017]. Available from: <http://elifesciences.org/lookup/doi/10.7554/eLife.24903>.
- Tiede, C., Tang, A.A.S., Deacon, S.E., Mandal, U., Nettleship, J.E., Owen, R.L., George, S.E., Harrison, D.J., Owens, R.J., Tomlinson, D.C. and McPherson, M.J. 2014. Adhiron: a stable and versatile peptide display scaffold for molecular recognition applications. *Protein Engineering, Design and Selection*. **27**(5),pp.145–155.
- Turkevich, J., Stevenson, P.C. and Hillier, J. 1951. A study of the nucleation and growth processes in the synthesis of colloidal gold. *Discussions of the Faraday Society*. **11**,p.55.
- Vaughan, T.J., Williams, A.J., Pritchard, K., Osbourn, J.K., Pope, A.R., Earnshaw, J.C., McCafferty, J., Hodits, R.A., Wilton, J. and Johnson, K.S. 1996. Human Antibodies with Sub-nanomolar Affinities Isolated from a Large Non-immunized Phage Display Library. *Nature Biotechnology*. **14**(3),pp.309–314.
- Visentin, J., Minder, L., Lee, J.-H., Taupin, J.-L. and Di Primo, C. 2016. Calibration free concentration analysis by surface plasmon resonance in a capture mode. *Talanta*. **148**,pp.478–485.
- Vo-Dinh, T. and Cullum, B. 2000. Biosensors and biochips: advances in biological and medical diagnostics. *Fresenius' Journal of Analytical Chemistry*. **366**(6–7),pp.540–551.
- Wagh, A. and Law, B. 2013. Methods for Conjugating Antibodies to Nanocarriers *In*: L. Ducry, ed. *Antibody-Drug Conjugates* [Online]. Totowa, NJ: Humana Press, pp. 249–266. Available from: https://doi.org/10.1007/978-1-62703-541-5_15.
- Wang, L., Zhu, Y., Xu, L., Chen, W., Kuang, H., Liu, L., Agarwal, A., Xu, C. and Kotov, N.A. 2010. Side-by-Side and End-to-End Gold Nanorod Assemblies for Environmental Toxin Sensing. *Angewandte Chemie International Edition*. **49**(32),pp.5472–5475.

- Wang, W., Ding, X., He, M., Wang, J. and Lou, X. 2014. Kinetic Adsorption Profile and Conformation Evolution at the DNA-Gold Nanoparticle Interface Probed by Dynamic Light Scattering. *Analytical Chemistry*. **86**(20),pp.10186–10192.
- Wang, X., Li, Y., Quan, D., Wang, J., Zhang, Y., Du, J., Peng, J., Fu, Q., Zhou, Y., Jia, S., Wang, Y. and Zhan, L. 2012. Detection of hepatitis B surface antigen by target-induced aggregation monitored by dynamic light scattering. *Analytical Biochemistry*. **428**(2),pp.119–125.
- Wang, Z. and Ma, L. 2009. Gold nanoparticle probes. *Coordination Chemistry Reviews*. **253**(11–12),pp.1607–1618.
- Weidle, U.H., Auer, J., Brinkmann, U., Georges, G. and Tiefenthaler, G. 2013. The emerging role of new protein scaffold-based agents for treatment of cancer. *Cancer Genomics & Proteomics*. **10**(4),pp.155–168.
- Wilchek, M. and Bayer, E.A. 1990a. [2] Introduction to avidin-biotin technology *In: Methods in Enzymology* [Online]. Elsevier, pp. 5–13. [Accessed 27 July 2017]. Available from: <http://linkinghub.elsevier.com/retrieve/pii/007668799084256G>.
- Wilchek, M. and Bayer, E.A. 1990b. [3] Applications of avidin-biotin technology: Literature survey *In: Methods in Enzymology* [Online]. Elsevier, pp. 14–45. [Accessed 27 July 2017]. Available from: <http://linkinghub.elsevier.com/retrieve/pii/007668799084257H>.
- Wu, L., Chen, K., Lu, Z., Li, T., Shao, K., Shao, F. and Han, H. 2014. Hydrogen-bonding recognition-induced aggregation of gold nanoparticles for the determination of the migration of melamine monomers using dynamic light scattering. *Analytica Chimica Acta*. **845**,pp.92–97.
- Xiang, M., Xu, X., Liu, F., Li, N. and Li, K.-A. 2009. Gold Nanoparticle Based Plasmon Resonance Light-Scattering Method as a New Approach for Glycogen–Biomacromolecule Interactions. *The Journal of Physical Chemistry B*. **113**(9),pp.2734–2738.
- Xie, C., Tiede, C., Zhang, X., Wang, C., Li, Z., Xu, X., McPherson, M.J., Tomlinson, D.C. and Xu, W. 2017. Development of an Affimer-antibody combined immunological diagnosis kit for glypican-3. *Scientific Reports*. [Online]. **7**(1). [Accessed 21 September 2017]. Available from: <http://www.nature.com/articles/s41598-017-10083-w>.
- Xiong, C. and Ling, L. 2012. Label-free, sensitive detection of Hg(II) with gold nanoparticles by using dynamic light scattering technique. *Talanta*. **89**,pp.317–321.
- Xu, X., Liu, X., Li, Y. and Ying, Y. 2013. A simple and rapid optical biosensor for detection of aflatoxin B1 based on competitive dispersion of gold nanorods. *Biosensors and Bioelectronics*. **47**,pp.361–367.

- Yang, X., Huang, J., Wang, Q., Wang, K., Yang, L. and Huo, X. 2011. A one-step sensitive dynamic light scattering method for adenosine detection using split aptamer fragments. *Anal. Methods*. **3**(1),pp.59–61.
- Yguerabide, J. and Yguerabide, E.E. 1998. Light-Scattering Submicroscopic Particles as Highly Fluorescent Analogs and Their Use as Tracer Labels in Clinical and Biological Applications. *Analytical Biochemistry*. **262**(2),pp.137–156.
- Yoo, E.-H. and Lee, S.-Y. 2010. Glucose Biosensors: An Overview of Use in Clinical Practice. *Sensors*. **10**(5),pp.4558–4576.
- You, C.-C., Miranda, O.R., Gider, B., Ghosh, P.S., Kim, I.-B., Erdogan, B., Krovi, S.A., Bunz, U.H.F. and Rotello, V.M. 2007. Detection and identification of proteins using nanoparticle–fluorescent polymer ‘chemical nose’ sensors. *Nature Nanotechnology*. **2**(5),pp.318–323.
- Zelensky, A.N. and Gready, J.E. 2005. The C-type lectin-like domain superfamily. *FEBS Journal*. **272**(24),pp.6179–6217.
- Zhang, J.-Q., Wang, Y.-S., He, Y., Jiang, T., Yang, H.-M., Tan, X., Kang, R.-H., Yuan, Y.-K. and Shi, L.-F. 2010. Determination of urinary adenosine using resonance light scattering of gold nanoparticles modified structure-switching aptamer. *Analytical Biochemistry*. **397**(2),pp.212–217.
- Zhang, L., Yao, Y., Shan, J. and Li, H. 2011. Lead (II) ion detection in surface water with pM sensitivity using aza-crown-ether-modified silver nanoparticles via dynamic light scattering. *Nanotechnology*. **22**(27),p.275504.
- Zhang, Y., Chen, Y. and Jin, G. 2011. Serum tumor marker detection on PEGylated lipid membrane using biosensor based on total internal reflection imaging ellipsometry. *Sensors and Actuators B: Chemical*. **159**(1),pp.121–125.
- Zhang, Y., Fei, W.-W. and Jia, N.-Q. 2012. A facile method for the detection of DNA by using gold nanoparticle probes coupled with dynamic light scattering. *Nanoscale Research Letters*. **7**(1),p.564.
- Zhang, Z., Lin, M., Zhang, S. and Vardhanabhuti, B. 2013. Detection of Aflatoxin M1 in Milk by Dynamic Light Scattering Coupled with Superparamagnetic Beads and Gold Nanoprobes. *Journal of Agricultural and Food Chemistry*. **61**(19),pp.4520–4525.
- Zhang, Z., Wang, S., Xu, H., Wang, B. and Yao, C. 2015. Role of 5-aminolevulinic acid-conjugated gold nanoparticles for photodynamic therapy of cancer. *Journal of Biomedical Optics*. **20**(5),p.051043.
- Zhao, W., Brook, M.A. and Li, Y. 2008. Design of Gold Nanoparticle-Based Colorimetric Biosensing Assays. *ChemBioChem*. **9**(15),pp.2363–2371.
- Zheng, T., Bott, S. and Huo, Q. 2016. Techniques for Accurate Sizing of Gold Nanoparticles Using Dynamic Light Scattering with Particular Application to

Chemical and Biological Sensing Based on Aggregate Formation. *ACS Applied Materials & Interfaces*. **8**(33),pp.21585–21594.

Zheng, T., Cherubin, P., Cilenti, L., Teter, K. and Huo, Q. 2016. A simple and fast method to study the hydrodynamic size difference of protein disulfide isomerase in oxidized and reduced form using gold nanoparticles and dynamic light scattering. *The Analyst*. **141**(3),pp.934–938.

Zheng, T., Pierre-Pierre, N., Yan, X., Huo, Q., Almodovar, A.J.O., Valerio, F., Rivera-Ramirez, I., Griffith, E., Decker, D.D., Chen, S. and Zhu, N. 2015. Gold Nanoparticle-Enabled Blood Test for Early Stage Cancer Detection and Risk Assessment. *ACS Applied Materials & Interfaces*. **7**(12),pp.6819–6827.

Appendices

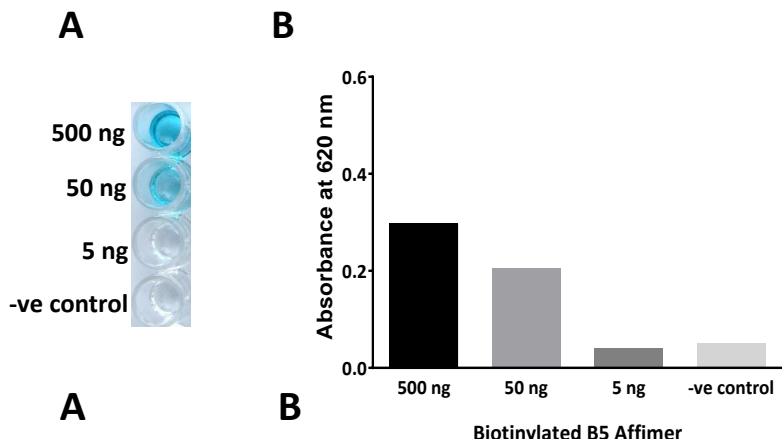
1. KingFisher Flex protocol 'Phage_display_pH_elution'

Protocol Step	Plate	Volume (ul)	Settings
Tipcomb	96 DW tip comb		
Pick-Up: Tipcomb	KingFisher 96 KF plate		
Collect Beads	Plate: Binding Microtiter DW 96 plate		Collect count 1 Collect time (s) 1
Binding	Plate: Binding Microtiter DW 96 plate	300	Beginning of Step Release beads [hh:mm:ss]: 00:00:00 Mixing/Heating Parameters Mix time [hh:mm:ss]: 00:00:10 Speed: fast Mix time [hh:mm:ss]: 00:01:00 Speed: slow End of step Collect beads, count: 5 Collect time (s): 30
Wash 1	Plate: Wash 1 Microtiter DW 96 plate	950	Beginning of Step Release beads [hh:mm:ss]: 00:00:00 Mixing/Heating Parameters Mix time [hh:mm:ss]: 00:01:00 Speed: slow End of step Collect beads, count: 5 Collect time (s): 30
Wash 2	Plate: Wash 2 Microtiter DW 96 plate	950	Beginning of Step Release beads [hh:mm:ss]: 00:00:00 Mixing/Heating Parameters Mix time [hh:mm:ss]: 00:01:00 Speed: slow End of step Collect beads, count: 5 Collect time (s): 30
Wash 3	Plate: Wash 3 Microtiter DW 96 plate	950	Beginning of Step Release beads [hh:mm:ss]: 00:00:00 Mixing/Heating Parameters Mix time [hh:mm:ss]: 00:01:00

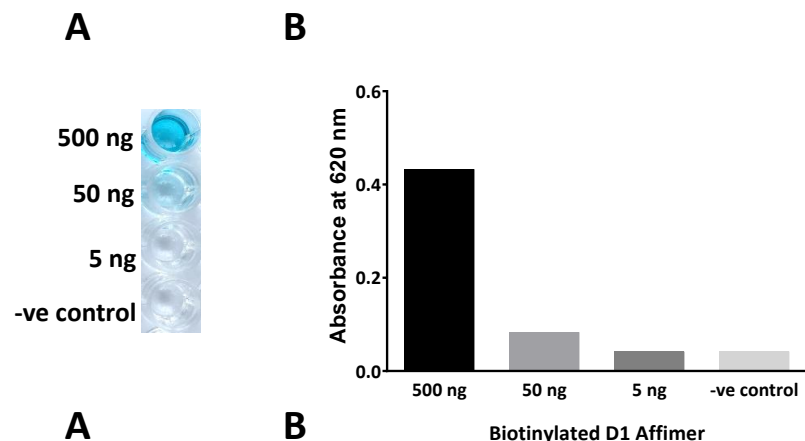
			Speed: slow End of step Collect beads, count: 5 Collect time (s): 30
Wash 4	Plate: Wash 4 Microtiter DW 96 plate	950	Beginning of Step Release beads [hh:mm:ss]: 00:00:00 Mixing/Heating Parameters Mix time [hh:mm:ss]: 00:01:00 Speed: slow End of step Collect beads, count: 5 Collect time (s): 30
pH Elution	Plate: pH elution KingFisher 96 KF plate	100	Beginning of Step Release beads [hh:mm:ss]: 00:00:00 Mixing/Heating Parameters Mix time [hh:mm:ss]: 00:07:30 Speed: slow Postmix[hh:mm:ss]: 00:00:05 Speed: Bottom mix End of step Collect beads, count: 5 Collect time (s): 30
Triethylamine Elution	Plate: Triethylamine KingFisher 96 KF plate	100	Beginning of Step Release beads [hh:mm:ss]: 00:00:00 Mixing/Heating Parameters Mix time [hh:mm:ss]: 00:03:30 Speed: slow Postmix[hh:mm:ss]: 00:00:05 Speed: Bottom mix End of step Collect beads, count: 5 Collect time (s): 30
Leave: Tipcomb	96 DW tip comb		

2. ELISA results of biotinylated Affimers

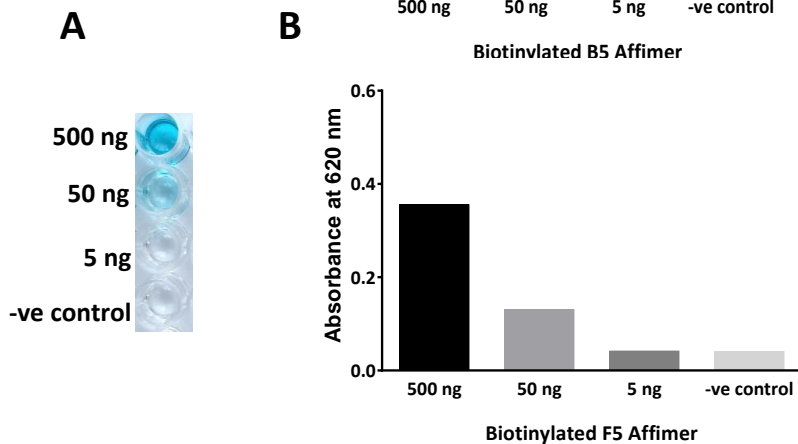
B5



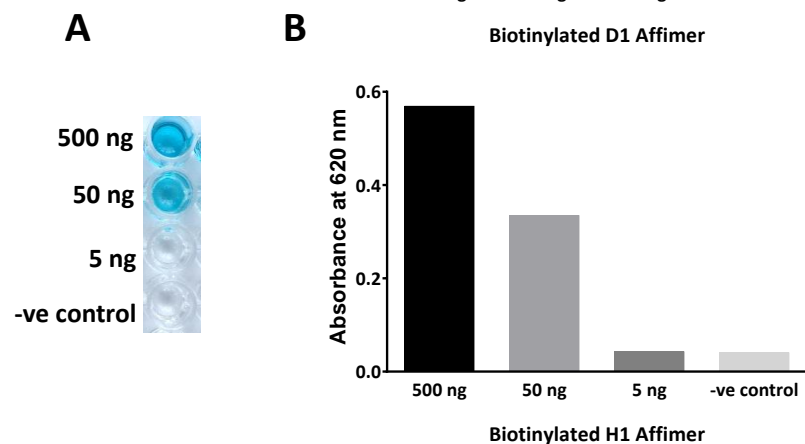
D1



F5

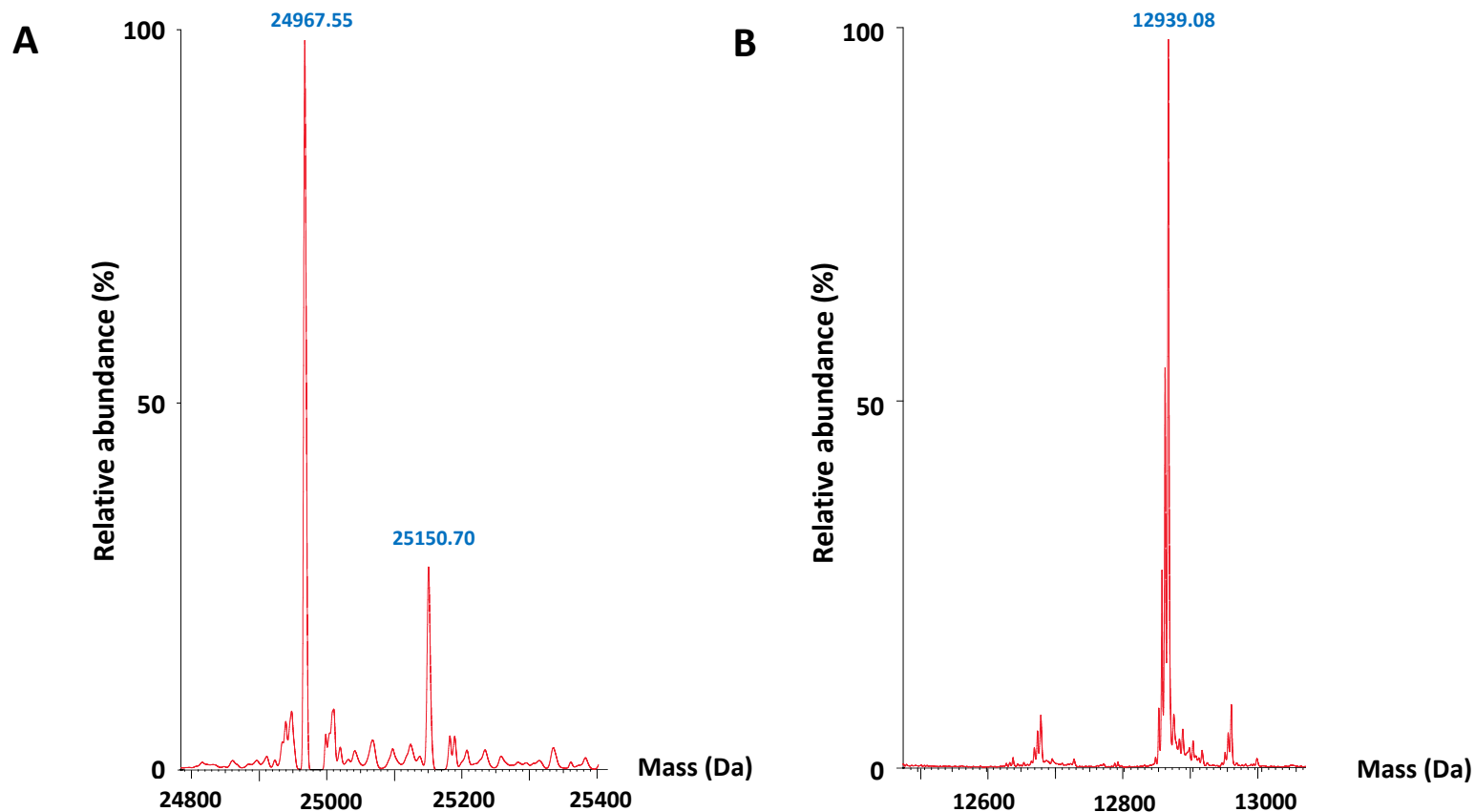


H1



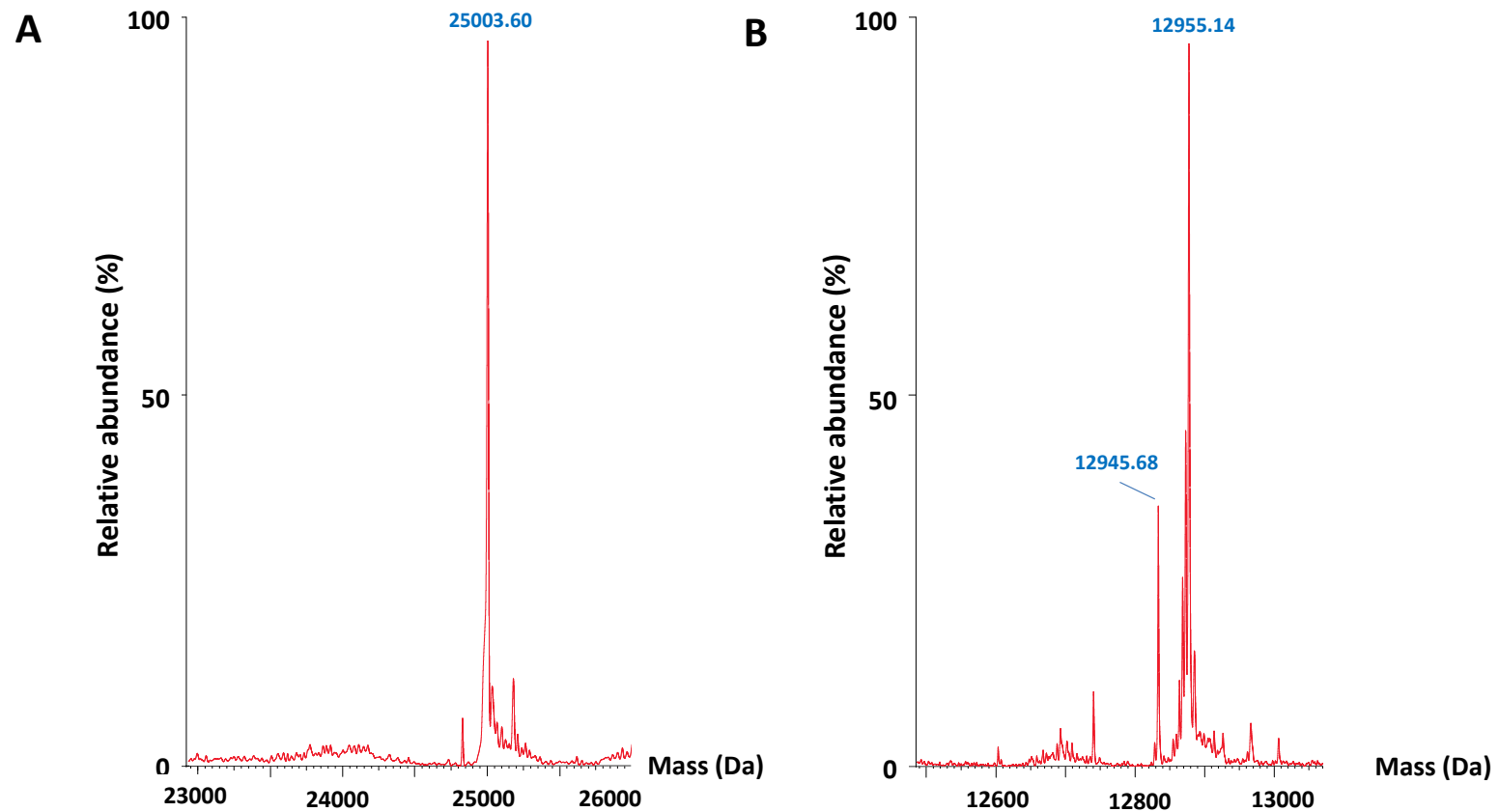
ELISA to validate biotinylation of Affimers B5, D1, F5 and H1 for AuNP functionalisation. (A), showing ELISA strip for three different dilutions of biotinylated Affimers 0.5 mg/ml (1, 1/10 and 1/100) and negative control (PBS buffer) from top to bottom; (B), showing the absorbance at 620 nm of each tested samples

3. Mass spectrum of Affimer B5 and biotinylated Affimer B5



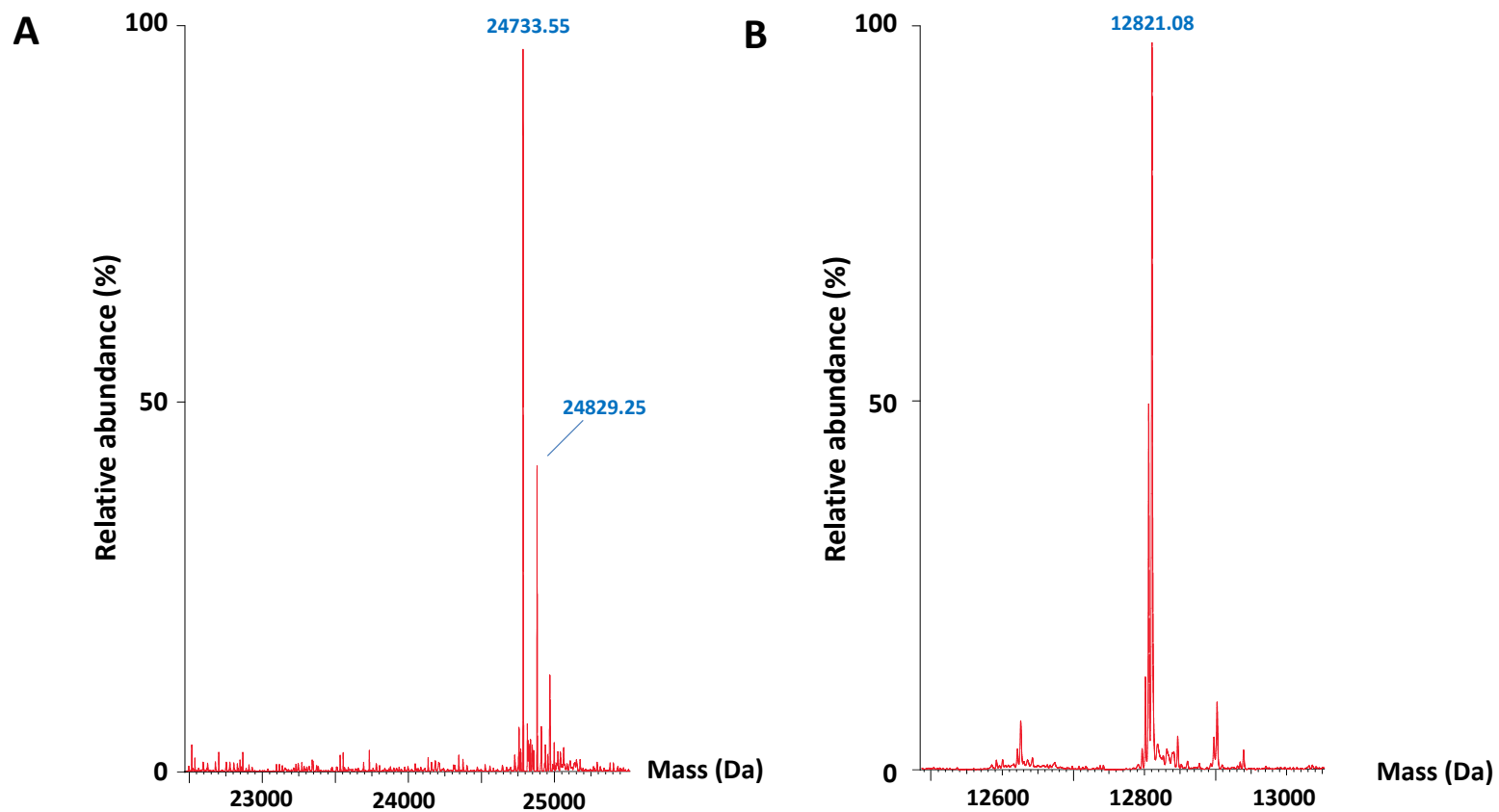
Mass spectrum of B5 Affimer. (A), showing B5 Affimer before biotinylation, highest peak at 24967.55 Da corresponding to Mr of dimeric B5 Affimer; (B), showing after biotinylation, highest peak at 12939.08 Da corresponding to Mr of B5 Affimer monomer plus biotin maleimide (Mr 451.54 Da).

4. Mass spectrum of Affimer D1 and biotinylated Affimer D1



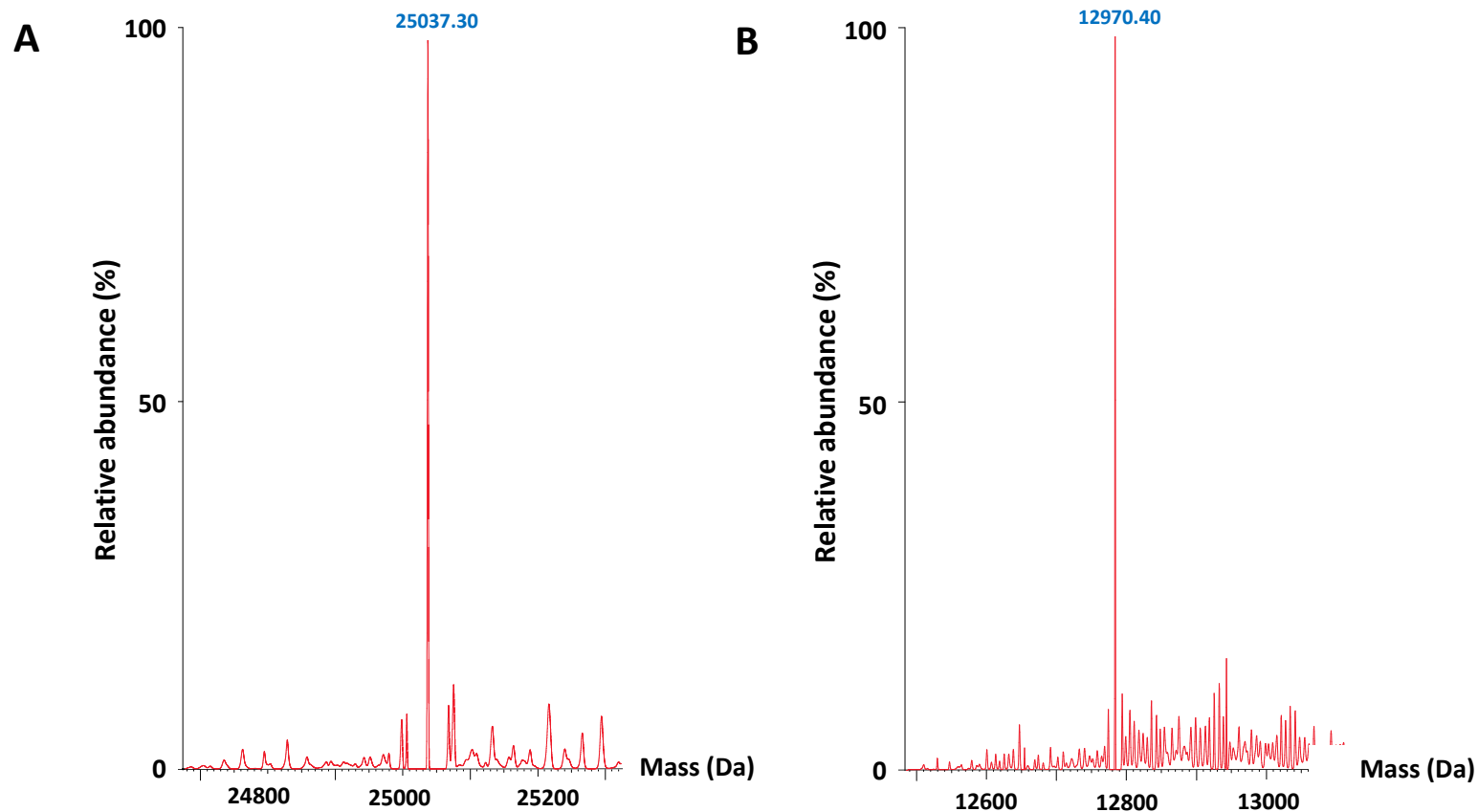
Mass spectrum of D1 Affimer. (A), showing D1 Affimer before biotinylation, highest peak at 25003.60 Da corresponding to Mr of dimeric D1 Affimer; (B), showing after biotinylation, highest peak at 12955.14 Da corresponding to Mr of D1 Affimer monomer plus biotin maleimide (Mr 451.54 Da).

5. Mass spectrum of Affimer F5 and biotinylated Affimer F5



Mass spectrum of F5 Affimer. (A), showing F5 Affimer before biotinylation, highest peak at 24733.55 Da corresponding to Mr of dimeric F5 Affimer; (B), showing after biotinylation, highest peak at 12821.08 Da corresponding to Mr of F5 Affimer monomer plus biotin maleimide (Mr 451.54 Da).

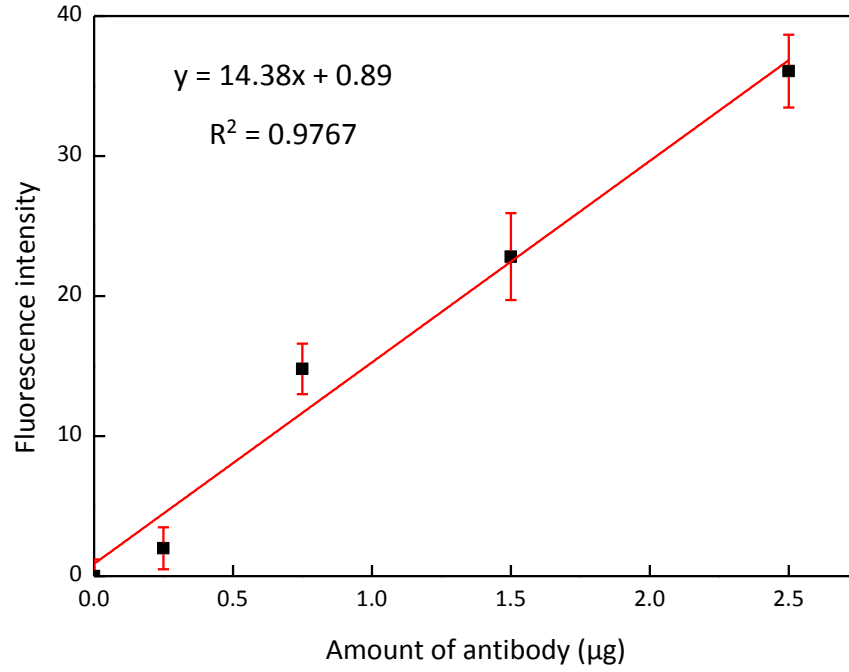
6. Mass spectrum of Affimer H1 and biotinylated Affimer H1



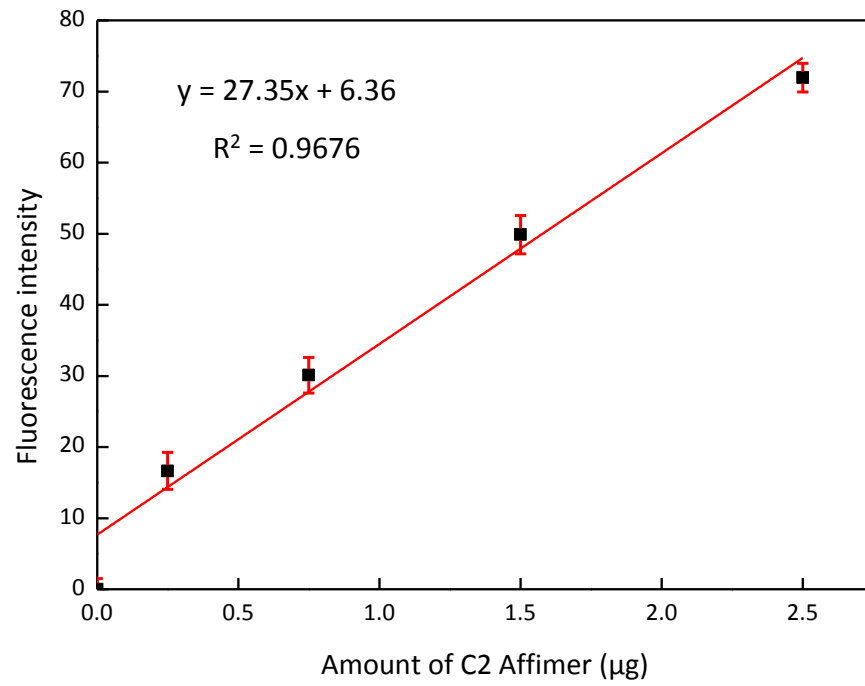
Mass spectrum of H1 Affimer. (A), showing H1 Affimer before biotinylation, highest peak at 25037.30 Da corresponding to Mr of dimeric H1 Affimer; (B), showing after biotinylation, highest peak at 12970.40 Da corresponding to Mr of H1 Affimer monomer plus biotin maleimide (Mr 451.54 Da).

7. Calibration curves prepared using NanoOrange™ fluorescent dye

A) IgG standard solutions

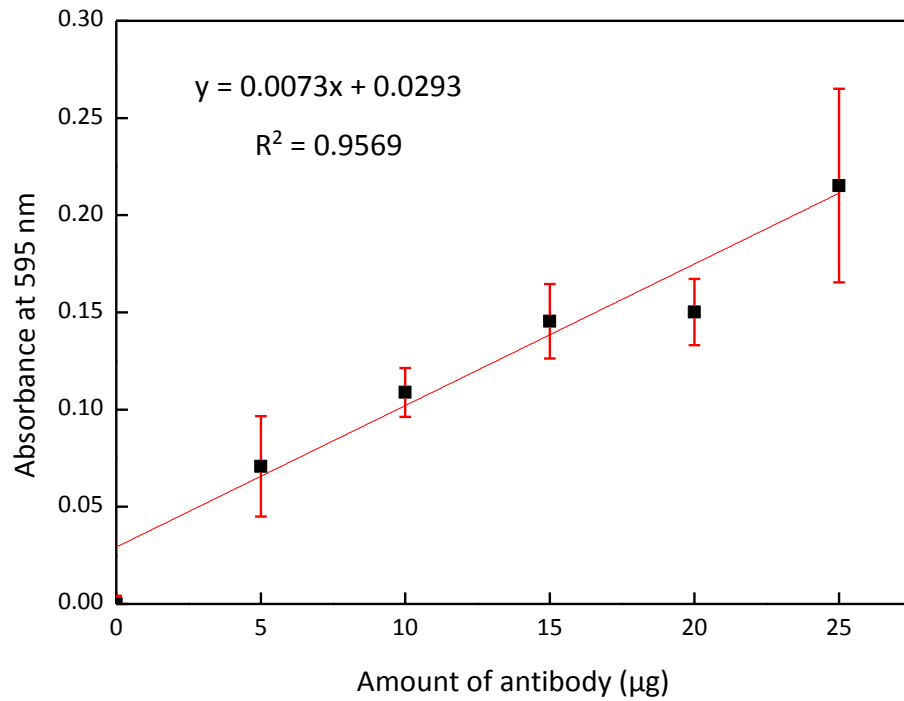


B) C2 Affimer standard solutions

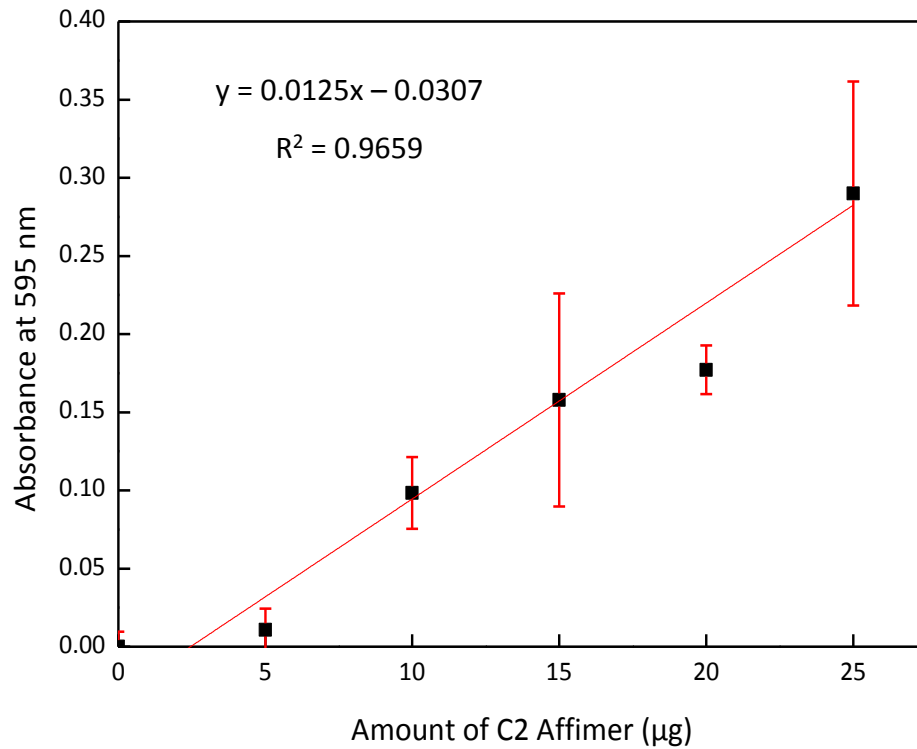


8. Calibration curves prepared using Bradford reagent

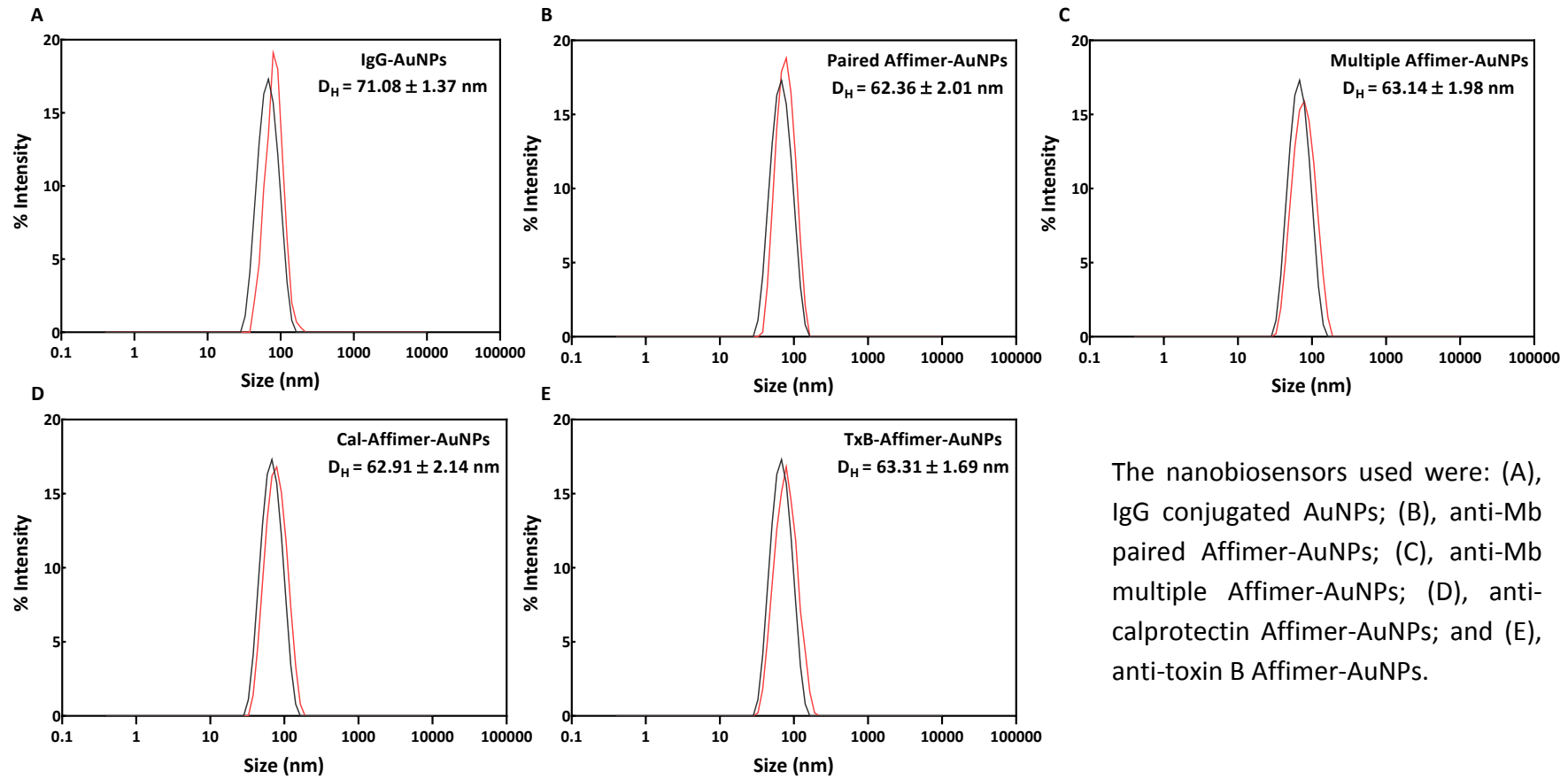
A) IgG standard solutions



B) C2 Affimer standard solutions

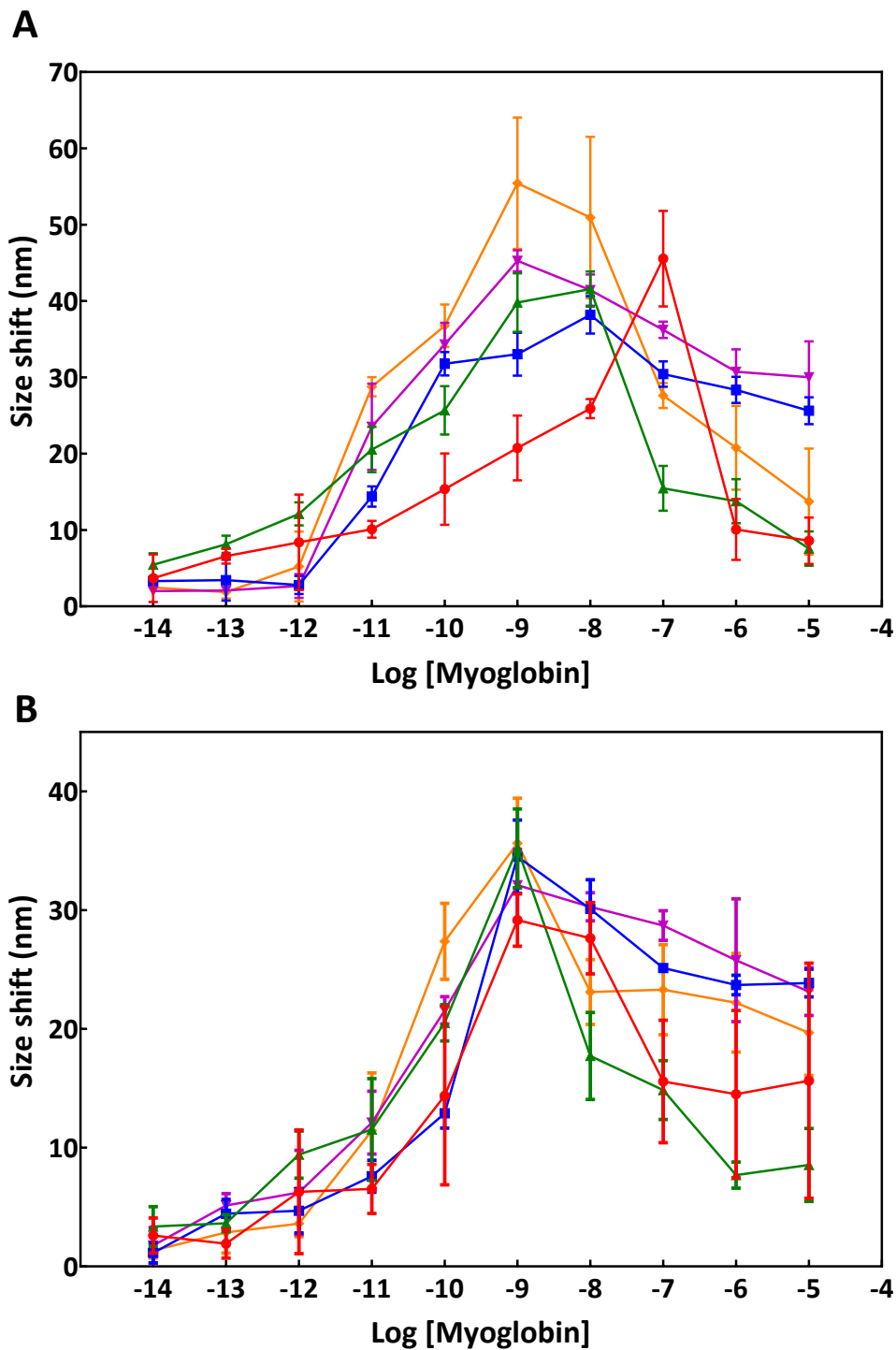


9. Size distribution plots of all nanobiosensors used



The nanobiosensors used were: (A), IgG conjugated AuNPs; (B), anti-Mb paired Affimer-AuNPs; (C), anti-Mb multiple Affimer-AuNPs; (D), anti-calprotectin Affimer-AuNPs; and (E), anti-toxin B Affimer-AuNPs.

10. Effect of AuNP size on the NP-coupled DLS size shift assay



Effect of AuNP size on the DLS assay for Mb detection. (A) and (B) represents IgG- and multiple-AuNPs, respectively; line graph represents AuNP core diameters of (•), 20 nm; (■), 40 nm; (■), 60 nm; (■), 80 nm and (■), 100 nm. Data are mean values \pm SD (n=3).

11. Poster presented at World Congress on Biosensors 2016 (Gothenburg, Sweden)

**A new analytical platform for biomolecules:
Nanoparticle size shift assay using synthetic binding proteins**

Thanisorn Mahatnirunkul^{1*}, Darren Tomlinson², Michael McPherson² and Paul Millner¹

¹ The Leeds Bionanotechnology Group, School of Biomedical Sciences, University of Leeds, UK.
² Leeds BioScreening Technology Group and Astbury Centre for Structural Molecular Biology.
sm12tm@leeds.ac.uk *

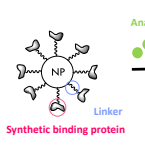
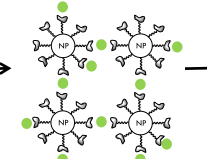
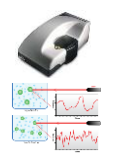



1. Why a new analytical platform?

- Detection of biomolecules usually involves labelling analytes with chromophores, fluorophores or radiolabels, which sometimes interfere with analytes and their molecular interactions.
- The tagging process also makes the established method complicated, complex, time-consuming and expensive.
- **Proposed applications for a new analytical platform:**
 - ✓ screening new drugs within the pharmaceutical industry
 - ✓ cheap and rapid diagnostic purposes by label-free approaches that minimize processing steps

2. What is the principle?

- Proposed assay is based on principle of optical biosensing.
- Synthetic binding proteins, which replicate antibody function, are conjugated onto nanoparticles (NPs) as bioreceptor elements.
- When the target analytes are added to the system, the binding of the target and immobilised binding protein will lead to aggregation of the NPs.
- The aggregation can be measured by dynamic light scattering (DLS) for complete quantitation
- **Dynamic light scattering (DLS):** analytical tool used routinely for measuring the hydrodynamic size of nanoparticles and colloids in a liquid environment.
- **Advantages:**
 - short duration analysis, no special expert required, cheap, sensitive to small change in size

3. Affimer vs Antibody

- It is an artificial protein that replicates antibody function selected by phage display.
- Library has around 1.3×10^{10} clones to be selected.
- Characterizes by ELISA and biolayer interferometry.
- **Compared with antibody:**
 - Inexpensive production system; genetic engineering and prokaryotic expression system
 - Better stability
 - Monomeric, small molecule
 - Do not contain internal cysteine

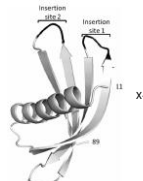


Figure 1: X-ray crystal structure of scaffold¹.

4. Nanoparticle size shift assay for myoglobin

- Myoglobin from equine heart was used as a model analyte.
 - common, cheap, have a lot of information and good supply availability

Preparation of nanoparticle probes

Labeling Affimers with biotin

+

Streptavidin AuNPs (OD 1)

=

Affimer-conjugated AuNPs probes

Probe	Target	Control
Myo-AbAuNPs	Anti-myoglobin antibody AuNPs	Positive control
Myo-AdAuNPs	Anti-myoglobin Affimer AuNPs	
Cal-AdAuNPs	Anti-calprotectin Affimer AuNPs	Non-specific control



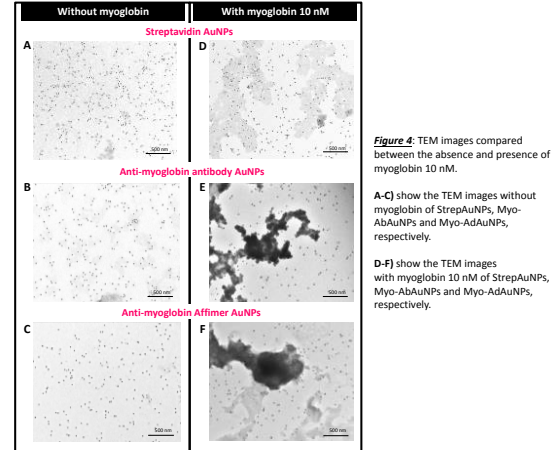
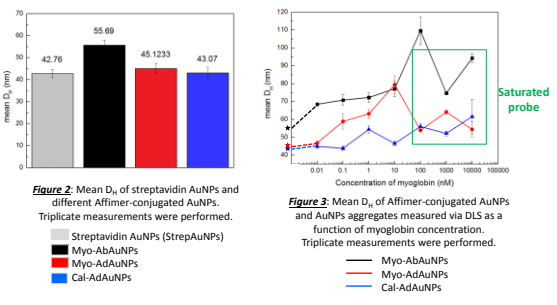

Myoglobin 10 pM – 10 μM
 Myoglobin 10 nM

Results and Discussion

- The DLS data (Figure 2) shows slight shift in size of both antibody and Affimer probes with narrow size distribution, which correlates to the TEM images (Figure 4A-C) that show no aggregation of the particles.
- The DLS results in Figure 3 show an increase in mean hydrodynamic diameter (D_h) with an increase in myoglobin up to 100 and 10 nM for anti-myoglobin antibody and Affimer systems, respectively.
- There was a slight shift in anti-calprotectin Affimer system (Control, Figure 3, blue line)
- Greater concentrations of myoglobin led to a decrease in D_h . This is probably due to the commonly observed phenomenon reported before^{2,3}, when all the bioreceptors are saturated with the analyte and lead to prevention of cross-linking between particles.
- TEM images in Figure 4 confirm the presence of aggregates in the anti-myoglobin antibody and Affimer system, also the absence of the aggregates in streptavidin AuNPs alone without bioreceptors when myoglobin 10 nM was added.

5. Conclusion

- These preliminary results show a potential of anti-myoglobin Affimer nanoparticles probe in detection of myoglobin in the concentration range from 0.1 – 10 nM, which was similar to antibody nanoparticles probe.
- Optimisation of the system is under investigation.



References:
 [1] C. Todd et al, Protein Engineering Design and Selection, 2014, 22.
 [2] X. Liu and Q. Huo, J. Immunol. Methods, 2009, 349, 38-44.
 [3] S. Dong, Biochem. Biophys. Res. Commun., 2009, 38, 10-12.

12. Poster presented at 5th International conference on bio-sensing technology (Riva del Garda, Italy)

